

PRINT ISSN : 2395-6011

ONLINE ISSN : 2395-602X



4th National Conference on “Recent Innovations in Science and Engineering”

Organised by

PES Institute of Technology -

Bangalore South Campus, Electronic City, Hosur Road, Bangalore – 560 100,
Karnataka, India

VOLUME 5, ISSUE 3, MAY-JUNE-2018

**INTERNATIONAL JOURNAL OF SCIENTIFIC
RESEARCH IN
SCIENCE & TECHNOLOGY**

Email : editor@ijsrst.com Website : <http://ijsrst.com>



4th National Conference on
“Recent Innovations in Science and Engineering”
in association with
International Journal of Scientific Research in Science and Technology

Print ISSN: 2395-6011 Online ISSN : 2395-602X

Volume 5, Issue 3, May-June-2018

Organised By
PES INSTITUTE OF TECHNOLOGY - BANGALORE SOUTH
CAMPUS,
Electronic City, Hosur Road, Bangalore – 560 100

Published By

Technoscience Academy
(The International Open Access Publisher)

Email: info@technoscienceacademy.com
Website: www.technoscienceacademy.com

About Us

PES was established in 1972 at Bangalore, the Silicon Valley of India. PES is focused on four main educational areas: Engineering, Medicine, Management and Life Sciences. The institutions offer both foundation courses in these areas, as well as specialization with a Bachelors/ Master/ PhD Degree. Today PES has more than 18,000 students, spread across four different campuses.

PES Institute of Technology, Bangalore South campus offers Bachelor of Engineering in Computer Science, Electronics, Information Science and Mechanical Engineering. Masters Program includes Computer Science, VLSI, Signal Processing, and MBA & MCA. The campus also houses Research Centers to pursue Ph.D in the area of Mathematics, Physics, Chemistry, Computer Science, Electronics, Information Science, Mechanical Engineering, Computer and Business applications. All programs are affiliated to VTU and recognized by AICTE.

In today's business scenario, the core competence in domain knowledge is a prerequisite to excel in a chosen field of specialization. This conference is a platform for budding engineers and researchers to bridge the gap between the domain knowledge and industrial practices in terms of recent innovations in science and engineering technology. PESIT BSC generously thanks all the authors from various institutions and industries who made RISE 2015, 2016 and 2017 conferences a great success with tremendous contribution of original work. We look forward for innovative technical research/project papers to be part of RISE 2018 conference from your esteemed institution.

Conference Topics:

1. New vistas in basic and applied science.
2. New horizons in various technology domains pertaining to CSE, ECE, ISE and ME.
3. Case studies on bench marking techniques and issues faced by practicing engineers.

Chief Patrons

Dr. M.R. Doreswamy, Chancellor : PES University

Prof. D. Jawahar, Pro Chancellor : PES University

Patron

Prof. Ajoy Kumar, COO : PES Institutions

Conference Chair

Dr. J. Surya Prasad, Principal & Director : PESIT- BSC

Convener

Dr. S.V. Satish, Professor, Mechanical Department : PESIT-BSC

Technical Committee

Dr. T. S. B. Sudarshan : Associate Director
Dr. Subrahmanya S. Katte : HOD, ME
Dr. Subhash S. Kulkarni : HOD, ECE
Dr. Sandesh B.J : HOD, CSE
Dr. Annapurna. D : HOD, ISE
Dr. Arti Arya : HOD, MCA
Dr. R. Duraipandian : HOD, MBA
Dr. Karthiyayini. O : HOD, S&H
Dr. Abida Begum. N : HOD, S&H
Dr. Shikha Tripathi : ECE
Dr. Rahmath Ulla Baig : ME
Dr. Kiran G. Bhat : ME
Prof. Haridasa Nayak : ME
Dr. Shashidhar Tantry : ECE

Dr. Prashanth Wali : ECE
Prof. K. Pattabhi Raman : ECE
Dr. Bajarangbali : ECE
Dr. Gowri Srinivasa : CSE
Dr. Snehanshu Saha : CSE
Dr. Sarasvathi. V : CSE
Prof. Anand M.S : ISE
Dr. S. Naveen Prasath : MBA
Dr. Revanasiddappa. M : S&H
Dr. Mohana Lakshmi : S&H
Dr. Muhammad Faisal : S&H
Dr. Deepa K. Nair : S&H
Dr. Nagesh H.M : S&H

Conference Management Committee

Prof. Animesh Giri : ISE
Prof. Karthik. S : ISE

Organizing Committee

Prof. Ananda. M: ECE
Prof. Chandru. A: ME
Prof. Bharathi. R: ISE
Prof. Jayanthi. R : MCA
Prof. Ravi Urs : MBA
Prof. Sabeeha. S : MCA

CONTENTS

Sr. No	Article/Paper	Page No
1	Determination of Soil PH and Development of a Web Application for Crop Selection Harshini S. R., Kavya D., B Harshitha, Ganapathi Bhat, Sreenath M V, Revanasiddappa M	01-07
2	Spectroscopic Studies and Thermal Behaviour of Chemically synthesized Silver Doped Polyaniline / Strontium Titanatepolymer Composite Vinay. K , Shivakumar. K , Revanasiddappa. M	08-11
3	Vehicle Exhaust Purification by Chemical Process Venkatesh. B. N , Shubham Kumar ,Dr. Revanasiddappa M, Mrs. SatyaVani N. L	12-15
4	3D Vibration Monitoring Sensor for Automobiles Using Internet of Things (IoT) Kanishkar P, Senthil Kumar S A, Ketan Pandit, Ganapathi Bhat	16-24
5	IOT Based Automatic Crack Analysis for Structures Using Vibrations Niraj Anil Babar, Noel Alben, Mohamad Amjad Arhaan	25-27
6	Smart Home Security -Intrusion Detection System” Security for Home Pooja Balageri V, Dr. Sarasvathi V	28-36
7	Substitution and Comparative Study of Solar Panel Efficiencies of Silver and Aluminium as a Reflector Kaushik. M	37-41

8	IoT Based Noise Pollution Reduction in Traffic Jams Pawan Terdal, Sanath Kumar, Mohak Rathore	42-46
9	IoT-Enabled Hydroponics Farm Siddhanth J Ajri, Abhishek Guragol, Adish S Rao, Rahul Suresh	47-51
10	Efficient Water Distribution using Blockchain Ashwin M, Ramya M, Apeksha B G, Prof. Animesh Giri	52-56
11	Introduction to Mobile Cloud Computing and Battery Optimization in Mobile Devices Nidheesh. S. N, Namitha. N. Deshpande	57-66
12	Tuning and Analysis of PID Controllers Using Soft Computing Techniques Bajarangbali, Sujay H S, Suman R, Chaithanya S, Narayanan S, Shamanth U	67-71
13	Determination of Dissolution of Plastic by Using Ostwald's Viscometer Disha Anil, Manavi Pai, Anjali Deshpande, Revanasiddappa M	72-76
14	Simulation Tool to Determine Presence of Impurities in an Organic Compound Using IR Spectroscopy Suyoga Srinivas, Ujwal Unnikrishnan, Yashas A, Revana Siddappa	77-79
15	Nir'Bhaya - A Concealed Women's Safety and Security Torch Dhanurdhar Murali, Alfhan Ahmed, Chinmayi Hegde, Apoorva Saxena	80-84
16	Finite Element Modelling of Stick-Slip Principle Based Inertial Slider S. Shashikanth, B. K. Karthik, V. Shrikanth	85-92

17	Open Source Blockchain Model of Journalism Shashidhar V, Suraj Dev Yadav, Prasad B Honnavalli	93-97
18	Synthesis and D. C. Electrical Conductivity Studies of Coordination Metal Complexes Jyoti C Ajbani, Kotresh Durgada, D Smitha Revankar, Neeraj Ajbani, Vinay K, Basavaraj Patel B M, M Revanasiddappa	98-101
19	Development of Closed-Form Solution for a Multi-Layered Composite Stack Subjected to Thermal Loads Sanidhya Kumar Sanu, B K Karthik, Vijay Vittal, B Rammohan	102-108
20	Mathematical Modelling and Automation of Real-time Queues Srikrishna C.N	109-116
21	Spectroscopic and Electromagnetic Interference-Shielding Effectiveness Studies on Polyaniline/DBSA/MoO₃ Composite at X-band Frequencies NagesaSastry. D , Vinay. K , Hiremath Suresh Babu , Revanasiddappa. M	117-119
22	Numerical Modeling of Dynamically Excited Non-Resonant Piezoelectric Sensor R. Abishek, V. Shrikanth	120-126
23	Cable-Driven Constrained Traversal Mechanism for Planar Motion B Datta Shreehari, K Lokesh Varun, P Vignesh, V Shrikanth	127-131
24	EyesPRO - Protect Your Eyes Pranav Manjunath, Nimisha V Arun	132-138
25	Effect of Schiff Base Ligands as Corrosion Inhibitors on Mild Steel Avinash Anupam, Atmanand Udameeshi, Revanasiddappa M	139-146

26	Effects Of Different Types of Water Solutions on Corrosion of Mild Steel Revanasiddappa.M, Avinash Anupam , Atmanand Y. Udameeshi	147-151
27	Qualitative Analysis of Ground Water Samples of 4 Sites in Hosakerehalli Locality of Bangalore South, Karnataka, India Sankarshana Rao R, Sanath Krishna, Pushkar Pramod Wani, S Sourav Revanasiddappa M	152-155
28	Crime Patterns and Prediction: A Data Mining and Machine Learning Approach Saptarshi Dutta Gupta, Vaibhav Garg	156-162
29	IoT Based Intelligent Lock Nidhi Shivhare, Aashi Garg, Ananda M.	163-168
30	Structural and Modal Analysis of Composite Leaf Spring Rohan P Sakale, Sharanbassappa Patil	169-175
31	Synthesis and Mechanical Properties of Araldite/Wooden Powder/Lead oxide/PPY/PANI Composites P M Surendar, Nagaraja K B, Navyakiran R M, N Rahul, J Yashas, Pachappan C, M Revanasiddappa	176-184
32	Real Time Analysis of Pollutants in Vehicles [R.T.A.P.V] Yash Bhardwaj, Shakti Ratan	185-190
33	Design and Analysis of CMOS Based Temperature Sensor and Its Readout Circuit Pankaja. H. C, Dr. Shashidhar Tantry	191-196

Determination of Soil PH and Development of a Web Application for Crop Selection

Harshini S. R.¹, Kavya D.¹, B Harshitha¹, Ganapathi Bhat¹, Sreenath M V¹, Revanasiddappa M²

¹Department of Information Science and Engineering PESIT- Bangalore South Campus, Hosur Road, Bangalore, Karnataka, India

²Department of Engineering Chemistry PESIT- Bangalore South Campus, Hosur Road, Bangalore, Karnataka, India

ABSTRACT

This paper discusses the determination of soil pH and development of a web application for the real time use. The pH values of the soil sample was determined experimentally and theoretically. It includes the design and development of a web-application that will display the most suitable crops that can be cultivated in the specific region, based on the input values of pH, rainfall, temperature and soil type prevalent in that particular area. This project is developed with the idea of helping farmers choose the most optimum crops to cultivate in order to maximize the quality of their yield.

Keywords: pH; glass membrane electrode; HTML, CSS, PHP

I. INTRODUCTION

pH was originally acronym of French clause 'pouvoirhydrogene' which can be translated into English as 'power of hydrogen' or 'potential of hydrogen'. pH is used to quantify acidic or alkaline nature of a chemical which is measured in terms of H⁺ ions concentration. pH is a scale of acidity from 0 to 14. Substances that are neither acidic nor basic have a pH of 7 and are called as neutral solutions. More acidic solutions have lower pH i.e. less than 7. More basic or alkaline solutions have higher pH i.e. greater than 7. pH is a measure of concentration of protons(H⁺) in the solution S.P.L. Sorenson introduced this concept in 1909. Letter p indicates a German word potenz, which means power or concentration. Letter H indicates hydrogen ion (H⁺). For calculating pH the formula is given as $pH = -\log_{10}[H^+]$

[H⁺] indicates concentration of H⁺ ions(also can be written as [H₃O]⁺), the equal concentration of

hydronium ions), measured in moles per litre (also known as molarity) [1]. Alkaline substances have concentration of hydroxide ions(OH⁻) instead of hydrogen ions. Great deals of agricultural losses are incurred every year in our country due to a variety of reasons by people who depend on agriculture as a livelihood. A number of reasons are: lack of awareness about the properties of the soil and land that they intend to cultivate on, unseasonal and irregular rains, etc. Even if they do know about the pH, rainfall, temperature and soil properties, they are unable to identify which crops would be the most suitable to grow within the constraints of their parameter values. Information regarding this, even though available, is not readily available to farmers in an easy manner.

Our project has been developed in an effort to ease the process of selecting the right crop to cultivate for farmers. Data collected from research and other authorized sources about crops and their optimum parameter values was entered into a database. An easy-to-use web page has been developed for the user.

Output will be displayed after performing manipulative and computational operations on the collected input data.

IMPORTANCE OF SOIL pH

Wide range of pH in solution culture can be tolerated by most of the plants, but they tolerate a wide range of acidity in the soil. Because of acidity of soil changes, the solubility of concentration of metal ion also changes. Plant growth gets affected by the varying concentration of metal ion in solution rather than the acidity itself. Many soil minerals dissolve and increase the concentration of metal ions to toxic levels under acidic conditions. The primary toxic level is aluminum is due to high levels of manganese and iron can also inhibit the growth of plants under the above conditions. The nutrients phosphorous, molybdenum, magnesium and calcium are less than the required amount in acidic soils.

Nutrient deficiencies occur in the alkaline conditions of the soil due to decrease in mineral solubility. Deficiencies in iron, manganese, copper, zinc and boron restrict the growth of plants. Due to less availability of phosphorus in alkaline soils it inhibits the uptake of potassium and magnesium [2].

pH VALUES FOR SOME COMMON CROPS:-

Table 1

Sl. No	Crop	pH range	Optimum temperature range [°C]	Average rainfall [cm]	Type of soil
1	Cotton	5.5-6.5	18-30	60-120	Deep black and alluvial soil

2	Jute	5.0-7.4	24-37	125-200	Sandy, alluvial and Clayey loam soil
3	Ragi	4.5-8.0	20-30	50-100	Alluvial and red soil
4	Tea	4.5-5.5	13-35	150-250	Sandy loam and laterite soil
5	Coffee	4.5-5.5	15-28	125-200	Loamy, red and laterite soil
6	Rubber	5.0-6.0	21-35	200-400	Loamy and laterite soil
7	Rice	5.5-6.5	16-32	150-200	Clayey, black lava soil
8	Tobacco	5.5-6.5	75-80	50-125	Sandy loam and alluvial soil
9	Sesame	5.5-8.0	21-23	45-50	Loamy and black soil
10	Wheat	6.0-7.0	15-26	25-100	Loamy and alluvial soil

pH VALUES FOR SOME SOIL SAMPLES:-

Table 2

Crop	Scientific pH	Determined pH[laboratory]	
		With silt	Without silt
Beans	6.0-7.5	7.1-7.5	7.1-7.6
Bitter gourd	5.5-6.7	5.1-7.3	5.3-7.5
Banana	5.5-6.5	7.6-7.7	7.9-8.0
Marie gold	5.5-7.5	6.7-7.6	7.0-7.9
Maize	5.5-7.0	6.8-7.7	6.9-7.8
ChowCh	6.5-7.5	7.0-7.3	7.4-7.6

1.RICE:

Rice is a food grain that contains a number of vitamins and minerals that are extremely healthy for us. Rice is a wonderful and versatile grain that complements practically any food. And there are more than 8000 different types of rice categorized by size and by the method used to process. Rice cultivation is best suited on the alluvial soil or on the fertile river basins, mixed soil or loamy soil or clayey soil. It is grown well in black lava soil. The soil of pH 5.5 -6.5 is suitable for the growth of rice [3].

2.GROUND NUT:

The peanut also known as the ground nut and taxonomically classified as ARACHIS HYPOGARA, is a legume crop grown mainly for its edible seeds. It is widely classified grown in tropics and subtropics, bring important to both small and large commercial producers. It is classified as both as legume and grain because of its high oil content, an oil crop [4].

For growing peanuts in containers fertile and light soil is required which is neutral in pH and well drained. Groundnuts can be well grown in loamy soil, black soil and red soil. It requires a pH range of 6.0-6.5 for good yield.

3.WHEAT

Wheat is a cereal grain of species triticum. People eat it most often in the form of bread. Wheat is the best source of vegetable protein content than other major cereals. Wheat cultivation is best suited in the soil with a clay loam or loam texture, good structure , moderate water holding capacity and heavy soil with good drainage. It requires an optimum pH range of 6.0-7.0. Wheat grows well even in alluvial soil.

4.CHOW CHOW

Scientific name of chow chow is sechiumedule. It is also called the vegetable pear. It is mostly handled like summer squash and generally cooked to retain in rispflavor. It is a rich in vitamin C and perfect cooling vegetable. Chow chow is one of the edible perennial plants belonging to the gourd family cucurbitaceae, along the melons, cucumbers and squash. Chow chow is also known as chayote, summer squash etc.[5] The soil with good drainage facility and preserving the soil moisture is suitable for chow chow crop. Chow chow cultivation is best well drained loamy soil and alluvial soil. Chow chow crop is slightly tolerant to acidic soil.The soil pH range is between 5.5-6.5.

5.MARIGOLD:-

Marigold is one of the most commonly used flowers for garden decoration. Itis also extensively used as loose flowers for making garlands for social and functions. It is adapted to different types of soil. Sandy loam soil with pH 5.6-6.5 is ideal for its cultivation. Acidic and alkaline soil is not suitable for cultivation. Marigold takes about 2months to complete vegetative growth and later enters into reproductive phase. Sufficient amount of moisture in soil is required at vegetative and flowering period [6].

6.BANANA:-

Banana is ranked as the second most important fruit crop in India. Its affordability, availability, varietal range, nutrition, taste and medicinal values makes it favorite fruit for all kinds of people. Its export potential is also good. The soil with good drainage, moisture and adequate fertility is best suited. Deep rich loamy or clayey loam soil is also essential. pH range between 6.0-7.5 is necessary.

7. BITTER GOURD:-

Bitter gourd can also be called as bitter melon which is a unique vegetable fruit that can be used as medicine and food. Bitter gourd grows in wide range of soils. For optimum growth and production it prefers soils that are sandy loam with good drainage and rich in organic matter. Alluvial soil is suitable for the growth of bitter gourd. A soil with pH value ranging from 6.0-7.5 is favorable for bitter gourd cultivation.

8. COTTON:-

Cotton is one of the most important cash crop in India and plays a prominent role in agricultural and industrial economy of the country. It is the basic raw material for the cotton textile industry. Deep well drained soils with good nutrient content and deep black alluvial soil is suitable for cultivation of cotton. Soil with pH range of 5.5-6.5 is favourable for growth of cotton crop.

9. BEANS:-

Beans belongs to a flowering plant family fabaceae, which is a seed of one of the several genera. Pole beans and bush beans more commonly called green beans are the major types of beans. Beans need a sunny well drained area rich in organic matter for its cultivation. Soggy, cold soil will cause the seeds to rot. Beans grow well in sandy soil, loamy soil and alluvial soil. Beans likes soils which are slightly acidic pH range around 6.0-6.5 gives better yield.

DEVELOPMENT OF FRONT-END WEB PAGE:

HTML and CSS codes have been used in our project to aestheticize and structure our web page in a user-friendly manner. A header provides information about all the sections present and a pleasant background has been added to enhance user experience. Form has been used to collect user input with appropriate headings to guide with what the expected input is.

DEVELOPMENT OF BACK-END DATABASE:

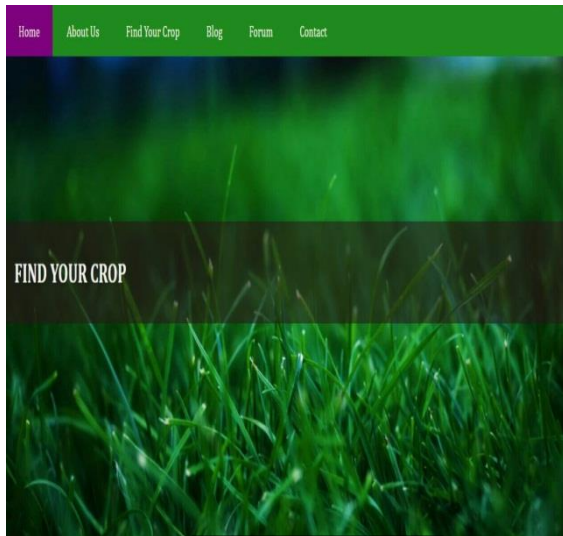
SQL and PHP have been used to handle the server side scripting and back-end database handling in our project. XAMPP software was used to establish a connection with the Apache web-server and enable working with MySQL. A database named "crops" was created and a table named "cropsinfo" was created to store details of crops collected under 9 columns, namely: SERIAL, NAME, pHLOW, pHHIGH, RAINLOW, RAINHIGH, TEMPLOW, TEMPHIGH and SOIL. Between the LOW and HIGH values of each parameter lies the range of those parameters where the crop is suitable to be cultivated. Individual records of crops were manually inserted into the table using SQL queries after establishing a connection with the database via a php-sql file. Crops that can be cultivated in more than one type of soil were entered each time with individual soil value to ease the extraction later.

EXTRACTING RECORDS FROM DATABASE BASED ON USER INPUT VALUES:

The POST method offered by PHP is used to collect information input by the user into PHP variables for further manipulation in a separate PHP file. The query used for extracting the correct crop for displaying is:

```
$query = "SELECT * FROM cropsinfo WHERE soil = 's$sol' AND phlow<=$phl AND phhigh>=$phh AND templow<=$templ AND temphigh>=$temph AND rainlow<=$rainl AND rainhigh>=$rainh";, where $sol, $phl, $phh, $templ, $temph, $rainl, $rainh are PHP
```

variables where user input values have been stored using the POST method. **Photographs:**

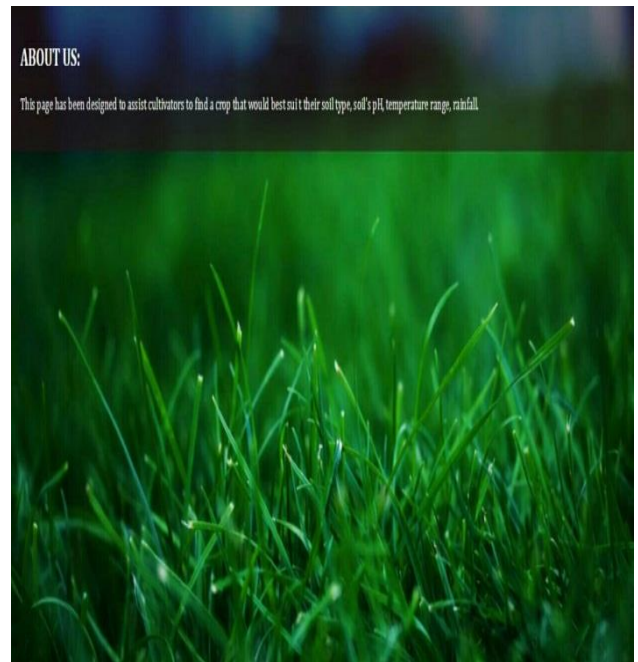


FRONT PAGE

NAME	pH-LOW	pH-HIGH	TEMP-LOW	TEMP-HIGH	RAIN-LOW	RAIN-HIGH	SOIL
Cardamom	5.5	7.5	10	30	200	300	Loamy
Pepper	5.5	7.5	10	30	200	300	Loamy
Chilies	5.5	7.5	10	30	200	300	Loamy
Arecanut	5.5	7.5	10	30	200	300	Loamy
Cinnamon	5.5	7.5	10	30	200	300	Loamy
Clove	5.5	7.5	10	30	200	300	Loamy

OUTPUT DISPLAYING CROPS THAT HAVE PARAMETER VALUES WITHIN THE RANGE THAT WAS GIVEN AS INPUT

ENTERING PARAMETER VALUES



Server: 127.0.0.1 Database: crops Table: cropsinfo

SELECT * FROM 'cropsinfo' ORDER BY 'serial' asc

Number of rows: 25

serial	name	phlow	phhigh	templow	temphigh	rainlow	rainhigh	soil
1	Cotton	5.5	6.5	18	30	60	120	Deep Black
2	Jute	5	7.4	24	37	125	200	Sandy
2	Jute	5	7.4	24	37	125	200	Alluvial
2	Jute	5	7.4	24	37	125	200	Clayey Loam
3	Ragi	4.5	8	20	30	50	100	Alluvial
3	Ragi	4.5	8	20	30	50	100	Red
4	Tea	4.5	5.5	13	35	150	250	Laterite
4	Tea	4.5	5.5	13	35	150	250	Sandy Loam
5	Coffee	4.5	5.5	15	28	125	200	Loamy
5	Coffee	4.5	5.5	15	28	125	200	Red
5	Coffee	4.5	5.5	15	28	125	200	Laterite
6	Rubber	5	6	21	35	200	400	Loamy
6	Rubber	5	6	21	35	200	400	Laterite
7	Rice	5.5	6.5	16	32	150	200	Black Lava
7	Rice	5.5	6.5	16	32	150	200	Clayey
8	Tobacco	5.5	6.5	75	80	50	125	Sandy Loam
8	Tobacco	5.5	6.5	75	80	50	125	Alluvial
9	Sesame	5.5	8	21	23	45	50	Loamy
9	Sesame	5.5	8	21	23	45	50	Black
10	Wheat	6	7	15	26	25	100	Alluvial
10	Wheat	6	7	15	26	25	100	Loamy
11	Green Gram	5	6.2	20	25	50	100	Loamy
11	Green Gram	5	6.2	20	25	50	100	Alluvial
12	Maize	5.5	7	21	27	50	100	Heavy Clayey
12	Maize	5.5	7	21	27	50	100	Alluvial

Server: 127.0.0.1 Database: crops Table: cropsinfo

serial	name	phlow	phhigh	templow	temphigh	rainlow	rainhigh	soil
13	Jowar	6	7.5	26	33	30	100	Black
13	Jowar	6	7.5	26	33	30	100	Sandy
14	Groundnut	6	6.5	20	25	50	100	Loamy
14	Groundnut	6	6.5	20	25	50	100	Red
14	Groundnut	6	6.5	20	25	50	100	Black
15	Sunflower	6.5	8.5	15	25	100	100	Black
16	Mustard	5.5	6.8	10	20	25	40	Alluvial
17	Soyabean	6	7.5	21	21	100	100	Alluvial
18	Linseed	6	7	15	30	45	75	Clayey Loam
18	Linseed	6	7	15	30	45	75	Alluvial
19	Castor	5	6.5	20	25	50	80	Alluvial
19	Castor	5	6.5	20	25	50	80	Sandy Loam
20	Sugarcane	6.5	7	20	36	75	120	Clayey Loam
20	Sugarcane	6.5	7	20	36	75	120	Alluvial
20	Sugarcane	6.5	7	20	36	75	120	Black
21	Coconut	5.5	8	20	35	150	250	Coastal Alluvial
22	Cashews	8	10	25	25	150	200	Laterite
22	Cashews	8	10	25	25	150	200	Sandy
23	Tur Dal	6.5	7.5	20	35	60	65	Sandy Loam
23	Tur Dal	6.5	7.5	20	35	60	65	Alluvial
24	Millets	5.6	8	20	30	100	200	Desert
24	Millets	5.6	8	20	30	100	200	Black
25	Pulses	5	6.5	20	30	50	75	Laterite
25	Pulses	5	6.5	20	30	50	75	Red
26	Oil Seeds	5.5	7	20	30	50	75	Alluvial
26	Oil Seeds	5.5	7	20	30	50	75	Loamy
27	Bajra	6.3	7	20	30	40	75	Desert
27	Bajra	6.3	7	20	30	40	75	Alluvial
28	Pea	6	7.5	24	30	60	140	Alluvial
29	Barley	6.5	7.5	1	2	39	43	Alluvial
29	Barley	6.5	7.5	1	2	39	43	Desert
30	Potato	5	6	7.2	26.6	50	70	Sandy Loam
30	Potato	5	6	7.2	26.6	50	70	Loamy

Server: 127.0.0.1 Database: crops Table: cropsinfo

serial	name	phlow	phhigh	templow	temphigh	rainlow	rainhigh	soil
30	Potato	5	6	7.2	26.6	50	70	Loamy
31	Onion	6	7	12.7	23.8	65	75	Alluvial
31	Onion	6	7	12.7	23.8	65	75	Clayey Loam
31	Onion	6	7	12.7	23.8	65	75	Sandy Loam
32	Cucumber	5.5	7.5	20	24	38	100	Clayey
32	Cucumber	5.5	7.5	20	24	38	100	Sandy Loam
33	Bitter Gourd	5.8	7.4	28	32	100	150	Alluvial
33	Bitter Gourd	5.8	7.4	28	32	100	150	Sandy Loam
34	Pumpkin	5.5	7	12.7	23.8	15	18.3	Laterite
34	Pumpkin	5.5	7	12.7	23.8	15	18.3	Sandy Loam
35	Watermelon	5.5	7	21	32	65	75	Fertile Loamy
35	Watermelon	5.5	7	21	32	65	75	Sandy
36	Muskmelon	6	6.5	18.3	35	80	150	Alluvial
36	Muskmelon	6	6.5	18.3	35	80	150	Well-Drained Loamy
37	Chow Chow	5.5	6.5	30	30	150	150	Loamy
37	Chow Chow	5.5	6.5	30	30	150	150	Alluvial
38	Mango	5.5	7.2	24	27	30	100	Red
38	Mango	5.5	7.2	24	27	30	100	Loamy
39	Apple	5	6.8	21	24	100	125	Alluvial
39	Apple	5	6.8	21	24	100	125	Heavy Clay
39	Apple	5	6.8	21	24	100	125	Loamy
40	Marigold	5.6	6.5	18	35	100	150	Sandy Loam
41	Banana	6	7.5	15	35	65	75	Alluvial
41	Banana	6	7.5	15	35	65	75	Clayey Loam
41	Banana	6	7.5	15	35	65	75	Rich Loam
42	Beans	6	6.5	15.5	26.6	60	65	Loamy
42	Beans	6	6.5	15.5	26.6	60	65	Sandy
42	Beans	6	6.5	15.5	26.6	60	65	Alluvial
43	Cardamom	5.5	7.5	10	30	200	300	Loamy
43	Cardamom	5.5	7.5	10	30	200	300	Laterite
44	Pepper	5.5	7.5	10	30	200	300	Loamy
44	Pepper	5.5	7.5	10	30	200	300	Laterite
45	Chillies	5.5	7.5	10	30	200	300	Laterite
45	Chillies	5.5	7.5	10	30	200	300	Loamy
46	Areca nut	5.5	7.5	10	30	200	300	Loamy
46	Areca nut	5.5	7.5	10	30	200	300	Laterite
47	Cinnamon	5.5	7.5	10	30	200	300	Loamy
47	Cinnamon	5.5	7.5	10	30	200	300	Laterite
48	Clove	5.5	7.5	10	30	200	300	Loamy
48	Clove	5.5	7.5	10	30	200	300	Laterite

Server: 127.0.0.1 Database: crops Table: cropsinfo

serial	name	phlow	phhigh	templow	temphigh	rainlow	rainhigh	soil
43	Cardamom	5.5	7.5	10	30	200	300	Loamy
43	Cardamom	5.5	7.5	10	30	200	300	Laterite
44	Pepper	5.5	7.5	10	30	200	300	Loamy
44	Pepper	5.5	7.5	10	30	200	300	Laterite
45	Chillies	5.5	7.5	10	30	200	300	Laterite
45	Chillies	5.5	7.5	10	30	200	300	Loamy
46	Areca nut	5.5	7.5	10	30	200	300	Loamy
46	Areca nut	5.5	7.5	10	30	200	300	Laterite
47	Cinnamon	5.5	7.5	10	30	200	300	Loamy
47	Cinnamon	5.5	7.5	10	30	200	300	Laterite
48	Clove	5.5	7.5	10	30	200	300	Loamy
48	Clove	5.5	7.5	10	30	200	300	Laterite

Query results operations: Print, Copy to clipboard, Export, Display chart, Create view

Bookmark this SQL query: Label: [] Let every user access this bookmark

IMAGES OF

IMAGES OF DATABASE

II. CONCLUSION

We have determined pH of the soil sample by using a glass membrane electrode. With the help of pH values a web application is developed for the real time application to the end users. This web application is useful for selecting a particular crop for cultivation depending upon the pH of the soil sample. Our web application will also provide information based on values of rainfall, temperature and soil type which helps to decide the particular crop for cultivation in the field.

III. ACKNOWLEDGEMENT

The authors would like to thank Dr J Suryaprasad, Principal, PESIT-BSC for his encouragement during the course of this project work.

IV. REFERENCES

- [1]. Wikipedia.org
- [2]. Nhb.gov.in
- [3]. Harvesttable.com
- [4]. Almanac.com
- [5]. Cropnutrition.com
- [6]. W3schools.com

Spectroscopic Studies and Thermal Behaviour of Chemically synthesized Silver Doped Polyaniline / Strontium Titanatepolymer Composite

Vinay. K ¹, Shivakumar. K ², Revanasiddappa. M ^{*3}

¹Department of Chemistry, PES Institute of Technology and Management, Shivamogga, Karnataka, India

²Department of Chemistry, PES Institute of Technology and Management, Shivamogga, Karnataka, India

³Department of Chemistry, PESIT-Bangalore South Campus, Bangalore, Karnataka, India

ABSTRACT

The present work is the study of thermal properties of IPANI/Ag/SrTiO₃ (PAS) composites synthesized via in-situ chemical oxidative interfacial polymerization using ammonium per sulfate as an oxidant at 0-30°C. The synthesized polymer composites were characterized by FT-IR analysis and their thermal stability was studied by TGA-DTA techniques. FT-IR patterns confirm the formation of the composite. The endotherms in the DTA profile are consistent with the change regions in the TG curve.

Keywords: Composite, Conducting, TGA, Polyaniline, strontium titanate.

I. INTRODUCTION

Conducting polymer composites blended with inorganic metal-oxides have attracted remarkable interest because of possible interactions between inorganic fillers and the host polymer matrices which may produce novel composite materials with superior properties [1-3]. These materials render the promise of achieving a new polymer composite matrix which exhibit remarkable features viz., reversibility, distinct electrical properties, simple method of polymerization, cost effective monomers and environmentally stable which increase their potential applications in LED's, battery electrodes, sensors, super capacitors, EMI shielding and corrosion coatings [12-14]. Structural conformation, distribution, stability and thermal properties of the composites were analysed using FT-IR and TGA-DTA techniques, and the results are presented here.

II. METHODS AND MATERIAL

Double distilled aniline (0.1M) monomer was dissolved in aqueous nitric acid (1M) solution in a beaker, an organic solvent; chloroform (10ml) was added to the beaker. Then, add 0.1M (NH₄)₂S₂O₈ solution and AgNO₃ (0.1M) solution separately dropwise, along the sides of the beaker to start oxidation at room temperature for about 2-4 hrs, a dark- greenish coloured precipitate was formed slowly at the junction and then gradually diffused into the aqueous phase. After 36 h; a dark greenish colour polyaniline matrix doped with shiny silver particles is obtained and the same is collected and washed with ethanol. SrTiO₃ powder was added to polymer solution with constant stirring in order to make the SrTiO₃ particles completely suspended in to the entire polymer solution. The reaction mixture was allowed to proceed at 30°C for about 4hrs. The precipitate so obtained was vacuum filtered, followed by washing with milli-Q water and acetone. Following this

procedure, different IPANI/Ag/SrTiO₃ (PAS) composites were prepared by varying 10%, 20%, 30%, 40% and 50% by weight of SrTiO₃ in IPANI/Ag matrix. The resulting composites were crushed in to fine grained powder and dried in oven at 80^o C to gain constant weight.

III. RESULTS AND DISCUSSION

A. FT-IR ANALYSIS

The important absorption bands of IPANI observed in the FT-IR spectra recorded for PAS-50% composite are in accordance with the published values found in the literature [4-8] and the corresponding band assignments are represented in the table 1. The Pure SrTiO₃ exhibits a characteristic broad band at 548 cm⁻¹ which is due to the Ti-O stretching vibration and the band at 1449cm⁻¹ may be ascribed to carboxylate group stretching mode [6,7].

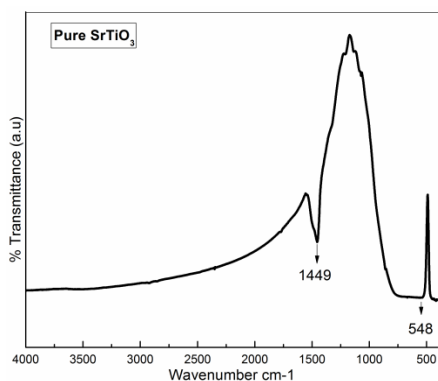


Figure 1a

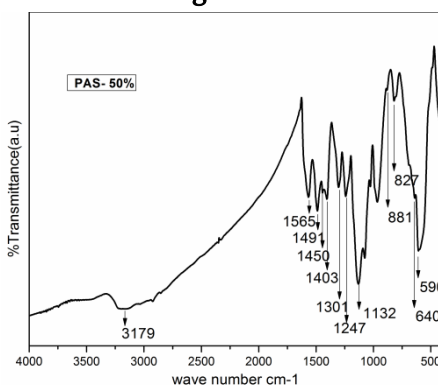


Figure 1b

Figure 1(a-b) represents FT-IR spectra of (a) Pure SrTiO₃ and (b) PAS-50% composite

Table 1. IR frequencies of PAS-50% composite and its band assignments

IR Frequencies (cm ⁻¹)	Band Assignments
3179	N-H stretching of aromatic amine
1565	N=Q=N ring stretching modes
1491	N-B-N ring stretching modes
1301	Asymmetric C-N stretching modes of the benzenoid moiety
1247	Conducting protonated form of IPANI
827	C-H out plane bending of p-disubstituted benzene ring

By vigilant observation of FT-IR spectra of the composite a well retained characteristics peaks of SrTiO₃ was observed, however the typical stretching frequencies are significantly shifted towards higher frequency region, suggesting weak vanderwaals interaction between the SrTiO₃ particles and polyaniline backbone [7,15].

B. THERMAL STUDIES

The TG curve of IPANI shows two stage weight loss behaviour, initial weight loss of about 3.90% below 150^oC ascribed to the removal of absorbed water molecules and acid dopants on the surface of the IPANI chain [9] and the major weight loss of 9.50% is occurred from 300^o-400^oC due to degradation of IPANI backbone [10]. Similar behaviour in the degradation process was also observed for silver doped IPANI, it shows higher onset degradation temperatures compared to IPANI due to the presence of more thermally stable silver particles [12].

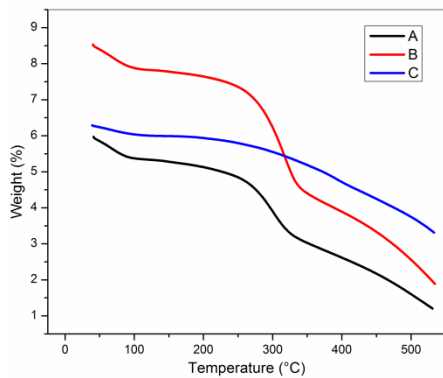


Figure 2a

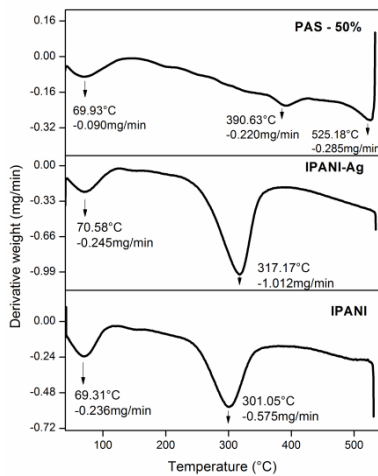


Figure 2b

Figure 2 Shows (a) TGA curves of A. IPANI, B. IPANI-Ag, C. PAS-50% composite. (b) Derivative weight loss pattern of IPANI, IPANI-Ag, and PAS-50% composite, which suggests most apparent weight loss steps corresponding to endothermic peaks in the region 40^o- 550^oC .

The TG thermogram of PAS-50% composite exhibit three distinctive decomposition patterns, from ambient temperature to 550^oC, the first step weight loss of 1.5% below 100^oC which is due to removal of moisture and volatile impurities, second step weight loss of 4.7% occurs in the range 300-350^oC, the third step weight loss of 3.5% in the range 350^o- 400^oC is mostly attributed to degradation of IPANI backbone [11] and the third step weight loss of 4.5% takesplace beyond 500^oC, which is due to decomposition of strontium titanate particles. The onset temperatures for three degradation stages of the composite are

69.93^o, 390.63^o, 382.65^o and 525.18^oC respectively. The decomposition rate of the polyaniline when combined with SrTiO₃ and silver particle is found to be different from that of the bulk IPANI. IPANI undergoes rapid thermal degradation at 301.05^oC; however the composite is stable up to 525.18^oC. This suggests that, the composite is thermally more stable compared to that of bulk IPANI. From the table 2, it is clear that, upon addition of strontium titanate particles in to the IPANI/Ag matrix, the thermal stability of the composite is notably enhanced.

Table 2. % weight losses and onset temperatures of synthesized samples

Sample	Steps	% Weight loss	Onset temperature (°C)
IPANI	1	3.9	69.31
	2	9.5	301.05
IPANI-Ag	1	2.9	70.58
	2	11.8	317.17
PAS-50%	1	1.5	69.93
	2	3.5	390.63
	3	4.5	525.18

IV. CONCLUSION

In the present work, IPANI/Ag/SrTiO₃ composites were successfully prepared by in-situ oxidative interfacial polymerization using ammonium per sulfate as an oxidizing agent. The weak vanderwaals interaction of IPANI chain with SrTiO₃ particles and the structural changes in the composite were confirmed by the FT-IR spectra. It was found that, the additive has considerable effect on the stability of the composite, suggesting that the synthesized composite is thermally stable up to 525^oC.

V. ACKNOWLEDGEMENT

The authors wholeheartedly acknowledge VGST, Government of Karnataka, for their financial support in the form of a research and development of infrastructure (No.: VGST/K-FIST (Li)/GRD-363/2014-15 dated 02/01/15). We are also thankful to the Principal and Management of PESIT-BSC, Bangalore for their kind cooperation to carry out this research work.

VI. REFERENCES

- [1]. G B. Shumaila, V. S. Lakshmi, M. Alam, A. M. Siddiqui, M. Zulfequar and M. Husain, *Current Applied Physics*, 11(2), 2010, pp. 217-222.
- [2]. Safenaz M. reda, Sheikha M, Al-Ghannam , *Advances in materials Physics and Chemistry* 2, 2012, pp. 75-81
- [3]. Z. Durmus, A. Baykal, H. Kavas, H. Sozeri, , *Physica B*, 406 , 2011, pp. 1114-1120.
- [4]. Asha, Sneh Lata Goyal, D Kumar, Shyam Kumar, N Kishore, *Ind. J. of Pure & Appl. phy*, 52, 2014 , pp.341-34.
- [5]. Y B Wankede, S B Kondawar, S R Thakare, P S More., *Adv. Mat. Lett.* 4(1), 2013, pp. 89-93.
- [6]. Syed Shahabuddin, Norazilawati Muhamad Sarih, Muhammad Afzal Kamboh, Hamid Rashidi Nodeh and Sharifah Mohamad, *Polymers*, 8, 2016, pp. 305.
- [7]. Parinitha M, A Venkateshulu, *International journal of latest research in science and Technology*, 2(1), 2013, pp. 495- 498.
- [8]. D. M. Nerkar, S. V Panse, S. P Patil, S. E Jaware and G .G Padhye, *Sensors & Transducers*, 202(7), 2016, pp. 76-82.
- [9]. R. J. Ramalingam, H. A. Al-Lohedan, T. Radhika , *Digest Journal of Nanomaterials and Biostructures*, 11(3), 2016, pp. 731-740.
- [10]. R.K. Paul, C.K.S. Pillai, *J. Appl. Polym. Sci.* 84, 2002, pp. 1438.
- [11]. K.A Vijayalakshmi, K. Vinutha, M. Revanasiddappa, S C Raghavendra, *MaterialsTechnology: Advanced performance materials*, 31(7), 2016, pp.400- 405.
- [12]. D. Rama Devi, B. Ganga Rao and K. Basavaiah, *World Journal of Pharmacy and Pharmaceutical Sciences*, 5(11), 2016, pp. 775-785.
- [13]. Siddalinga Swamy D, Raghavendra S C and Revanasiddappa M, *Materials today Proceedings Elsevier*, 5(1), 2018, pp. 1379-1386.
- [14]. Nithin, Kumara N, Siddesh Chincholia, Preran R, Hegdea, Shivagiria, S Y and Revanasiddappa, M, *Materials today Proceedings, Elsevier* ,5(1), 2018, pp.501-507.
- [15]. Vinay K, Shivakumar K and Revanasiddappa M, *International Journal of Emerging Technologies in Computational and Applied Sciences*, 21, 2017, pp. 22-26.

Vehicle Exhaust Purification by Chemical Process

Venkatesh. B.N¹, Shubham Kumar², Dr.Revanasiddappa M³, Mrs.SatyaVani N.L⁴

¹Department of Computer Science PESIT Bangalore South Campus, Bangalore, Karnataka, India

²Department of Computer Science PESIT Bangalore South Campus, Bangalore, Karnataka, India

³Department of Science and Humanities PESIT Bangalore South Campus, Bangalore, Karnataka, India

⁴Department of Science and Humanities PESIT Bangalore South Campus, Bangalore, Karnataka, India

ABSTRACT

Pollution has always been a menace to our environment. Air is the most susceptible to pollution. A major part of air pollutants consist of the exhaust of vehicles. While measures have been taken to suppress the amount of these pollutants entering the atmosphere, it is either ineffective or too expensive. An alternate solution to this problem can be the chemical purification of the exhaust gases. The setup described here has a 4-stage filtering mechanism for utmost reduction of harmful particles present in the exhaust. The first stage involves bubbling of the exhaust through water to remove any particulate matter. In the second phase, the moist gas is passed through sulphuric acid, resulting in the elimination of any bacteria and oxidation of harmful chemicals like Carbon monoxide. The third stage involves the subsequent conversion of these oxides to their respective bases with the help of sodium hydroxide. In the last step, neutralization of carbon dioxide is ensured by passing the gas through lime water. This is a cost effective solution to the increasing amount of pollutants in the atmosphere due to motor exhausts. If implemented, we can ensure a more sustainable and breathable air for the years to come.

Keywords: Environmental issues, Air pollution, Solar Energy, Chemical process.

I. INTRODUCTION

The release of **air pollutants** into the atmosphere is called air pollution. These **pollutants** mainly consists of gases or particulate matter and can they can be obtained from various sources. It occurs when harmful or excessive quantities of substances including harmful gases, particulates and biological molecules are introduced to earth's atmosphere. Carbon monoxide, sulphur dioxide, nitrogen oxides, ozone, particulate matter and lead are some of the major contributors of air pollution.

A major pollution contributor, Passenger vehicles produces significant amounts of nitrogen oxides, carbon monoxide, and other pollutant. Out of all the

major contributors Seventy-five percent of carbon monoxide is produced by the emissions of automobiles. In urban areas, harmful emissions produced from automotive are responsible for anywhere between 50 and 90 percent of **air pollution**. That's quite a lot of polluted air coming from our vehicles. By reducing vehicular emissions, we can cut down more than half of the pollutants in air.

Our implementation uses a passive and self-efficient way to reduce the emissions. Vehicular exhaust consists mainly of carbon components. Out of these Carbon dioxide, released as a consequence of fuel combustion along with water, is a passive component. However this happens only when the efficiency of the engine is 100% i.e. an ideal engine. In non-ideal

engines, however, in addition to CO_2 , active components like Carbon monoxide are released. This is due to the incomplete combustion of the fuel in the engine.

II. METHODS AND MATERIAL

For the experimental setup, the following components were used:

- Airtight containers
- Intake fan (Voltage rating=12V)
- Transmission pipe
- Solar panel (Output Voltage=12V)

The following chemicals were utilised for the purification of the exhaust gas:

- Water
- Sulphuric acid- H_2SO_4 (98%)
- Sodium Hydroxide AR grade - NaOH (5%)
- Lime Water- CaOH (5%)

III. DISCUSSION

Initially, the exhaust is taken through the intake fan. The exhaust is then passed through a 4-stage purification process. The processes are as follows.

A. Stage-1

The raw exhaust is taken through the transmission pipe submerged in water. This exhaust is bubbled through water. Due to this, particulate matter present in the exhaust is removed and these form a sediment.



Figure 1. The air is sucked through intake fan.

B. Stage-2

The particulate-free gas is then passed through concentrated sulphuric acid. In this stage microorganisms and other harmful gas molecules are removed. In addition to this sulphuric acid also removes the moisture content present in the gas.



Figure 2. The intake air is passed through water and H_2SO_4 .

C. Stage-3

The dry gas is then passed through Sodium Hydroxide (NaOH). NaOH is a strong base which facilitates conversion of carbon molecules into their respective carbonates. These carbonates thus formed are salts and are stable.



Figure 3.This air is then bubbled through NaOH.

D. Stage-4

The gas is then bubbled through Lime Water (CaOH) which turns milky indicating that Carbon Dioxide (CO_2) is converted into Calcium Carbonate (CaCO_3). Thus the exhaust is purified by 4-stage chemical process.



Figure 4.This air is finally passed through lime water which turns milky and the bag which was filled with air is completely transparent.

IV. OBSERVATION

For this experiment the fumes produced by burning paper was passed through the setup.

A transparent plastic bag was attached to the outlet. It was observed that the gas filling the bag was completely transparent unlike the blackish fumes of the burnt paper.



Figure 5.Experiment setup.

V. CONCLUSION

This experiment demonstrates the purification of exhaust by chemical process. The transparent air filled in the bag indicates that the impure air is purified to a high degree. Hence it can be inferred that the exhaust gas of vehicles can be purified in a cost effective and efficient way through chemicals and this method can be used to purify the air to high degree.

VI. ACKNOWLEDGEMENT

We would like to thank Dr.Revanasiddappa M, Professor in the Department of Engineering Chemistry, PESIT-Bangalore South Campus, Bangalore, and Mrs.SatyaVani N.L Professor in the Department of Engineering Mathematics, PESIT-Bangalore South Campus, Bangalore, who helped us in the paper. We are very grateful to them for their precious time spent on us. Also would like to thank Mrs.SatyaVani N.L for giving us an opportunity to participate.

VII. REFERENCES

- [1]. <http://www.iea.org/publications/freepublications/publication/WorldEnergyOutlookSpecialReport2016EnergyandAirPollution.pdf>
- [2]. "Air Pollution Causes, Effects, and Solutions". National Geographic. 9 October 2016.
- [3]. Gehring, U.; Wijga, A. H.; Brauer, M.; Fischer, P.; de Jongste, J. C.; Kerkhof, M.; Brunekreef, B. (2010). "Traffic-related air pollution and the development of asthma and allergies during the first 8 years of life". *American Journal of Respiratory and Critical Care Medicine*. 181 (6): 596–603. doi:10.1164/rccm.200906-0858OC.

3D Vibration Monitoring Sensor for Automobiles Using Internet of Things (IoT)

Kanishkar P^{*1}, Senthil Kumar S A², Ketan Pandit³, Ganapathi Bhat⁴

^{*1}Department of Information Science and Engineering, PESIT South Campus, Bangalore, Karnataka, India

²Department of Computer Science and Engineering, PESIT South Campus, Bangalore, Karnataka, India

³Department of Mechanical Engineering, PESIT South Campus, Bangalore, Karnataka, India

⁴Department of Information Science and Engineering, PESIT South Campus, Bangalore, Karnataka, India

ABSTRACT

Internet of Things (IoT) is considered to be the backbone of forth industrial revolution. It seeks to create a network of physical objects/processes, omnipresent sensors and computer systems, so as to provide a smart solution to day to day problems by bridging gap between real and information world. Reducing of mechanical vibrations and shocks generated is one of the major challenges in automobile industry. Whole-body vibrations (WBV) are the most serious of all the vibrations. Continuous exposure to these vibrations not only adversely effects human health, but also decreases durability and fuel economy of automobiles. Longer the exposure, greater will be the effect on health. Musculoskeletal disorders (WMSD) like Low Back Pain (LBP), fatigue and numbness of muscles, joint pain etc., are some of the disorders caused by these vibrations. To avoid long-term health risks associated with WBV, vibrations generated in automobiles need to be accurately measured and analyzed. The aim of this paper is to develop a cost effective easy and user friendly sensor for the purpose of frequent monitoring of the excessive vibrations produced in vehicles. This project consists of active experiments conducted on selected structural elements of bike, car and bus. The observations were made in all the three orthogonal axes for different constant rotational velocity (gears), using an arduino based accelerometer.

Keywords: Internet of Things, Whole-body vibrations, musculoskeletal disorders, Low Back Pain, cost effective, user friendly, constant rotational velocity, arduino, accelerometer.

I. INTRODUCTION

The Internet of Things (IoT) is an emerging technology whose purpose is to overcome the gap between objects in the physical world and their representation in information systems i.e., realizing a world where in physical objects are seamlessly integrated into the information network [1]. Facilitating these objects with the possibility to communicate with each other and to analyse the information recorded from the surroundings would

generate a possibility of wide range of applications [2, 3]. One such application is monitoring of mechanical vibrations produced in automobiles. These vibrations are produced due to a number of different sources like engine (incomplete combustion, knocking etc.) [4], roughness of road surfaces, gear box (during transmission), tires etc. [5] Periodic monitoring and attempts to decrease these vibrations are very vital, given its adverse effects on heath of passenger/driver, fuel economy and vehicular structure. Whole-body vibrations occur when the human body is supported

on a surface which is continuously vibrating. As a mechanical and biological system, prolonged exposure to WBV leads to musculoskeletal disorders like low back pain [5, 6], spinal degeneration, muscle fatigue, joint pain, physiological effects such as increase in heart rate, increase in muscle tension, gastrointestinal issues, respiratory disorders, reproductive organ damage etc. [7-10]

The prediction of discomfort caused by WBV is very essential in automobile industry, so as to design a customer friendly vehicles. The injury potential of vibrations is expressed in terms of an average measure of the acceleration (R.M.S. value) [11]. According to ISO standard for a comfortable ride, the rms acceleration must be less than 0.315 m/s^2 and the vibration is very uncomfortable if it's more than 1.25 m/s^2 . [12]

II. DESIGN OF SENSOR

The sensor (figure 1) designed consists of ADXL 335 triple axis accelerometer (bandwidth: 0.5 to 1600Hz for x and y axis and 0.5 to 550 Hz for z axis), arduino UNO board (ATmega328 microcontroller) and arduino IDE (programming software which interprets code in SKETCH language). Accelerometer was fixed on to positioning pin (figure 3), to be placed on vibrating surface under observation. The output set in serial monitor is at

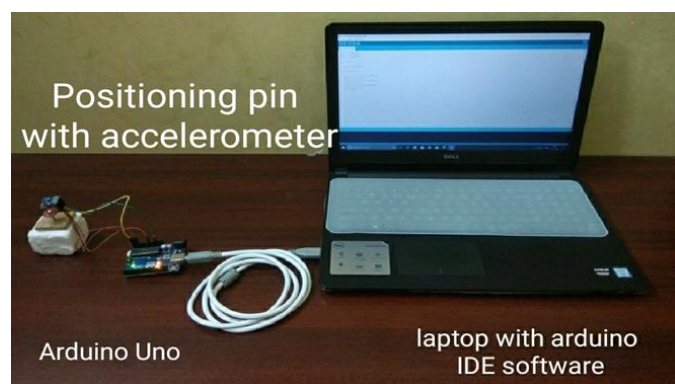


Figure 1. Vibration monitoring system setup

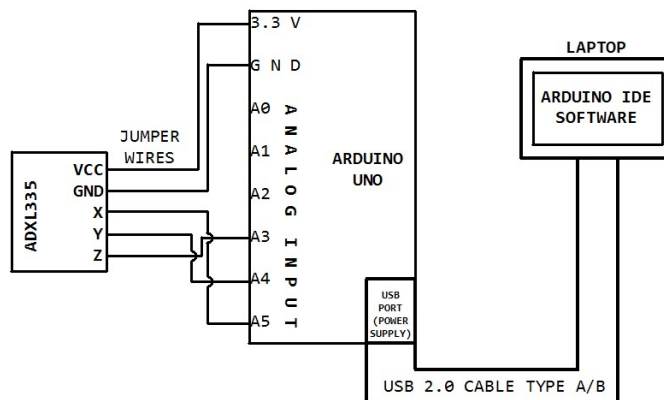


Figure 2. Circuit diagram of the sensor system

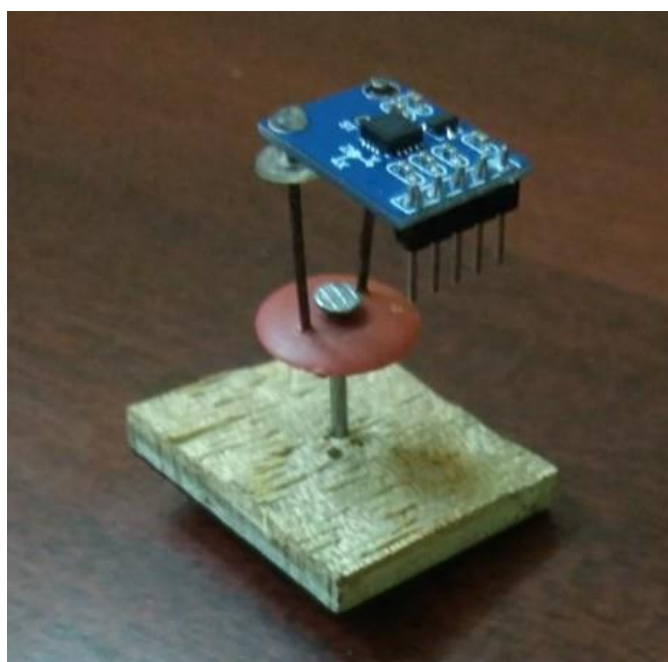


Figure 3. Positioning pin with accelerometer fixed on to it

III. INSTALLATION AND TESTING OF SENOR

A. Monitoring of vibrations in bike

Accelerometer is mounted on the positioning pin which is in turn fixed on to the casing of the gear box adjacent to the engine (94.5 cc) of a bike (Figure 4). Observations were made during neutral state, first gear, second gear, third gear and fourth gear. Corresponding graphs were generated with the help of arduino IDE software.

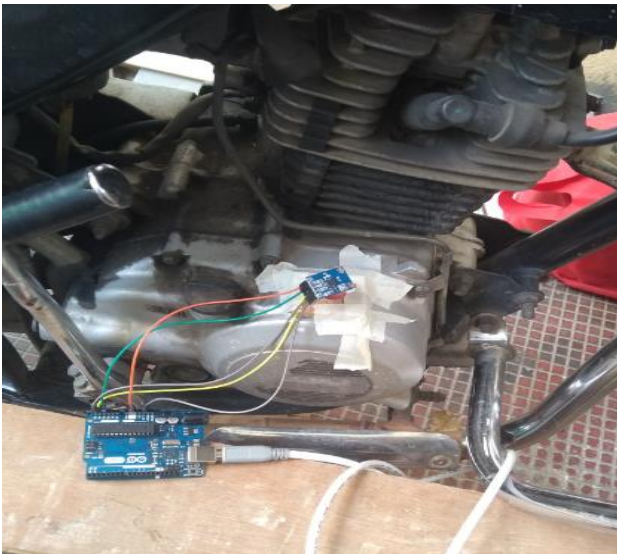


Figure 4.Installation of the sensor to the bike under observation.

B. Monitoring of vibrations in car

Accelerometer is mounted on the positioning pin with thermocol/polystyrene base (functioning as a shock absorber to prevent damage to the sensor) which is fixed onto the casing of the engine (Figure 5).

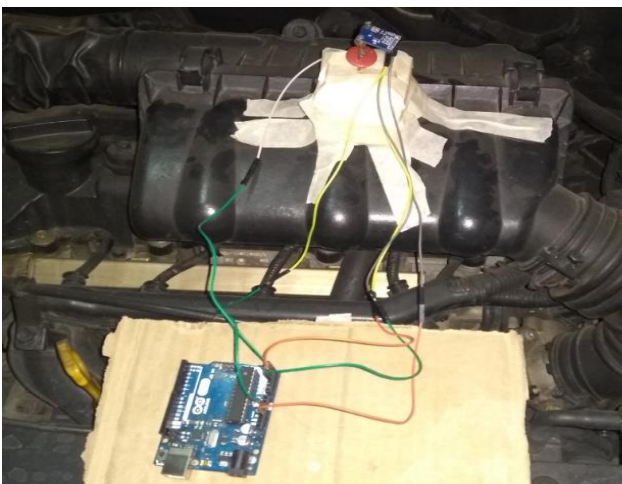


Figure 5.Installation of the sensor to the car under observation.

Observations were made during neutral state with and without acceleration. Graphs were plotted in similar manner as that of the bike.

C. Monitoring of vibrations in bus

The sensor system identical to that of the car was fixed to record observations at two different locations that

generate most of the vibrations, namely:- tires and the engine (diesel) as shown in Figure 6 and 7 respectively. Tires are complex composites made of rubber, steel and polymers, which absorb and transmit forces generated by the vehicle and the road surface [14]. Graphs were generated using the same procedure.

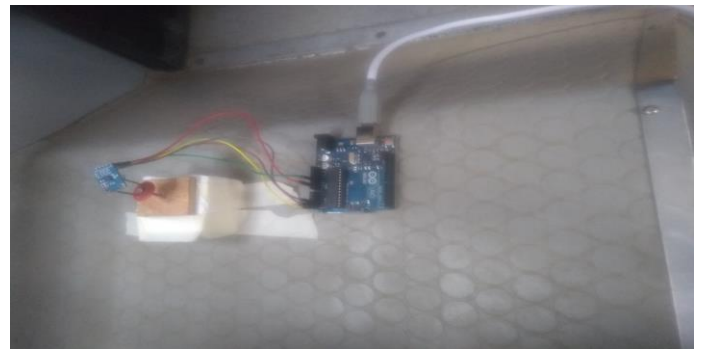


Figure 6. Installation of the sensor above the tire of the bus

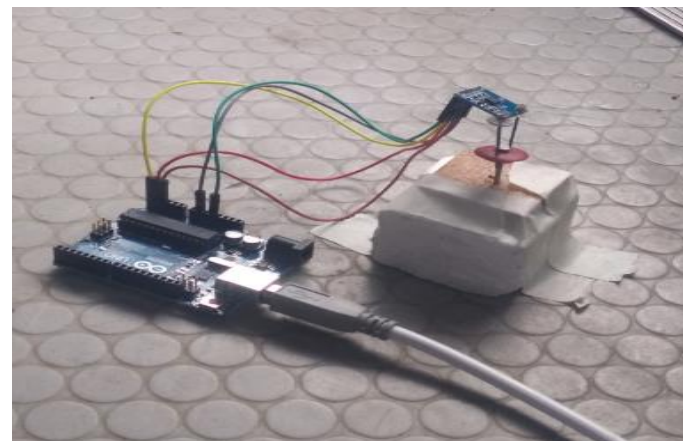


Figure 7. Installation of the sensor adjacent to the engine of the bus

IV. RESULTS AND DISCUSSION

Graphs were plotted, taking the time taken for code to processes two consecutive output statements along x axis and serial data (data from accelerometer along x, y and z axis) along y axis using arduino IDE. The engine of the vehicles are accelerated periodically. X axis is represented by purple curve, y axis by yellow curve and z axis by blue curve. (Special filters were used to improve quality of the graphs obtained for inclusion in the paper.)

i. Output of vibrational analysis of the bike

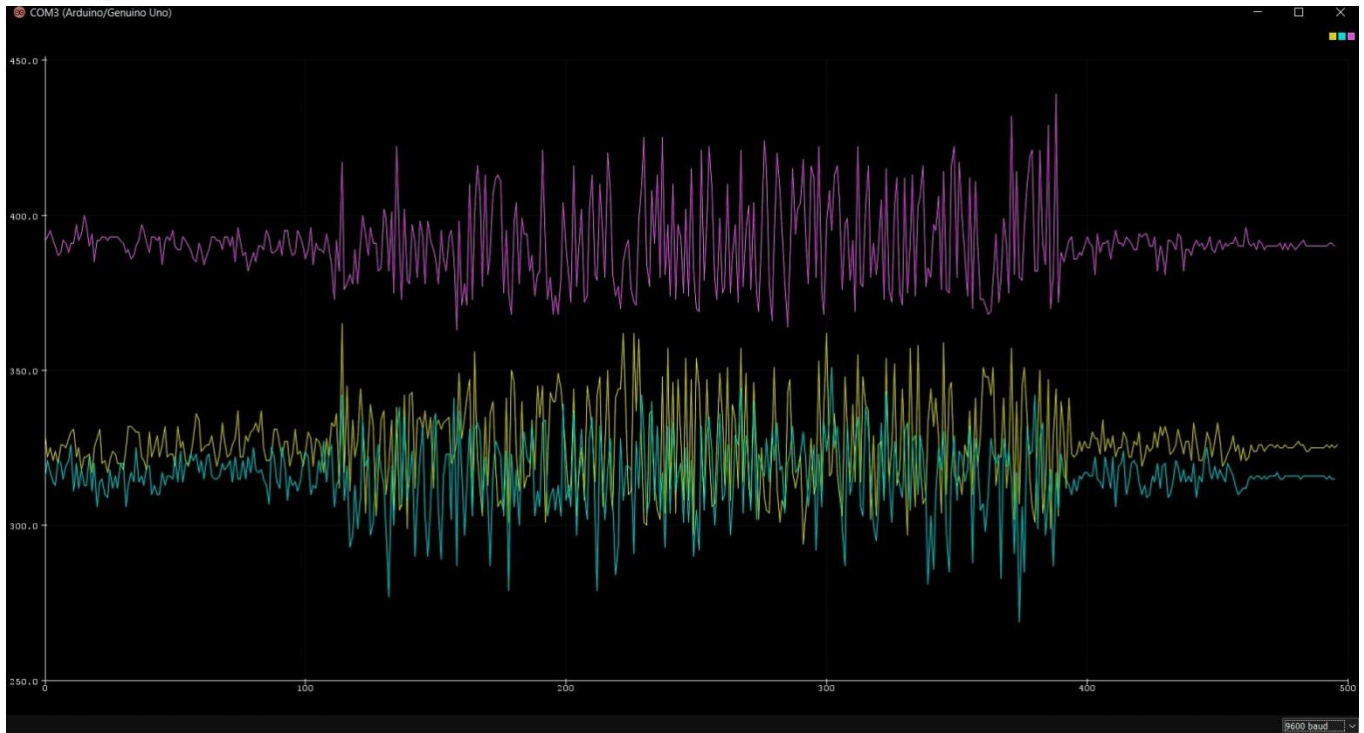


Figure 8. Monitoring of the bike in neutral state

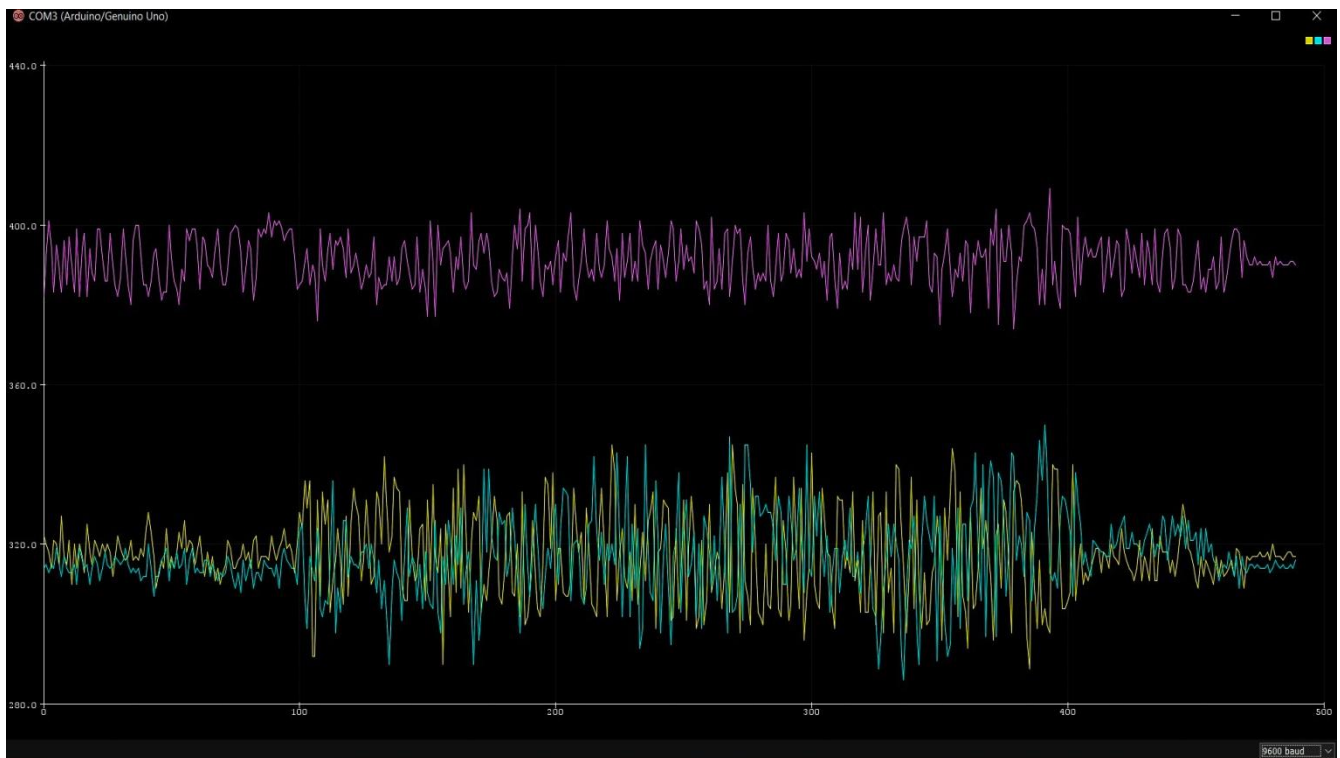


Figure 9. Monitoring of the bike in first gear

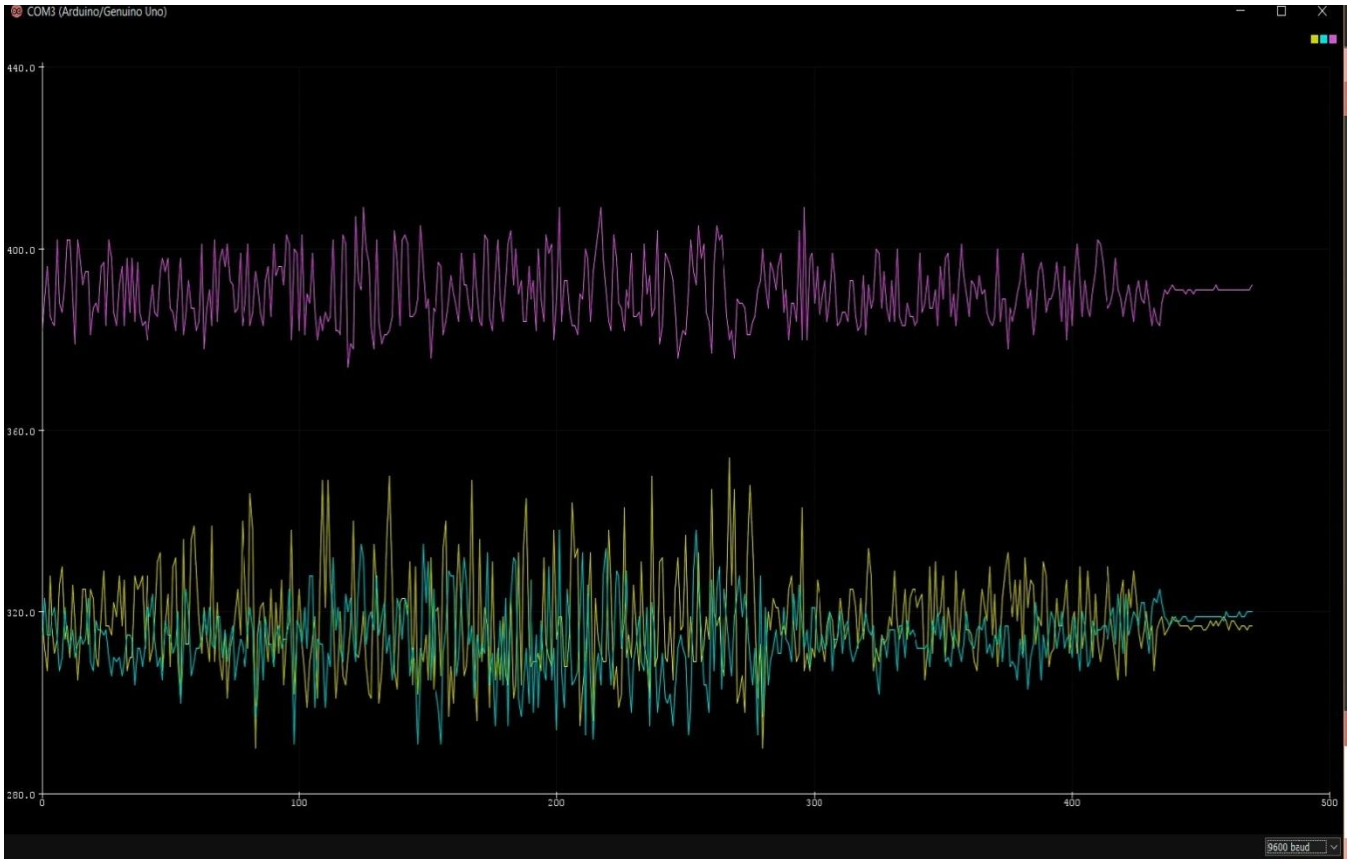


Figure 10. Monitoring of the bike in second gear

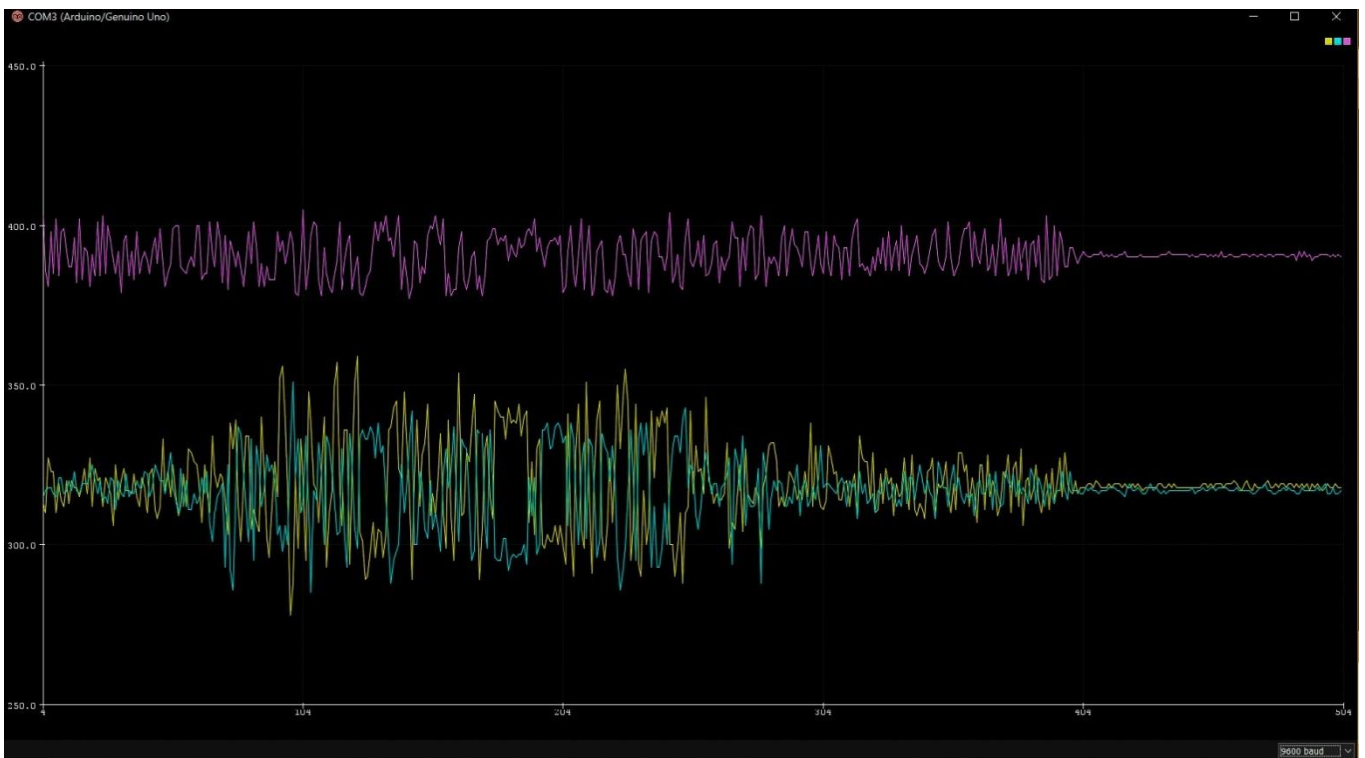


Figure 11. Monitoring of the bike in third gear

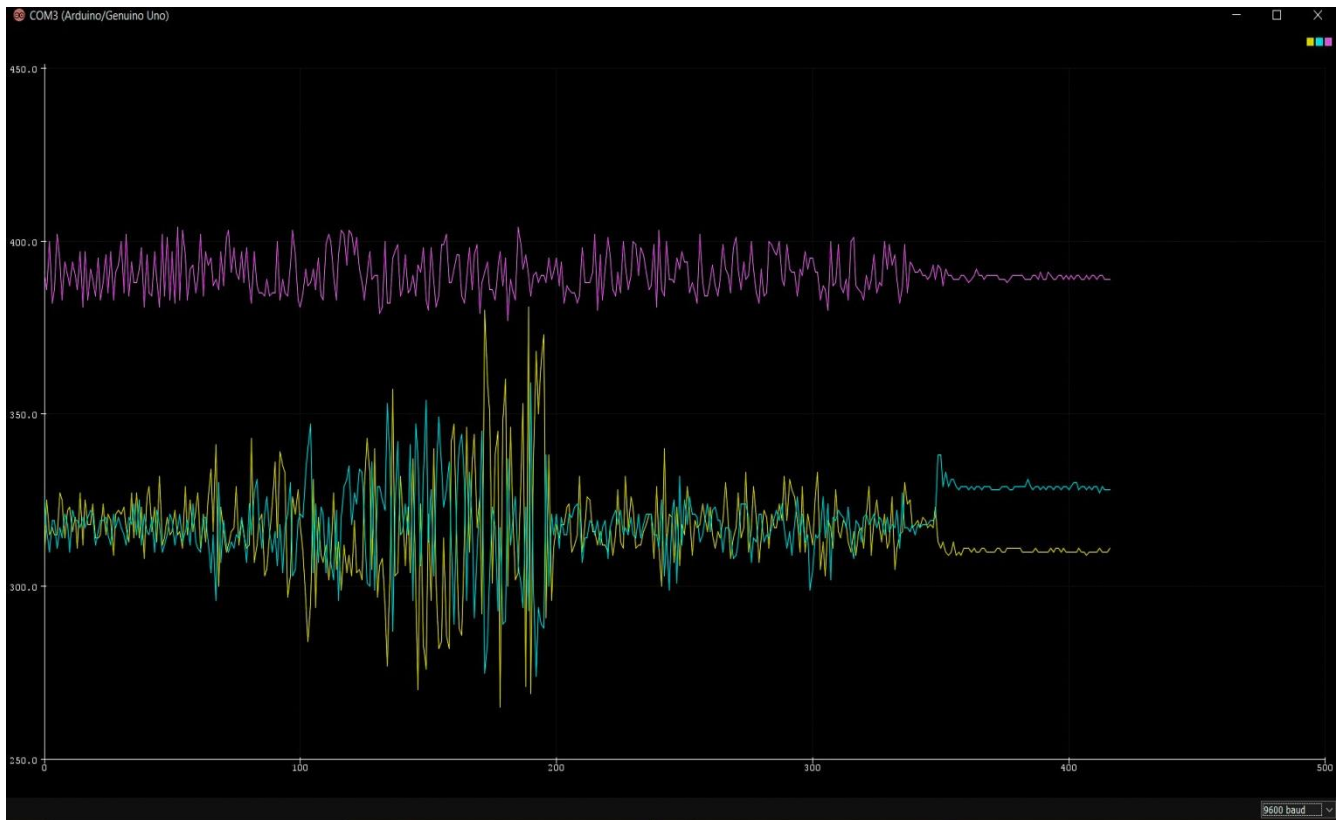


Figure 12. Monitoring of the bike in forth gear

ii. Output of vibrational analysis of the car

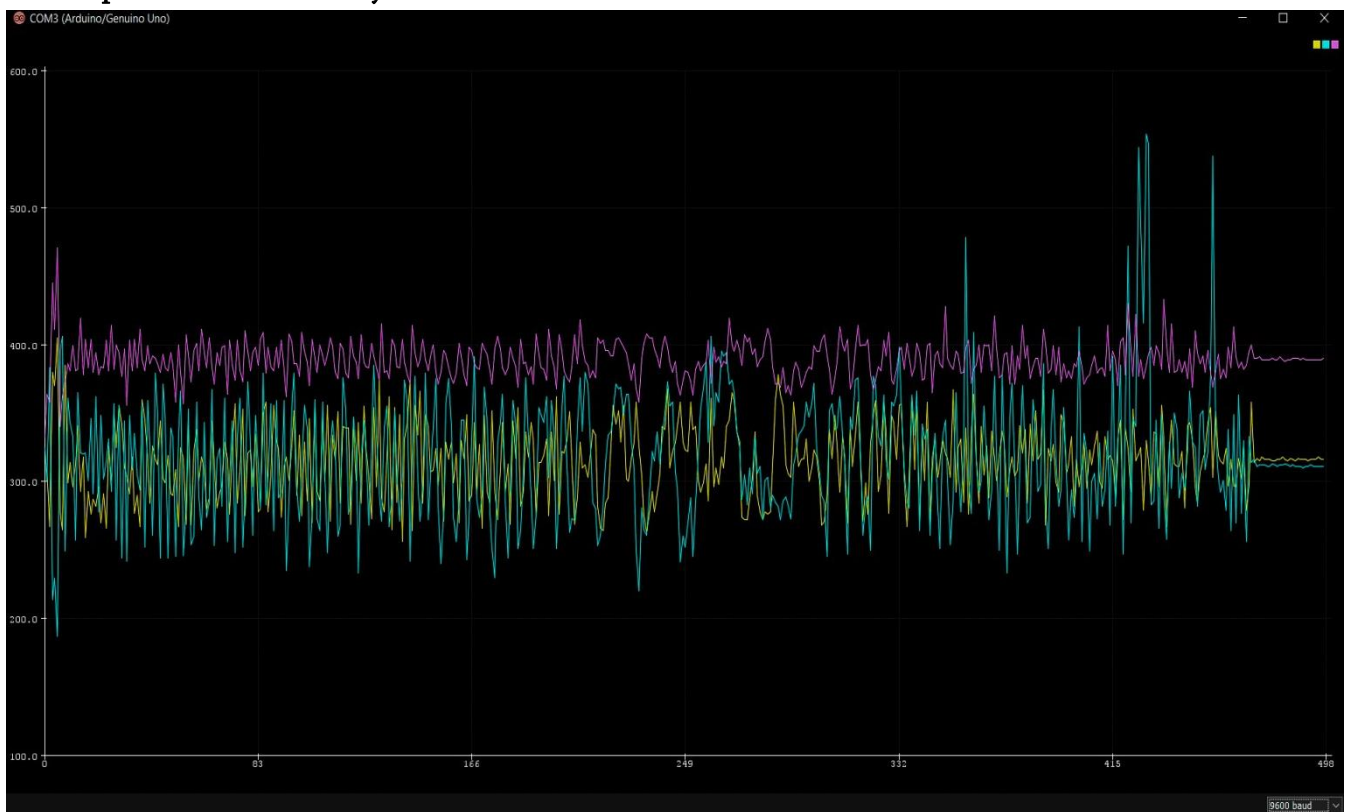


Figure 13. Monitoring of the car in neutral state without being accelerated

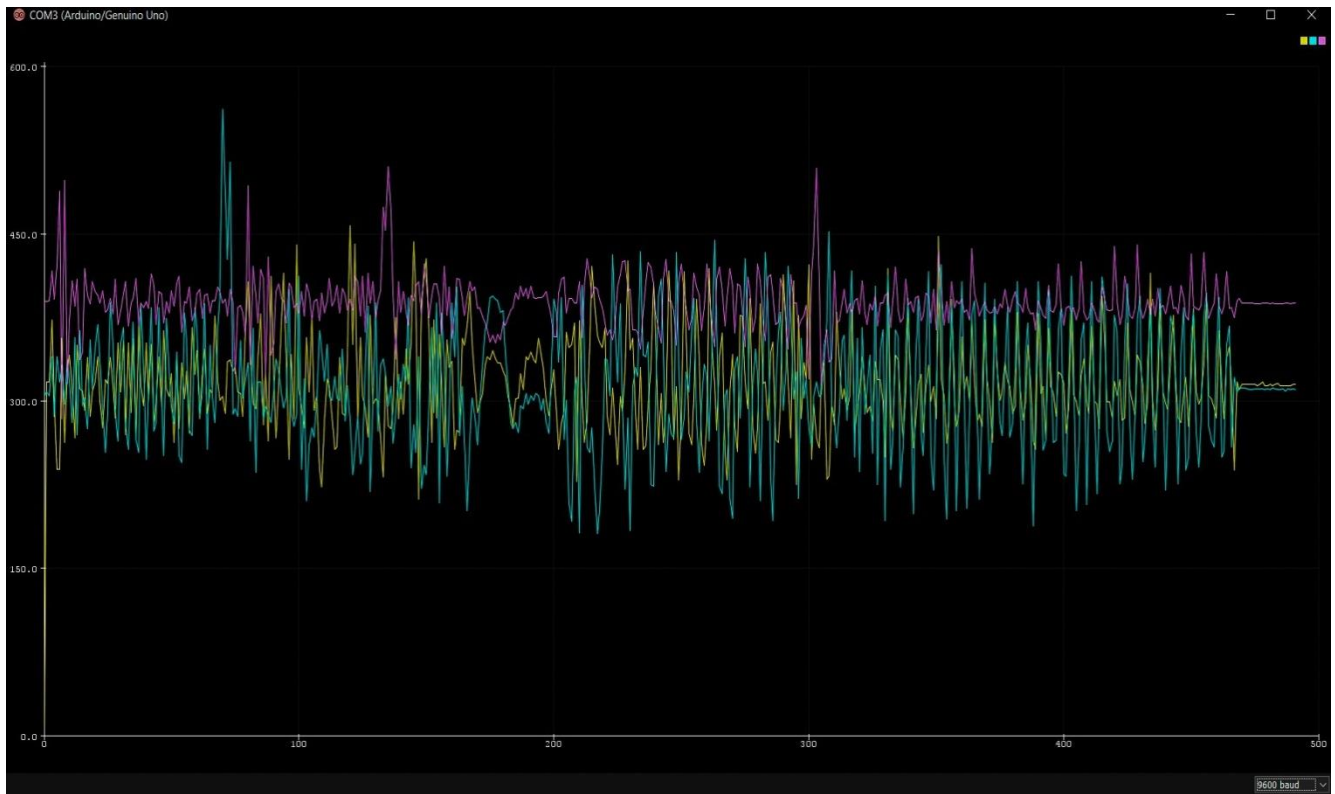


Figure 14. Monitoring of the car in neutral state while being accelerated

ii. Output of vibrational analysis of the bus

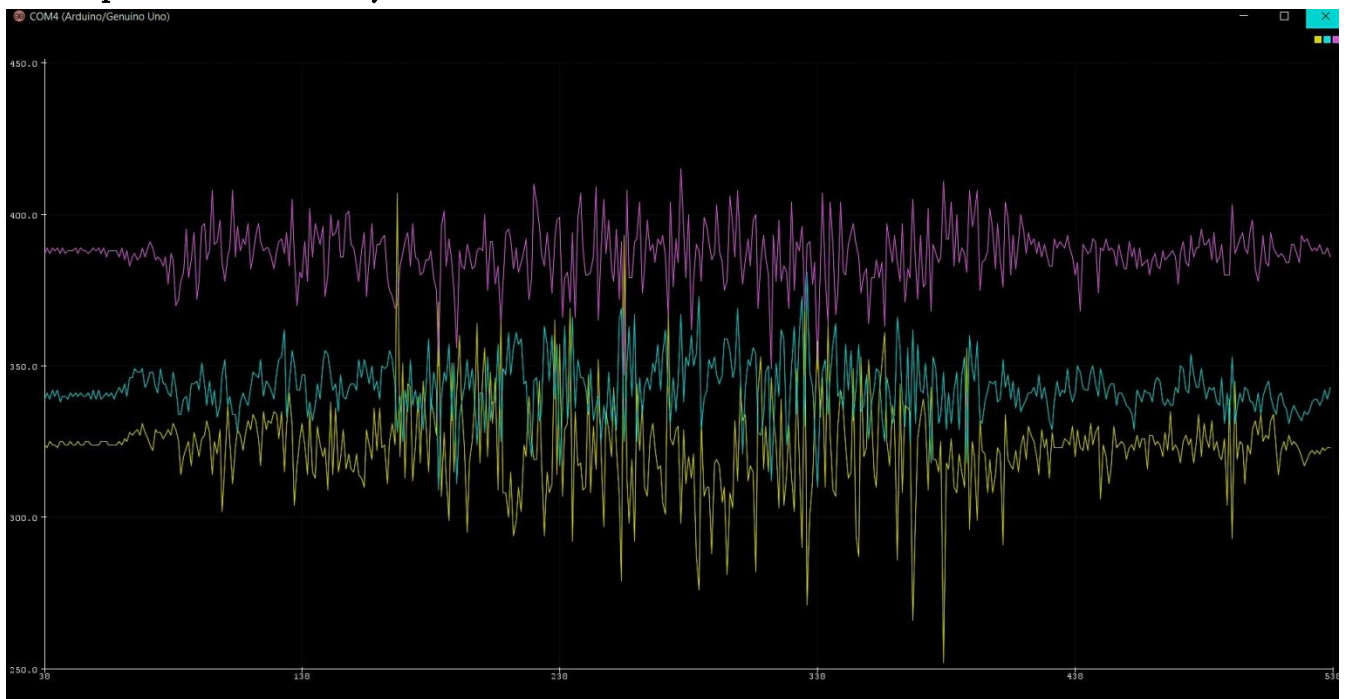


Figure 15. Monitoring of the bus with sensor positioned above one its tire

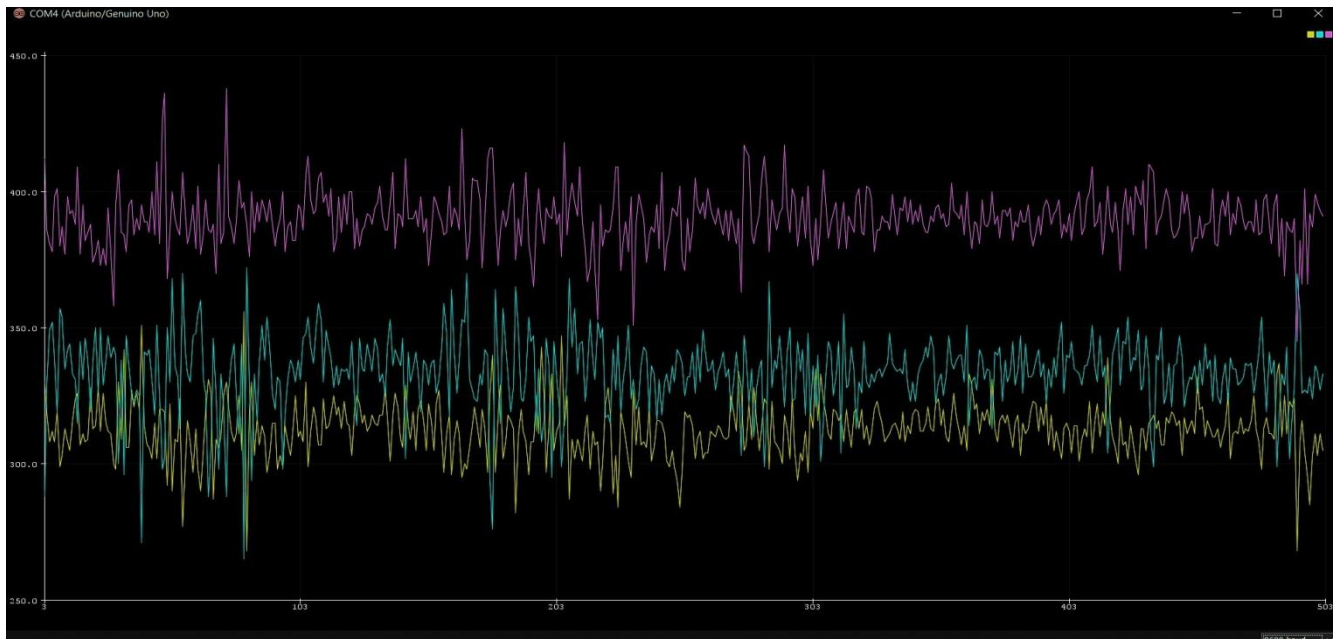


Figure 16. Monitoring of the bus with sensor positioned above its engine

V. ADVANTAGES OVER CONVENTIONAL SYSTEMS

Commercially used vibrational monitoring systems work on different techniques like eddy currents, piezoelectric effect, photonics, capacitive sensing etc. These systems are very expensive and need skilled operator to use them. However, arduino based sensor provides a versatile and an inexpensive cross-platform (compatible with multiple operating systems), with an open source and extensible software and hardware components adding to its credentials. Also, arduino has a very low power and maintenance requirements.

VI. CONCLUSION

Thus, monitoring of vibrations were made in vicinity of key structural components/sources of vibrations for various automobiles as required by this project. Unsteady fluctuations in vibrations generated were recorded over a given time interval by developing a cost effective and user friendly arduino based sensor.

VII. REFERENCES

- [1]. Rolf H. Weber, Romana Weber, Internet of Things, springer
- [2]. Luigi Atzori, Antonio Iera, Giacomo Morabito, The Internet of Things: A survey Elsevier
- [3]. J Gubbi, Rajkumar B, Slaven M, Marimuthu P, Internet of Things (IoT): A Vision, Architectural Elements, and Future Directions
- [4]. Katu U.S., Desavale R.G. and Kanai R.A, Effect Of Vehicle Vibration On Human Body-RIT
- [5]. A Rozali, K Rampal, M T Shamsul B, M S Sherina, S Shamsul A Khairuddin, A Sulaiman, Low Back Pain and Association with Whole Body Vibration Among Military Armoured Vehicle Drivers in Malaysia
- [6]. Garg, and J. S. Moore, 1992. "Epidemiology of low back pain in industry", *Occup. Med.*, 7: 593-60.
- [7]. International Organization for Standardization, 2005, Human response to vibration- measuring instrumentation. International Standard, ISO 8041

- [8]. Griffin, M.J., 1990, Handbook of human vibration. Academic Press, London, ISBN: 0-12-303040-4.
- [9]. Zhen Zhou, Michael J. Griffin, Response of the seated human body to whole body vertical vibration: discomfort caused by mechanical shocks.
- [10]. Review of methods for evaluating human exposure to whole-body vibration Appendix W4A to Final Report May 2001
- [11]. Massimo Bovenzi, Carel Hulshof Risks of Occupational Vibration Exposures, Annex 21 to Final Technical Report
- [12]. Rajesh Kumar R, M.N. Vinod kumar A review on WBV and its effects in automobile drivers IOSR Journal of Mechanical and Civil Engineering (IOSR-JMCE) e-ISSN: 2278-1684.
- [13]. Min-Soo, Takabumi F, Tae-gu K, Setsuo M, Health Risk Evaluation of Whole-body Vibration by ISO 2631-5 & ISO 2631-1 for Operators of Agricultural Tractors and Recreational Vehicles.
- [14]. Ketan Pandit, Karthik R, Preeta Sharan & Anup Upadhyaya, MOEMS based sensor for tire carcass deflection monitoring in automobile using photonic crystals

IOT Based Automatic Crack Analysis for Structures Using Vibrations

Niraj Anil Babar, Noel Alben, Mohamad Amjad Arhaan

Department of ECE, PES Institute of Technology- Bangalore South Campus, Bangalore, Karnataka, India

ABSTRACT

This paper presents a mechanism based on IOT-automation that can detect cracks in structures (Living Spaces and Flyovers). The system gathers information from the magnitude of vibrations produced by the structure using vibration sensors which relay information to a database for further data collection, analysis, and future reference. After the gathered data is analyzed, the concerned authorities are notified about the condition of the structure.

Keywords: IOT, Vibration Sensors, Database.

I. INTRODUCTION

The design of a structure is related to the type and amount of load it is meant to carry.

Under static load conditions, natural vibrations of the structure act as a restoring force to keep the load in place. Under optimal conditions, these vibrations are low in magnitude, but are affected by various natural phenomena and structural defects. Cracks are usually the first visual signs of structural defect. Cracks develop whenever stress in a particular component of the structure exceeds the strength of that component. Since cracks are sometimes not visible on the exterior of the structure,

maintenance fails to record them, leading to a structural failure as the cracks grow undetected in size and number. The development of cracks directly relates to the magnitude of vibration that a building experiences in static conditions. There is a lack of technology implemented for vibrational analysis to detect cracks in structures. Our system collects the data from these vibrations, and using a predetermined cut-off value based on the type of structure and load it undertakes, a prompt information report will be

sent to the maintenance department. Inbuilt buzzers and LEDs will determine the location of the detected vibrational anomaly and subsequently, the location of the crack. Further, our system incorporates the concept of Internet Of Things technology to create a database for all structures making use of this system, allowing for future reference and accessibility of maintenance information.

II. WORKING AND CONSTRUCTION

Analysis of the natural vibration modes of the structure can be used to understand the behavior of the structure.

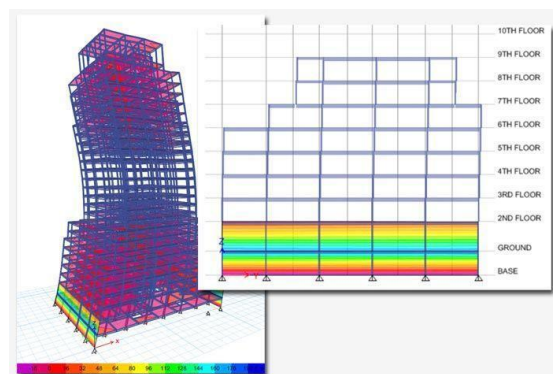


Figure 1. Eigen-Vector modal analysis which finds the natural vibration modes of the structure.

For the prototype our team constructed a miniature bridge of moderate structural strength. Connected Piezo Electric Sensors (a device that uses the piezoelectric effect, to measure changes in pressure, acceleration, temperature, strain, or force by converting them to an electrical charge.) which were used as vibration sensors for the experiment. Due to the application of a load, the magnitude of vibration in the structure changed, causing a change in pressure. An electric charge was then generated by the sensors, which was in turn relayed to an externally powered Arduino. Using Arduino IDE codes, we converted this signal into analytical data and it provided graphical representation of the recorded vibration. The graph is a representation of voltage generated by the piezo electric sensor v/s time. LEDs and Buzzers were connected to the Setup, which enhanced the effectiveness of maintenance and repair with accurate location of the anomaly. Further, we developed a mobile application which received a signal to send a text message to the concerned authorities when the magnitude of vibration crosses the predetermined threshold value. The message is sent to ensure that the authorities give proper attention proper attention to the condition of the structure.



Figure 2.1.The prototype model, with RC car used as Load.

The bridge was constructed in three phases.

1. 0% deformity was the first phase, representing ideal condition with almost no cracks.



Figure 2.2: Phase 2, with 30% deformity. The presence of cracks is detected with the signal sent by the Piezo Electric Sensor. The Vibration travels to Phase 3(70% deformity) through the body of the structure. At Phase 3 The presence of increased deformity and cracks is detected even before load passes through the section. (As shown in **Figure 2.3**)



Figure 2.3.Phase 3, with 70% Deformity and cracks. The LED's light up and the Buzzer Signals Location of the vibrational Anomaly.

Once the maintenance crew has access to the aforementioned site, they can connect to the system easily via Bluetooth using the mobile app to receive accurate statistical data with all the generated values.

Components Used:

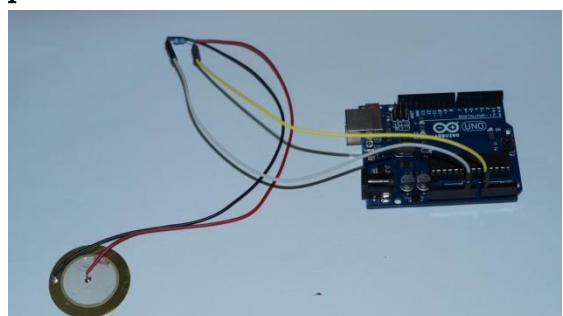


Figure 2.5.The Arduino (Externally Powered) with the Piezo Electric Sensor.

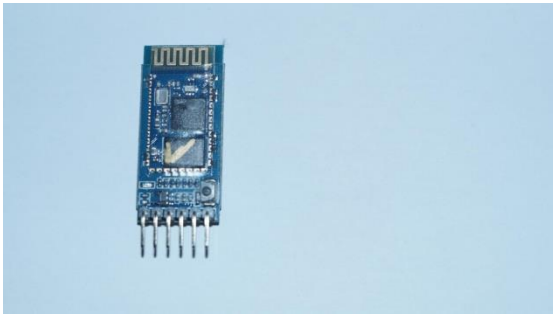


Figure 2.6.The Bluetooth Module

IV. CONCLUSION

The design of this system aims to ensure coordinated and timely maintenance of structures with precise data collection and transmission for future reference. The database collected from multiple systems can be accessed and used for cost effective and efficient maintenance and repair of the structures. With further developments this system could be further improved to be self sustaining, wherein the Piezo electric sensors themselves generate the power required to run the Arduinos and the entire setup.

A bread board was used to make all the connections, along with LEDs and Buzzers.

III. RESULTS

The experiment proved successful with expected values at each phase. At peak values a message was sent to one of our phones.

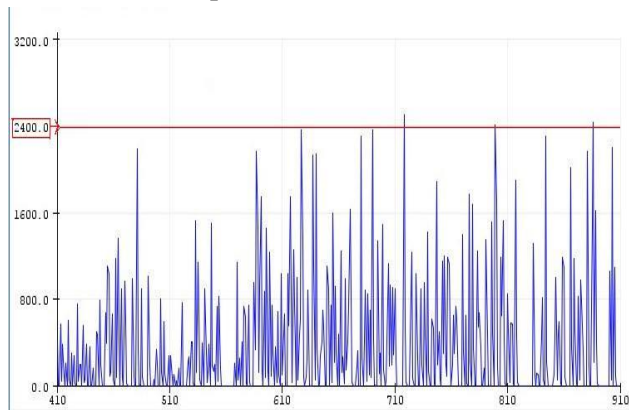


Figure 2.4.The data is presented in a graphical format where the cut-off value is shown in red. At this point, a text message will be sent to authorities regarding the condition of the structure.



Figure 2.5.Text message received after experiment.

Access to all the data was made through simple Bluetooth connection with the app.

V. ACKNOWLEDGEMENT

We would like to thank our institute, PESIT-BSC, for giving us an environment and the opportunity to work on this project. We give our special thanks to Dr.Revanasiddappa, who was our mentor and graciously lent his valuable time, towards the cause of our project.

VI. REFERENCES

- [1]. <https://cic.com.vn/en/san-pham/etabs-2013-integrated-analysis-design-and-drafting-building-systems>
- [2]. <https://www.arduino.cc/en/Tutorial/KnockSensor>

Smart Home Security -Intrusion Detection System”

Security for Home

Pooja Balageri V, Dr. Sarasvathi V

Department of CSE,PESIT-BSC Bangalore, Karnataka, India

ABSTRACT

The “Internet of things” (IOT), is a system of interconnected, interrelated computing devices, digital and mechanical machines, physical objects, moving objects, with each object having unique IP address assigned to it, it plays an influential role in almost all the fields one of them is security, an important prospect of security is providing a security for home. Home Intrusion Detection [10] is IOT conceptualization which provides a security for home. The paper entitled “Smart Home Security-intrusion detection system” is a IOT based concept by the name itself witnesses that it is providing a security for home using the sensors and actuators. Passive Infrared Sensor (PIR) sensors are used to detect the motion of moving objects and magnetic door sensors are used to detect the state of door, Raspberry PI 3 model B is used as an interfacing, computing device, buzzer and Light Emitting Diode (Led) is used as actuators. The proposed intrusion detection system sends a Text SMS to owner and activates the Buzzer, Led at home.

Keywords: Raspberry Pi, twilio Api, sensors, actutatos, pir sensor.

I. INTRODUCTION

IoT is an emerging concept it has a simmering effect in most of the fields such as home automation, smart city, smart manufacturing, Health care, Automotive, wearables and one of the most important fields is security. An important prospect of security is providing a security for home. Security is degree of opposition, protection from harmful activity, or a state of feeling stable. From earlier to till now the security is important aspect in almost all the fields few of them are communication security, computer security, application security, information security, home security, physical security. Our intrusion detection system plays a valuable role in protection of home from the third person or the intruder. Our proposed system provides a security for the home without always keeping eye on home all the time.

The security plays an important role in layman’s life. Providing a security for the homes is the major

concern now-a-days. Keeping an eye on the home all the time is impossible and it may sometime be more expensive. In case of big Buildings and bungalow it becomes difficult to keep an eye on every area of the property to have a look at it physically by a single person. it easy to fool the person keeping an eye on home easily.

The proposed system provides a security for the home with a less expenses using the Raspberry PI as the main component, which acts as a physical interface between the physical environment and the computer.

II. REVIEW OF LITERATURE

In the field of IOT [10] many proficient has contributed their knowledge, mainly in the field of home introduction detection. Many have worked and explored about the providing a security for the home using the concept of IOT. The many sensors can be used to provide a protection for the home from the intruder some of them are PIR sensor [1] which senses

the motion of the moving object, Magnetic door sensor [2] senses the door state, Raspberry PI camera module [3] which captures the image of intruder.

HIVE: Home Automation System for Intrusion Detection [4] which uses the ZigBee sensors and actuators and also used Firebase for services such as a cloud database and user authentication. This system can enhance security and safety for home. Smart home automation system for intrusion detection [5] provides an implementation of smart home automation system along with the intrusion detection to minimize the damages for the home. Home Monitoring and Security system [6] which gives the implementation of PIR sensor, temperature sensor, humidity sensor to measure and detect the motion of the intruder which helps in making home secure with less expensive sensors.

PIR-sensor based human motion event classification [7], the modified passive infrared radiation sensor is used to detect the motion and based on motion detected the classification is done. Active Compressive Sensing via Pyroelectric Infrared Sensor for Human Situation Recognition [8], the design and implementation of the PIR sensor is demonstrated in this paper

III. PROPOSED SYSTEM

A. System Architecture:

The architecture shown in figure 1 is the architecture of the proposed intrusion detection system.

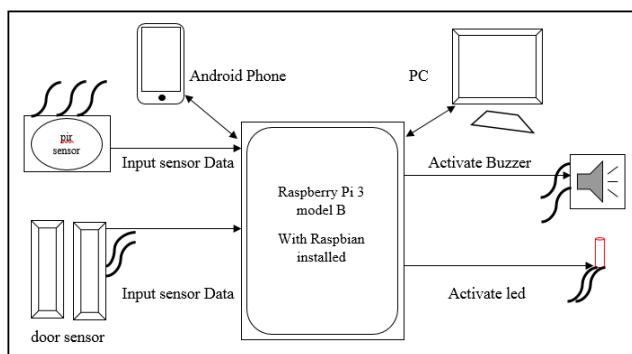


Figure 1. Architecture of Intrusion detection system

The main component in the proposed system is the Raspberry PI which is the interface between the physical environment and the computing environment. Here in this paper we are using Raspberry PI 3 model B along with the SD card containing the installed RaspbianOs it contains inbuilt python packages which provides a basics for writing code to control the sensors and actuators.

The Android phone can be used to login to Raspberry PI using Raspberry PI's dynamic IP address and control the Raspberry PI using Android phone. The commands are given from phone which is in the same network as the Raspberry PI.

The PIR sensors are used to detect the motion of the object moving in front of it and a pair of door sensors is used which detects the state of door and both these sensors send the input information to the Raspberry PI to which they are connected. The Raspberry PI activates the Buzzer and a led based on the input given by the input sensors. If motion is detected then it turns on led and buzzer indicating that someone is moving around home. If the one magnet is moved away from the other then the Raspberry PI activates the led and buzzer indicating that door is open.

The Raspberry PI uses twilio API to send the alert text SMS to the owner person. When the motion is detected the it sends the alert message to owner. When door is left open then the door sensor senses it and sends the signals to the Raspberry PI which in turn sends the text message to authorized remote owner.

IV. IMPLEMENTATION DETAILS

The following are the components used in this implementation of the Home intrusion detection system, Hardware Components are Raspberry PI 3 model B, PIR sensor, T-SEN-DR-003-N/C Magnetic Door sensor, 5mm Red Led, HXD Buzzer Software components are NOOBS (Raspbian), VNC viewer,

Advanced IP Scanner, Android Application such as Network Scanner and Mobile SSH. Twilio API for text messages, Programming language used is Python

A. Raspberry PI 3 model B: Raspberry PI 3 [8] is the third-generation Raspberry PI. It has many features such as A1.2GHz CPU, 64-bit quad-core ARMv8 processor, 802.11n wireless LAN, Bluetooth of version 4.1 and has BLE (Bluetooth Low Energy). The Raspberry PI 3 model B has 4 USB ports for connecting external devices such as keyboard, mouse etc, and one full HDMI port for connecting monitor to Raspberry PI, RAM is 1GB, it has one ethernet RJ45 port for network connectivity, it has a 1 camera interface and a display interface, it also has a 40 GPIO Pins (General Purpose Input Output Pins) for connecting various sensors and actuators. it provides a slot for placing a SD card in which the Raspbian OS is been installed.



Figure 2.Raspberry PI 3 model B outlook

The figure 3 is the Pin diagram of Raspberry PI 40 GPIO Pins.

The Pins are normally grouped as:

- ✓ GND-for ground connection.
- ✓ GPIO-General Purpose input output Pin.
- ✓ 3.3V- 3.3 volts power supply
- ✓ 5V- 5 Volts power supply
- ✓ DNC- ID_SD (I2C EEPROM)

	Pin No.		
3.3V	1	2	5V
GPIO2	3	4	5V
GPIO3	5	6	GND
GPIO4	7	8	GPIO14
GND	9	10	GPIO15
GPIO17	11	12	GPIO18
GPIO27	13	14	GND
GPIO22	15	16	GPIO23
3.3V	17	18	GPIO24
GPIO10	19	20	GND
GPIO9	21	22	GPIO25
GPIO11	23	24	GPIO8
GND	25	26	GPIO7
DNC	27	28	DNC
GPIO5	29	30	GND
GPIO6	31	32	GPIO12
GPIO13	33	34	GND
GPIO19	35	36	GPIO16
GPIO26	37	38	GPIO20
GND	39	40	GPIO21

Figure 3. Raspberry PI 3 model B Pin Diagram

B. PIR Sensor: PIR is used to detect the motion of the human moment in and out of sensor range. PIR sensor is small and less expensive, it consumes less power. The figure 3.4 shows the outlook of Pir sensor and figure 3.5 shows the inside view of the Pir sensor. It is made up of pyroelectric sensor which can detect the levels of infrared radiation. Figure 3.7 shows the working of Pir sensor, everything emits a radiation which above the room temperature those radiations are in infrared range, the PIR sensors reads the infrared radiation and detects the moment of object in its range.

PIR sensor is made up of little circuitry, capacitors and the resistors, it has a Micro power PIR Motion Detector IC BISS0001, this chip is used for processing of sensor output before sending out of sensor and emit the output in digital form. PIR sensor is in Rectangular in shape, it outputs Digital pulse high (3V) when it detects the motion and digital low when no motion is detected. The range to which it is capable of sensing is up to 6 meters. The PIR sensor has 3 Pins one is VCC for connecting a power supply to PIR, one for Ground connection GND and the other is the OUT which is the output Pin of PIR sensor as shown in figure 3.6.

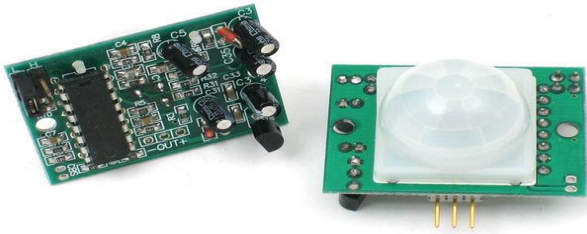


Figure 4. PIR sensor Outlook

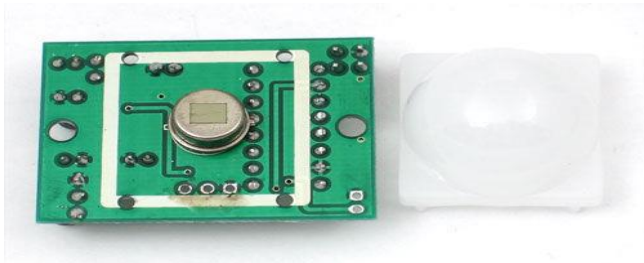


Figure 5. PIR Sensor inside view

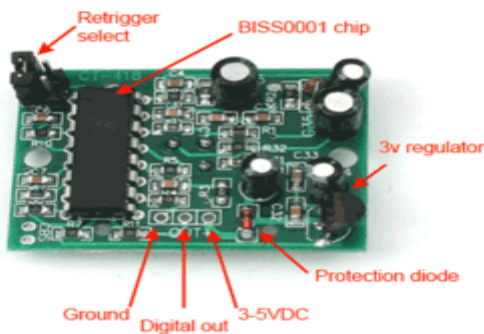


Figure 6. PIR sensor Pin Diagram

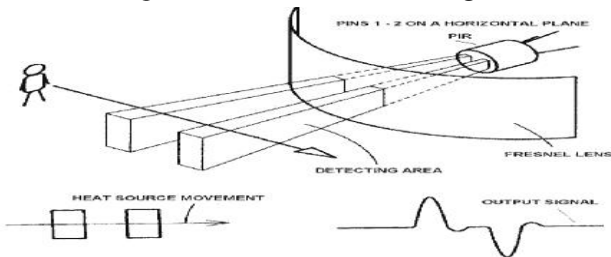


Figure 7. working of PIR sensor

C. BT-SEN-DR-003-N/C Magnetic Door sensor: is a Reed switch, which is enclosed in an ABS plastic shell as shown in figure 3.8. When it is open—no connection between the two wires. The other half is a magnet. when this magnet is away from other with a 5" then the door is said to be open else it is in a closed state. These sensors are commonly used to detect the state of door is it closed or open. Maximum rated current is 100mA and maximum distance is 15mm.

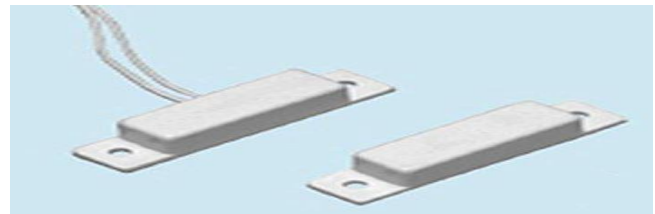


Figure 8. Magnetic Door sensor

D. HXD Buzzer: HXD buzzer is long working buzzer which beeps when it is triggered by an action. Its rated voltage is in the range of 1.5~12 VDC and a operation voltage is 1.2~16VDC and the sound output is greater than 85DB.

E. NOOBS: NOOBS are also known as Net Out of Box Software. The NOOBS are an easy OS (operating system) installer for Raspberry PI It contains Raspbian OS which is installed in Raspberry PI using SD card. It provides an option for user to select the alternative OS which can be downloaded and installed.

F. VNC Viewer: VNC is the Virtual Network Computing which is a graphical desktop system that uses the RFB (known as Remote Frame Buffer) protocol for controlling the computer remotely. In this proposed system, we use VNC viewer for controlling the Raspberry PI which is connected by an ethernet cable to the computer. Figure 9 shows the login screen to pi using VNC viewer.

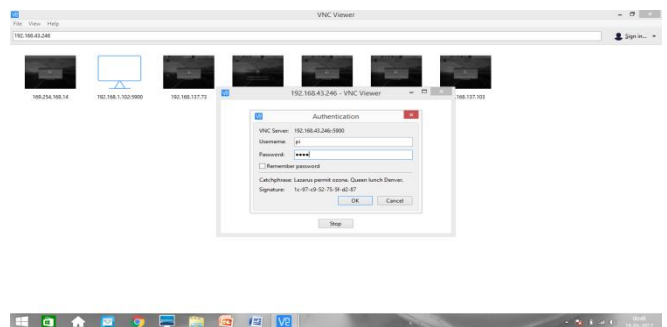


Figure 9. Login screen of Raspberry PI into Raspberry PI

G. Advanced IP Scanner: The Raspberry PI is assigned a unique dynamic address whenever it is connected to the computer and joined to the Network. To know the Raspberry PI Dynamic, address the Advanced IP

scanner is used which shows the connected live and dead Devices within the network. The below is the Fig 3.10 showing the Advanced IP Scanner with Raspberry PI dynamic IP address, the Blue node indicate that the System is alive and running state.

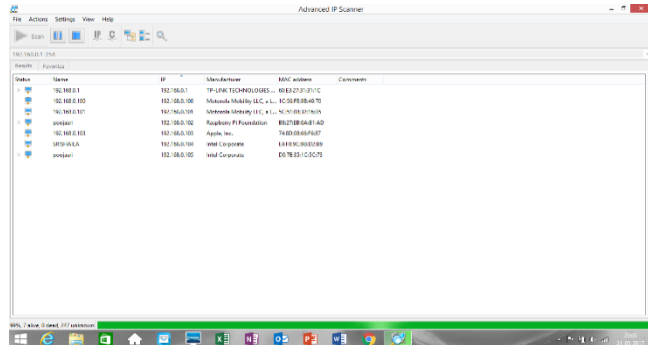


Figure 10.Advanced IP scanner showing the status of Raspberry PI within the network.

H. Twilio API: Twilio API allows Messaging. This API allows user to send messages using twilio Rest API and Receive SMS from the twilio Number, in this each user is given a public and private key and a unique twilio assigned phone number using which the messages are sent to mobile numbers of user. Twilio API supports python programming language.

I Android Apps: **Network Scanner** is an Android App used in Smartphone to detect the devices connected within that network and their IP address. Which is used to connect the Raspberry PI from the android Phone.

Mobile SSH is an Android App based on putty SSH library which is used to control the Raspberry PI remotely and give commands from the Android phone to Raspberry. The Username and password is entered from Mobile SSH android App to get connected to the Raspberry PI wirelessly.



Figure 11. Mobile SSH connecting to Raspberry PI using PI id and password

J. Programming language: Python, Raspbian comes with ainbuild packages for python the Raspbian contains both python 2.7 as well as python 3 but for this paper we are using python 2.7. [9] Python is a High-level programming language commonly used because of its simplicity and ease of learning. Python interpreters are available for many operating system. Python supports the object oriented and structured programming language.

K. Connections

The fig 3.17 shows the Pin connection of the Raspberry PI to Bread board and to the Sensors.

The Raspberry PI 3 model B has 40 GPIO Pins to connect the sensors and actuators. The +ve Pin of PIR sensor is connected to 5v Pin of Raspberry PI, -ve Pin is connected to common ground, the out Pin of PIR sensor is connected to Pin 11 and 15. One Pin of door sensor is connected to 16 as +ve , other to ground Pin 20.Led +ve Pin is connected to 13 and other Pin to the ground. HXD Buzzer One Pin is connected to Pin 12 and other to ground.

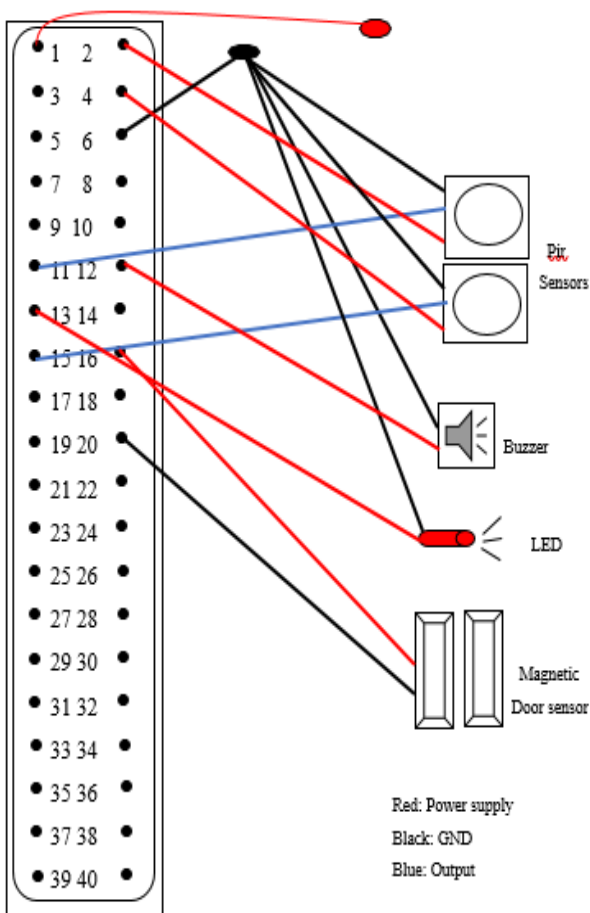


Figure 12. Pin connections

V Experimental Results

The following figures shows the result of the proposed system. When no objects move around the home then led and buzzer remains off which is shown in figure13.1, figure 13.2 is Raspberry PI screen and figure13.3 is mobile ssh screen in normal screen.



Figure13.1.when sensors are in normal state.

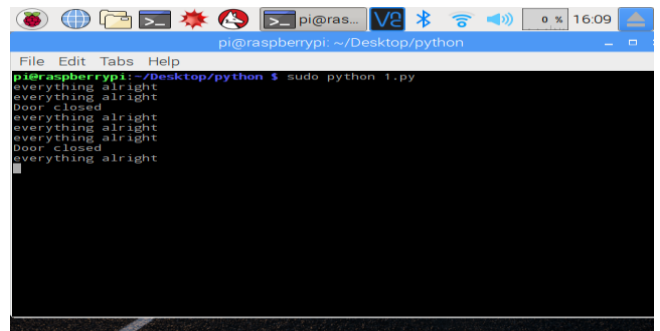


Figure 13.2. PC Screen shot showing that everything is alright



Figure 13.3.showing the snapshot of mobile when all sensors are in normal state

When objects or person moves right side of the home then the Led glows along with the buzzer beep as shown in fig 4.4. The text SMS is sent to authorized person's phone number fig 4.6 shows the screen shot of the text SMS.

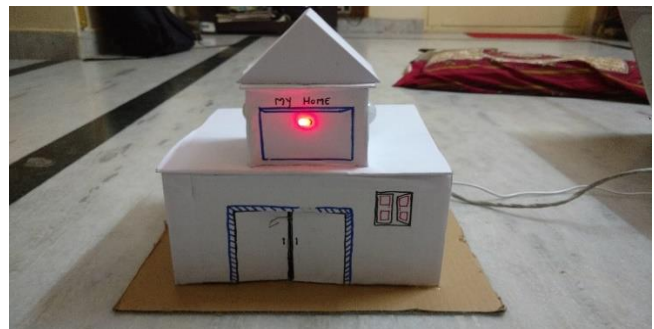


Figure 13.4.the blinking of Led and Buzzer is on when someone moves right side of home

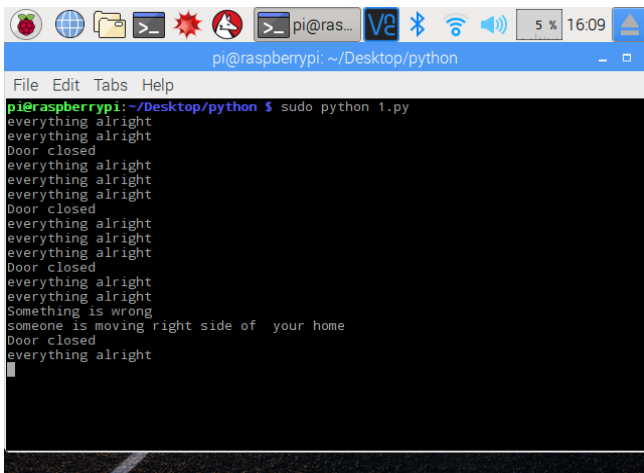


Figure 13.5. When person moves right side of the house

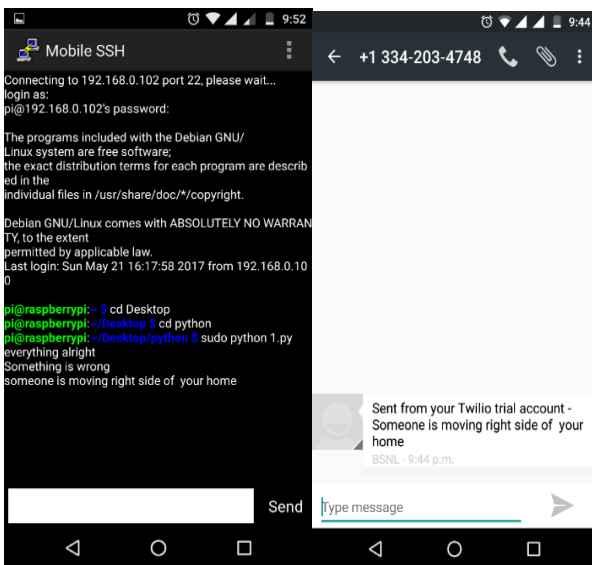


Figure 13.6. mobile snapshot showing the Someone is moving right side of the home in Mobile SSH and also the text message received by the owner

When objects or person moves left side of the home then the Led glows along with the buzzer beep as shown in figure13.7. The text SMS is sent to authorized person's phone number figure13.9 shows the screen shot of the text SMS.

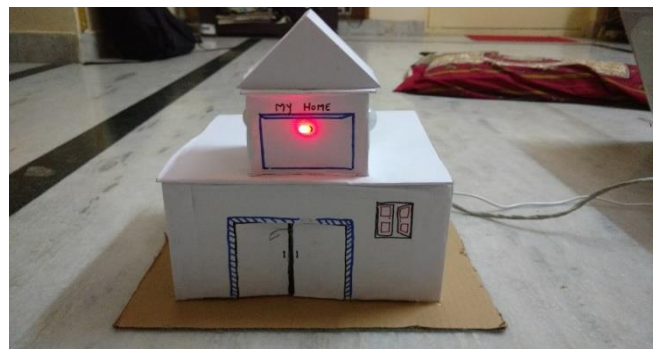


Figure 13.7. showing when the person moves left side of the home then led and buzzer activates.

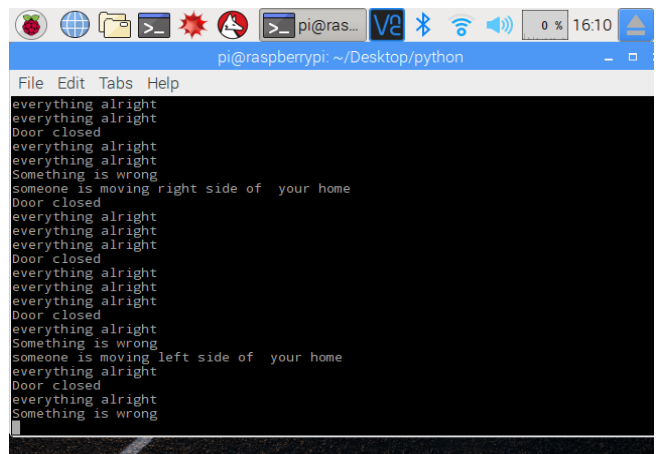


Figure13.8. when someone moves left side of the home

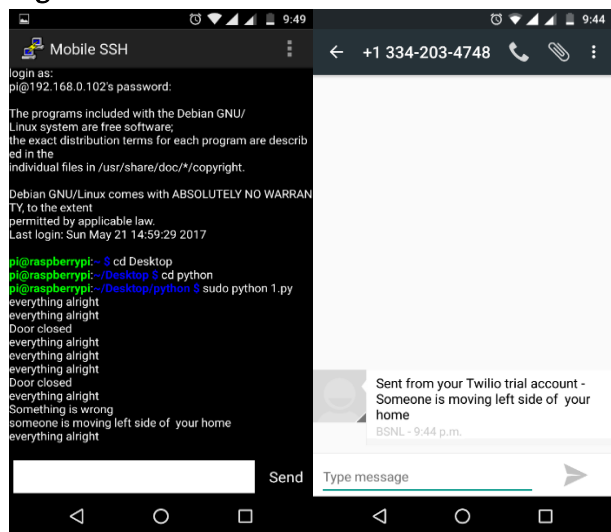


Figure 13.9. mobile snapshot showing the Someone is moving right side of the home in Mobile SSH and also the text message received by the owner.

When the door of the home is left open then the led and buzzer activates as shown in figure13.10 along with these the Alert text SMS is sent to the authorized

owner's phone number, the mobile phone screen shot is shown in figure13.12.

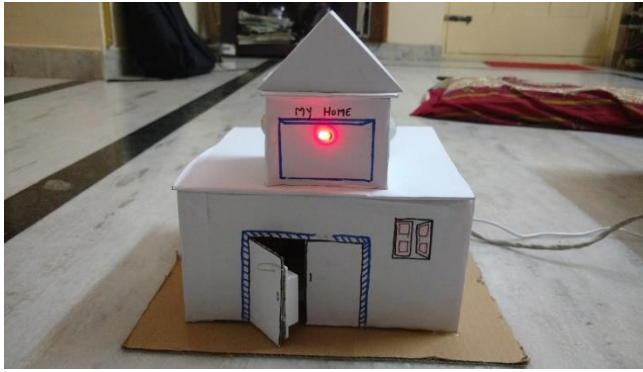


Figure 13.10.when home door is open it blinks led and buzzers

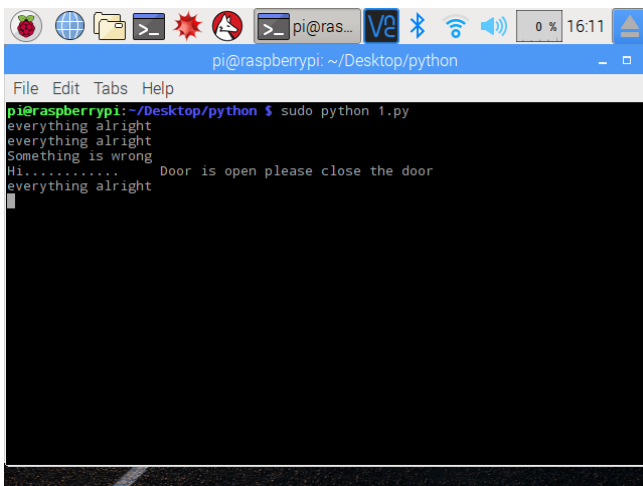


Figure 13.11. When the door is open, it gives an alert message

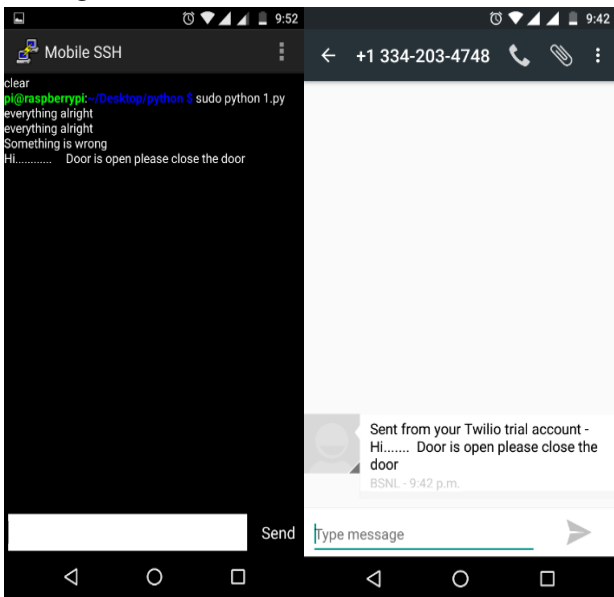


Figure 13.12.snapshot shop of mobile phone when the door is open

V. ADVANTAGES AND APPLICATIONS

- ✓ The security for the home using a low-cost sensor. It is efficient to use this concept for big bungalow.
- ✓ It can also be used to monitor particular objects in a room or a public place such as gold showrooms museums.
- ✓ It alerts immediately to user even when they are away from home, it is also possible to send messages to multiple phone numbers from using this paper.
- ✓ This can be implemented in private buildings.
- ✓ Using PIR sensor and door sensor it is possible to keep an eye on restricted places in office all the time.

VI. CONCLUSION

In this paper, the security for home is provided using the various low-cost input sensors and output actuators. The Python programming language is used for designing and controlling the sensors and triggering actuators. RaspbianOs is installed in Raspberry PI using the SD card. The text message is sent to owner's mobile phone whenever input sensor detects the changes. The PIR sensors detect the human motion and sends signals to the Raspberry PI which in turn activates the Led and the Buzzer, also sends an alert Text message to the owner's mobile phone, Similarly, when the door sensor detects that the other part of magnet is away from it, it sends signals to the Raspberry PI which in turn activates the led and Buzzer also sends alert text SMS to owner's phone. For the Future enhancement, the Raspberry PI camera model can be used with this paper to capture the image of intruder whenever PIR sensor detects the motion and send the image of the intruder to the remote person.

VII. REFERENCES

- [1]. "The PIR sensor" <https://learn.adafruit.com/pir-passive-infrared-proximity-motion-sensor?view=all>
- [2]. "The magnetic sensor" <https://www.adafruit.com/product/375>
- [3]. "The HXD Buzzer" [https://www.adafruit.com/product/1367'](https://www.adafruit.com/product/1367)
- [4]. A. Daramas, S. Pattarakitsophon, K. Eiumtrakul, T. Tantidham, N. Tamkittikhun, "HIVE: Home Automation System for Intrusion Detection", Student Project Conference (ICT-ISPC), 2016 Fifth ICT International, 25 July 2016
- [5]. Suresh S., J. Bhavya S Sakshi, K. Varun, G. Debarshi, "Home Monitoring and Security system", ICT in Business Industry & Government (ICTBIG), International Conference on 06 April 2017
- [6]. O. Urfaliglu, Emin B. Soyer, B. Ugur Toreyin, A. Enis Cetin, "PIR-sensor based human motion event classification", Signal Processing, Communication and Applications Conference, 2008. SIU 2008. IEEE 16th, september 2008
- [7]. Rui Ma, Fei Hu, Qi Hao, "Active Compressive Sensing via Pyroelectric Infrared Sensor for Human Situation Recognition", IEEE Transactions on Systems, Man, and Cybernetics: Systems (Volume: PP, Issue: 99) 22 June 2016
- [8]. Agus Kurniawan, Berlin, "getting started with Raspberry PI 3", March 2016
- [9]. Alex Bradbury, Ben Everard, "Learning Python with Raspberry PI" 12 Mar 2014.
- [10]. Arshdeep Bahga, Vijay Madisetti, "Internet of Things A HANDS-ON APPROACH", 2015.

Substitution and Comparative Study of Solar Panel Efficiencies of Silver and Aluminium as a Reflector

Kaushik.M

Department of Computer Science and Engineering, PESIT south campus, Hosur Road Electronic city, Bangalore, Karnataka, India

ABSTRACT

Solar energy and solar rays as a whole are a worldwide wealth and help in generation of large amounts energy often not put to good use by us. In an attempt to promote use of sustainable energy resources such as solar energy, it is important to venture into efficiency of solar energy and improvements herewith. Hence this pioneering research tackles ways to compare Silver (as used in mirrors) and Aluminium as possible reflectors of solar energy and see which one is more efficient, cost efficient, easily replaceable and most suited for real world non functional requirements of the common man. Hence, this paper seeks to promote the use of Aluminium as opposed to Silver reflectors.

Keywords: Silver, Aluminium, mirror, cost efficiency, Solar, foil

I. INTRODUCTION

Current theories suggest that solar Energy is still an undiscovered field of Science, full of opportunities for research and development. In this Paper we take an incremental and comparative research study, where we try to replace or substitute mirrors used in solar light reflection onto a Solar cell with Aluminium foil so as to decrease cost efficiently and make it more accessible to all without decreasing the output of the solar panel to a considerable level. We have taken up Aluminium foil as a component of study as it is easily available and other theories prove that it has considerably good reflectivity of light and it can possibly replace mirrors and provide with the similar output in a small scale event. Through this paper we can Understand the potential uses of the use of Aluminium foil other than just being a accessory in cooking.

II. EXPERIMENTAL METHOD

The apparatus used for the experiment are as follows:

1. Solar Panel -7.5V and 1.3W output, Resistance of 43.103 ohm
2. Plane mirrors- 3X4 inches dimensions
3. Aluminium foil on cardboard plane- 3X4 inches dimensions
4. Multimeter,Laser for calibration and positioning of mirrors

The theory behind this experiment is to test the reflectivity of Aluminium foil compared to mirrors when used to reflect sunlight onto the solar cell. We perform this experiment once indoors and once outdoors keeping the mirrors parallel to the plane of the sun so as to maximize reflectivity and calculate the amount of light falling on the panel when the sun and panel are not aligned. The setup used was kept 50° inclined to the plane keeping the mirror in the plane. The Voltage is used as a parameter to calculate the output to get visible values. All voltage values were calculated using Multimeter connected to the ends of the solar panel. Every setup has 3 iterations performed and their average value taken as final result. The temperature, date and time of experimentation is

recorded and other temperature conditions are manipulated and obtained results are recorded and respective graphs are drawn for further comparison. The **wrinkling** of the foil during its preparation is considered **negligible**.

There are **3 setups** in the experiment

1) **Solar setup using mirrors**

2) **Solar setup using foil**

3) **Control setup without any reflectors**

All three setups were **performed indoors and outdoors** for comparison and revelation of glitches in the components. The **Laser** was used to **position** the

mirrors in angles which would direct the sunlight falling on them towards the solar cell, this will maximize the amount of sunlight falling on the panel to get **comparable outputs** for our study. The angle at which the setups were kept was calculated by the above method. The Aluminium foil was wrapped around cardboard pieces with dimensions as the mirrors and kept in the same angle and position of the mirrors. All 3 setups were experimented on at different times of the day and compared for a final conclusion.

Observations and Graphs

1) INDOOR

Temperature = 24-27°C Setup1 (with mirrors)

Table 1

Time	1 st	2 nd	3 rd	Average (Volt)	Power (Watt)
8:00am	7.37	7.39	7.40	7.387	1.265
9:00am	7.56	7.55	7.55	7.554	1.323
10:00am	6.05	6.04	6.05	6.054	0.850
11:00am	5.46	5.45	5.45	5.454	0.690
12:00pm	5.04	5.04	5.03	5.044	0.590

Setup2 (with foil)

Table 2

Time	1 st	2 nd	3 rd	Average (Volt)	Power (Watt)
8:00am	7.40	7.42	7.44	7.420	1.277
9:00am	7.56	7.55	7.56	7.564	1.327
10:00am	5.95	5.94	5.95	5.954	0.822
11:00am	5.33	5.35	5.34	5.340	0.661
12:00pm	4.95	4.94	4.95	4.950	0.568

Setup3 (control setup)

Table 3

Time	1 st	2 nd	3 rd	Average (Volt)	Power (Watt)
8:00am	7	7.01	7	7.003	1.137
9:00am	7.34	7.34	7.44	7.343	1.250
10:00am	5.72	5.73	5.72	5.723	0.759
11:00am	5.1	5.1	5.2	5.103	0.604
12:00pm	4.74	4.74	4.75	4.743	0.521

2) OUTDOOR

Temperature = 25-29°C Setup1 (with mirrors)

Table 4

Time	1 st	2 nd	3 rd	Average (Volt)	Power (Watt)
8:00am	8.82	8.81	8.82	8.823	1.806
9:00am	8.46	8.46	8.46	8.46	1.660
10:00am	8.06	8.06	8.07	8.074	1.512
11:00am	7.52	7.52	7.52	7.52	1.311
12:00pm	7.30	7.29	7.29	7.293	1.233

Setup2 (with foil)

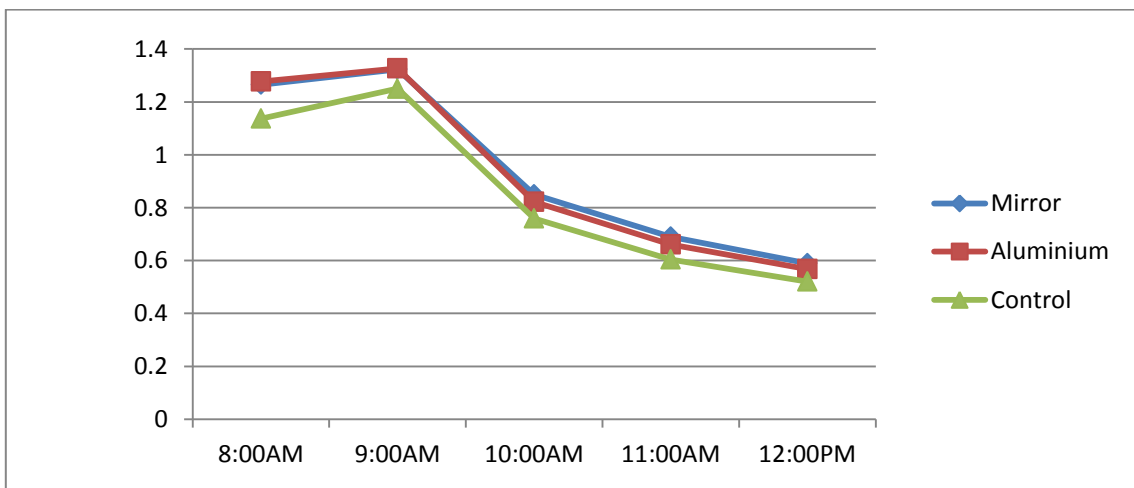
Table 5

Time	1 st	2 nd	3 rd	Average (Volt)	Power (Watt)
8:00am	8.73	8.72	8.72	8.723	1.765
9:00am	8.48	8.48	8.49	8.484	1.669
10:00am	8.08	8.08	8.09	8.083	1.515
11:00am	7.47	7.48	7.47	7.473	1.295
12:00pm	7.26	7.26	7.25	7.263	1.223

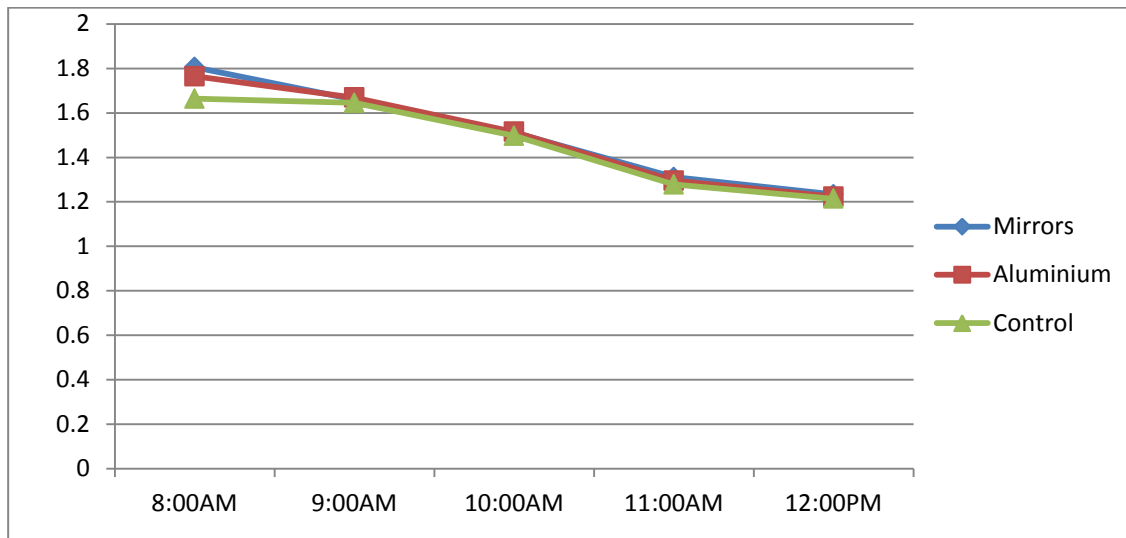
Setup3 (control setup)

Table 6

Time	1 st	2 nd	3 rd	Average (Volt)	Power (Watt)
8:00am	8.47	8.47	8.47	8.47	1.664
9:00am	8.42	8.43	8.42	8.423	1.645
10:00am	8.03	8.04	8.03	8.034	1.497
11:00am	7.42	7.42	7.41	7.423	1.278
12:00pm	7.22	7.24	7.24	7.235	1.214



Graph1. INDOOR setup (Time (X-Axis) vs Power output(Y-Axis) in Watt)



Graph 2.OUTDOOR setup (Time(X-Axis) vs Power output(Y-Axis) in Watt)



Figure 1

III. RESULT AND DISCUSSION

According to the results obtained we can successfully say that aluminium foil can surely substitute silver mirrors for the reflection of light onto a solar cell so as to decrease cost and maintain similar efficiency. Some theories suggest that aluminium and Silver mirrors have similar reflective index with mirrors being higher. Due to this theory, we can get close values of Power output. Other than the fact that this theory was proved to be right, it is hard to maintain Aluminium foil is hard to maintain as mirrors are sturdier and easier the manufacture for this use. We can make the aluminium sturdier by placing it in between 2 plain transparent glass, this process can make it sturdier and help keep the Aluminium from wrinkling and also decrease the chance of the foil

heating up too much. The only drawback of this theory is that in a large scale production of electrical energy from solar energy we can obtain very high and easily comparable values of output.

IV. CONCLUSION

From the above Observations we can see that there is clear difference between the Power output in all the setups both outdoor and indoor and by this we can conclude that, **Aluminium can act as a good and reliable substitute for Silver mirrors in the reflection of solar light onto a solar cell.**

V. ACKNOWLEDGEMENT

I would like to show my Gratitude to Dr.Revanasiddappa, PESIT bsc for sharing his pearls of wisdom with me during the course of this research. I would also like to thank my classmate Mr. Naren Anant Kulkarni for his insights and comments for the research. I would also like to thank PESIT bsc for providing me with this opportunity to present my research at RISE.

VI. REFERENCES

- [1]. Azom Articles
- [2]. www.rollitup.org
- [3]. www.ieeexplore.org
- [4]. Explorable.com
- [5]. Investigation of reflective materials by John Harrison
- [6]. Researchgate.net
- [7]. cs.trains.com

IoT Based Noise Pollution Reduction in Traffic Jams

Pawan Terdal, Sanath Kumar, Mohak Rathore

Department of Information Science and Engineering, PES Institute of Technology, South Campus, Bangalore, Karnataka, India

ABSTRACT

Due to the increasing population of vehicles on road, the noise pollution levels have risen beyond limits. No longer can a person travel from one place to another without being subjected to high intensity noise coming from vehicles. This noise can have varying effects on a person, such as hearing impairment, high blood pressure, stress etc. At traffic signals or traffic jams, people tend to honk relentlessly adding nothing but noise to the environment. This paper tries to solve this problem by proposing an IoT-Based solution. With the use of an ESP-8266 microchip and a sound sensor, the noise produced in the traffic can be reduced by cutting down on the unnecessary honking by drivers. Reduction in the levels of noise pollution helps to increase productivity, reduce stress etc.

Keywords: IoT, traffic jams, noise pollution, honking, environment, technology.

I. INTRODUCTION

The decrepit state of public transport in our country is driving up sales of private vehicles at an alarming rate. This is reflected in the substantial increase in traffic especially in the urban areas. According to a study done by World Resource Institute in Bangalore, traffic moved at the speed of 35 km in an hour in 2005 as compared to 9.2 km in 2016. Increase in traffic and congestion has led to several negative impacts, one of which is the drastic increase in the noise pollution. A noise study conducted by Kalra's NGO in Gurgaon, has shown that the recorded levels on some of the busy stretches of the city went well towards the 60-70 dB bracket, when the acceptable range for the human ears is of around 40-50 dB.



Figure 1

II. LITERATURE SURVEY

In Gwalior city noise level survey was undertaken along four roads namely Tansen Road (Site I), Jinsi Nala Road (Site II), Kilagate Road (Site III) and Laxmibai road (Site IV). Noise level was recorded with the help of a sound level meter at the edge of road for every interval of 15 sec. A weighted noise level dB(A) was measured. [2]

Table 1
Sound Level in dB(A)

75.3	81.3	75	69.8	69.8
70.6	77	73.8	72.9	71.3
81.3	72.7	72.6	96.7	78.5
69.8	74.2	71.2	77.8	70.3
72.5	71.9	80.9	72.7	27.8
76.3	78.8	75.7	77.6	85.3
85.6	72.2	75.4	73.8	82.6
71	74.8	72.1	91.6	79.8
74.4	78.4	71	70.9	78.3
98.3	71.3	81	68.9	71.2
73.9	73	73.9	69.8	68.6
71.4	79.5	80.1	75.6	72.9
90.2	76.3	76.4	70.6	73.1
69.3	84.7	71	73.3	78.3
71.2	73.7	74.3	78.4	75.3
73.4	72.6	80.5	71.3	75.3
75.2	81.2	78.9	82.3	74.8
78.4	75.3	80.6	75.6	79.3
69.4	72	68.2	84.2	72.3
72.3	70.9	87.6	72.5	75.8
69.3	86.3	76	73.8	71.1
76.2	83.2	71.6	78.5	69
69.8	73.5	76.6	89.1	80.2
79.6	76.9	70.8	74.2	75

The main contributor to these figures is the noise generated by honking from vehicles such as cars, bikes and trucks. In the same study, it was noted that vehicular honking in cities has reached an alarming level and contributes approximately 70% of the noise pollution in our environment.

III. LITERATURE SURVEY CONTINUED

A soundless horn system was proposed in [1]. In this system, a camera, a processor, a transceiver and a LCD display is used. A vehicle intending to overtake another vehicle captures the number plate of the vehicle to overtake using ANPR(Automatic Number Plate Recognition System). It then sends a request with its own vehicle ID(VID) as the source and the number plate captured(VNUM) as the destination. This request signal is transmitted through a DSRC(Dedicated Short-Range Communications) transceiver. This signal is received by all the vehicles within the range of the transceiver. Each vehicle checks the destination field with its vehicle ID.

The vehicles whose number does not match with the destination of the request, discard the request. The request signal appears as a notification on the LCD display of the on board equipment of the target vehicle. The target vehicle sends an acknowledgement signal containing its own VID and allowance of pass to the requested vehicle. This pops up on the LCD of the source vehicle indicating whether it can overtake the target vehicle or not. In this way, the motive of horn is achieved without using any honking mechanism.

IV. IMPLEMENTATION

The proposed system consists of a NodeMCU board which runs on the ESP8266 Wifi-enabled microchip and a sound sensor. The device is fitted inside a vehicle and is connected to the vehicle's horn. The sound sensor is placed near traffic signals and other tactically chosen locations where congestions or pile-ups are frequent.

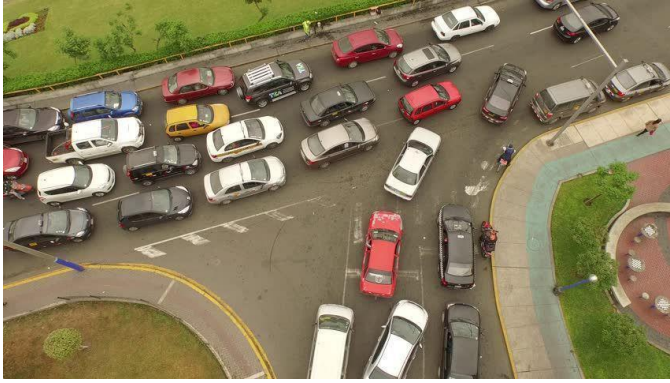


Figure 2

Table 2. Relation Between Adc And Decibel Values

ADC value	dB
460	44
480	47
500	59
508	60
550	61
600	63
613	65
700	70
859	78

i) TECHNICAL SPECIFICATION

The sound sensor measures the noise at the traffic signal/jam and sends this analog value to the microprocessor. The board has an in-built Analog-to-Digital converter(ADC) which always returns a value between 0 and 1024. This is because according to the ESP8266 datasheet, the ADC pin has 10 bit resolution. This means that analog reading will return a value between 0 to 1024. This digital value is sent to the server from where the data is read by the vehicles. The following table[3] gives a suitable relationship between the ADC value and the decibel value-

During traffic jams and congestions, we see that a lot of drivers honk excessively and unnecessarily. This is of no use and only adds up to the noise pollution in the environment.

So, what we propose is this:

The sensors that are located near the signals and other points sense the sound level around and send this information to the server. If the sound level is above a certain threshold (around 60dB) the value for the intensity of the horn is reduced. All the vehicles around that sensor read this updated value from the server and accordingly the intensity of its horn will be reduced. This ensures that the sound intensity coming out of the vehicles is kept in check and unnecessary honking doesn't add to the overall noise

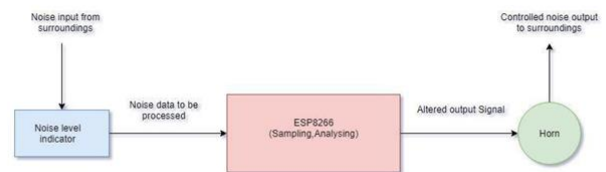


Figure 3

V. RESULTS

From the survey[2] we found out that the average noise levels on the roads were crossing levels as high as 90dB. For a human ear, continuous exposure to high noise levels, of over 70 dB can be harmful.

In India, the horn level for a car is about 95 dB. The entire purpose of our paper is to reduce noise pollution caused by honking. So, for this sake we cut down the horn level as follows-

We set the threshold value to be at 60dB.

So if average noise level in the surrounding is

- ✓ below the threshold - do nothing
- ✓ between 60 dB and 80 dB - reduce the horn level intensity of vehicles by 30%
- ✓ between 80 dB and 100 dB - reduce the horn level intensity of vehicles by 40%

Table 3 gives a suitable relationship between minimum and maximum values of decibels, ADC and volts

Table 3.Min And Max Values Of Decibels,Adc And Volts

	ADC	VOLTS	dB
Min	0	0	7.83
Max	1023	3.3	100.23

The graph depicted below gives a clear picture of the impact caused by the system. We see that as the noise levels in the surrounding increases, the intensity of the horn decreases accordingly.

In particular, at $t = 25$ sec(approx), the noise level crosses the threshold (60 dB) and hence there is a sharp decrease in the intensity of the horn in the surrounding vehicles.

This ensures that the noise level in the surrounding remains at an ideal level which helps to keep the noise pollution in check.

Table 4. Tabular Representation Of The Results

Time (sec)	Sound Sensor Reading(ADC value)	Value in volts	Sound (dB)	Updated Horn Level(dB)
0	460	1.48	44	95
10	480	1.55	47	95
20	500	1.61	59	95
30	508	1.63	60	95
40	600	1.93	63(-30%)	67
50	613	1.97	65	67

60	700	2.25	70	67
70	859	2.76	78	67
80	863	2.77	86(-40%)	59
90	877	2.82	88	59
100	885	2.85	92	59
110	895	2.88	95	59
120	899	2.89	97	59

Sound Level Variation

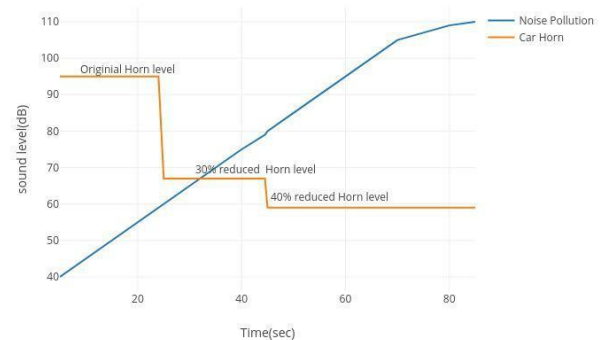


Figure 4

VI. CONCLUSION

In India like many developing countries the residents of cities are now becoming aware of environmental problems that result from the transportation facilities in general from road traffic and in particular from automobiles. Traffic noise is a major factor of environmental pollution. Noise affects human body in a number of ways ranging from Psychological to Physiological, e.g. auditory damage, speech interference, sleep interference, general annoyance, reduces the working efficiency, increases blood pressure & fatigue etc.

While the paper presents an honest attempt to reduce noise pollution, it also faces several obstacles and shortcomings which are as follows

- ✓ The proposed idea depends heavily on internet connectivity. Thus, internet should be accessible freely and conveniently across the city.
- ✓ The usage of the system is restricted to junctions and gridlocks or any such places where congestions are frequent.
- ✓ The system cannot tell the difference between noise from a horn and other loud noises such as that of sirens or loudspeakers.

VII. ACKNOWLEDGEMENTS

The authors would like to thank Prof. Bharathi R for her guidance and support throughout this work.

VIII. REFERENCES

- [1]. PrRajiv Kapoor, Rajesh Birok, Divi Sai Manoj Department of Electronics and Communication Engineering "Soundless Horn And Remote Patroller" 2014 IEEE International Conference on Vehicular Electronics and Safety (ICVES)
- [2]. P. D. Marathe "Traffic noise pollution" IJED: Vol. 9, No. 1, (January-June 2012)
- [3]. <https://circuitdigest.com/microcontroller-projects/arduino-sound-level-measurement>

IoT-Enabled Hydroponics Farm

Siddhanth J Ajri, Abhishek Guragol, Adish S Rao, Rahul Suresh

CSE, PES Institute of Technology, Bengaluru, Karnataka, India

ABSTRACT

Farming in India is carried out through mundane, outdated methods. Most farmers lack the necessary knowledge or expertise to carry out effective agriculture and rely on predictions, which oftentimes, fails. This leads to low yield, poor quality crops grown year after year, thus, putting the consumer at a loss of essential nutrients in their diet and also leaving the farmers with a very low profit margin for their crops. Since we are aware of the benefits of proper soil moisture and its quality, air quality and irrigation in the growth of crops, such parameters cannot be ignored. With the aim of revolutionizing the Indian Agricultural Business and also optimizing natural resources to procure higher yield and profits for our Farmers, the paper proposes remote access, self-sustained IoT-enabled Hydroponics Farm as a viable solution to rising crises in the Agro-Business.

Keywords: Hydroponics, Indoor Farming, IoT, Sustainable Development, Energy Optimization

I. INTRODUCTION

Weather and Climate have become highly unreliable in India, and throughout the World. It is this predicament that calls for a move to more prudent Indoor Farming methods. Hence, we have chosen to explore the technique known as Hydroponics to utilize in our Indoor Farm.

Hydroponics is a technique used to grow plants without the use of soil, instead the root system is placed in a water-base nutrient rich solution that is supported using an inert medium such as rock wool, perlite, vermiculite, peat moss, or clay pellets. The basic premise behind hydroponics is to allow the roots of the plant to come in direct contact with the nutrient solution, while also having access to oxygen, which is essential for proper growth.

The reason we have chosen to implement Hydroponics is due to its various advantages, namely greatly increased rate of growth in plants. With the proper setup, plants will mature upto 25% faster and produce upto 30% more than the same plants grown

in soil. Hydroponics also involves careful control of nutrient solutions and pH levels. A hydroponic system will also use less water than soil-based plants because the system is enclosed, which results in less evaporation and also due to the reuse of water. It also contributes to reduced waste and pollution from soil runoff and offers improved pest control.

One of the commonly cited drawbacks is that the initial cost of setting up a Hydroponics Farm is quite high. Our implementation is designed to eliminate this drawback by helping to optimize and increase the energy/cost efficiency of a Hydroponics farm by making use of setup called the 'Solar Flower.' Determining weather conditions based on sensor readings, the 'Flower' would be able to switch between functioning as a solar tracking system (thus increasing energy efficiency by 60%), as well as, a rain water harvesting system. The solar energy that is harvested and stored, would in turn be used to power the smart farm.

Plants use only certain regions of the light spectrum for growth. Hence using LED grow lights, we will be

able to set up an indoor farm under a controlled environment, that can promote the 24*7 growth of crops by providing them with only their required light recipe for their optimal growth.

Making use of the best combination of hydroponic nutrient solutions in the implemented hydroponics system, the rate of growth of certain crops can be improved, compared to that achieved by traditional growing techniques.

Since all the components including the Solar Flower and all the electronic components for the farm are IoT-enabled, the entire farm can be controlled remotely through our Web Interface, thus, making this Self-Sustained Ecosystem facilitate maximum yield through minimal effort. This sort of Farming technique is especially useful in arid regions where water is scarce, as the same water is reused by replenishing the required nutrient solutions after every flow cycle, when the water passes through the Nutrient tank.

II. PROPOSED SYSTEM

All the necessary configuration and powering of the components was done using Arduino Uno and Node MCU 1.0 Microcontroller boards and the prototype model was implemented in the following manner.

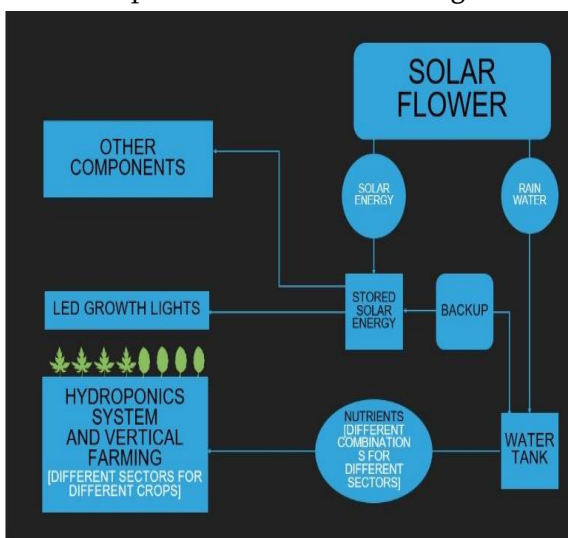


Figure 1. Block Diagram

The first sector in the farm will be the powering sector consisting of the Solar Flower. The Solar Flower setup consists of Solar Tracking Panels, constructed using LDRs, wherein based on the amount of light falling on the resistor the value of resistance varies. Using this varying resistance, the average of the four LDR's are calculated to determine in which direction the panel must rotate. The Solar Flower is provided with a Humidity sensor, and through its readings the Flower is able to detect if it is likely to rain or not, and accordingly configures itself to Rain Mode, wherein the Panels align themselves in the shape of an inverted umbrella, in order to harvest rain water which will be stored in Water tank, which is responsible for storing water that is used for irrigating the Crops being grown. Thus, both Solar energy and Rain water can be harvested successfully using this setup.

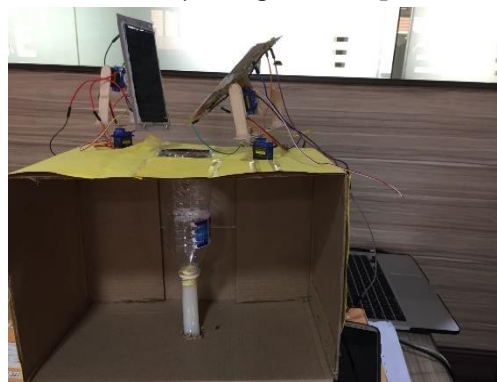


Figure 2. Solar Flower setup

Separate and preferably vertically arranged sectors for the growth of different plants are set up and pipes are laid from the Water Tank to each of these sectors. The pipes will have openings where the saplings will be placed. The water flowing to each sector was monitored and controlled in the prototype with the help of Hall Effect Flow Sensors and Solenoid Valves, which are powered by 12V Adapters. The water flowing through each valve can be monitored on the Webpage and adjusted so that each crop is provided with just enough water as needed.

LED Grow Lights are set up in each sector, with the colour of LED being used depending on the type of Crop being grown. These LEDs are powered by the Solar energy harvested by the Flower, failing which the Node MCU used to configure it is sufficient to power it.



Figure 3. Plantation sector, provided with LEDs

The final sector is the Nutrition Tank, that replenishes the nutrients that were drawn by the plants, and this water is then resupplied back to the Water tank and can be used for the next water flow cycle.

Each of the above functionalities are provided webpage access. All the webpages were written in HTML and connected to the Web through the ESP 12E Module of the Node MCU. The webpages are hosted on a local Server set up on a Raspberry Pi using Flask.

III. RESULTS AND DISCUSSION

A. Demonstration of Working Prototype

For the demonstration of the working of our prototype model, first, all the Arduino and Node MCUs were configured accordingly, and Water was poured into the setup to emulate the situation of rainfall. Water flowed through the pipes to reach the Valves, which remained open until a certain, predefined amount of water had flown through the Flow sensors. Upon reaching the flow limit configured earlier, the valves closed, preventing the excessive flow of water to Plantation sectors.

Each of the components could be controlled from the webpage successfully, i.e. the Switching between Rain Mode and Solar Energy mode, the Opening and closing of the valves, the LED Switching circuits etc. A home button was provided on each webpage to go back to the Home page of the Server, where the user again has the option to choose to control any of the functionalities of the Farm.

B. Nutrient Solution

The hydroponic nutrient solution is the only source of nutrients to the crop being grown and thus, it is of utmost importance to utilise a well-balanced solution, that contains all the organic and inorganic nutrients, as required by the plant.

Several factors have to be taken into account when choosing fertilisers for preparing a hydroponic nutrient solution:

- ✓ Water Quality - salinity, concentration of possibly harmful elements (like sodium, chlorides and boron).
- ✓ The nutrients required and their concentrations in the hydroponic nutrient solution.
- ✓ Proportional mix of the nutrients.
- ✓ The pH of the hydroponic nutrient solution and its outcome on uptake of nutrients by plants.

The following figures illustrate the ideal nutrients that could be utilised to grow the various crops tested so far.

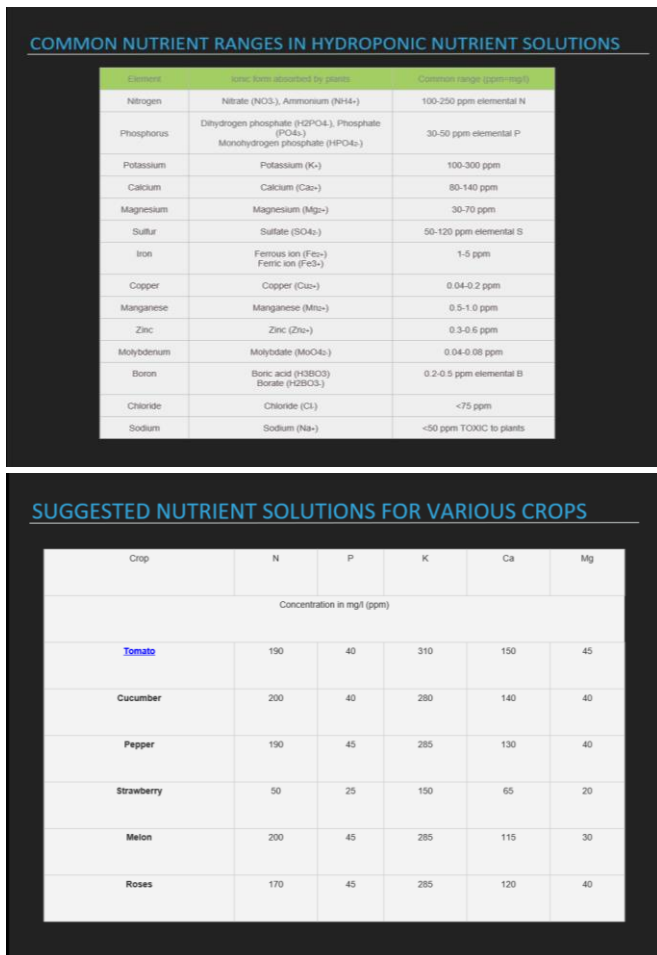


Figure 4. Nutrient solutions required by various crops

C. LED Grow Lights

Lighting mechanisms are used to create a specific light recipe for each plant, giving them the wavelength, intensity and frequency, they require for photosynthesis in the most energy-efficient way possible. This engineered lighting makes it possible for us to control size, shape, texture, colour, flavour, and nutrition with razor-sharp precision and increased productivity.

It was found that further investigation pinpointed the more specific effects of different light wavelengths on plants grown indoors. The findings of these studies provide the basis of LED light recipes:

- ✓ Light of wavelength 630 - 660 nm is essential for the growth of stems, as well as the expansion of leaves. This spectrum of red light

also regulates seed germination, dormancy periods and flowering.

- ✓ Light of wavelength 400 - 520 nm needs to be carefully mixed with light in other spectra since long exposure to light in this wavelength may stunt the growth of certain plant species. Light in the blue range also affects the chlorophyll content present in the plant as well as leaf thickness.
- ✓ Light of wavelength 500 – 600 nm was once believed to be unnecessary for plants, but recently it has been proved that this wavelength penetrates through thick top canopies to support the leaves in the lower canopy.
- ✓ Light of wavelength 720 – 740 nm penetrates through dense upper canopies to support the growth of leaves located lower on the plants. Exposing plants to IR light reduces the time a needed to flower. Another benefit of far red light is that plants exposed to this wavelength tend to produce larger leaves than those not exposed to light in this spectrum.

IV. CONCLUSION

Agriculture is one of the oldest implementations of Mankind and yet has seen very slow advancements in technology. Thus, the digitisation of the Farming sector is the need of the hour. The use of Hydroponics indoor farms, that provide remote access to users through IoT and whose energy consumption has been optimised to reduce cost exponentially is bound to not only improve the Nutrition standards of the Country, due to the better quality of produce, but also offers a viable solution to desertification, as otherwise barren land in arid regions can now be utilised to set up such modular self-sustained indoor farms.

On the whole, it would positively influence the General Economy of the Country while also

providing the platform to truly revolutionise the Agricultural business in India.

IV. REFERENCES

- [1]. A Hall Effect sensor-based syringe injection rate detector, Mukherjee, B et al, IEEE Conference Publications, 2012
- [2]. First Nguyen NT, McInturf SA, Mendoza-Cózatl DG. Hydroponics: A Versatile System to Study Nutrient Allocation and Plant Responses to Nutrient Availability and Exposure to Toxic Elements. *Journal of Visualized Experiments: JoVE*. 2016;(113):54317. doi:10.3791/54317.
- [3]. www.raspberrypi.org
- [4]. www.arduino.cc
- [5]. www.simply-hydroponics.com/grow-systems
- [6]. www.uponics.com/best-led-grow-lights
- [7]. www.aerofarms.com/technology
- [8]. www.smart-fertilizer.com/articles/hydroponic-nutrient-solutions
- [9]. www.theconversation.com/improving-upon-the-sun-led-lights-fuel-plant-growth-in-space-89631

Efficient Water Distribution using Blockchain

Ashwin M, Ramya M, Apeksha B G, Prof. Animesh Giri

Department of Information science and Engineering, Pesit Bangalore South Campus, Hosur Road,
Electronic City, Bangalore, Karnataka, India

ABSTRACT

Inspired and encouraged by the recent surge in interests around blockchains and its various applications, we propose and scrutinize an idea of block chains used for efficient and equitable water distribution/management in cities. Blockchains enable a distributed peer to peer network analogous to an open ledger where the peers can verify and validate the data therefore eliminating the possibility of falsification. The problem with water management (distribution) in cities (especially those inhabited by people belonging to both extremes of financial status) is that it is unfair or partial. The distribution of water is done in such a way as to please those who are financially well-off, whereas the pleas and worries of the economically backward are ignored. In our proposed idea, the water distribution is based on the population density and the corresponding need in amount of water [assessed based on a few factors discussed below]. A blockchain is used because every node can verify whether they are receiving their equitable share of water or not. Cost assessing metrics and ways of payment are also discussed.

Keywords: water distribution system, blockchains, population density.

I. INTRODUCTION

Blockchains, as of now, are being implemented at its budding stage in various fields and industries, mainly Finance/Banking. Other fields include health care, real estate and the government sector. The reason behind the interest in blockchains is that with a block chain being implemented in an application, it can run in a decentralized fashion without the need of a centre of authority, and still achieve the same functionalities, which wasn't previously possible.

Falsification of data is eliminated as the network of peers is decentralized and security of the data is ensured through the heavy use of cryptography, this brings authoritativeness in all transactions in the network.

Now, the problem we hope to solve using blockchains, Water Management (Unfair Water

Distribution). It is evident in almost all the cities that the people who are financially well-off are free from various problems faced by the economically backward; one such problem is the availability of water. It only makes sense that water should be distributed to the different areas in a city based on their population density. We discuss a way to ensure that there is a proper water distribution system. Equitable distribution of water is what we hope to achieve through our proposed idea.

The paper is structured as follows: Section II deals with the drawbacks of the existing system. Section III gives an explanation of blockchain and its working, Section III and IV deals with the explanation and implementation of the proposed idea followed by the advantages, limitations and future prospects of the system.

II. DRAWBACKS OF EXISTING SYSTEM

A. Incomplete coverage and inadequate infrastructure.

There is an incomplete and inaccurate coverage of water distribution by the public supply. Many parts of cities are deprived of water. Many cities do not have any kind of infrastructure system in place for proper water distribution.

B. Losses in distribution go unnoticed

The major problem in cities is huge losses of water during distribution. This is due to leakage from broken distribution pipes and incomplete metering and billing. The leakages can occur in distribution pipes or in storage tanks and these leakages are often unnoticed or paid no heed to.

C. Improper maintenance

The water distribution systems in cities often suffer from inadequate maintenance.

This is the main cause of distribution losses. Hence the water distribution system will not last for a longer time.

III. BLOCK CHAIN AND ITS WORKING

The block chain is an incorruptible digital ledger of economic transactions that can be programmed to record not just financial transactions but virtually everything of value and this is the driving force behind the implementation of block chains in all of its applications.

By storing blocks of information that are identical across its network, the block chain cannot be controlled by any single entity and has no single point of failure. The network is also transparent as the access to data is open to peers within the network (public). To sum up, block chain is a robust, incorruptible and transparent network of peers, ideal

for maintaining transactional details of anything with value.

The best way to explain a block chain network is to imagine it to be a continuously growing and self-auditing network which checks any transaction or data verifies and validates the same and adds it as a new block to the existing blockchain.

The working of a block chain network is as follows:

1. Firstly, there is a request for a transaction from within the network.
2. The request is broadcast to all the peers in the network.
3. The network of nodes, then verify and validate the transaction.
4. Once verified, the transaction is added to the existing block chain, as a new unalterable and permanent block.

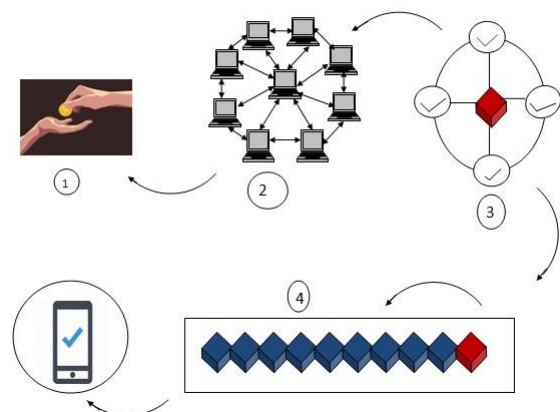


Figure 1. Illustration of steps involved in a blockchain network.

IV. AN OVERVIEW OF THE PROPOSED SYSTEM

The Block chain network proposed here is a tweaked version of regular blockchains being used at present, to ensure certain functionalities.

The network of nodes contains all the houses (or any individual building with its own water connection), and three other nodes:

1. Water Board, the node which is in charge of the distribution of water,
2. Revenue and Billing, the board which deals with the payment,
3. Population Board, which deals with data of the population of the areas present in the cities

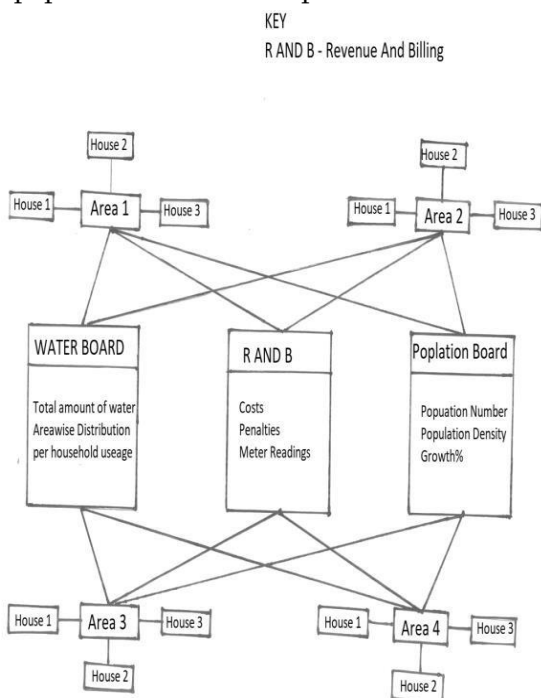


Figure 2. The nodes involved in the proposed system

The main function of these three nodes is to relay information/data to other nodes in the network, the validation of transactions is still left to the peers and not in the hands of the WaterBoard.

The Water Board has the data about total amount of water, area wise distribution, Demand increase/decrease%.

The Revenue and Billing node has data about the costs, penalties, and meter readings.

The Population Board has the data about Total Population, Population density, growth %.

Now with these nodes transmitting/broadcasting the data to the network, all the peers are open to check if they are receiving the equitable amount of water or not. If not, they can approach the Water Board regarding the same.

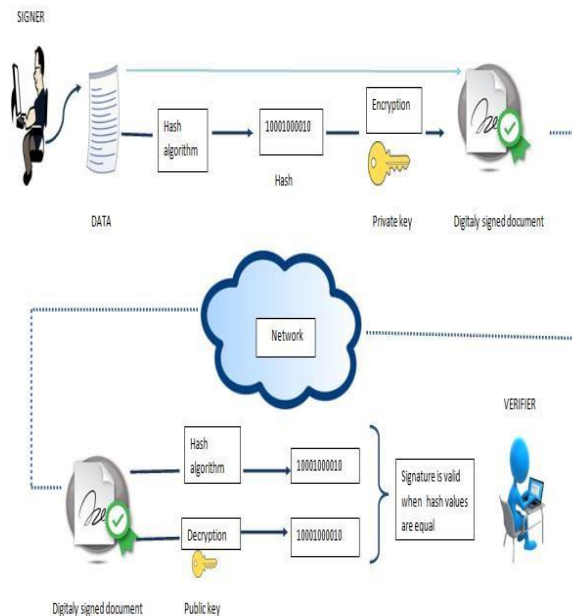


Figure 3. Hashing, Encryption and Validation of data and blocks.

V. THE PROPOSED SYSTEM AND BLOCKCHAIN IN THE NETWORK

Like a typical Blockchain network, the role of the miners in the proposed remains the same, validating the data before the block is added to the existing chain, using various algorithms. The miners, here are operating without any incentive, so likely to be a government official.

Hashing and encryption of the data and adding digital signatures, is done just like in any quintessential block chain network, illustrated in Figure 4 above.

The network of nodes (discussed earlier) is decentralized and therefore enables the usage of block chain. The blocks here refer to any group validated transactions which contain data about the amount of water received and amount of water used by the nodes in the network. With the data from the Water Board regarding the distribution of water to the respective

areas, each node can check if their area has received the equitable share from the main water distribution board, and if their house or building has received the equitable share of water from the area-wise pumping station.

The distribution of water to each area is ascertained by the population density of the area. The data on the population distribution and density is processed using an algorithm which partitions the total water available to the areas in such a way that the ratio of water supplied to that of population, is maintained constant for all the areas.

With the data broadcasted from the three nodes (Water Board, R and B, Population Board) each node is open to run some simple algorithms to calculate the rightful amount of water it, or the area the node (building with water connection) is in, should receive. With this information each node is capable to validate any transaction. A typical transaction in this system would contain the details about the water received and consumed by a node and the corresponding charge for the usage. With these details the payment for the water usage by a node is done to the Revenue and Billing through crypto currency.

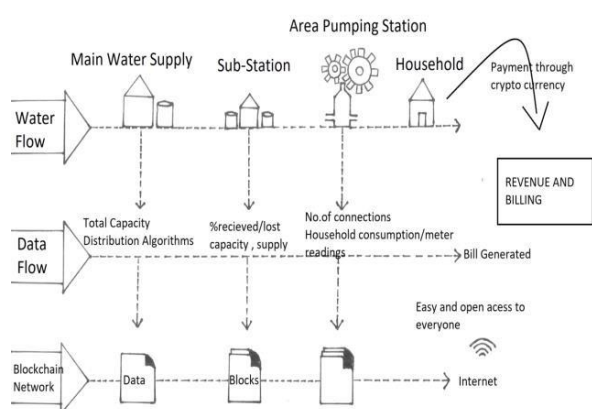


Figure 4. Flow of data in the network

VI. ADVANTAGES OF PROPOSED SYSTEM

A Transparency

As block chain is a distributed, peer to peer network, all data is accessible by all the peers in the network. So through this all people can know how much water they are allotted. Hence equality is assured.

B Scalability

Once the system has been implemented in a city, the addition of new nodes or the increase in the network is accommodated with relative ease and doesn't affect the functional performance of the system.

C Incorruptible

Falsification of data is almost impossible to achieve in a network implementing blockchain. Therefore hacking the network or any other malicious activities are futile.

D Detection of leakages or pilferages

Using the system, the net consumption of water can be easily determined, with this data any abnormalities are evident and can be identified, these include leakages and pilferages.

VII. LIMITATIONS OF PROPOSED SYSTEM

A. Complexity

Blockchains technology involves an entirely new vocabulary. Thankfully, there are several efforts at providing glossaries and indexes that are thorough and easy to understand.

B. Reliance on Government Bodies

Though the network of peers are open to access the data regarding water consumption, the government (Water Board) still is the unit which relays the original data (Total amount of water available to the city). This might pave way to bureaucracy and bias.

C. Need for a basic water connection already in place

This system can be implemented only if there is a proper water connection system already in place in the city (With water measurement meters, pumping stations etc). Otherwise, the installation of such a

system is essential for the implementing the proposed system.

D. Favorable to people with access to technology

Though the system might solve the problem of unfair water distribution, the people who don't have access to technology (smart phones, computers) might still not be direct participants of the network; hence they are at the mercy of others to ensure that they get their rightful share of water.

VIII. FUTURE PROSPECTS

A. Payment

Cashless payment, crypto currency promises to be the norm in the future. Lots of technical advancements in this field are almost certain to happen, and these advancements can easily be implemented in the proposed system as well.

B. Automation and Prediction

After the system is in place, up and running, there are a lot of features that could be added to enhance its functionalities.

Developments in IOT and machine learning are on the rise, with proper implementation, IOT can be used to automate the entire distribution system and Machine learning, to predict patterns of draught and water availability to ensure better preparedness.

IX. CONCLUSION

With water being a scarce commodity of late, it is paramount that everyone gets their rightful share and uses it wisely. Hence we require a sustainable water management/distribution system.

With the proposed system in place, fair water distribution in a city is certain. This system in combination with right knowledge about block chain among people can solve most of the problems of the current water managing/distribution system. By using blockchains as the building block, this

system ensures an equitable and secured water distribution system.

As blockchain is emerging out as a new technology, much advancements will be made in this field. This will help the proposed system enhance its functionalities so that most of the limitations can be overcome.

X. REFERENCES

- [1]. Blockchains and smart contract for internet of things-DOI10.1109/Access.2016.2566339.
Source:IEEE Xplore
- [2]. What is blockchain technology? - <https://blockgeeks.com/guides/what-is-blockchain-technology/>
- [3]. The energy block chain: How blockchain could be a catalyst for the distributed grid. - <https://www.greentechmedia.com/.../the-energy-blockchain-could-be-a-catalyst-for-the-distributed-grid>
- [4]. Distributed ledger technology: beyond block chain - <https://www.gov.uk/government/...data/.../gs-16-1-distributed-ledger-technology.pdf>
- [5]. In India, water problems are 'man made': Comments on the draft water policy-2012-
- [6]. www.indiawaterportal.org/articles/india-water-problems-are-man-made-comments-on-the-draft-water-policy-2012

Introduction to Mobile Cloud Computing and Battery Optimization in Mobile Devices

Nidheesh. S. N¹, Namitha. N. Deshpande²

¹Department of Computer Science, PES University, Bangalore, Karnataka, India

²Department of Computer Science, PESIT BSC, Bangalore, Karnataka, India

ABSTRACT

With the recent advances in the field of science and technology, there has been a steep increase in the number of people using smartphones connected to the internet. This has opened up countless new possibilities to be explored in the field of Mobile Cloud Computing as a potential technology for mobile network providers and cloud computing services. The basic framework of the Mobile Cloud Computing is to integrate cloud services in the mobile environment providing the user with a multitude of benefits such as increased battery life, increased storage and bandwidth, decrease in the power consumed by the mobile device, with increased security and privacy of the user's data. In this paper, we give an overview of the definition and architecture of mobile cloud computing and explore the possibilities of the implementation of this technology in increasing the battery power of a mobile device.

Keywords: Mobile Cloud Computing, Computational Offloading, Battery optimization, Power Consumption

I. INTRODUCTION

A. What is Cloud computing?

Cloud computing is an Information Technology model which enables the user to access the configurable system resources and also avail higher level services with least management effort and comparatively faster speed, often over the Internet. This has led to the development of mobile device applications such as Google Apps, Twitter and many more renewing the way we make use of Communication Technology. Cloud computing is all about sharing resources to attain consistency and carrying out tasks with greater efficiency with increasing size or speed of operation. Third-party clouds help the organizations to focus on their main/essential business rather pay out unwanted time on computer framework and maintenance. Sometimes the administrators might incur unexpected operating expenses, to overcome this issue cloud provides "pay-as-you-go" model. After the launch of Amazon EC2 in 2006, there has been significant

amount of growth in this field due to availability of high holding ability networks, low-cost computer devices and storage spaces as well as virtualization, service-oriented architecture and self-governing and utility computing.

B. Advantages and benefits of cloud computing

- The Organisations need not invest on data centres and servers, instead only pay when they make use of/consume resources (pay-as-you-go).
- Hundreds of customers are aggregated in the cloud, which helps the organisations to focus on their core business.
- Organisations using cloud computing can eliminate the task of guessing the infrastructure capacity. It helps the user to access as much or as little as needed.
- In this environment, the resources just a click away which reduces the access time from weeks to just a few minutes

- It allows the organisation to focus on their customer needs and not on infrastructure expenses.
- It is easy to utilize your application in multiple regions in just a click away.

C. Mobile Cloud Computing

- A combination of cloud-computing along with mobile-computing which is a human-computer interaction enabling data transmission and wireless networks, to not only provide business opportunities to mobile network providers and cloud computing companies but to unify a plethora of information which can be accessed unrestricted, with infinite storage and mobility which can be used by any mobile device anywhere with an internet connection, regardless of heterogeneous environments and different platforms.
- Basically mobile cloud computing uses cloud computing to deliver applications to mobile devices. Using a cloud, applications can be built, revised and sent to various devices with different operating systems. Thus every mobile device can access applications via the mobile cloud which otherwise cannot be supported.
- Mobile cloud computing enables users to have a secure and fast connection to a sea of integrated information from various sources regardless of the place of origin or where it resides. When a mobile application is created and made public, the IT^[18] professionals usually do not have the resources to maintain and manage the application. However the mobile cloud providers help them run the application whilst allowing modifications and updates to the application. Demanding applications put a strain on the device and reduces its performance. Integrating a flexible

cloud infrastructure will help with difficult workloads.

- Mobile devices (E.g., Smartphone and tablet PC) are increasingly becoming an essential part of day to day human activities as the most effective, efficient and reliable communication tools. Not bounded by time and place of usage.

Table 1

1	MCC	Mobile Cloud Computing
2	BTS	Base Transmission Station
3	HA	Higher Architecture
4	IP	Internet Protocol
5	LaaS	Infrastructure as a Service
6	PaaS	Platform as a Service
7	SaaS	Software as a Service
8	AWS	Amazon Web Service
9	GCP	Google cloud Platform
10	SSS	Simple Storage Service
11	GAE	Google App Engine
12	AMR	Amazon Map Reduce
13	RPC	Remote Procedure Call
14	VNC	Virtual Network Computing
15	PC	Personal Computer
16	RBF	Remote Buffer Framework
17	Power	Consumption Difference
18	IT	Information Technology
19	API	Application Program Interface

II. WORKING PROCEDURE

A. Mobile cloud computing architecture

From the concept of MCC ^[1] we can draw a general outline of the architecture present as shown in Figure 1. Any given mobile device connected to the internet by the mobile network has a base station which can be an access point, satellite or a BTS^[2] that establish a link between the mobile network and the mobile device. When a mobile user requests information, the

central processor transmits a signal to the servers that are connected to the mobile network providers.

Once the request is received by the mobile network providers they provide services such as authorization, authentication and accounting based on the HA [3] which acts as a router and provides information based on the user's location so that the IP[4] address does not have to change every time the user connects to the internet and the information of the user which is already stored in their database.

The processed information is provided to the user via the cloud services. This mechanism is also known as tunnelling. The cloud has service oriented architecture with the support of API's [19] and multiple programming models which benefits the end user with the required information. It also involves creating market oriented clouds and a web based delivery system in the clouds.

The details of cloud architecture can be explained using the TrustCube architecture, E-Recall architecture, Layered architecture, Open Mobster architecture and many more. But in this paper we focus on the Layered and Open Mobster architecture of mobile cloud computing.

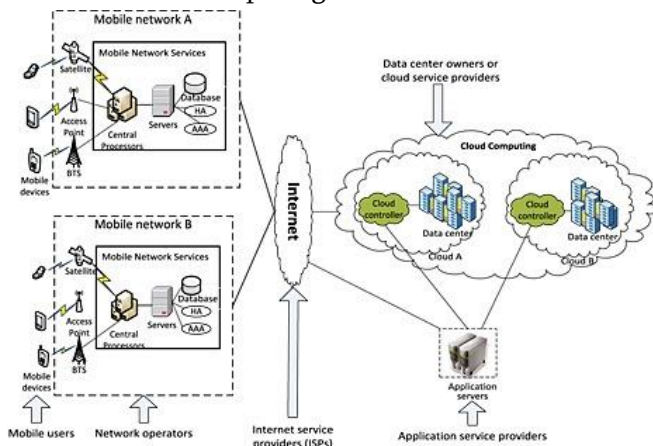


Figure 1. Architecture of Mobile Cloud Computing

We first focus on the Layered Architecture which contains in its upper layers, Infrastructure as a Service[5] (IaaS), Platform as a Service[6] (PaaS) and

Software as a Service[7] (SaaS) along with data centre layer.

- 1) IaaS : Here the cloud service provider usually hosts information that is present in an on-premises data centre including a virtualization and hypervisor layer supporting servers, storage and a networking hardware system. When a user prefers IaaS, then he has a pay-per-use basis where he pays only for the services used. Thus clients save cost as they pay for only the services used. Amazon Web Services [8] (AWS), Google Cloud Platform [9] (GCP), Simple Storage Service [10] (SSS) are some of the private providers for IaaS cloud services. This kind of a cloud structure can be dynamically shrunk or expanded according to the users need.
- 2) PaaS : This gives the users an advanced platform to build, repair, test and deploy custom applications. Here the third party provides the hardware and software tools required for the application development over Platform as a Service cloud computing. Hence the client does not have to externally install the tools that are required to run the new application. It helps provide a resilient and optimized environment where key processes such as the application hosting and java development can be provided by the cloud services. Platform as a Service cloud computing also enables development teams not present at the same location to work together on a same project. Google App Engine [11] (GAE), Microsoft Azure, Amazon Map Reduce [12] (AMR) are some of the cloud services providing PaaS.
- 3) SaaS : It is a distribution model in which an external third party provider hosts and maintains the application and makes it available to the user over the internet. It supports a software distribution model with custom and specific requirements. This model

eliminates the cost of hardware acquisition which the companies will require if they run and maintain the applications on their own servers. It also provides services such as software licensing, installation and support. Salesforce is a leading SaaS^[10] provider. To allow multiple sharing folders and files simultaneously Microsoft's Live Mesh is also preferred.

- 4) Data Centre Layer: A hardware facility and cloud infrastructure is provided by this layer. A plethora of servers linked to a high speed broadband are maintained in the data centre to provide services to the client. In most cases, a data centre is built in places where there is high power stability and where the risk of disaster is next to zero.
- 5) The data centre layer plays a crucial role in this layered architecture due to the fact that some sort of a hardware backup is always required in case the software is hacked or it fails. It also contains lots of servers holding up the cloud.

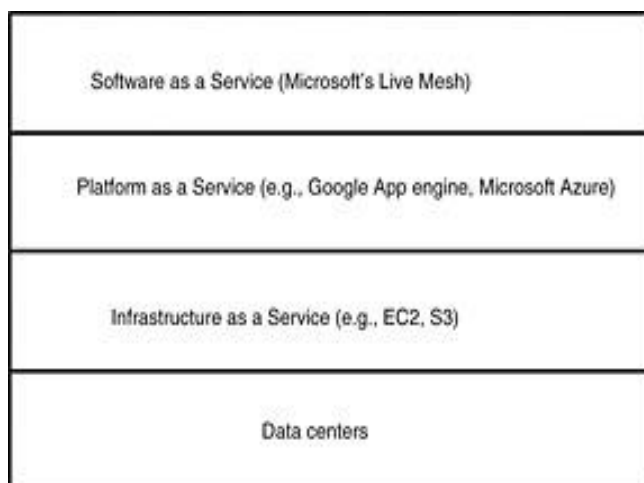


Figure 2. Layered Architecture of Mobile Cloud Computing

Although the Mobile cloud computing architecture is layered, it is not necessary that the top layers need to be built on the layers below it. Services provided by one layer maybe provided by other layers also. For example data storage facility is provided by both the

IaaS^[5] and the PaaS^[6] mobile cloud computing models. Overall, the layered architecture provides the users with flexibility and reliability.

B. Open Mobster Architecture

The open mobster architecture is an advanced cloud based platform that can be used for the incubation and development of cloud connected mobile applications. It aids in the seamless transition and synchronization between the data that is present in the cloud and the information that is available in the device. It provides a basic body framework for the production of end-to-end Location Aware Apps. It provides features such as RPC ^[13] (Remote Procedure Call) which is essential in invoking cloud based services in a mobile device connected to the internet. It is a server-side layered business structure where any low level programmer can become an app developer using cloud based services on the open mobster platform. There is a fixed RPC - API structure that is used to maintain the procedural calls.

The method of uniting cloud data and information stored in the mobile so that the client has unrestricted access to the information is categorised under the following procedures

- 1) Sync: It is maintained and controlled on the open mobster platform. Any changes made to the data present on the mobile device or on the cloud is automatically backed up and synced. Changes made will appropriately be reflected the next time the user boots up the application or according to the setting set by the user
- 2) Offline Application: An offline application is an unrestricted and secure platform to coordinate between low level services. Once the users set the setting to sync automatically, the application will manage all synchronisation settings
- 3) Network: It is a channel and a medium of communication between the cloud based

services and the mobile devices. The underlying functioning of network need not be explained

- 4) Security: The in-built security component provides authentication and authorization services to confirm if the device which has requested for the information has in fact the clearance to access the information that is present in the cloud. A device needs to be securely provisioned before it has access to the cloud system. Once it has registered the credentials, it must be stored in a secure database so that it can be verified every time the user requests information

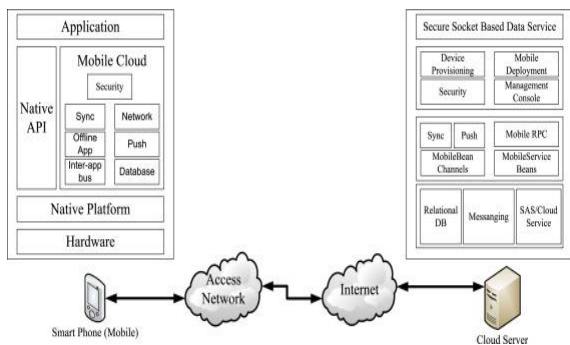


Figure 3. Open Mobster Architecture of Mobile Cloud Computing

Overall the open mobster has some similarities compared to the layered architecture system but it includes more features and has a better user interface.

III. OPTIMIZATION

A. Computational Offloading to Extend Energy in Mobile Devices

Energy efficiency is a basic factor for mobile devices. Poor processing ability and limited energy have become serious issues for Smartphones. To overcome these issues, efforts have been made to offload the tasks from mobile client onto the cloud with greater computational ability. The mobile devices in traditional computational ability find it difficult to execute high-bandwidth occupying videos; we can overcome this issue by offloading complex tasks onto

the cloud to minimize the computation time required and battery usage. Here we are going to focus on computational offloading, which can be used to save energy in battery dependent devices i.e., mobiles. An input device, namely, a Virtual Network Computing [14] (VNC) client is loaded onto the local mobile device and connected to the VNC [14] server, which is installed in the cloud. This reduces the energy consumption in devices by 67.19% when compared to traditional methods.

Previously, mobile devices were only used to send text messages or to make calls. They did not support any kind of applications. Due to the tremendous growth in the field of web and multimedia recently, mobile devices have gained enough preparation ability, an efficient battery and other such factors. Mobile devices are made to use cloud services along with mobile environment which together is termed as Mobile Cloud Computing (MCC) [1]. There are many applications accessing cloud services today, namely, Gmail, Google Maps, Microsoft Live Mesh, Apple's MobileMe and many more.

There are four essential methodologies implied to spare the energy and expand battery life

- Adopting new semiconductor technology
- Forbear from wasting energy
- Execute programs slowly
- Eliminate computation altogether

B. Offloading Computation to Save Energy

Transferring computation from one device to another is not an ideal thought. Presently, the popular client-server model is mobile client servers to ship web browsers, search the internet and shop on the web. Rather than service providers supervise the programs that are currently running on their servers, virtualization allows the cloud owners to run self-decisive applications from varied clients on virtual devices.

Computation Offloading is a system that transfers resource-intensive computations from a mobile device to server or cloud. Cloud based computation offloading enhances applications processing ability, utilizing less battery and performs tasks that were not able to execute previously due to lack of mobile services. Also, cloud provides storage services. As demonstrated in the architecture part, combining mobile environment with cloud computing determines a collection of issues and problems, with real difficulties to be resolved.

In cloud computing, the hardware is sufficiently capable to handle the services and facilities, however for the mobile devices, the software is less compatible than what is required. Hence, mobile devices alone cannot perform the complex computations in required execution time. The amount of mobile gadget clients and mobile application offerings are rising real quick. Nowadays, everybody use smartphones. These devices have capacities equivalent to those of modern day PC's. However, there are limitations for mobile devices.

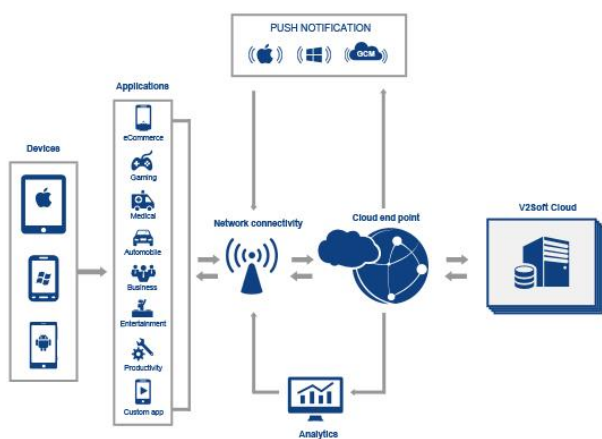


Figure 4. General Architecture of Mobile Cloud Computing

C. The Proposed Model

The framework architecture is the novel model that characterises the structure, behaviour and other features of the bodywork. A construction modelling is a formal description and representation of a framework. The framework architecture involves

system components, properties of these components and the connections between them.

The novelty of our proposed system is that it not only considers resource utilization and future consumption demand, but takes offloading based decisions considering factors like delay tolerance, favourable network bandwidth, cloud capacity and energy consumption. This makes the proposed model better than already existing traditional offloading framework. Fog computing (Cisco, 2013) provides the type environment to users where they can store and process their application using the resources available in the neighbouring devices, creating cloud like environment. The proposed framework suits very well with fog and edge computing application thereby reducing the load on host device making it more user friendly. Issues related to limited battery life can be resolved by virtualization. The local machine can be a laptop or PC [15]. A remote machine can be workstation.

Figure below shows that the cloud is an enormous layer of new and large number of services. The act of accessing a remote servers system, instead of a local server or PC [15], provides storage, processing and overseeing of information. In the cloud, virtual images from mobile devices are stored, starting in the physical mobile device. Whenever a particular application containing the image is accessed from physical mobile device, essential parameters such as execution time, memory usage, power consumption and so on are estimated. If offloading is enabled, then the control is passed onto series of input events of VNC [14].

At the same time, the application is run remotely, the output is sent to physical mobile device as video stream utilising VNC. VNC is a graphical desktop sharing system that utilises the RBF [16] protocol to remotely control alternate device. It transfers the

mouse and console events starting from one device onto the next.

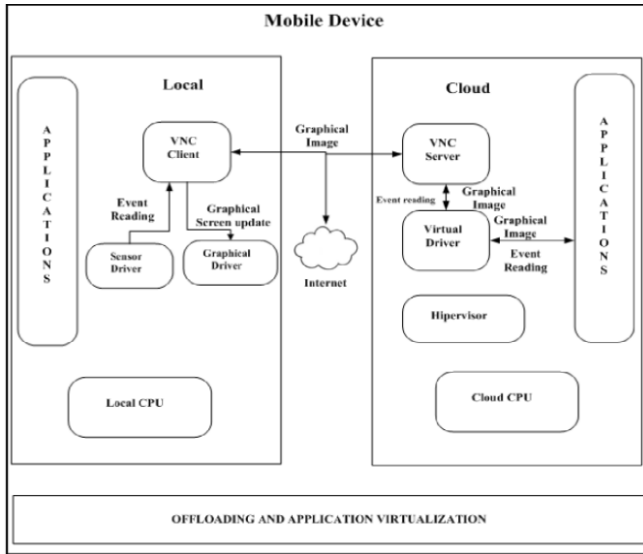


Figure 5. Novel Software Architecture for Offloading

D. Analysis of Energy for Offloading

For offloaded services, the energy consumption for offloading should not be greater than the power of execution.

- Let us assume that there are E computation instances. Let S_c be the speed of cloud server, S_m be the speed of mobile device.
- The task takes E/S_c seconds on the server and E/S_m seconds on the mobile device.
- Let B be the bytes of information traded by cloud and the mobile device, BW be the bandwidth, it takes B/BW seconds to transmit the information.
- Assume mobile expends P_c watts in figuring, P_i for idling and P_{sr} for sending and receiving information.
- Available primary memories are S_x And S_y , average execution time is T_x and predicted tolerance delay is T_y . E_l And E_c is the power consumption by local mobile device and cloud respectively.

There is a necessity for an application to execute in cloud if the following three conditions are true

1. $S_x > S_y$
2. $T_x > T_y$

3. $E_l > E_c$

The bandwidth of the network should be higher to transfer and receive data. If all the above mentioned conditions are met, then load the application to the cloud.

Total Energy = $E_c + \text{Energy}_{(\text{offloading})}$

Energy is saved when the bandwidth is sufficiently large. T_x should be tolerable both during offloading and execution. Every time the application is accessed on physical mobile device, basic measurements such as execution time (T_x), size of the application (S_x) and delay tolerance (T_y) are calculated.

E. Calculation of Energy Consumption in Local Devices

We have to make note of the current available capacity of our system before running an application. Only then the application should be executed. After completing the execution of the application, take note of the capacity. An important thing to be taken care of is to terminate all the background applications. Finally, calculate the difference between two capacities to find out the total power consumption.

F. Calculating Power Consumption in the Cloud System

We have to make sure that all the background running applications are terminated. Using the IP address and password establish a remote instance, login is validated to access the cloud. Before running the application, the current capacity is noted down. Only then the application is executed. In the cloud system, select the application to be executed. After completion of execution, note the capacity of the system. Finally, calculate the difference between these two capacities to find out the total power consumption. (table of values)

To calculate the Power Consumption Difference (PCD) [17], take the difference between total power consumption of cloud and local device. The results

show that the power consumption can be reduced by offloading complex applications to the remote cloud. Much energy can be saved, which indicates that the user can have longer battery life compared to local execution.

Table 2

T_{ex} (in hrs)	E_{ecl} (in mWh)	E_{ecc} (in mWh)	% of energy saving
0.5	8,333	3,131	62.00466
1.0	11,134	3,705	66.3565
1.5	12,600	3,849	69.11614
2	14,841	4,214	71.29145

Notes: T_{ex} : time consumed to execute the video application (in hrs).
 E_{ecl} : energy consumption from local execution (in mWh).
 E_{ecc} : energy consumption from remote cloud execution (in mWh).

Let us consider a local machine running a video that is stored in the device. The energy consumed by the central processing unit is shown by the blue line and whereas the power consumed when it is streamed from the cloud is shown by the red line. We can see how there is significantly less power consumed when it is streamed from the cloud.

This is represented in figure shown below. It is a graph showing the power consumed by a device during local execution and power consumed by the device during remote cloud execution.

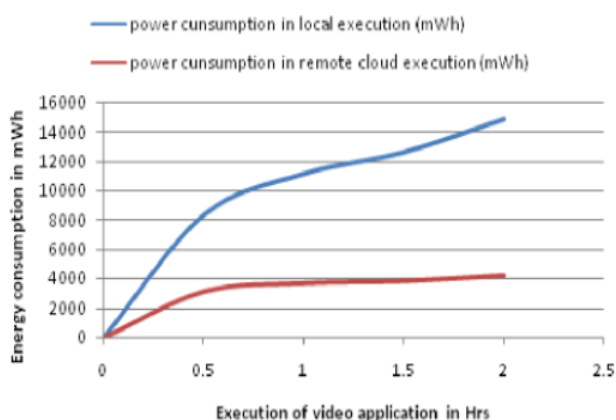


Figure 6. Graph comparing power consumptions

IV . APPLICATIONS

A. Mobile Cloud Computing Applications

- 1) Mobile commerce: For commerce using mobile devices, we use a business model, mobile commerce (m-commerce). The m-commerce applications generally handle tasks such as mobile ticketing, mobile payments and transactions, mobile messaging and so on. They are used in many classes and hence their functioning can be divided as shopping, finance and advertising. These applications have to overcome numerous challenges such as high complexity of mobile configurations, low network bandwidth and security. Hence these applications are integrated with cloud computing.
- 2) Mobile learning: Mobile learning (m-learning) is based on the concept of electronic learning and mobility. Traditional m-learning applications have many drawbacks such as insufficient educational resources, low transmission rate, high cost of networks and devices. Cloud-based m-learning applications are introduced to resolve these issues. For example, accessing a cloud with large storage capacity provides learners high processing speed, richer resources in terms of data size and longer battery life. Another application of MCC [1] in learning implemented for researches and undergraduate genetics students is “Cornucopia” and “plantation pathfinder” implemented to provide collaborative spaces and information for visitors visiting gardens.
- 3) Mobile healthcare: To minimize the limitations of traditional treatment, we use applications of MCC [1] in medical field. Mobile healthcare (m-healthcare) assists the user in maintaining patient health records, saving storage space and also privacy of the services provided. There are mainly five health care applications provided by MCC in the present environment, namely, Comprehensive health monitoring services,

Intelligent emergency management system, Health-aware mobile devices, General access to health-care records, General lifestyle incentive management

- 4) Mobile Gaming: Mobile game (m-game) is a potential market for service providers. We can offload game engines requiring large resources such as graphic resources to the cloud with the help of m-game. Offloading can save significant amount of energy, which increases the playing time for the user. The objective is to increase the user's experience considering the communication and computing costs.
- 5) Other practical applications: These may include Keyword-based searching, Voice-based searching, Tag-based searching

In addition, there are MCC ^[1] applications used to detect traffic lights for the blind, to control different corners in house using a mobile device and many more. Thereby, we can conclude that MCC ^[1] is probably a current technology with enormous applications in the near future.

V. CONCLUSION

Mobile Cloud Computing is one of the technologies of the future as it combines the best features of both Mobile Computing and Cloud Computing. It provides us with an elegant solution to the battery problems and limitations in the modern day smartphones and gives us an efficient solution to the storage problems. That traction will push the revenue of Mobile Cloud Computing to \$5.7 billion.

With that in mind, this paper has provided a brief overview of this potential technology and how it has applications in not only the security but also in the e-commerce and healthcare sectors.

We wish to conduct more research on specific applications of MCC which will play an important

role in the implementation of this technology. Finally the future research details have been outlined.

IV. REFERENCES

- [1]. ProfDinh, Hoang T.; Lee, Chonho; Niyato, Dusit; Wang, Ping, "A survey of mobile cloud computing: architecture, applications, and approaches" , *Wireless Communications & Mobile Computing* , Volume 13 (18)-Dec 25, 2013
- [2]. Khan, Atta ur Rehman; Othman, Mazliza; Khan, Abdul; Abid, Shahbaz; Madani, Sajjad, "MobiByte: An Application Development Model for Mobile Cloud Computing" *Journal of Grid Computing* , Volume 13 (4)-Apr 23, 2015
- [3]. Wang, Ning; Wu, Jie, "Maximizing the user's benefit in the mobile cloud computing" *Association for Computing Machinery* — Oct 3, 2016
- [4]. "Mobile cloud computing: innovation and creativity perspectives" *International Journal of Technology Marketing*, Volume(12) 1- Jan 1,2017
- [5]. Bahl, Paramvir; Han, Richard Y.; Li, Li Erran; Satyanarayanan, Mahadev, "Advancing the state of mobile cloud computing" *Association for Computing Machinery* — Jun 25, 2012
- [6]. Hayes, Brian, "Cloud computing" *Communications of the ACM* , Volume 51 (7)-Jul 1, 2008
- [7]. Ko, Jaejun; Lee, Jongwon; Choi, Young-June, "Computation offloading for energy efficiency of smart devices" *Association for Computing Machinery* — Sep 11, 2017
- [8]. Thanapal, P.; Durai, M.A. Saleem, "Energy saving offloading scheme for mobile cloud computing using CloudSim" *International Journal of Advanced Intelligence Paradigms* , Volume 10 (1-2): 18-Jan 1, 2018
- [9]. Vakiliinia, Shahin; Qiu, Dongyu; Ali, Mustafa, "Optimal multi-dimensional dynamic resource

allocation in mobile cloud computing" EURASIP
Journal on Wireless Communications and
Networking , Volume 2014 (1)-Nov 28, 2014

- [10]. Rupinder Pal Kaur Amanpreet Kaur Assistant
Professor, Assistant Professor Guru Nanak
College for Girls, Guru Nanak College for Girls,
Sri Muktsar Sahib, Punjab Sri Muktsar Sahib,
Punjab, "Perspectives of Mobile Cloud
Computing: Architecture, Applications and
Issues" International Journal of Computer
Applications (0975-8887) Volume 101– No.3,
September 2014

Tuning and Analysis of PID Controllers Using Soft Computing Techniques

Bajarangbali, Sujay H S, Suman R, Chaithanya S, Narayanan S, Shamanth U

Department of Electronics and Communication, PESIT-Bangalore South Campus Hosur Road, Bangalore, Karnataka, India

ABSTRACT

In this paper, we are looking at a method to tune a PID controller given that we know the system transfer function beforehand. Here we will be tuning the controller using soft computing methods which involve Particle Swarm Optimization (PSO) and Genetic Algorithms (GA). These techniques like PSO and GA are very well known to find the best global minima. Thus, such a feature of these techniques is used to minimize the errors such as IAE (Integral Absolute Error), ITAE (Integral Time Absolute Error) and ISE (Integral Squared Error). By reducing the errors, the best value for the three PID parameters, K_p , K_i and K_d are determined. The PID controller will be tuned for linear processes with and without time delay.

Keywords: Genetic Algorithm (GA), Particle Swarm Optimization (PSO), IAE (Integral Absolute Error), ITAE (Integral Time Absolute Error), ISE (Integral Squared Error).

I. INTRODUCTION

A PID (Proportional Integral Derivative) controller is a feedback type of controller which is used in many industrial applications. The PID controller continuously calculates the error and applies a control signal based on the Proportional, Integral and Derivative Gains and hence the name “PID Controllers”.

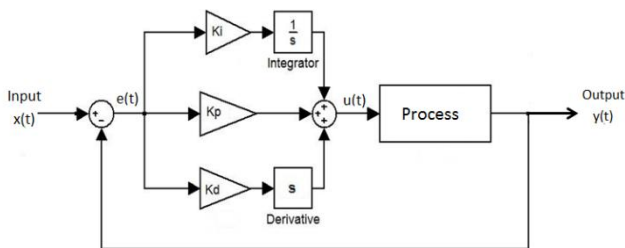


Figure 1. PID Controller Closed Loop System

The PID constitutes three critical parameters, proportional, integral and derivative gain denoted by K_p , K_i and K_d respectively. In brief, effect of each of the coefficient is as explained below:

Proportional Parameter (K_p): The proportional gain term is directly proportional to the present error produced by the system. Here, the error is the deviation of the output from the set-point value. It is like the ratio of the output value to the error value. Increasing this increases oscillations which will never settle, but makes the system response much faster.

Integral Parameter (K_i): The integral gain parameter calculates the error over a certain period of time. Thus, the output produced by the I term is not only dependent on the present output but also on the past output values. This helps greatly in eliminating steady state error.

Derivative Parameter (K_d): The derivative gain term comes into action when the rate of change of error is large. Thus, the D term is regarded to see the future errors and reduce them. Increasing the derivative term makes the controller more aggressive and hence must be used with caution.

All the three terms, i.e., proportional, integral and derivative terms are summed to compute the output of the PID controller. If, $u(t)$ is regarded as the controller

output, the PID controller can be represented mathematically as:

$$u(t) = K_p \cdot e(t) + K_i \int_0^{\infty} e(\tau) d\tau + K_d \cdot \frac{de(t)}{dt} \quad (1)$$

In the Laplacian domain, the PID controller is represented as:

$$L(s) = K_p + \frac{K_i}{s} + K_d \cdot s \quad (2)$$

System Performance Assessment

Academic measures are ones that are calculated on paper based on the expected response from the system. The three measures are IAE (Integral Absolute Error), ITAE (Integral Time Absolute Error) and the ISE (Integral Squared Error).

Mathematically, they are given as:

$$ISE = \int e^2(t) dt \quad (3)$$

$$IAE = \int |e(t)| dt \quad (4)$$

$$ITAE = \int t \cdot e(t) dt \quad (5)$$

ISE - This error type calculates the integral over the square of error in time. It is found to help in correcting sufficiently large errors that are present for a short period of time, rather than those small errors which can last either for short or long period of time. Hence quick responses can be achieved, but small percentage of steady state oscillations will be present.

IAE - Similar to ISE, it only integrates the absolute value of error over time instead of the square of error value. It is helpful in reducing constant errors or small persistent oscillations. It does however produce slower responses.

ITAE - This error calculates the integral of the time weighted absolute value of the error over time. It can be definitely more tedious to calculate, but is often used as it produces the best results in most cases. It eliminates errors that are persistent for large period of time as it weights heavily for those errors at a later

period of time than those at the beginning. But, initial response is found to be quite sluggish which are quite essential to reduce the sustained oscillations.

II. IMPLEMENTATION

A. Soft Computing

Soft computing, in computer science is a method to find out the inexact solution to really hard problems. These solutions are generally an approximation that include uncertainty and are partially true.

Soft computing techniques include Evolutionary Computation (EC), Fuzzy Logic (FL), Probabilistic Reasoning (PR) and Machine Learning (ML).

In our study, we have chosen Evolutionary Computation. Evolutionary Computation involves algorithms that are inspired biologically, i.e., we have 'tried' to copy the way humans or living organisms interact with nature and one other. The copy is undoubtedly not accurate as a lot of research is still going on in the current field and only about 20% of the actual reason for human evolution, interaction with nature and one another could probably be justified. These algorithms can also be considered as a sub-field of artificial intelligence.

The algorithms we have considered under Evolutionary Computation are:

1. Genetic Algorithm
2. Particle Swarm Optimization

These algorithms look to solve many minimization problems (can also be maximization). They are believed to be really good at finding the global minima (or maxima) rather than ball parking in and around local minima's (maxima's). Thus they are employed where there is no known algorithm that can compute the exact solution in polynomial time. These algorithms initially start with random initialization of population (in case of genetic

algorithm) or swarm (in case of Particle Swarm Optimization). Then the algorithm is repeated iterative steps until the best possible solution is found. Thus to apply these algorithms to our Tuning of PID controller, we must thus define an “OBJECTIVE FUNCTION” which has to be minimized.

We have already discussed the four different types of errors (ISE, IAE, ITSE, ITAE). So, now we must define when and where which error must be used as the objective function.

B. Error Selection

To apply evolutionary computation for the tuning of PID controllers, the system transfer function must be known. Since the system is completely known before we begin our tuning process, we have to analyse the system. An analysis must be done such that it leads us to the correct selection of error definition to be used as our objective function.

In case the system response shows a large deviation from the set point, ISE criteria should be used because squaring the error term contributes more to the cost which eventually drags the optimization algorithm towards a set of controller parameters that ensures minimization of that cost. In case of small deviation errors, squaring the term would actually reduce its contribution to the cost. Hence IAE criterion is used for such cases. When the error persists for a long time, ITAE criterion helps because the presence of time as a multiplier to the error term actually augments its effect on the cost term at high values. Generally ITAE criterion is not used because time is not under anyone’s control and squaring of time as it increases only shows larger errors and affects the objective (cost) function negatively.

To get a quantitative measure of the objective function, the following steps are followed:

1. For the given open loop transfer function, step response is plotted.
2. The step response is analysed.

3. Based on the above mentioned criteria, a suitable cost function is determined, i.e. either ISE or IAE or ITAE.
4. The selected cost function is minimized and thus the controller parameters are tuned.

Once, we have finalized the objective function, we run the algorithm and verify our results.

C. Genetic Algorithm

The Genetic Algorithm procedure is as follows:

Step 1: [Start] A random population of chromosomes are generated which represents the total number of solutions that are required for the problem.

Step 2: [Fitness] The fitness of each of the randomly created chromosome in the population is evaluated.

Step 3: [New population] A new population is created by repeating following steps till the new population is complete:

- [Selection] Select any two parent chromosomes from a population based on their fitness. It is generally taken as better the fitness, bigger is the chance of a chromosome to be selected as the parent.
- [Crossover] With a crossover probability rate of 4, crossover the parents to form new offspring i.e. children. If in case, no crossover is performed, offspring is taken as the exact copy of its parents.
- [Mutation] With a mutation probability of 8, mutate the new offspring at each of the locus.
- [Reproduction] Place newly created offspring in the new population.

Step 4: [Replace] Use new generated population in the previous step for a further run of the algorithm.

Step 5: [Test] If the end condition has been satisfied, stop and return the best obtained solution in the current population.

Step 6: [Loop] Go back to step 2. The generation is repeated for 100 iterations.

D. Particle Swarm Optimization

The Particle Swarm Optimization procedure is as follows:

Step 1: Initially, a random number of particles (agents) that belong to a swarm moving around in a search space looking for the best solution is setup.

Step 2: Each particle is then treated as a point in a N-dimensional vector space which will adjust its flying based on its own flying experience as well as the flying experience of the other agents.

Step 3: [pbest] Each agent always keeps track of its coordinates in the solution space which are associated with the best solution that has been achieved so far by that agent. The value of the best solution is called personal best, **pbest**.

Step 4: [gbest] Another best value that is kept track by the PSO is the best value obtained so far by any particle in the neighbourhood of that particle. This value is called **gbest**.

Step 5: PSO accelerates each and every agent toward its pbest and gbest locations hence finding the optimum solution.

III. RESULTS AND COMPARISON

Example 1

The following transfer function is considered from the paper-N A Rahman[3].

$$G(s) = \frac{-0.365s + 0.657}{s^2 + 1.642s + 1.982} \quad (6)$$

In the paper, the PID parameter values were $K_p = 2.2324$, $K_i = 2.4070$, $K_d = 1.0736$. Tuning the controller based on our proposed method, the values of K_p , K_i and K_d were respectively found to be 3.3856, 4.0761, 2.0501.

The step response of both the results are:

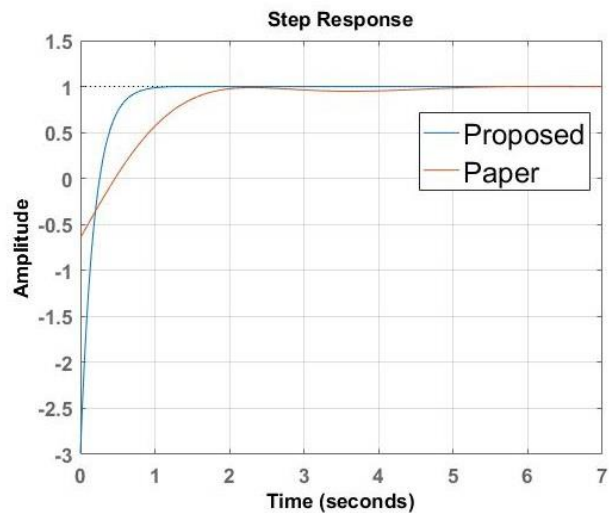


Figure 2. Example 1

Table 2: Comparison 1

	Typ e	ISE	IAE	ITAE	t_r	OS	t_s
Pape r	GA	0.04 2	0.04 4	0.01 3	1.31	0.18 3	4. 4
Prop .	PSO	0.08 0	0.03 1	0.00 4	0.41 3	NA	0. 7

Here, we can see that the rise time has a significant decrease of 68%, the settling time of 84% and 0 overshoot compared to 0.183.

Example 2

The following transfer function is considered from the paper-RuchiJain[5].

$$G(s) = \frac{1.91 \times 10^6}{s^2 + 666.7s + 1.948 \times 10^6} \quad (7)$$

In the paper, the PID parameter values K_p , K_i and K_d were 14.9, 29.93 and 29.96 respectively. Tuning the controller based on our proposed method, the values of K_p , K_i and K_d were respectively found to be 98.4, 99 and 97.6.

The step response of both the results are:

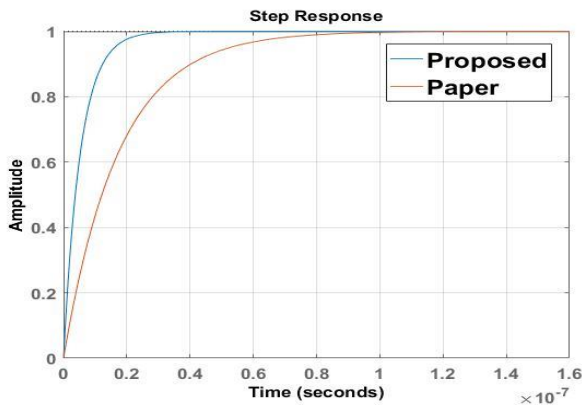


Figure 3. Example 2

Table 2. Comparison 2

	Typ e	ISE	IAE	ITA E	t_r	O S	t_s
Pape r	PSO	0.00 1	0.00 8	0.023	3.8 4	0	6.8 4
Prop.	PSO	0.00 1	0.00 2	0.003	1.1 8	0	2.1

It can be seen from the results that an improvement of 69% in rise time and settling time is achieved in the proposed method.

IV. CONCLUSION

In this paper, we looked at improving the performance of the PID controller using modern techniques such as Machine Learning's subclass which include the Genetic Algorithm and Particle Swarm Optimization. In the results that we obtained, we can say with the right choice of error selection, a much better PID controller tuning can be done. Both the academic measures such as ISE, IAE and ITAE as well as the practical measures such as settling time, rise time and peak overshoot prove that the PID controller tuned using error minimization criteria proposed in this paper, yield good results.

V. REFERENCES

[1]. Cheng-Ching Yu; Autotuning of PID Controllers. A Relay Feedback Approach 2nd

Edition; Published by Springer-Verlag London Limited 2006.

[2]. B.Nagaraj, S.Subha, B.Rampriya; Tuning Algorithms for PID Controller Using Soft Computing Techniques; IJCSNS International Journal of Computer Science and Network Security; VOL.8 No.4, April 2008.

[3]. Tengku Ahmad Faris Ku Yusoff, Mohd Farid Atan, Nazeri Abdul Rahman, Shanti Faridah Salleh and Noraziah Abdul Wahab; Optimization of PID Tuning Using Genetic Algorithm; Journal of Applied Science and Process Engineering; Vol. 2, No. 2, 2015.

[4]. Ahmad Ali and Somanath Majhi; Design of Optimum PID Controller by Bacterial Foraging Strategy; IEEE International Conference on Industrial Technology, 601 605, 2006.

[5]. Ruchi V. Jain, M.V. Aware, A.S. Junghare; Tuning of Fractional Order PID controller using particle swarm optimization technique for DC motor speed control; 1st IEEE International Conference on Power Electronics, Intelligent Control and Energy Systems (ICPEICES-2016).

[6]. Greg Birky, Thomas Mc Avoy, Bjorn Tyreus; DicodeAn Expert System for Designing Distillation Column Controls; IEEE, American Control Conference, 1989.

[7]. Deepyaman Maiti, Ayan Acharya, Mithun Chakraborty, Amit Konar; Tuning PID and PID Controllers using the Integral Time Absolute Error Criterion; 4th International Conference on Information and Automation for Sustainability, IEEE 2008.

[8]. A. Visioli; Tuning of PID controllers with fuzzy logic; IEEE Proceedings - Control Theory and Applications, 2001.

[9]. J.G. Ziegler, N.B. Nichols; Optimum settings for Automatic Controller

Determination of Dissolution of Plastic by Using Ostwald's Viscometer

Disha Anil¹, Manavi Pai¹, Anjali Deshpande¹, Revanasiddappa M²

¹Department of Information Science and Engineering, PESIT South Campus, Bangalore, Karnataka, India

²Department of Engineering Chemistry, PESIT South Campus, Bangalore, Karnataka, India

ABSTRACT

This study shows the extent of decomposition of different type of plastics or polymers when used to store hot food or beverages. By using Ostwald's viscometer, we determine the difference between the viscosity coefficients of different samples stored in polymeric substances to that of distilled water. This difference helps us assess the degree of dissolution of many polymeric materials and likely impact the choices that we make towards the betterment of our health.

Keywords: Ostwald's viscometer; viscosity coefficients;

I. INTRODUCTION

Plastic is by far the most valued invention made by man. It has become one of the most popular materials and has played an important role in the modern human society because of its many benefits. Being economical and cheap, it is preferred in manufacturing various products. Because of its lightweight and resistance to corrosion, it has replaced many other materials. Although plastic has its many advantages we tend to blindside its disadvantages. It not only harms the environment but often leaches itself indirectly into the human body. It affects both the consumers as well as the workers involved in the manufacture of it. As we reuse and recycle these materials, simultaneous degradation of the polymer occurs to very small extent. Our work aims to scientifically prove that the so called 'harmless plastic' could lead to catastrophic problems in humans and can have a gradual effect on our health.

II. EXPERIMENT

a. INSTRUMENT: Ostwald's Viscometer

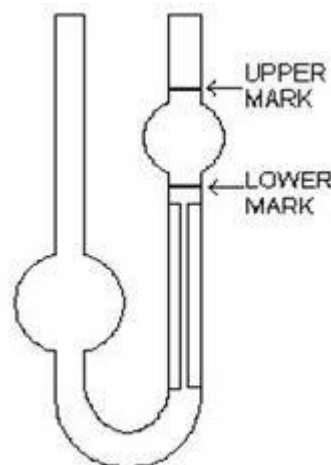


Figure 1

b. PROCEDURE:

- ✓ Heat the water 80°C and transfer it into different polymer containers whose capacity to withstand at any kind temperature is to be determined.
- ✓ Leave the water in the different polymer containers overnight.

- ✓ Now, take the viscometer, beaker and a 10cm cube pipette and clean it with water, followed by acetone. Dry these apparatus in the hot oven for 5-10 mins.
- ✓ Take them out and let it cool till room temperature.
- ✓ Take distilled water in the beaker and pipette out 10 ml of it into the wider mouth of the viscometer.
- ✓ From the other mouth of the viscometer, suck in the water until the upper mark, A.
- ✓ Calculate the time of flow of distilled water from marking A to B.
- ✓ Meanwhile, measure the temperature of the water-bath in which the viscometer is to be placed, with the help of a mercury thermometer (in °C).
- ✓ Take a few more readings for the same sample for accuracy and find the mean time of flow.
- ✓ Repeat the above procedure for other water samples stored in the different polymeric containers.
- ✓ Using the formula given below, the viscosity coefficient for each of them and compare them to that of the distilled water (which is the reference).
- ✓ Tabulate and compare the values of the water samples from different type of polymeric containers.

III. FORMULA

$$\eta_l = \frac{d_l t_l \eta_w}{d_w t_w}$$

Where d_l and d_w are the densities of the liquid and water respectively, t_l and t_w is the mean time of flow of the liquid and water, η_l and η_w are the viscosity coefficients of the liquid and water. In our experiment, the density of the sample water is

assumed to be the same as the density of the distilled water.

IV. OBSERVATION TABLE

Important Measurements:

1. Temperature of the lab= 27°C
2. Viscosity coefficient of distilled water $\eta_w = 8.545$ millipoise
3. Mean time of flow of distilled water $t_w = 63.18$ seconds

After 12 hours of storage,

Table 1

Container Used	Mean time of flow of sample water t_l (in sec)	Viscosity coefficient of sample water (in millipoise)
Plastic Bag	64.70	8.750
Tupperware	63.2	8.547
Paper Cup	63.65	8.608
Plastic Cup	64.735	8.755

After 1 week of storage,

Table 2

Container Used	Mean time of flow of sample water t_l (in sec)	Viscosity coefficient of sample water (in millipoise)
Bisleri Bottle	66.16	8.948

V. ANALYSIS

As seen in the above observation table, we have recorded and calculated the viscosity coefficients of the water samples stored in different types of containers such as plastic bag, soda bottle, Tupperware bottle, plastic and paper cup. The water samples in plastic bag, Tupperware bottle, plastic and paper cups are stored and kept in their respective containers for

almost 12 hours, whereas the water sample in the soda bottle is stored for over a week (Assuming that the drinks in the soda bottles are often consumed after a few days of packaging).

As reference, the coefficient of viscosity of distilled water is taken as 8.545 millipoise at 27 °C. From the table, the water sample from plastic bag and plastic cup records the viscosity coefficient value of 8.75 millipoise (approx.), which is almost 0.205 millipoise less than the reference value.

Water sample stored in the paper cup records a viscosity coefficient of 8.608 millipoise, which is 0.063 millipoise less than the reference value.

The closest recorded value of viscosity coefficient to the reference value is that of the water sample stored in the Tupperware bottle. The water sample from the soda bottle that was kept for over a week records a viscosity coefficient value of 8.948 millipoise, this shows the highest deflection (0.403 millipoise) from the reference value.

VI. PLASTIC BAG/CUP

a. Description: Polyvinyl Chloride (PVC) or Plastic #3 is commonly used to make plastic bags. It is the second most widely used plastic resin in the world. Its use has decreased over the years due to the serious health and environmental issues being faced. The base monomer, Vinyl Chloride, can be combined with numerous chemicals to create materials whose properties include versatility, ease of blending, strength, toughness, clarity and transparency.

b. Why We Chose: Plastic is used on a day to day basis and is often used to carry hot liquids. Due to this, there could be dissolution of plastic into the liquid which could affect our health in future.

c. Toxicity: PVC is considered the most toxic and hazardous plastic. It leaches a variety of chemicals such as Bisphenol A, phthalates, lead, dioxins, mercury and cadmium. Manufacture of this plastic puts not only the workers but the surrounding communities at risk due to the carcinogens. PVC when burnt produces dioxins, commonly known as human carcinogens, which could also cause cancer. Phthalates in soft forms of PVC often are the cause for asthma and allergic symptoms in children.

d. Use: PVC is used in manufacture of toys, take-out containers, squeeze bottles, mouthwash bottles, blood bags, medical tubing etc.

VII. TUPPERWARE

a. Description: Tupperware bottles and containers are generally made of Low Density Polyethylene or Polypropylene. Low density polyethylene (LDPE) or Plastic #4 are widely used plastics. They have the simplest structures of a plastic polymer making it easy to process. It is made from low density, branching chains of polyethylene which has properties including strength, toughness, flexibility, resistivity to moisture and ease of sealing.

Polypropylene (PP) or Plastic #5 is similar to polyethylenes but is stiffer and more heat resistant. The simple chemical structure makes it versatile and its crystallinity is high, in-between LDPE and HDPE.

b. Why We Chose: Tupperware is used to store food and water in almost every household. Not only is it used for storing food but is also used as a container to heat food in.

c. Toxicity: Being relatively stable, both LDPE and PP are considered safer plastics and are used for storage of food and drinks. LDPE when exposed to ultraviolet rays can leach the endocrine disruptor nonylphenol, which is added to LDPE as a stabilizer.

In a study, heated PP is suggested to cause asthma to the workers based on their exposure to it.

d. Use: LDPE is commonly used as grocery bags, coatings for paper milk cartons, cups and can also be used for wire and cable covering. PP is used not only as food and medicinal containers but also used in disposable diapers and sanitary pads, thermal vests and appliance parts.

VIII. PAPER CUPS

a. Description: Paper cup is a disposable cup made out of paper which is often coated with plastic or wax to prevent the leaking or soaking of the liquid through the paper. Initially clay was used to coat the paper cups, but as it resulted in the drinks tasting and smelling weird. On invention of coating the paper cup with a thin layer of polyethylene or wax to the paper cups, the coating of paper cups clay stopped.

b. Why we chose: Paper cups are used to serve beverages (hot or cold).

c. Toxicity: The wax present in the paper cup coating melts when a hot beverage is poured into it. The acids in our stomach normally flushes out the small amounts of wax ingested. If ingested in large amounts accumulates and causes obstruction in the intestine.

IX. BISLERI/ SODA BOTTLES

a. Description: Polyethylene terephthalate (PET or PETE) commonly known as polyester or Plastic #1, is the most known type of polymer. It is the most widely used polymer in the world. It is known for its properties of clarity, strength, toughness, barrier to liquid and glass. It is popularly used for food and drinks packaging as it acts as a barrier between liquid and glass. In soda bottles, it makes sure that the oxygen doesn't spoil the contents inside the bottle nor

does it allow the carbon dioxide that makes the drink fuzzy get out.

b. Why We Chose: This type of polymer is the most widely used for many different purposes which mainly include storing food and drinks. It is predicted that during this storage period, that a little of the container material might get incorporated into the stored food or drink.

c. Toxicity: PET is known to release or leach antimony. It releases more when the liquid is kept in the container for a long time and also, in warmer temperatures. It causes respiratory problems and skin irritation and in females, menstrual problems and miscarriages.

d. Use: Bottles (water, soft drink, juice, beer), jam jars, oven-ready and microwaveable meal trays, detergent and cleaner containers.

X. PLASTIC CONTAINERS

a. Description: Polystyrene (PS) or Plastic #6 is also known as Styrofoam as it is a foam puffs up with air. The monomer styrene is made up of benzene. Apart from being foamy and soft, the can be made clear, glassy and hard and can be used for harder applications.

b. Why We Chose: This is used to make foam containers as well as harder conditions. These containers are used as take-out food containers and hence there might be a possibility of getting dissolute or decomposed into the liquid or food stored in it.

c. Toxicity: Polystyrene food containers can leach styrene, which is considered to be a human carcinogen and a brain and nervous system toxicant. Studies have shown that this has effects on genes, lungs, liver and the immune system. The leaching of

styrene from polystyrene containers is increased when the food or liquid stored is hot or oily.

d. Use: Styrofoam food containers, egg cartons, disposable cups and bowls, take-out food containers, packaging, CDs & DVDs cases, hangers, medicine bottles, smoke detector housing.

XI. CONCLUSION

The outcome of this research has proven that every type of plastic decomposes to some extent. Tupperware and paper cups show the least dissolution when compared to plastic bags and plastic cups. The plastic materials used in the manufacture of Tupperware and paper cups have a lesser impact on our body. Bisleri bottles are often reused. Results have shown that the dissolution of Bisleri bottles that have been stored over a week is maximum and hence should be avoided. Although some plastics are proven to be safer than the others, it is best to replace these plastics with glass and steel.

XII. ACKNOWLEDGMENT

We would like to thank Mr.Chandrashekhar for providing the lab equipment to us to carry out this experiment. We would also like to thank the management of PESIT South Campus for allowing us to carry out this research and giving us this opportunity.

XIII. REFERENCES

- [1]. PESIT- BSC Chemistry Lab Manual
- [2]. Life Without Plastic- Common Plastics #1 to #7-
https://www.lifewithoutplastic.com/store/commo_n_plastics_no_1_to_no_7#.Wr3c4ohubIU

Simulation Tool to Determine Presence of Impurities in an Organic Compound Using IR Spectroscopy

Suyoga Srinivas¹, Ujwal Unnikrishnan¹, Yashas A¹, Revana Siddappa²

¹PESIT South Campus, Department of Information Science and Engineering, Bangalore, Karnataka, India

²PESIT South Campus, Department of Science and Humanities, Bangalore, Karnataka, India

ABSTRACT

The popularity of using IR Spectroscopy in elucidation of organic and inorganic compounds in both research and industry has driven development of an array of IR Spectral analysis of tools and databases. IR Spectroscopy is used to identify and study the component chemicals. It relies on infrared radiations and can provide detailed information about the structure, dynamics, and functional groups involved. The paper outlines the development of simulation tool to obtain the IR Spectra of the compound by entering its name. The position of the peaks is obtained through interaction of infrared radiation with the various functional groups present in the given compound.

Keywords: IR Spectroscopy, Interaction of IR Radiation with compound.

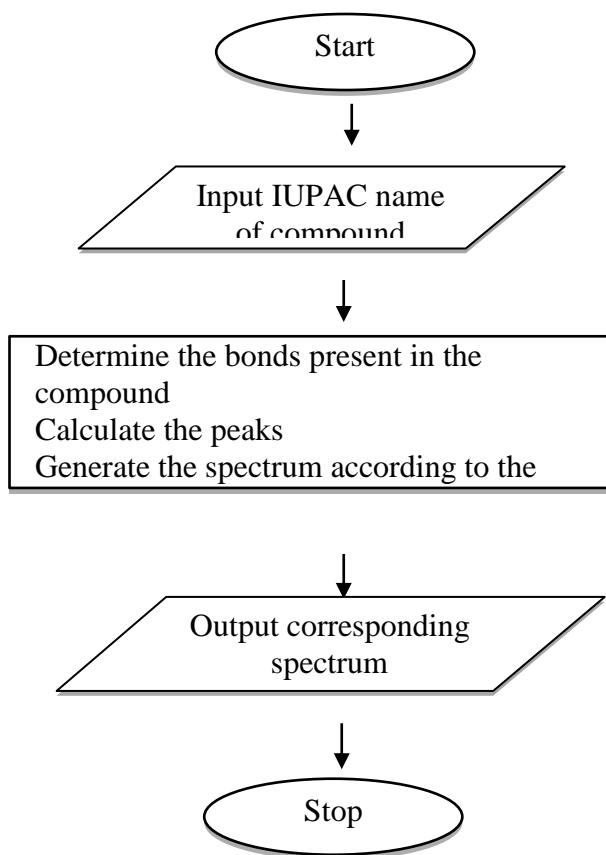
I. INTRODUCTION

Infrared spectroscopy or commonly known as IR Spectroscopy is based on the Principle that the molecules absorb frequencies that are characteristic of their structure. The absorptions occur at resonant frequencies, i.e. the frequency of the radiation absorbed is similar to the vibrational frequency. The masses of the atoms, the associated vibronic coupling and the molecular potential energy surfaces affect the energies. Various types of bonds respond to the IR radiation differently. For example, triple bonds and double bonds are shorter and stronger than single bonds, and therefore vibrate at higher frequencies. The types of atoms involved in the bonds are also relevant. For example, O-H bonds are stronger than C-H bonds, so O-H bonds vibrate at higher frequencies. Therefore various functional groups present in the compound can be identified using IR spectroscopy. IR radiation is absorbed only in presence of the dipole moment. In general, the stretching frequency of a bond which has a dipole

moment, causes the absorption in IR spectrum. If the bond is symmetrically substituted, has zero dipole moment, its stretching vibration is very weak or absent in the spectrum (IR-active v/s IR-inactive vibrations). Molecular collisions, vibrations and rotations cause change in symmetry in bonds with zero dipole moment and thus produce weak absorptions. The objective of our tool is to generate a theoretical IR Spectrum which can be used to compare with the experimental graph that is obtained when Infrared radiation is allowed to pass through an organic compound prepared in the laboratory.

An example can be considered to observe how the peaks can be obtained

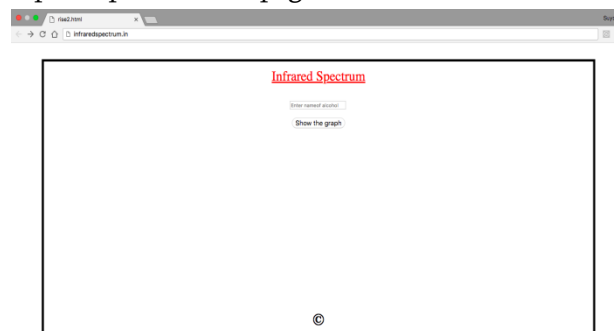
II. METHOD



The flow chart shows the procedure to determine the theoretical IR spectrum merely based on the information about the functional groups available. First, the IUPAC name of the compound has to be given as input to the simulation tool. After the data corresponding to respective peaks are fetched from the database, the graph between transmittance v/s wave number. The spectral lines of theoretical data and sample are compared. After comparison, a conclusion can be drawn regarding the presence of impurities. If the spectral lines are same then we can say that there are no impurities present otherwise we say there are some sort of impurities present.

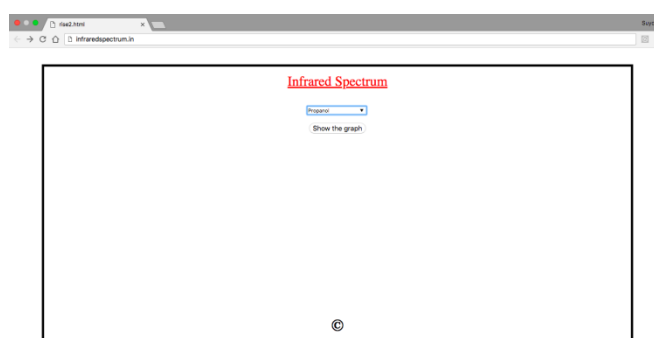
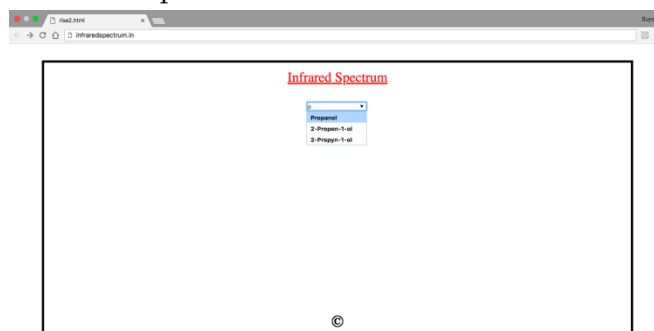
III. RESULTS AND DISCUSSION

Step 1. Open the webpage.



Step 2. Enter the compound.

The compound can be either entered by name or by selecting desired compound from dropdown box. Here the dropdown box is shown.



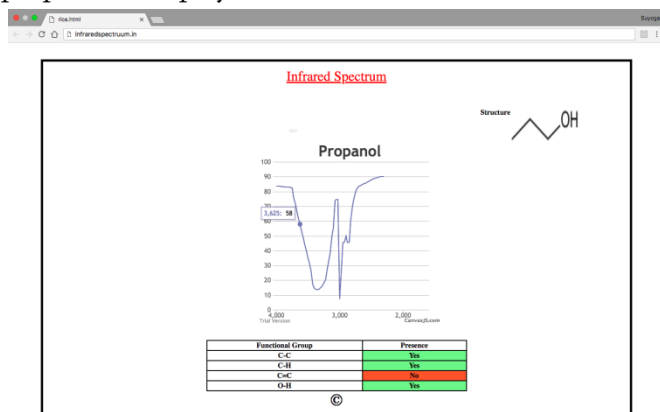
Here, the name of the compound is entered through keyboard.

Propanol is selected/entered.

Step 3. Spectrum is displayed.

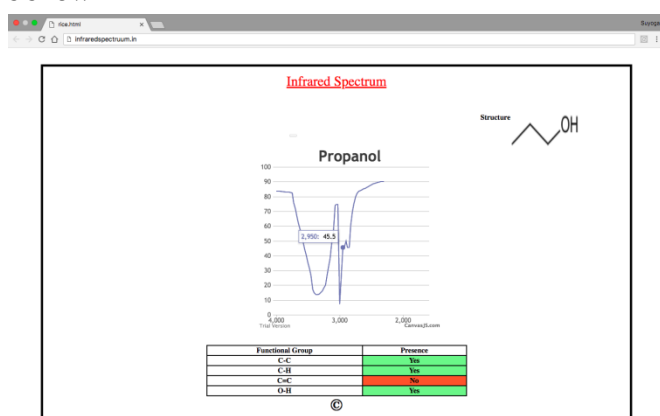
If a valid compound is entered, the bonds present are found out, hence the peaks are calculated. Structure, a table containing the bonds present and the spectra are displayed.

As propanol is entered, table, structure and spectra of propanol is displayed.

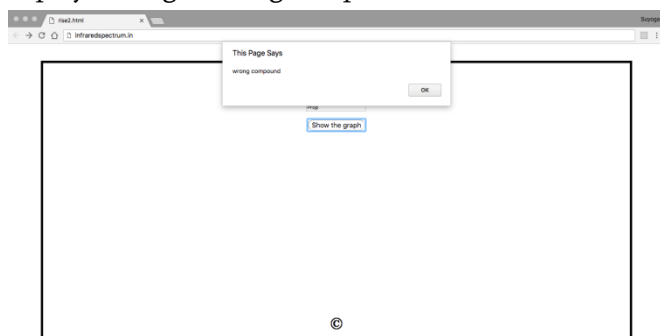


On moving the cursor along the spectra, wavenumber and its corresponding absorbance can be determined.

In the case below, the cursor is moved to the wavenumber 2950. Its corresponding absorbance 45.5 is shown



If a wrong compound is entered, user is alerted by a display stating a wrong compound has been entered.



IV. CONCLUSION

1. For finding impurities in pharmaceuticals: Several regulatory authorities like the International Conference on Harmonization (ICH), the United States Food and Drug administration (FDA), and the Canadian Drug and Health Agency (CDHA) are accentuating on the purity requirements and identifying impurities in Active Pharmaceutical Ingredients (APIs) .
2. For obtaining pure organic compounds in the chemistry laboratory for amateur experiments.

V. ACKNOWLEDGEMENT

We are highly thankful to our learned faculty, Revanasiddappa for his guidance, encouragement and support throughout the completion of this paper work. We sincerely thank our parents for their support. We have tried our level best to gather relevant information subjected to this research. Lastly, we thank PES Institute of Technology for conducting RISE, which gave us a platform to present our paper..

VI. REFERENCES

- [1]. <https://webbook.nist.gov/chemistry>
- [2]. <https://en.wikipedia.org/wiki>
- [3]. Elementary Organic Spectroscopy by YR Sharma

Nir'Bhaya - A Concealed Women's Safety and Security Torch

Dhanurdhar Murali¹, Alfhan Ahmed¹, Chinmayi Hegde², Apoorva Saxena²

¹Department of Electronics and Communication Engineering, P.E.S Institute of Technology - Bangalore South Campus (formerly PES School of Engineering), Bangalore, Karnataka, India

²Department of Computer Science Engineering, P.E.S Institute of Technology - Bangalore South Campus (formerly PES School of Engineering), Bangalore, Karnataka, India

ABSTRACT

Due to the socioeconomic changes and degraded ethical standards of society, women's safety has become a major issue which has come to notice of the government as well. Physical and sexual harassment has hindered freedom provided to a woman and also has created a sense of fear even in the minds of an independent woman. Unfortunately, not much action has been taken for their safety; so, we decided to take it into our own hands to make an electronic device that takes a leap towards ensuring their safety and provide them with a sense of security. The best way for a woman to be safe is to be able to defend herself. In our proposed system, we intend to make a product that a person in danger can use to alert and in extreme cases-defend oneself. The product is equipped with features that can be used in such times: Button activated GSM and cloud-based SOS call/SMS, an optional high-lumen light got by a setup of 7 - 900LM LEDs and lenses that can act as a blinder to distract an attacker, a loud siren (120dB) to get attention of surrounding people, a location-tracking system using GPS and a 200kV-400kV taser using a high-voltage electric arc generator, step-up boost converter. All above features are concealed inside a regular looking torch. The prototype has been made with wood and leather for aesthetic purposes and this product can be extended to any people who may have the need to defend themselves; i.e. the elderly against poachers and dogs, children of suitable age and even trekkers and adventure enthusiasts in their survival kit

Keywords: Internet of Things(IoT), TASER, high voltage arc generator, GPRS, GSM, GPS, System on Chip(SoC), SOS

I. INTRODUCTION

The rape case in New Delhi that happened in December 2012 never ceases to make people have second thoughts about how safe our World is; especially cities for women who dream to be independent. With increasing population in cities, women security has become a major concern. It hinders their freedom and a lot of times, makes them hesitant about taking up jobs in areas less known to them.

The idea behind this project is to make a portable torch that comes with a variety of features to ensure

the users safety. The features so discussed are implemented as follows.

The remainder of this paper has been divided as follows. Chapter 2 talks about the methodology involved including the software and the hardware description. The results and discussion of the project have been briefed in Chapter 3 and onwards.

II. METHOD and MATERIAL

To proceed with our proposed model, let us follow the flow chart of implementation of the proposed technique given in figure 1.

The implementation starts when the person senses danger around her. She would have two choices: either she can use the torch and press the button once or she can use the Google Voice Assistant in her smart phone and say “Help” or “I am in danger”. This will activate an alert system - the location tracking with GPS and automated SOS call and messages including a google maps link to her location indicating danger is sent to her loved ones, using the SIM800L GSM/GPRS/GPS module. If the woman is out of danger or if it was not an attacker at all, she can say “False alarm” or “I am out of danger” on her google voice assistant to turn the tracking off and let her beloved know she is safe. If the user feels more threatened, she can press the same button twice to activate the combination of a 120dB siren and a high lumen LED. Siren grabs the attention of the public which acts as a call for help and the LED lights can as a blinder that makes the attacker visually hindered for a short period of time, in which the user can choose to run away from the scene or defend herself with a TASER.

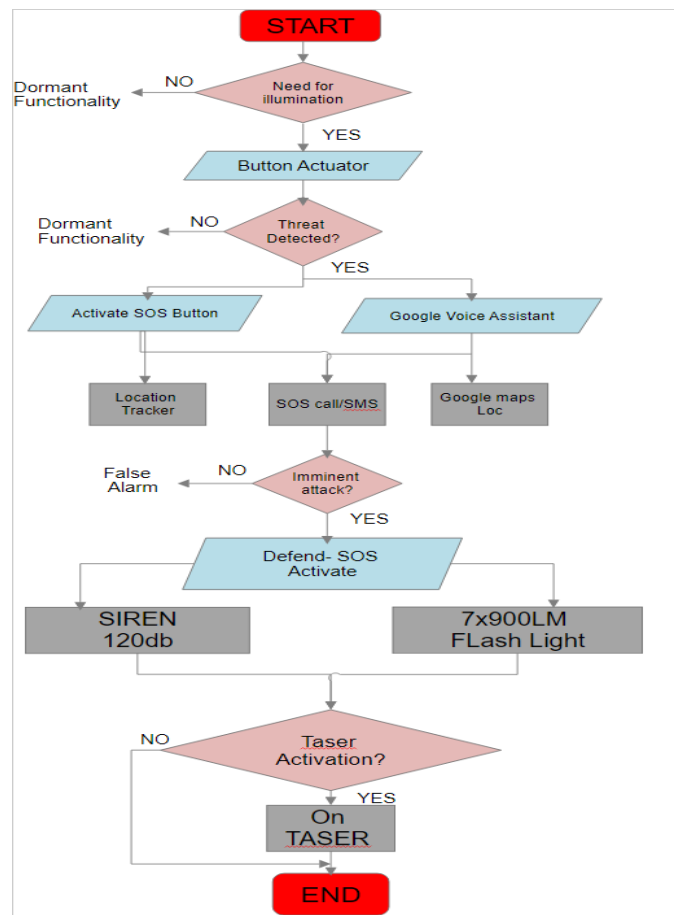


Figure 1. Flow chart

Suppose the attacker continues to approach the user, the user can actuate the taser with an activation trigger which temporarily paralyzes the attacker and inflicts immense pain. A taser is a high voltage and low current device that is non-fatal in the regular use but can inflict a great amount of pain to an attacker due to the high voltage and also paralyse them as the current interferes with the brain signals in the incident area. TASER stands for Thomas A Swift's Electronic Rifle; and is basically a step up boost converter which converts a low DC voltage, typically in the range 3.5-7.2V to a very high voltage in the range 100kV-1000kV a current in the range 3-10mA.

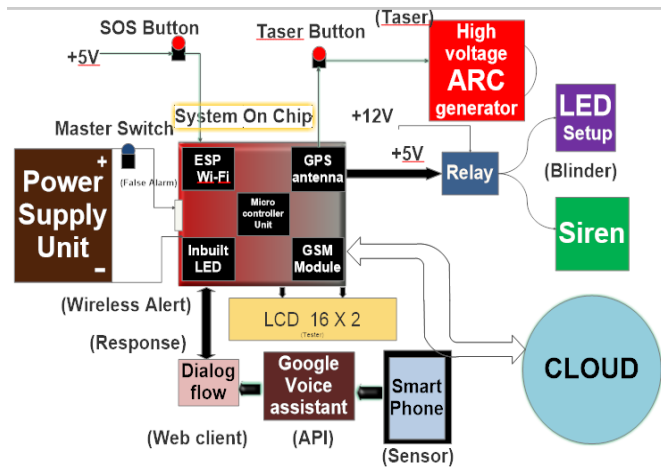


Figure 2. Block diagram

2.2 Methodological constraints

There are certain constraints that have to be abided by, to ensure the expected results.

The user must say “Help” or “I am in danger” to the Google Voice Assistant to activate SOS calls and location tracking. Saying other triggers-words would not be understood by the application, though it can be incorporated if desired. The same goes for “False alarm” and “I am out of danger”.

With the current materials and components, there might be a slight delay in sending of message and there is always the uncertainty whether or not the message/ call has been delivered.

2.3 Requirements

2.3 a) HARDWARE REQUIREMENTS

- ATmega 32
- GPS/Glonass module
- GSM SIM module
- WIFI module esp8266
- Siren
- Batteries
- Level shifter IC's
- Relay
- LM357 comparator IC
- And general hardware components such as jumpers and voltage regulators

(1) Microcontroller ATmega32:-

The Atmel ATmega32 is an 8 bit, low power, microcontroller with upgraded RISC architecture. It operates on a voltage between 2.7 - 5.5 V. It works on a frequency of 16 MHz. ATmega32 can even handle analog inputs. Three inbuilt timers/counters, two 8 bit and one 16 bit timers. It includes one successive approximation type ADC in which total 8 single channels are selectable. It has a selectable reference. Either an internal 2.56v reference voltage can be used or any external reference.

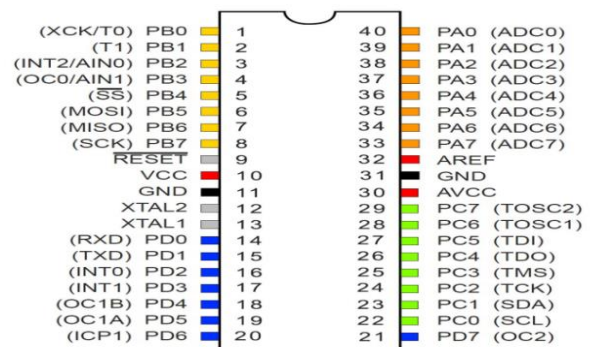


Figure 3. ATmega32

We are using the ATmega32 microcontroller as a processing engine and a cloud gateway. The output values from the filter stages is read by the ADC port of the board and are averaged to get an optimum reading. Then the finalized pulse rate and SpO2 values are uploaded to the cloud using a Wi-Fi module connected to the board.

(2) Esp8266:-

ESP8266 is a highly integrated chip designed for the needs of a new connected world. It offers a complete and self-contained Wi-Fi networking solution, allowing it to either host the application or to offload all Wi-Fi networking functions from another application processor.

ESP8266 has powerful on-board processing and storage capabilities that allow it to be integrated with the sensors and other application specific devices through its GPIOs with minimal development up-front and minimal loading during runtime.

ESP8266 Interfacing

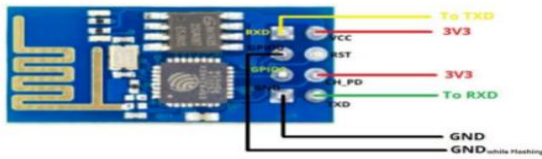


Figure 4.ESP8266 Wi-Fi module pin config.

III. APPLICATION

The product can be used as a preventive and safety measure in the following situations:

- i. Stalkers while walking
- ii. Unsafe neighbours
- iii. Attempted physical or sexual assault
- iv. Domestic violence
- v. Essential backpack for adventure enthusiasts
- vi. Safety and security of the elderly against dogs and malicious people
- vii. Making a wearable security device having a few of the modules of this project

(3) GSM:-

A GSM modem is a device which can be either a mobile phone which can be used to make a processor communicate over a network. A GSM modem requires a SIM card to be operated and operates over a network range subscribed by the network operator. It can be connected to a computer through serial, USB or Bluetooth connection.

IV. FUTURE SCOPE



Figure 5. SIM800L GSM/GPRS/GPS module

- i. With better and smaller components, the product can be made a lot more compact to fit into something as small as a lipstick or jewellery which makes it a lot more portable.
- ii. The device can be equipped with a video-camera, recordings of which is stored in memory card or USB. that can be enabled simultaneously with the siren-LED combination. This can be used to collect proof against the criminal.
- iii. A part of the device can be coated with rape-drug sensing chemical, rohypnol that changes colour when such a chemical comes in contact with it. This can alert the user.
- iv. The product can also be equipped with a hidden camera detector that helps the user be alerted.

(4) GPRS:-

GPRS (General Packet Radio Service) is a service within the GSM network, just like the two most popular services SMS and voice connections. GPRS is used for transmitting data in the GSM network in form of packets

V. CONCLUSION

2.3 b) SOFTWARE REQUIREMENTS:

1. HTML for designing web page
2. Programmer's notepad as a C-code compiler
3. ATX flasher to create and dump the HEX file into the microcontroller
4. Dialogflow web client
5. Google voice assistant on smart phone

It is known that crimes can never be completely ended but the best that can be done is to keep oneself safe and our product promises to do so. Not only does it help the user and her beloved be alert about their safety in various types situations, it can also help her save herself as discussed.

VI. ACKNOWLEDGMENT

We would like to express our sincere gratitude to the institute, PESIT-BSC for providing us with a conducive environment and the required facilities that helped us in completing the project. We would also like to thank the department of ECE for co-operating with us. We would like to express a deep sense of gratitude to Mr.Pattabhi Raman and Mr.Ananda M, Professors who has been very supportive. They have been extremely important in the completion of this project.

VII. REFERENCES

- [1]. https://en.wikipedia.org/wiki/Taser_safety_issues
- [2]. http://www.slate.com/articles/news_and_politics/explainer/2006/11/how_do_tasers_work.html
- [3]. <http://www.tacticalogy.com/blinding-flashlight-self-defense/>
- [4]. <https://www.streetdefender.com/>

Finite Element Modelling of Stick-Slip Principle Based Inertial Slider

S. Shashikanth, B. K. Karthik, V. Shrikanth

Department of Mechanical Engineering, PES University, Bengaluru, Karnataka, India

ABSTRACT

Inertial sliders are positioning devices and are used to a position with a resolution ranging from few hundred nanometres to few millimeters. The inertial sliders are used in microprobe applications as they allow precise positioning, high resolution, practically unlimited travel range and can be made very compact. This work presents a finite element model to study the displacement due to friction model on stick-slip principle. In this work, finite element analysis involves mechanical and electro-mechanical coupled model. FEA of Lead Zirconium Titanate (PZT) plate is carried out under the mechanical model. The maximum displacement obtained for exponential input waveform. Finite element modeling of inertial slider subjected to different input waveforms such as linear, quadratic, cubic and exponential waveforms is carried out under the electro-mechanical coupled model and the results obtained are compared with semi-analytical results obtained by solving the differential equations derived from the lumped model, the results are directly compared to obtain good agreement.

Keywords: Inertial slider, Piezoelectric actuator and Stick-slip

I. INTRODUCTION

The positioning with sub-micrometer accuracy over distances of several millimeters is very important in many applications such as scanning tunneling microscopy and scanning probe microscopy, where the demand is on high precision, very large travel speed and minimization. Precision manufacturing and engineering require increased accuracy for the production of devices. This has resulted in miniaturization and subsequent development of nanotechnology. Miniaturization enables devices to be developed for new functions and applications. Assembly and machining of very small parts starting from a few millimeters to a few microns require very precise handling of the tools.

Piezoelectric devices provide extremely small displacement which is the range of few picometers

made of lead zirconium titanate (PZT) [1]. The piezomaterial can be operated over millions of cycle without any deterioration. The advantages are microsecond response, very high force generation and practically no wear and tear.

The precision positioning systems generally incorporate the stick-slip effect. Long displacement range with a very high resolution, simple in construction, very compact and high stiffness are the advantages of stick-slip actuators [2]. The piezoelectric actuator used the inertial slider in friction drive mechanism to process exchanging periods of sliding and sticking between piezoelectric actuator and slider to produce steps during the movement and the input waveforms control the step size.

Pohl [3] designed a piezoelectric fine positioning device which utilizes the principle of inertial sliding,

in order to create translation motion, sawtooth waveforms are applied to the piezoelectric actuator. The positioning device provides step size of 40-200 nm. Renner et al. [4] developed a linear translation device using piezoelectric induced stick-slip motion for low-temperature application in scanning tunneling microscope (STM). To obtain vertical motion used cycloidal waveform instead of the sawtooth signal to activate the motion. Niedermann et al. [5] voltage are applied to the piezoelectric plate to drive a stage with the utilization of stick-slip effect to produce the shear deformation. C N Woodburn et al. [6] developed a linear inertial slider to accomplish miniaturized in any direction and it is mainly for SPM cryogenic and ultra-high vacuum environment.

Erlandsson and Olsson [7] developed a three-axis micro-positioner using the inertial slider principle for the use of atomic force microscope. The device works reliably in an ultrahigh vacuum system and permits positioning with submicron precision.

From the detailed review of the literature, the precision positioning devices mainly incorporate the stick-slip effect induced friction drive stage, it can be concluded that the conventional mechanical systems are often less suitable for this application as they tend to be complex, have a problem with backlash. The inertial sliders have many advantages such as precise positioning, very compact and provide fine resolution with relatively large travel speed.

II. INERTIAL SLIDER

Inertial sliders are positioning devices used to position an object in the desired direction with a resolution ranging from few hundred nanometres to few millimeters. The inertial slider is as shown in Fig. (1). A shear piezoelectric plate (PZT-5A) of area $5 \times 5 \text{ mm}^2$ and 0.75 mm thickness is bonded between copper beryllium (Cu-Be) electrode plate of area $5 \times 6 \text{ mm}$ and thickness 0.25 mm with the help of silver

epoxy resin. A steel ball is placed above the Cu-Be plate. The bottom plate is fixed to the mounting block with cyanoacrylate glue.

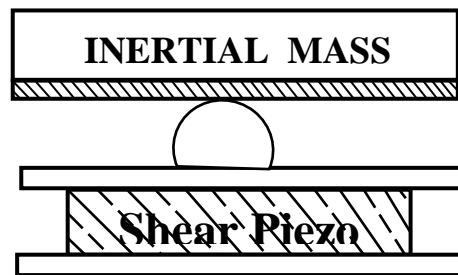


Figure 1. Sectioned view of inertial slider

A. Working principle

The stick-slip principle is used to design the inertial slider. The fine motion of the slider is possible by proper management of inertia and frictional forces. The piezoelectric actuator utilized the inertial slider to process exchanging periods of sliding and sticking between actuator and slider to produce steps during the movement. A ramp during which the slow rise of the input voltage and then rapid drop to zero. During the slow rise of voltage, the inertial mass follows the piezoelectric material movement due to friction sticking occurs ($a < \mu g$), but due to slipping ($a > \mu g$) that occurs during the sudden drop of voltage, the inertial mass cannot follow the piezoelectric movement. The input waveforms control the step size. Hence due to gradual deformation followed by a sudden drop of voltage results in a stepping motion of the inertial mass with respect to the piezoelectric actuator. Those single step movement of the slider is controlled by stick-slip principle.

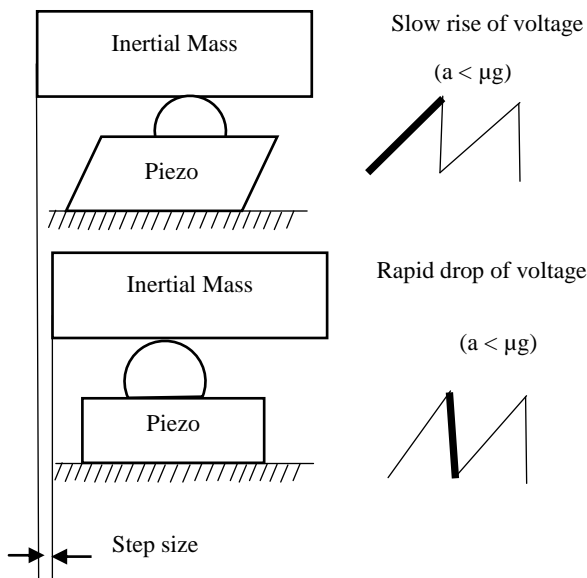


Figure 2. Working principle of inertial slider

B. Friction models

Friction is the primary factor in the inertial slider since the surface characteristics directly influence the step size of the slider. A comprehensive friction model that captures all the phenomena related to friction in a mechanical system, such as Stribeck effect, pre-sliding motion, stick-slip motion, hysteresis etc. However, Karnopp model and Luger friction model are used in this work to study the effect of static friction and then the effect of kinetic friction on the performance of the slider.

1) Coulomb friction model

$$F = \begin{cases} F_c \cdot \text{sgn}(\dot{x}), & \text{if } x \neq 0 \\ F_a, & \text{if } x = 0 \text{ and } F_a < F_c \end{cases} \quad (1)$$

$$F_c = \mu F_n \quad (2)$$

Where F is a frictional force, \dot{x} is sliding speed. F_a is applied force. F_c is coulomb friction force

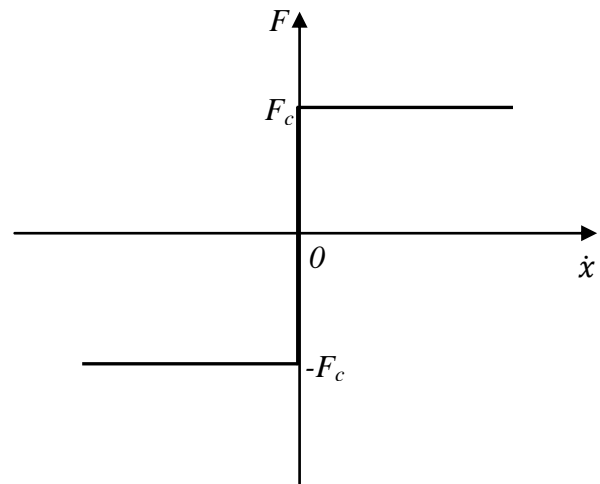


Figure 3. Coulomb friction model

There is no sliding between the contact surface when the Coulomb friction force is more than the applied force. Coulomb friction value varies from 0 to F_c and depending on the direction of sliding it may be positive or negative value.

2) Stribeck friction model

Stribeck friction is represented by

$$F = \left(F_c + (F_s - F_c) e^{-(|\dot{x}|/v_s)^i} \right) \text{sgn}(\dot{x}) + k_v \dot{x} \quad (3)$$

where F is a frictional force, F_c is coulomb friction force, \dot{x} sliding speed, F_s the static friction force, k_v the viscous friction coefficient, v_s stribeck velocity, Stribeck friction force takes F_c and F_s as lower and upper limit respectively.

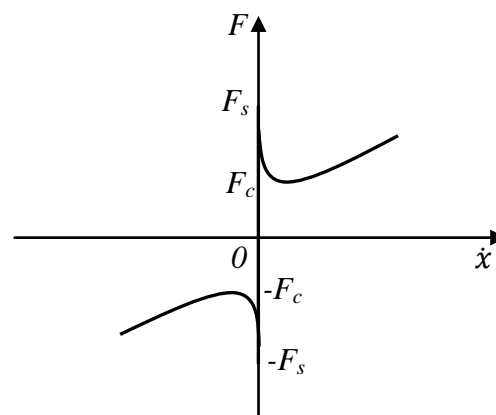


Figure 4: Stribeck friction model

3) Karnopp friction model.

Karnopp model [8] proposed the frictional force occurs in the stick-slip effect is

$$F = \text{sgn}(v)[\mu_k \lambda(v) + \mu_s(1 - \lambda(v))]N \quad (4)$$

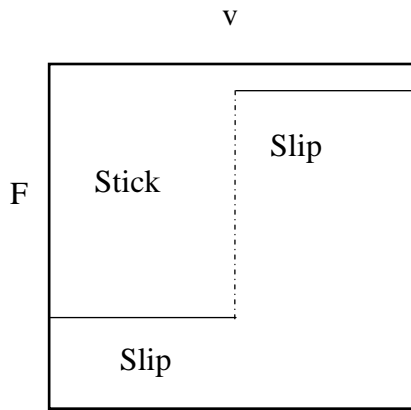


Figure 5. Karnopp friction model

Where μ_s and μ_k are static and kinetic friction coefficients, v is the velocity and N is the normal load, where $N = (m_1 + m_2)g$, $\lambda(v) = 0$ when $|v| \sim 0$ and $\lambda(v) = 1$ when $|v| > 0$.

4) Luger friction model

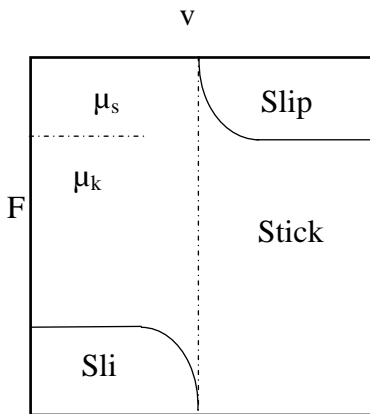


Figure 6. Luger friction model

Canudas et al. [9] proposed the Luger model by combining Dahl model with steady-state friction.

$$F = \text{sgn}(v)[F_k + (F_s - F_k)e^{-(v/v_s)^2}] \quad (5)$$

F_s and F_k are static and dynamic friction forces, v_s is the stribek velocity.

III. PROBLEM FORMULATION

A. Mechanical model

FEA of single PZT is carried out under the mechanical model. PZT of area $5 \times 5 \text{ mm}^2$ and 0.75 mm thickness. PZT material type used in the analysis is PZT 5A

The meshed model of PZT is shown in Fig.7 is a hexahedron mesh consists of 20000 elements with an element size 0.0001 m .

The analysis has been carried out in ANSYS software. The bottom face of the PZT plate is fixed and the force equivalent to voltage is applied to the top face of the bottom PZT plate.

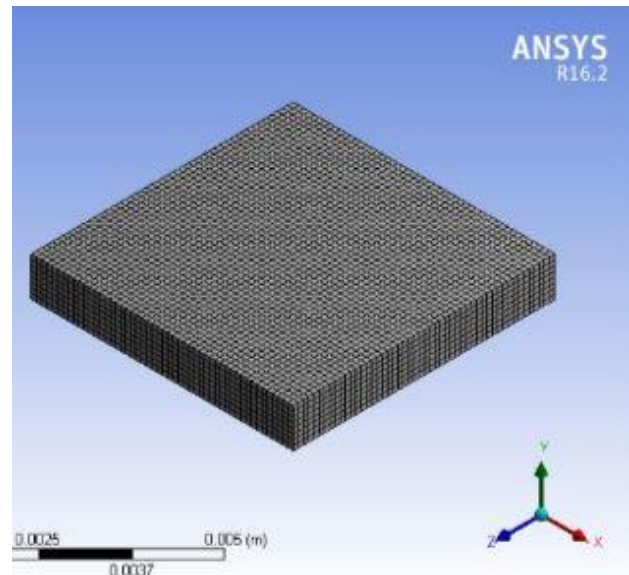


Figure 7. Meshed model of PZT Plate

B. Electro-Mechanical coupling model

FEA of the inertial slider is carried out under Electro-Mechanical coupling model. The inertial slider is designed based on the stick-slip principle. A shear piezoelectric plate (PZT-5A) of volume $5 \times 5 \text{ mm}^2$ and 0.75 mm is bonded between copper beryllium (Cu-Be) electrode plate of area $5 \times 6 \text{ mm}^2$ and thickness 0.25 mm by means of conducting silver epoxy resin. The two steel balls are positioned on the top of Cu-Be plate. These balls help to increase the stiffness of the drive. The base plate is fixed to the mounting obstruct with a thin layer of cyanoacrylate glue.

The meshed model of the inertial slider is shown in Fig.8 is a hexahedron mesh consists of 218337 elements with an element size 0.0001m.

The stick-slip principle is used to design the inertial slider. The voltage is applied to the top face of the piezoelectric actuator due to its indirect effect it undergoes shear deformation and mounting block is fixed. During the slow rise of voltage, the inertial mass follows the piezoelectric material movement because of friction sticking occurs ($a < \mu g$), whereas it can't take after a sudden piezoelectric withdrawal because of its inertia, hence slipping occurs ($a > \mu g$), due to the sudden drop of voltage. For the electrical boundary condition, the **bottom** surface of the PZT plate should be grounded in order to create a potential difference.

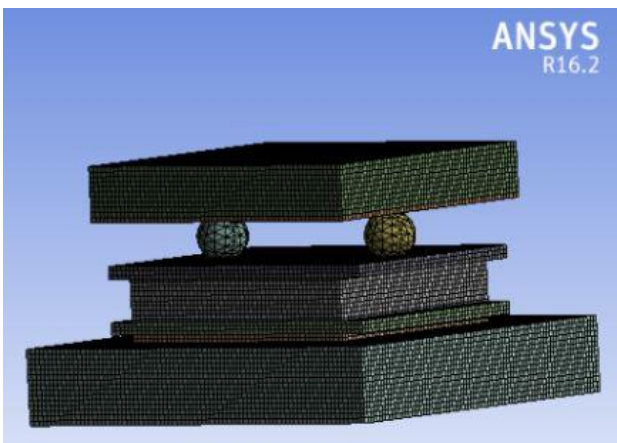


Figure 8. Meshed model of inertial slider

C. Lumped model of the inertial slider

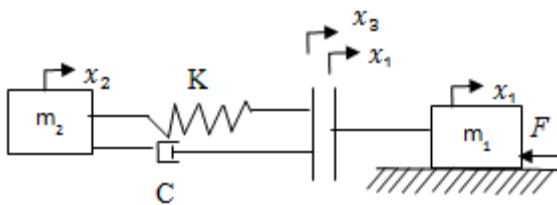


Figure 9. Lumped model of the inertial slider

$$\begin{aligned} m_1 \ddot{x}_1 + c(\dot{x}_3 - \dot{x}_2) + k(x_3 - x_2) + F &= 0 \\ m_2 \ddot{x}_2 - c(\dot{x}_3 - \dot{x}_2) - k(x_3 - x_2) &= 0 \end{aligned} \quad (6)$$

Where m_1 is inertial mass and m_2 is the mass of piezoelectric actuator respectively. C is the damping co-efficient of the piezoelectric material. K is the

stiffness of the piezo material. x_1 is the displacements of the inertial mass and x_2 is the displacement of the piezoelectric actuator respectively. F is the frictional force involved in the motion of the inertial mass. $x_3 = x_1 - s$. Where $s = d_{15} V$ and d_{15} are the applied displacement and charge constant of the piezo material and V is the input voltage.

Linear waveform $V(t) = V_0 \left(\frac{t}{t_p} \right)$

Quadratic waveform $V(t) = V_0 \left(\frac{t^2}{t_p^2} \right)$

Cubic waveform $V(t) = V_0 \left(\frac{t^3}{t_p^3} \right)$ and

Exponential $V(t) = \left(\frac{V_0}{2^{15}} \right) (e^{10.39(t/t_p)} - 1) \quad (7)$

The applied input waveforms for linear, quadratic, cubic and exponential waveforms as shown in Fig.10. The applied input voltage is changed into a displacement as per the relation $s = d_{15} V$. The maximum displacement obtained when the applied input waveform is exponential. The quadratic and cubic waveforms gives a displacement slightly higher than that for a linear input waveform.

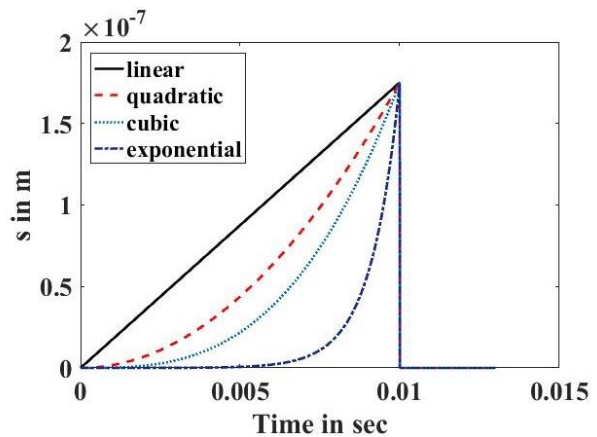


Figure 10. Input waveforms

The time parameters of the linear input signal are shown in Fig.11. A ramp during which the slow rise of the input voltage and then suddenly drop to zero voltage. During the slow ramp of input voltage or rise time (t_r), the inertial mass follows the piezoelectric movement because of friction sticking occurs. The slipping of the piezo leg is determine by drop time (t_d)

of the input signal. The delay time (t_D) is the time during which the piezo is at rest. t_p is the total time period of the input signal. The time period of the input signal is $t_p = t_r + t_d + t_D$.

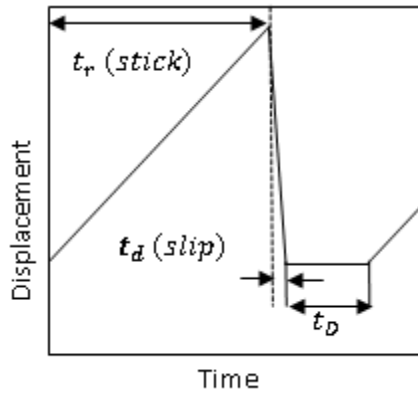


Figure. 11. Time parameters of the input signal

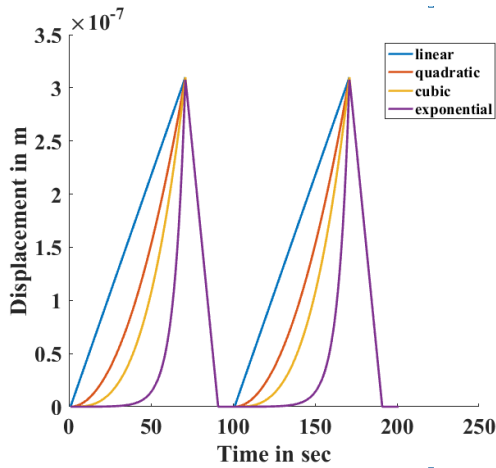


Figure.12 (a). Simulation result of PZT Plate

Figure 12 (b) shows the semi-analytical results of PZT plate obtained by solving the equation of motion. In both the cases the maximum displacements of PZT plate obtained are in good agreement

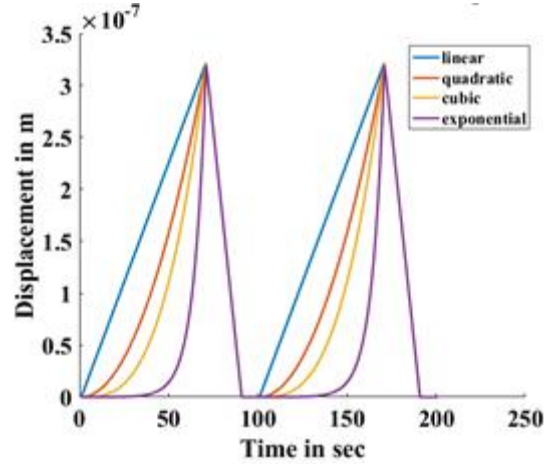


Figure.12 (b). Semi-analytical result of PZT Plate

B. Simulation results of Electro-Mechanical coupled model

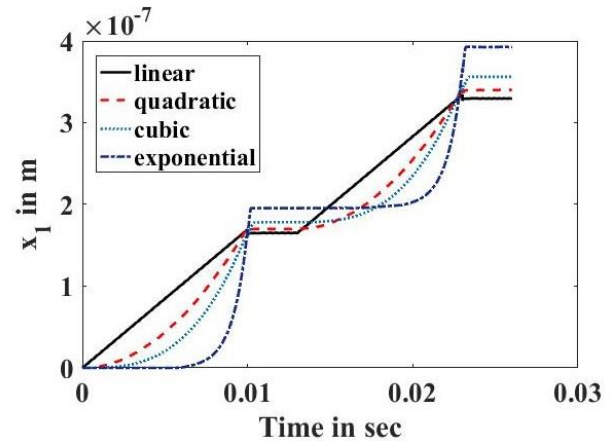


Figure.13 (a). Simulation result of inertial slider

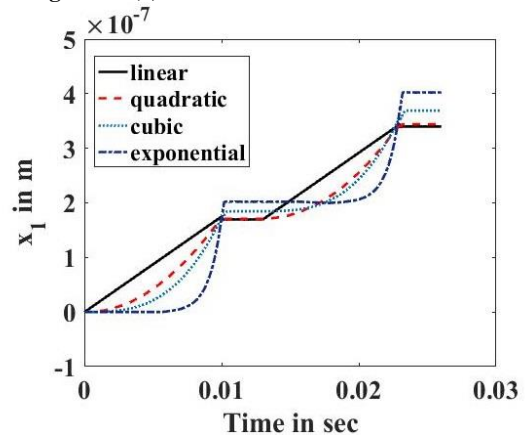


Figure.13 (b). Semi-analytical result of inertial slider

IV. RESULTS AND DISCUSSIONS

A. Simulation results of the mechanical model

1) Displacement of single PZT plate

Figure 12 (a) shows the simulation result of PZT plate. The analysis has been carried out in ANSYS software. Simulation is carried out for the following condition: the bottom face of the PZT plate is fixed and the force magnitude of 140N equivalent to 300V is applied to the top face of the PZT plate. The time parameters t_r , t_d and t_D are 12ms, 4 μ s and 3ms respectively. Displacement of plate the the is 322.13nm obtained in Ansys.

Figure 13 (a) shows the simulation result of inertial slider. Simulation is carried out for the following condition: the voltage is applied to the top face of the piezoelectric actuator and mounting block is fixed. Due to exponential drop during the slipping phase, the slider experiences a backward movement and the net displacement is not as much as the applied displacement. When compared with the linear, quadratic and cubic waveform, slider gets the highest velocity and acceleration when the exponential waveform is applied.

Figure 13 (b) shows the semi-analytical results of inertial slider obtained by solving the equation of motion. The maximum displacement of the slider when the input waveform is exponential. The quadratic and cubic waveform gives a displacement slightly higher than that for a linear input. The displacement obtained by the finite element method are very close to the Semi-analytical results.

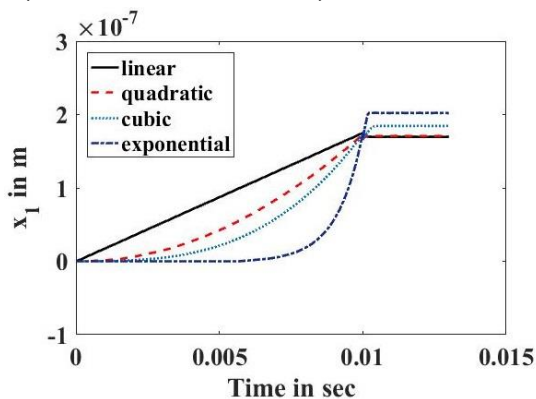


Figure 14. Displacement of the slider x_1

From the above results, it is found that the Step size of the inertial slider varies for the different input waveforms is shown in Fig.14. During sticking phase input waveforms such as linear, quadratic, cubic and exponential waveforms move the slider, by the same amount but during the slipping phase there is an exponential drop as a result in the backward motion of the slider and the net displacement of the slider is less than the applied displacement. The size of the slider is reliant on the velocity just before the beginning of the slip, because of which the slider has the maximum velocity and acceleration when the exponential

waveform is applied. Higher the velocity and acceleration, larger step size, Hence, when the exponential signal is applied the step size is much larger than the other input signal. The maximum displacement of the slider when the input waveform is exponential followed by cubic, quadratic and linear input waveform.

V. CONCLUSIONS

FEA of mechanical and electromechanical coupled model has been carried out. Both mechanical model and electro-mechanical subjected to different input waveforms. Any periodic waveforms can move the slider when input amplitude is slowly increased and then suddenly dropped to zero. The displacement of the slider is maximum when exponential ramp input is applied. The FEM results obtained are compared with semi-analytical results obtained by solving the differential equations, both the results are in good agreement.

VI. REFERENCES

- [1]. A. H Holman, P. Scholte, W. C. Heerens, and F. Tuinstra, "Analysis of piezo actuators in translation constructions," *Review of scientific instruments*, vol. 66, no. 5, pp. 3208–3215, 1995.
- [2]. A. Bergander, J.-M. Breguet, C. Schmitt, and R. Clavel, "Micropositioners for microscopy applications based on the stick-slip effect," in *Micro mechatronics and Human Science*, 2000. MHS 2000. Proceedings of 2000 International Symposium on. IEEE, 2000, pp. 213–216.
- [3]. D. W. Pohl, "Dynamic piezoelectric translation devices," *Review of Scientific Instruments*, vol. 58, no. 1, pp. 54–57, 1987.
- [4]. C. Renner, P. Niedermann, A. Kent et al., "A vertical piezoelectric inertial slider," *Review of scientific instruments*, vol. 61, no. 3, pp. 965–967, 1990 .
- [5]. P. Niedermann, R. Emch, and P. Descouts, "Simple piezoelectric translation device,"

- Review of scientific instruments, vol. 59, no. 2, pp. 368–369, 1988.
- [6]. C N Woodburn, A W Mckinnon, D A Roberts, M E Taylor and M E Welland, “A one-dimensional piezoelectric-driven inertial micropositioner with vertical capabilities,” *Meas. Sci. Technol.* 4 (1993) 535-537.
- [7]. R.ErlandssonandL.Olsson,“Athreexaxis micromicropositionerforultra high vacuum use based on the inertial slider principle,” *Review of scientific instruments*, vol. 67, no. 4, pp. 1472–1474, 1996.
- [8]. D. Karnopp, “Computer simulation of stick-slip friction in mechanical dynamic systems,” *Journal of dynamic systems, measurement, and control*, vol. 107, no. 1, pp. 100–103, 1985.
- [9]. C. Canudas de Wit, H. Olsson, K. Astrom, and P. Lischinsky, “A new model for control of systems with friction,” *IEEE Transactions on automatic control*, vol. 40, no. 3, pp. 419–425, 1995.

Open Source Blockchain Model of Journalism

Shashidhar V¹, SurajDev Yadav², Prasad B Honnavalli³

¹Department of Computer Science and Engineering, PES Institute of Technology- Bangalore South Campus, Bangalore, Karnataka, India

²Department of Computer Science and Engineering, PES Institute of Technology- Bangalore South Campus, Bangalore, Karnataka, India

³Department of Computer Science and Engineering, PES University, Bangalore, Karnataka, India

ABSTRACT

The emergence of the blockchain, earlier blockchain technology, and cryptocurrency has changed the way the world deals with commerce [1]. The success of blockchain in cryptoeconomics has led to its application in many domains. This left people with a blockchain as a way to achieve consensus and security in a peer-to-peer application for any class of asset. In this article, we propose the application of blockchain technology to journalism. It is essential because it allows us to maintain archives that cannot be censored or altered after the fact.

Keywords:Blockchain, Ethereum, Distributed Ledger, Journalism, Smart Contract, Open Source, Investigative Journalism.

I. INTRODUCTION

In 1991 the two scientists Stuart Haber and W. Scott Stornetta initiated work on a chain of blocks which was cryptographically secured. The efficiency of their system was improved in 1992, when they incorporated Merkle trees into their design, which allowed collection of multiple documents into one single block [2]. A blockchain is a constantly growing list of records, which are called blocks. The first block in a blockchain is known as the genesis block. Each block is linked to its previous and successive block and is secured using cryptography.

The first successful implementation of blockchain technology was done in 2009 by Satoshi Nakamoto, when he implemented blockchain as a core component of the cryptocurrency bitcoin [3]. Here the blockchain is used as a public ledger to record all the transactions that take place on the network.

Prior to the invention of the blockchain, the coordination of individual activities on the internet and at the same time ensuring the integrity of data was impossible without a central body. Unrelated individuals relied on the central authority to confirm the occurrence of events. Computer scientists also believed that the distributed group of people could never reach a consensus without the support of the common clearinghouse. This is a well-known computer science problem commonly referred to as the “Byzantine Generals Problem” [4].

Information in a blockchain becomes transparent and verifiable using mathematical puzzles that require a great amount of computation thus making it difficult for a potential attacker to tamper the contents of a shared database. The attacker will need to own at least 51 percent of the total computational power of the entire network to succeed, the probability of which is close to impossible [5]. This way the blockchain solves the “Byzantine Generals Problem”.

II. EXISTENTIAL CRISIS FACING JOURNALISM

The advent of the digital age along with great technological advancements has changed the face of journalism. Facebook, Twitter, and other social media platforms have taken over the traditional methods of journalism. This has led to certain challenges like fake news, misleading advertisements creating issues of trust.

The public has witnessed the power of fake news in the 2016 United States Presidential Elections. This had led to dwindling public confidence and lesser support for media in the face of rising clickbait. Often we see biased journalism in favour of a political figure or an organization. A USA TODAY/CNN/Gallup poll found that only 36 percent of Americans believe news organizations get the facts straight, as compared with 54 percent in mid-1989 [6]. Majority of the public is of the opinion that the media likes to feed on sensational news rather than reporting the most important ones. These factors urged us to propose a new methodology of journalism “The Blockchain Model”.

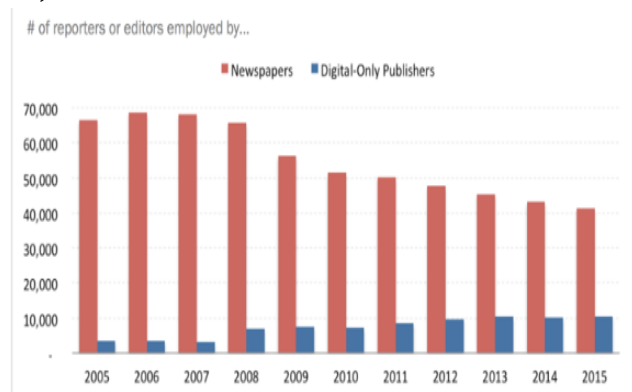


Figure 1. A graph showing how digital form of journalism is taking over the traditional form [7]

III. BLOCKCHAIN MODEL OF JOURNALISM

The model constitutes three major components. The first one is the author, the second one is the reader and the third one is the blockchain network which connects both the author and the reader.

This particular model is set up on Ethereum like blockchain platform and the information transaction happens through smart contracts [8]. Ethereum is a blockchain platform which allows the users to create smart contracts. The smart contract is the phrase used to describe computer code that can facilitate the exchange of money, content, property, shares, or for that matter anything of value.

The model classifies the users of the network into two groups. One is the author and the other is the reader. The author is the end user who is responsible for reporting the news through the creation of smart contracts. The reader is another end user who reads the articles written by the author.

The blockchain technology comes into play when the authenticity of the news being reported has to be determined. When the smart contracts are run on the blockchain, they run exactly as programmed – respecting the integrity and confidentiality of the Information.

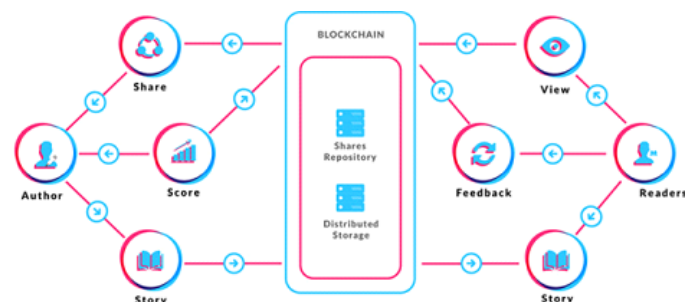


Figure 2. A block diagram illustrating how the blockchain model of journalism is going to work

A reader on the network can subscribe to one or more authors. They get notified every time an author publishes an article. The authors get ratings for their articles. The ratings are given by the readers. The readers can also post comments related to the article. The readers, in turn, receive feedback from the authors and other readers on the network for their comments.

In the blockchain network, any change that has to be made needs to be converted into a block and few complex mathematical algorithms have to be run to cryptographically hash the particular block and then place it on the network [5]. This process is known as mining. A miner is an investor that devotes time, computer space and energy to sorting through blocks.

In this model, we propose a concept of news mining. Not any miner on the network can verify the authenticity of the news. A person who wishes to perform mining for the news network should register himself with the geographical location where he lives. In this way, he will be allowed to mine (verify) the news which is easily accessible to him. This further ensures the blocking of fake news. If the news is false it is immediately rejected and not placed on the network and reported.

In any blockchain network, the miner gets paid in two forms [5]. They are block rewards and transaction fees. Since we propose an open source model, the miner gets paid in only block rewards. The miner also gets credit points for identifying the fake news which enhances his probability of winning the mining race.

One of the features of the blockchain is that it is immutable [9]. This feature is exploited in this model to provide a solution to fake reporting. The author of a particular article has to think twice before he publishes his article on the network. If the article is found to contain fake news the corresponding author will lose his credibility on the network.

IV. ADVANTAGES OF THE MODEL

A. Decentralization of Authority

The full-fledged implementation of this model on a large scale will make newsrooms completely powerless. The power to report an incident, bring awareness about any issue completely lies in the hands

of the general public leading to the eradication of biased journalism.

B. Creates an Open Source Awareness

A series of polls conducted over a seven month period, by the Center for Policy Attitudes and Center for International and Security Studies at the University of Maryland, found that Americans receiving their news from non-profit organizations were inclined to have accurate perceptions [6]. This only goes to prove the fact that a body of like-minded people who are not working for any financial benefits are more likely to produce good quality news compared to the commercial newsrooms.

C. An Advertisement Free Platform

The digitization of news through the web has made the media more of a market place for advertisements than news display.

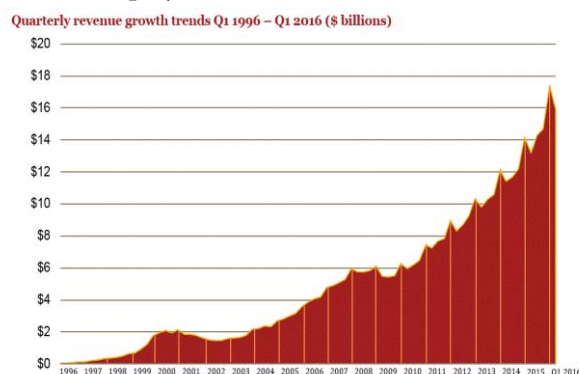


Figure 3. A graph showing digital revenue earned by the newsrooms [10]

The above graph clearly indicates that the newsrooms have become greedy for money and are not interested in spreading news for the benefit of the society.

D. The Reporter Remains Anonymous

In September 2012, UNESCO's International Programme for the Development of Communication concluded that journalism is one of the most dangerous professions in the world. This encourages ingenuity in reporting the news and masking of the original news due to fear.

In the blockchain platform, every end user on the network is anonymous to the other. This way the author does not have to disclose his identity to anyone and can report news truthfully and fearlessly.

E. An Alternative Form of Investigative Journalism

It is a form of journalism in which the journalists assess a particular subject in great depth. Often these subjects are political delinquency, corporate misconduct, and other major issues. Since this form of journalism takes several months or years they are often not encouraged by newsrooms and are often practiced by freelance journalists. Our model places a fantastic platform for these type of journalists to pursue their subjects of keen interests. They can turn their findings into a series of articles on our platform.

To carry out investigative journalism as an organization is very expensive. The graph below illustrates and projects the expenses. If not carried out by renowned organizations the readers would doubt the authenticity of the investigation. Our model is a perfect solution to this problem. By the application of blockchain model, we can keep the expenditure to a minimum while not compromising on the authenticity.



Figure 4. A graph showing the amount of money spent by organizations on investigative journalism [11]

F. Accountability

In this model, each and every reporter is responsible for his or her own actions. The accountability is thus traced back to only one person and not an organization or a newsroom as in traditional

journalism. The world has witnessed many situations in which due to the mistake of one reporter or an editor the entire news organization associated with the news had to be banned or shut down temporarily leading to many innocent employees losing their jobs. Since our model eradicates the concept of newsrooms such happenings can be prevented.

V. CONCLUSION

The blockchain technology is finding its application in various fields. We predict that over the years our open source platform model for news might lead to a general public awareness and be a successful platform like the Open Source Initiative of the computer science domain.

We hope that our model provides a permanent solution to the fake news menace which is currently creating havoc in the society. Also, this gives rise to a feeling of collective responsibility in the society. The blockchain model on a large scale can change the way the society has seen news reporting. It has the potential to reconstruct the job description of a journalist.

This model not only serves as a tool to prevent the wrong information from propagating but also allows access to the right information to every individual who aspires for it at free of cost. Thus through the evolution of blockchain technology, we propose a model to bring about a revolution in the journalism industry.

VI. REFERENCES

- [1]. David Lee Kuo Cheun, "Handbook of Digital Currency, Bitcoin, Innovation, Financial, Instruments, and Big Data", Singapore Management University.
- [2]. Haber, Stuart; Stornetta, W. Scott (January 1991)." How to timestamp a digital document".

- Journal of Cryptology. 3 (2): 99–111.
Doi:10.1007/bf00196791.
- [3]. Satoshi Nakamoto, "Bitcoin: A Peer-to-Peer Electronic Cash System", <https://bitcoin.org/bitcoin.pdf>.
 - [4]. Leslie Lamport et al., "The Byzantine Generals Problem", 4 ACM Transactions on Programming Languages and Systems at 382 (July 1982).
 - [5]. Joshua A. Kroll, Ian C. Davey, and Edward W. Felten, "The Economics of Bitcoin Mining or, Bitcoin in the Presence of Adversaries", Princeton University.
 - [6]. <http://www.dailysource.org/about/problems>
 - [7]. US Bureau of Labor Statistics Occupational Employment Statistics.
 - [8]. Vitalik Buterin, "A Next Generation Smart Contract & Decentralized Application Platform", <https://ethereum.org/pdfs/EthereumWhitePaper.pdf>.
 - [9]. Research Handbook on Digital Transformations, "A Primer on Blockchain Technology", Pg.233.
 - [10]. IAB/PwC Internet Ad Revenue Report, FY 2016
 - [11]. <https://busy.org/@infovore/making-a-change-with-blockchain-revolutionizing-the-advertising-and-publishing-industry>

Synthesis and D. C Electrical Conductivity Studies of Coordination Metal Complexes

Jyoti C Ajbani¹, Kotresh Durgada², D Smitha Revankar¹, Neeraj Ajbani³, Vinay K⁴, Basavaraj Patel B M¹, M Revanasiddappa*¹

¹Department of Chemistry, PESIT-Bangalore South Campus, Bangalore, Karnataka, India

²Department of Chemistry, Vijayanagarcollege, hosapete, Karnataka, India

³Department of Electrical Engineering, Tolani FG, Polytechnic college, Adipur, Gujarat, India

⁴Department of Chemistry, Channabasaveswara Institute of Technology, Gubbi, Karnataka, India

ABSTRACT

Conductivity of Schiff base metal complexes has become much importance to study the nature of synthesized transition metal complexes and attracted utmost attention of research scholars to synthesize some novel solid complexes having super functional properties viz, electrical, optical and magnetic properties. These complexes have extended their unique contribution in the field of bio-chemistry and material sciences. The present work is a sincere attempt to investigate the D.C electrical conductivity of some riluzoleschiff base transition metal complexes. The D.C electrical conductivity measurements of the prepared complexes were studied in the temperature range 364-454K.

Keywords: Coordination Complexes; Resistivity; Electrical conductivity; Schiff base ligand.

I. INTRODUCTION

In recent years, conducting metal complexes have been widely studied and have become a crucial concern for the scientific community because of their wide applications which includes high temperature coatings, electrode and display materials, lasers and homogeneous catalysts [1-5]. One of the fundamental methods to synthesize conducting organometallic complexes involves complexing transition metals with conjugated bridging Schiff base ligands. Due to their pliability and various structural aspects, a wide range of benzothiazoleschiff base metal complexes has been prepared and their complexation behaviour was examined.

II. METHODS AND MATERIAL

Synthesis of HL¹ ligand (HL¹= Riluzole, 6(trifluoro methoxy) benzothiozole – salicylaldehyde Schiff base): Riluzole, 6(trifluoromethoxy) benzothiozole (0.05M, 1.18g) was taken in a dry and cleaned round bottom flask. To this 0.6 ml (0.05M) of salicylaldehyde and 1-2ml of ethanol was added. The round bottom flask capped with water condenser was subjected to microwave irradiation at 50% intensity (450watt) for 6 minutes with an interim of 30 seconds. TLC was used to supervise the reaction. The resulting mixture was separated and dissolved in ethanol and the excess solvent was evaporated by rota-evaporater. The yellow orange crystals so obtained were separated on drying and stored in a desiccator.

Preparation of (Co, Cu, Cd, Zn and ZrO) metal complexes of HL¹ ligand

Metal (II) chlorides in ethanol (0.002mol) and Schiff base HL¹ (0.002mol) were taken in a round bottom flask and kept in microwave for 2-3mins at 50% intensity in an ethanolic medium. A pinch of sodium acetate was then added to the reaction mixture and kept in microwave for another 8-9mins. The separated metal (II) complexes were filtered and washed with distilled water containing small quantity of ethanol and dried in vacuum over fused calcium chloride. The complexes were purified using soxhlet extractor taking alcohol as a solvent. ZrO (II) complexes were prepared in methanol medium and same procedure was adopted. Electrical conductivity of the solid complexes can be measured with BPL – INDIA million mega meter R M 160 m K IIIA over wide temperature

III. RESULTS AND DISCUSSION

On the basis of spectral data, we can say that, the coordination of imines and Riluzole compounds to the central metal atom can take place through the donor sites. Different metal complexes investigated over the temperature range 364-454 K exhibit significant electrical properties. These complexes show increased behaviour of electrical conductivity with rise in temperature according to the following relation:

$$\sigma = \sigma_0 \text{Exp} (- E_a / KT)$$

Figures 1-3 shows the variation of logarithmic conductivity values with the reciprocal of absolute temperature. Most of the complexes show semiconducting behaviour in the temperature range 440-350K. Semiconducting properties of co-ordination complexes with isoterphthaldehyde 2-hydroxy-5-methylacetophenone-S-methyldithiocarbazate have also been reported by J. T. Makode [7]. Semi conductivity studies of polymeric schiff bases and their polychelates have been reported in the literature [6-8]. The synthesized complexes show low electrical conductivity which can be interpreted based on their

semiconducting properties. The delocalization of electron or hole in these complexes exhibiting semi-metallic behaviour is a characteristic of hopping mechanism. The electron or hole drifts from one localized metal site to the nearest neighbour, which results in generating atomic polarization. The electron occupied at new localized metal site is thermally energized so that it can migrate to the adjacent site [9-10].

Table 1. Summary of Activation Energy, E_a

Samples	E _a (eV)	E _a (cal/mol)	E _a (kcal/mol)
Co [(C ₁₅ H ₈ F ₃ N ₂ O ₂ S)(H ₂ O) ₃ Cl]]	0.36 6	8440.4	8.440
Cu [(C ₁₅ H ₈ F ₃ N ₂ O ₂ S)(H ₂ O) ₃ Cl]]	0.18 7	4329.6	4.329
Cd [(C ₁₅ H ₈ F ₃ N ₂ O ₂ S)(H ₂ O) ₃ Cl]]	0.08 5	1970.0	1.970
Zn [(C ₁₅ H ₈ F ₃ N ₂ O ₂ S)(H ₂ O)Cl]]	0.14 4	3336.1	3.336
ZrO [(C ₁₅ H ₈ F ₃ N ₂ O ₂ S)(H ₂ O)Cl]]	0.07 1	1655.3	1.655

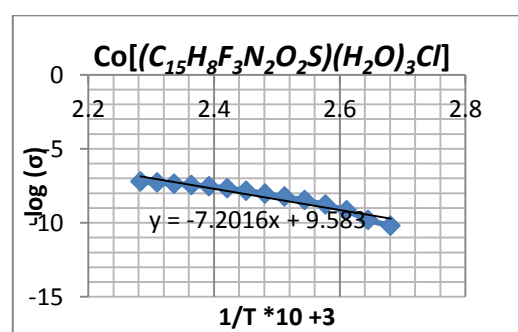


Figure 1a

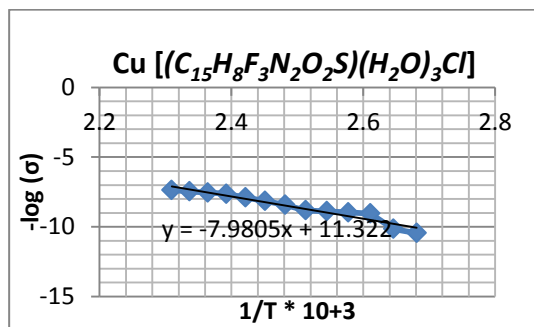


Figure 1b

Figure 1(a-b): DC-Conductivity of Co (II) and Cu (II) complex of HL¹ ligand

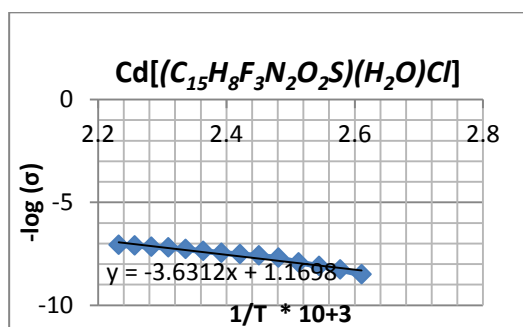


Figure 2a

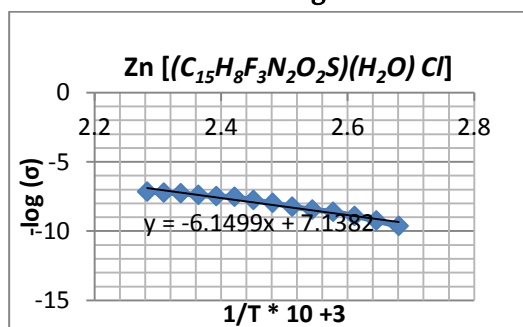


Figure 2b

Figure 2(a-b) . DC-Conductivity of Cd (II) and Zn(II) complex of HL¹ ligand

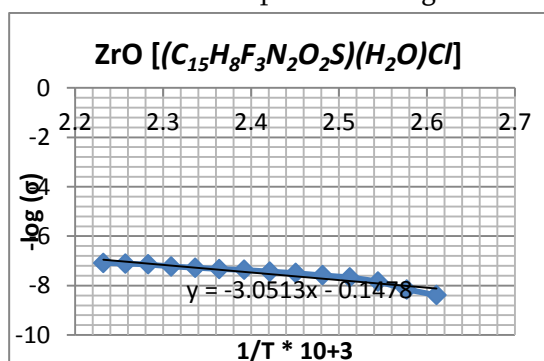


Figure 3. DC-Conductivity of ZrO (II) complex of HL¹ ligand

IV. CONCLUSION

In the present work, different transition metal complexes of riluzoleschiff base were successfully synthesized using microwave irradiation. The synthesized complexes were investigated for their D.C electrical conductivity over the temperature range 364-454 K. The observed electrical conductivity of the complexes increases with increasing temperature. At lower temperature range 300-360K they behave as non-conductor, however they exhibit semi-conducting properties in the temperature range 370-453K. The orders of the activation energy for the synthesized metal complexes are as follows.

$$\text{Co} > \text{Cu} > \text{Zn} > \text{Cd} > \text{ZrO}$$

V. ACKNOWLEDGEMENT

The authors wholeheartedly acknowledge VGST, for their financial support in the form of a research grants vide (No.: VGST/K-FIST (L₁)/GRD-363/2014-15 dated 02/01/15).. We are also thankful to the Principal and Management of PESIT-BSC, Bangalore for their support to carry out this research work.

VI. REFERENCES

- [1]. Prof. Ian Manners, Article first published online: 22 DEC 2003
- [2]. Verlagsgesellschaft M B H, Germany, Angewandte Chemie International Edition in English, 35(15), 1602–1621, 1996.
- [3]. Alaa S. Abd-El-Aziz; Weinheim Macromolecular Rapid Communications, 23(17), 995–1031, 2002.
- [4]. D. Kumar and R. C. Sharma, Eur. Polym. J. 34(8), 1053-1060, 1998.
- [5]. Paul Nguyen, Paloma Gomez-Elipse, and Ian Manners, Canada Chem.Rev., 99 (6), 1515–1548, 1999
- [6]. Jack M. Harrowfield, Gyu Hwan Jang, Yang Kim, Pierre Thuery and Jacques Vicens; J. Chem. Soc., Dalton Trans, 18, 252, 2002.

- [7]. J. T. Makode, *Revue Roumaine de Chimie*; 48(6), 433-437, 2003.
- [8]. F. Cherioux, L. Guyard P. Audebert, *Journal: Cheminform* , 30(5),2010.
- [9]. D Smita Revankar, Jyoti C Ajbani and Revanasiddappa M *Chem. Sci.Rev. Lett* , 5(20), 96-100, 2016.
- [10]. Jyoti C Ajbani, D Smita Revankar, M. Revanasiddappa, Veerabhadra Swamy and S. Shankar, *Int. J. Chem. Sci.* 13(4), 1673-1692, 2015.

Development of Closed-Form Solution for a Multi-Layered Composite Stack Subjected to Thermal Loads

Sanidhya Kumar Sanu¹, B K Karthik², Vijay Vittal³, B Rammohan⁴

Department of Mechanical Engineering, PES University, Bangalore, Karnataka, India

ABSTRACT

Design and assessment of thermal stresses in multi-layered composites has always been area of major concern, as delamination/debonding of the laminae poses a serious issue in the failure of the laminate structure. Stresses at interface can be obtained more swiftly by analytical method when compared to finite element method. In the current work, a comparison has been made between finite element model and first order approximated analytical formulae derived using classical plate theory for a cantilever beam type composite laminate structure with orthotropic material properties. A three-layered structure with orthotropic material properties subjected to uniform thermal load is presented. A comparison has been made among obtained results, Ansys results and the results from similar work carried out in published journal paper. Results obtained from the present work was found to be in close comparison to the Ansys results, stating quantitatively 10.7% from the Ansys results calculated at interface-2, while qualitatively both of them follows the similar trend.

Keywords: Composite laminate, Uniform thermal load, ILSS, Closed-form, Unidirectional lamina, and Multilayered stack

I. INTRODUCTION

A number of scholars have proposed research models for multi-layered composite stack, including experimental and theoretical models. Experimental modeling is a rational approach, but its application entails considerable time and significant expense while in case of theoretical modeling the results can be evaluated in less time and even expenses are less. Several analytical solutions for multi-layered structures have been proposed, but most of them can only be applied to isotropic materials. However, a number of applications necessitates orthotropic properties, hence efficient and practically correct estimation of the interlaminar stresses of these structures are vital for the design and evaluation of delamination/debonding failures. Coefficient of thermal expansion (CTE) mismatch is one of the major reason for delamination subjected to thermal stresses in case of adhesively bonded laminates.

Many researchers have deliberately worked on failure mechanics in multi-layered structures among them first was Timoshenko [1], who studied interlaminar stresses in laminate structures and used simple beam theory to calculate curvature of a bimetallic beam under uniform temperature change. Multi-layered beams and plates, with interfacial stresses, thermal stresses, and free-edge problems, was later studied by Grimado [2], Chen and Nelson [3], and others. Their study was focussed on the methods used in structural mechanics, theory of elasticity and elementary methods of strength of materials.

Chen and Nelson [3] derived a closed-form solution to obtain stress distribution in bonded materials for structures used in electronic devices, due to their thermal expansion mismatch.

Pagano [4, 5] used a different approach, he treated each layer independent of the laminate and

considered them as a homogeneous body in equilibrium and used ply mechanics to analyze composite laminates. This is called “layer equilibrium”. Rehfield and Valisetty [6] provided another alternative for layer or sub-laminate models, they developed a refined theory for homogeneous plates and laminated structures.

Suhir [7-11] developed a method for predicting interfacial stress in single and multi-layered heteroepitaxial structures. To estimate the thermal stresses in two-layer bonded finite joints he introduced a concept of longitudinal and transverse interfacial compliance and combined them into an engineering approach. Suhir [12] also derived a closed-form equation to determine the magnitude and trend of stresses in bi-material thermostats under uniform temperature change. By making assumptions on the compatibility conditions at the interfaces, he extended his approach to multi-layered thin stacks. Pao and Eisele [13] noted a drawback in Suhir solution, they noticed that it does not satisfy the free boundary condition. Therefore, without imposing additional assumptions on the interface they an extension to multi-layered thin stacks was made from Suhir’s bimetal model.

Wen and Basaran [14] presented a paper which is an addition to the Valisetty’s [15] work, they carried work on the calculation of interlaminar shear stress along the interfaces subjected to thermal load. At the end, a comparison was made between the analytical model results and FEM results. Basaran and Zhao [16] worked on the mesh sensitivity of the laminate structure.

II. ANALYTICAL METHOD

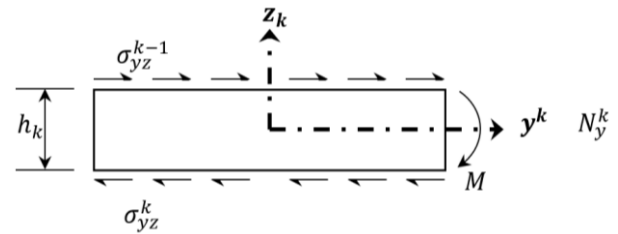


Figure 1. Beam Type Plate

Analytical model for a generic N layered composite laminate stack is developed by using general equations in classical plate theory [17] and macro-mechanical analysis of laminates [18] given as follows. Figure 1 represents k^{th} layer for N layered model.

As it is known that orthotropic materials has 9-elastic constants containing 3-Young's moduli E_x, E_y, E_z , 3-Poisson's ratios $\nu_{yz}, \nu_{zx}, \nu_{xy}$, and 3-shear moduli G_{yz}, G_{zx}, G_{xy} which can be written in compliance form, as shown below:

$$\begin{bmatrix} \varepsilon_{xx} \\ \varepsilon_{yy} \\ \varepsilon_{zz} \\ \varepsilon_{yz} \\ \varepsilon_{zx} \\ \varepsilon_{xy} \end{bmatrix} = \begin{bmatrix} \frac{1}{E_x} & -\frac{\nu_{yx}}{E_y} & -\frac{\nu_{zx}}{E_z} & 0 & 0 & 0 \\ -\frac{\nu_{xy}}{E_x} & \frac{1}{E_y} & -\frac{\nu_{zy}}{E_z} & 0 & 0 & 0 \\ -\frac{\nu_{xz}}{E_x} & -\frac{\nu_{yz}}{E_y} & \frac{1}{E_z} & 0 & 0 & 0 \\ 0 & 0 & 0 & \frac{1}{2G_{yz}} & 0 & 0 \\ 0 & 0 & 0 & 0 & \frac{1}{2G_{zx}} & 0 \\ 0 & 0 & 0 & 0 & 0 & \frac{1}{2G_{xy}} \end{bmatrix} \begin{bmatrix} \sigma_{xx} \\ \sigma_{yy} \\ \sigma_{zz} \\ \sigma_{yz} \\ \sigma_{zx} \\ \sigma_{xy} \end{bmatrix} \quad (1)$$

With plane stress and strain assumption σ_3, τ_{23} and τ_{13} are set to zero, it's determined that

$$\gamma_{23} = 0 \text{ and } \gamma_{13} = 0 \quad (2)$$

hence by the plane-stress assumption, it is noted that there can be no shear strains at all in the 2-3 and 1-3 planes. The plane-stress assumption results to a

relation relating only $\varepsilon_1, \varepsilon_2, \gamma_{12}$ and $\sigma_1, \sigma_2, \tau_{12}$, regardless of the fact that ε_3 is not zero.

$$\begin{bmatrix} \varepsilon_1 \\ \varepsilon_2 \\ \gamma_{12} \end{bmatrix} = \begin{bmatrix} S_{11} & S_{12} & 0 \\ S_{12} & S_{22} & 0 \\ 0 & 0 & S_{66} \end{bmatrix} \begin{bmatrix} \sigma_1 \\ \sigma_2 \\ \tau_{12} \end{bmatrix} \quad (3)$$

The relation among stresses and strains for the state of plane stress, together with the shear stress-shear strain relation is written as

$$\begin{bmatrix} \sigma_1 \\ \sigma_2 \\ \tau_{12} \end{bmatrix} = \begin{bmatrix} Q_{11} & Q_{12} & 0 \\ Q_{12} & Q_{22} & 0 \\ 0 & 0 & Q_{66} \end{bmatrix} \begin{bmatrix} \varepsilon_1 \\ \varepsilon_2 \\ \gamma_{12} \end{bmatrix} \quad (4)$$

The Q_{ij} are called the reduced stiffnesses.

Now adding thermal effect into Eqn. 4 gives following equation.

$$\begin{bmatrix} \sigma_1 \\ \sigma_2 \\ \tau_{12} \end{bmatrix} = \begin{bmatrix} Q_{11} & Q_{12} & 0 \\ Q_{12} & Q_{22} & 0 \\ 0 & 0 & Q_{66} \end{bmatrix} \begin{bmatrix} \varepsilon_1 - \alpha_1 \Delta T \\ \varepsilon_2 - \alpha_2 \Delta T \\ \gamma_{12} \end{bmatrix} \quad (5)$$

As every ply has its own fiber orientation, therefore it's really important to convert them to global coordinate by using transformation matrix [T].

$$\begin{bmatrix} \sigma_1 \\ \sigma_2 \\ \tau_{12} \end{bmatrix} = [T] \begin{bmatrix} \sigma_x \\ \sigma_y \\ \tau_{xy} \end{bmatrix} \quad (6)$$

where

$$T = \begin{bmatrix} m^2 & n^2 & 2mn \\ n^2 & m^2 & -2mn \\ -mn & mn & m^2 - n^2 \end{bmatrix} \quad (7)$$

where, $m = \cos\theta$, $n = \sin\theta$

$$\begin{bmatrix} \varepsilon_x \\ \varepsilon_y \\ \gamma_{xy} \end{bmatrix} = [T]^T [S] [T] \begin{bmatrix} \sigma_x \\ \sigma_y \\ \tau_{xy} \end{bmatrix} \quad (8)$$

$$\begin{bmatrix} \varepsilon_x \\ \varepsilon_y \\ \gamma_{xy} \end{bmatrix} = \begin{bmatrix} \bar{S}_{11} & \bar{S}_{12} & \bar{S}_{16} \\ \bar{S}_{12} & \bar{S}_{22} & \bar{S}_{26} \\ \bar{S}_{16} & \bar{S}_{26} & \bar{S}_{66} \end{bmatrix} \begin{bmatrix} \sigma_x \\ \sigma_y \\ \tau_{xy} \end{bmatrix}$$

where, the "compliance matrix $[\bar{S}]$ or \bar{S}_{ij} " is defined by,

$$[\bar{S}] = [C]^{-1} = ([T]^{-1}[C][T]^{-T})^{-1} = [T]^T [C]^{-1} [T] = [T]^T [S] [T] \quad (9)$$

$$\sigma_{xz}^k = \frac{Q_{11}^k}{2} \left(z^2 - \frac{h_k^2}{4} \right) \left(\frac{-\kappa_x + \nu_{12}(-\kappa_y)}{x} \right) \quad (13)$$

Using Eqn. 10 to calculate overall force and moment in the composite structure after application of thermal load ΔT .

$$\begin{Bmatrix} N_x \\ N_y \\ N_{xy} \\ M_x \\ M_y \\ M_{xy} \end{Bmatrix} = \sum_{k=1}^N [\bar{Q}]_k [\alpha]_k (z_k - z_{k-1}) \Delta T \quad (10)$$

where,

N = resultant forces

M = resultant moments

$$\begin{Bmatrix} \varepsilon_x^0 \\ \varepsilon_y^0 \\ \gamma_{xy}^0 \\ \kappa_x \\ \kappa_y \\ \kappa_{xy} \end{Bmatrix} = \begin{bmatrix} A_{11} & A_{12} & A_{16} & B_{11} & B_{12} & B_{16} \\ A_{12} & A_{22} & A_{26} & B_{12} & B_{22} & B_{26} \\ A_{16} & A_{26} & A_{66} & B_{16} & B_{26} & B_{66} \\ B_{11} & B_{12} & B_{16} & D_{11} & D_{12} & D_{16} \\ B_{12} & B_{22} & B_{26} & D_{12} & D_{22} & D_{26} \\ B_{16} & B_{26} & B_{66} & D_{16} & D_{26} & D_{66} \end{bmatrix}^{-1} \begin{Bmatrix} N_x \\ N_y \\ N_{xy} \\ M_x \\ M_y \\ M_{xy} \end{Bmatrix} \quad (11)$$

where,

$[A_{ij}]$ = stiffness matrix

$[B_{ij}]$ = bending coupling matrix

$[D_{ij}]$ = bending stiffness matrix

The three strains $\varepsilon_x, \varepsilon_y$ and γ_{xy} at any point on the normal line given the three strains $\varepsilon_x^0, \varepsilon_y^0$, and γ_{xy}^0 and the three curvatures κ_x, κ_y , and κ_{xy} , and the distance z from reference surface.

$$\begin{aligned} \{\varepsilon_x\}_k &= \varepsilon_x^0 + z\kappa_x \\ \{\varepsilon_y\}_k &= \varepsilon_y^0 + z\kappa_y \\ \{\gamma_{xy}\}_k &= \gamma_{xy}^0 + z\kappa_{xy} \end{aligned} \quad (12)$$

Integrating the equation used in classical plate theory and using Eqn. 4 and Eqn. 11 we get the equation for Interlaminar Shear Stress in x and y-direction

$$\sigma_{xz}^k = \frac{Q_{11}^k}{2} \left(z^2 - \frac{h_k^2}{4} \right) \left(\frac{-\kappa_x + \nu_{12}(-\kappa_y)}{x} \right) \quad (13)$$

$$\sigma_{yz}^k = \frac{Q_{22}^k}{2} \left(z^2 - \frac{h_k^2}{4} \right) \left(\frac{-\kappa_y + \nu_{12}(-\kappa_x)}{y} \right) \quad (14)$$

where, $k = k^{\text{th}}$ layer of the composite structure

Q^k = Reduced Stiffness for k^{th} layer

κ = Curvature

h = Thickness of each layer

III. CASE STUDY

For better clarification, a case study has been taken into consideration for a generic three-layered composite laminate stack with orthotropic material properties [14] subjected to a uniform thermal load of $\Delta T = 100^\circ\text{C}$. Thermal loads leads to thermal stresses owing to different CTE in different layers. Figure 2 and Figure 3 describes the geometry of the model and Table.1 indicates the dimension and material properties of the model.

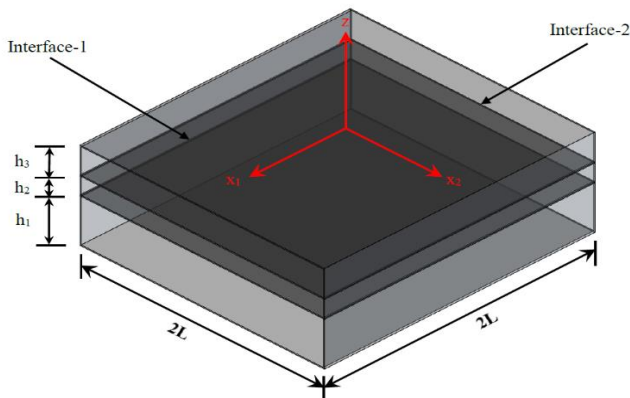


Figure 2. Three-layered model

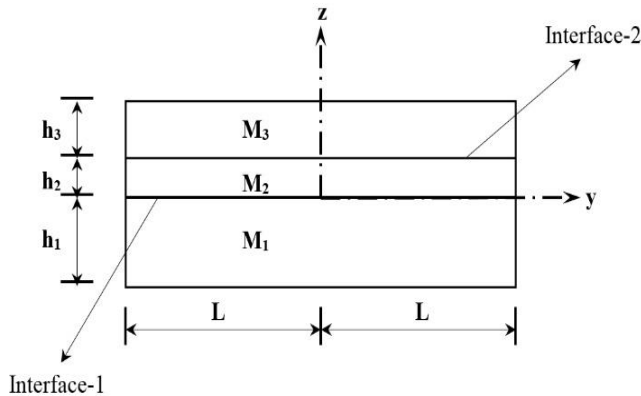


Figure 3. 2-D view of three-layered model

Table 1. Material properties and dimension of considered model

	M1	M2	M3
$E_1(\text{GPa})$	11	15	13
$E_2(\text{GPa})$	140	138	16
$E_3(\text{GPa})$	11	15	13

$G_{12}(\text{GPa})$	5.5	5.9	2.7
$G_{13}(\text{GPa})$	5.5	5.9	2.7
$G_{23}(\text{GPa})$	5.5	5.9	2.7
ν_{12}	0.29	0.21	0.16
ν_{13}	0.29	0.21	0.16
ν_{23}	0.3	0.21	0.16
$\alpha_1(e-6/^\circ\text{C})$	0.36	0.9	0.5
$\alpha_2(e-6/^\circ\text{C})$	28.8	23	18
$\alpha_3(e-6/^\circ\text{C})$	28.8	23	18
h(mm)	0.508	0.0508	0.14
2L(mm)	15.24		

In the present model assumed boundary conditions @ $y=0$ are

$$\begin{aligned} U_y^1 &= 0 & \phi_y^1 &= 0 \\ U_y^2 &= 0 & \phi_y^2 &= 0 \\ U_y^3 &= 0 & \phi_y^3 &= 0 \end{aligned} \quad (15)$$

$$\sigma_{yz}(0,0) = 0 \quad \sigma_{yz}(0,h_k) = 0$$

Using the boundary condition given by Eqn. 15 an Ansys model has been developed and inter-laminar shear stress has been calculated at interface-1 and at interface-2 as shown in Figure 4 and Figure 5.

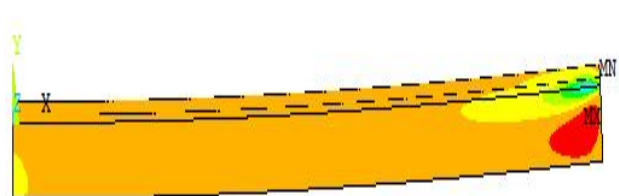


Figure 3. Ansys Model

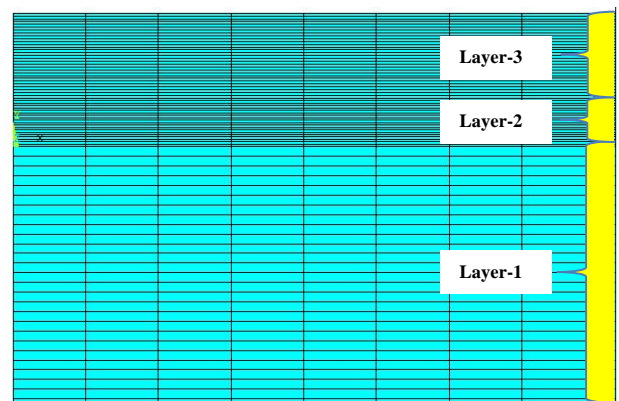


Figure 4. Ansys mesh exaggerated view

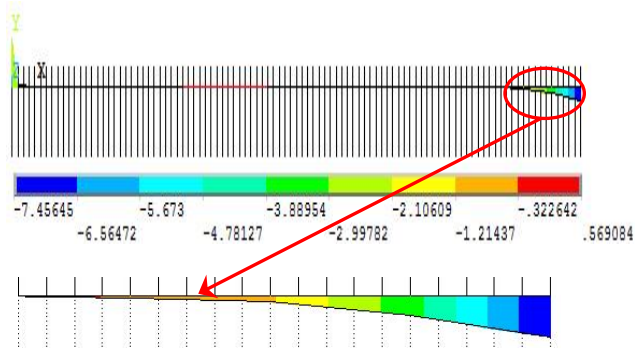


Figure 5. Ansys results at Interface-1

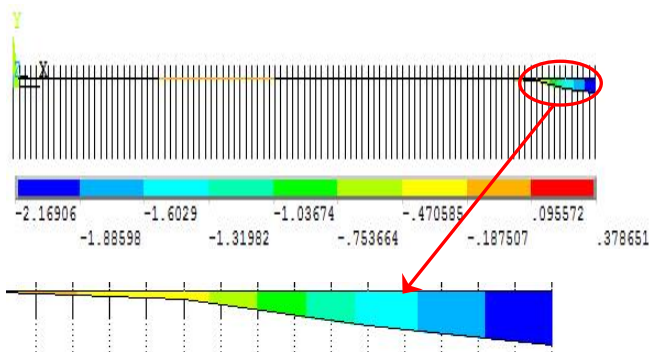


Figure 6. Ansys results at Interface-2

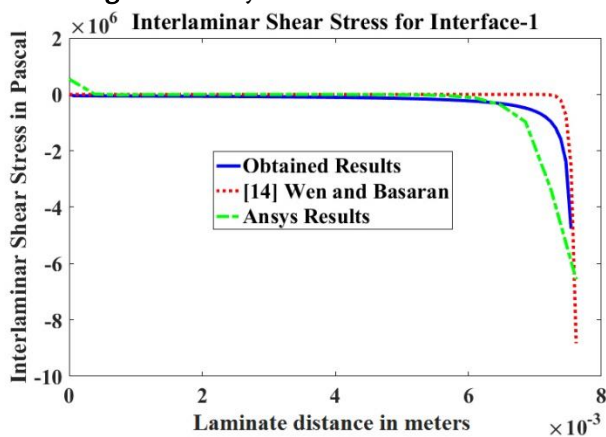


Figure 8. Comparison of ILSS at interface-1 between Derived Model, Wen & Basaran [14] and Ansys Results

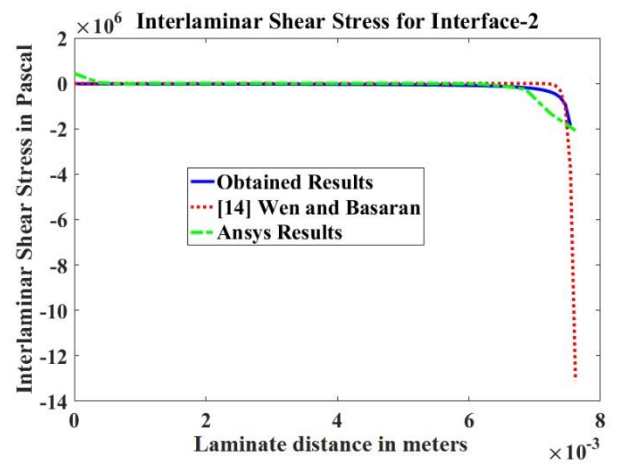


Figure 9. Comparison of ILSS at interface-2 between Derived Model, Wen & Basaran [14] and Ansys Results

The exaggerated view shown in Figure 6 and Figure 7 shows ILSS in interface-1 and interface-2 respectively at the near free edge.

Again using boundary condition given by Eqn. 15 and using Eqn. 14 to calculate inter-laminar shear stress (ILSS) at interface-1 and interface-2 for which a Matlab code has been developed.

Results from Ansys model, analytical model and the results from equation for work carried out by Wen and Basran [14] are plotted, as shown below.

IV. RESULTS AND DISCUSSIONS

To calculate the interlaminar shear stress a number of methods were suggested. In the present paper, the method proposed uses stiffness in each layer, overall strain and overall curvature of the laminate stack to calculate ILSS. Overall strain and overall curvature for the structure was calculated by using ABD matrix. ABD matrix was calculated for each layer using the given material properties and was later reduced to single ABD matrix [19], which represented properties for overall structure of the model. Simultaneously, resultant forces and resultant moments were calculated for the structure with $\Delta T = 100^{\circ}\text{C}$. Using ABD matrix

and resultant forces and resultant moments overall strains and curvatures for the model was calculated as indicated in Eqn. (12). By considering curvatures and thickness of each layer we obtain strains in each layer. Strain obtained from Eqn. (13) represents the strain along the thickness of the considered layer, different approach can be used to obtain the strain distribution along the length of the structure and also to calculate displacements in x, y and z-direction.

The analytical results shown in Figure 8 and Figure 9 was analyzed and compared with two other results which were obtained from Ansys APDL code [20] and from the work carried out by Wen and Basaran [14]. The Ansys mesh model contained in total of 10000 elements which is very fine mesh and according to the study carried out by Basaran and Zhao [16] it is predicted to produce a reasonable result. The results for ILSS at interface-1 and interface-2 were extracted from Ansys model, creating first set of data for comparison. In the work of Wen and Basaran [14], they developed a first-order approximated analytical model to calculate ILSS at different interfaces, using those equations to calculate ILSS at interface-1 and interface-2 creating another set of data for comparison. Using the data extracted from Ansys model, Wen and Basaran model and from Eqn. 14 altogether, graphs were plotted as shown in Figure 8 and Figure 9. Results from Eqn. 14 refers to the method suggested in this paper by using classical plate theory and macro-mechanical approach.

As it can be noticed from Figure 8 and Figure 9 that the distribution of interfacial shear stress at interface-1 and interface-2 is in good agreement to the Ansys results while when compared with the Wen and Basaran model a substantial difference can be noticed. In terms of the quantitative comparison, it has been found that there is difference of 27.5% was found between Ansys results and calculated results at interface-1 and 46% difference between Wen and Basaran model and calculated results. Whereas, for

interface-2 the difference was found to be 10.7% between Ansys results and calculated results and 85.8% between Wen and Basaran model and calculated results. The comparison of results was done for the data at the near free edge.

V. SCOPE FOR FUTURE WORK

The present work can be extended to laminates subjected to gradient thermal loads and also to laminates with different thermal load. Laminates used in this paper uses unidirectional fiber orientation but it can also be extended to bidirectional fiber orientation.

VI. CONCLUSIONS

The derived analytical model to calculate ILSS was comparable with the Ansys results. When compared qualitatively both Ansys results and evaluated results follows similar trend. It can also be concluded that compared to Ansys modeling and meshing, a simple calculation by using derived equation can yield faster results.

VII. REFERENCES

- [1]. Timoshenko, S., 1925, "Analysis of Bi-Metal Thermostats", J. Opt. Soc. Am., 11, pp. 233-255.
- [2]. Grimado, P. B., 1978, "Interlaminar Thermoelastic Stresses in Layered Beams", J. Therm. Stresses", 1, pp. 75-86.
- [3]. Chen, W. T., and Nelson, C., 1979, "Thermal Stresses in Bonded Joints", IBM J. Res. Dev., 23.2., pp. 179-188.
- [4]. Pagano, N. J., 1978, "Stress Fields in Composite Laminates", Int. J. Solids Struct., 14, pp. 385-400.
- [5]. Pagano, N. J., 1974, "On the Calculation of Interlaminar Normal Stress in a Composite Laminate", J. Compos. Mater., 8, pp. 65-82.
- [6]. Rehfield, L. W., and Valisetty, R. R., 1984, "A Simple Refined Theory for Bending and Stretching of Homogeneous Plates", AIAA J., 22.1., pp. 90-95.

- [7]. Suhir, E., 1986, "Stresses in Bi-Metal Thermostats", ASME J. Appl. Mech., 53, pp. 657-660.
- [8]. Suhir, E. 1986, "Stresses in Adhesively Bonded Bi-Material Assemblies Used in Electronic Packaging", Elect. Pack. Mat. Science-II, MRS Symp. Proc., pp. 133-138.
- [9]. Suhir, E. 1986, "Calculated Thermally Induced Stresses in Adhesively Bonded and Soldered Assemblies", Int. Symp. Microelect., pp. 383-392.
- [10]. Suhir, E. 1987, "Stresses in Multilayered Thin Films on a Thick Substrate, Heteroepitaxy-on-Silicon II", MRS Symp. Proc, 91, pp. 73-80.
- [11]. Suhir, E. 1988, "An Approximate Analysis of Stresses in Multilayered Elastic Thin Films", ASME Winter Annual Meeting, WA/APM-14.
- [12]. Suhir, E., 1989, "Interfacial Stresses in Bimetal Thermostats", ASME J. Appl. Mech., 56, pp. 595-600.
- [13]. Pao, Y.H., and Eisele, E., 1991, "Interfacial Shear and Peel Stress in Multi-Layered Thin Stacks Subjected to Uniform Thermal Loading", ASME J. Electron. Packag., 113, pp. 164-172.
- [14]. Wen, Y., and Basaran, C., 2003, "Thermomechanical Stress Analysis of Multi-Layered Electronic Packaging", ASME J., 125, pp.134-138.
- [15]. Valisetty, R. R., and Rehfield, L. W., 1983, "A Theory for Stress Analysis of Composite Laminates", AIAA Paper 83-0833-CP, 24thAIAA/ASME/ASCE/AHS Structures, Structural Dynamics, and Materials Conference, Lake Tahoe, NV.
- [16]. Basaran, C., and Zhao, Y., 2001, "Mesh Sensitivity and FEA for Multi-layered Electronic Packaging", ASME J. Electron. Packag., 123.3., pp. 218-224.
- [17]. O.C. Zienkiewicz, R.L. Taylor, and J.Z. Zhu, 2013 "The Finite Element Method: Its Basis and Fundamentals" Seventh Edition ISBN: 978-1-85617-633-0, Elsevier
- [18]. Autar K Kaw, 2006, "Mechanics of Composite Materials", Second Edition, CRC Taylor and Francis
- [19]. George Z. Voyiadjis, Peter I. Kattan, 2005, "Mechanics of Composite Materials with Matlab", Springer
- [20]. Ever J. Barbero, 2014, "Finite Element Analysis of Composite using Ansys", Second Edition, CRC Press, Taylor and Francis Group

Mathematical Modelling and Automation of Real-time Queues

Srikrishna C.N

Department of Information Science and Engineering PES Institute of Technology – South Campus, Bangalore,
Karnataka, India

ABSTRACT

The traditional Queue System followed today is quite certainly failing in managing huge crowds, especially in urban populated areas. There are even instances where the customers (users) have to wait for hours to get simple tasks done. It is important to manage these systems effectively by the Organizations in order to improve customer experience. While the Token Queue System provides a fairly acceptable solution, it has many problems of its own. In a token system, waiting physically in the building premises is inevitable. The design discussed in this paper holds the prime idea of completely automating the Token System, where users' waiting time is almost negligible. Using the classical Queue Theory and Poisson's Probability Distribution, it is possible to predict the arrival of the users and the average service time, for a particular service. It uses minimal resources and is cost effective. This paper discusses a model that uses these ideas to build a system that automates the traditional queuing system. It aims not only to minimize the customer wait time, but also reduce the crowds at the service area.

Keywords: Queues, Queue theory, Token System, Automation, Smart phones.

I. INTRODUCTION

Arnold O. Allen, in his famous book - 'Probability, Statistics, and Queue Theory'[1], describes "Waiting in line for service is one of the most unpleasant experiences of life on this planet." It is indeed a dreadful experience which most of the people go through. For an organization, higher the unhappy customers, the more is their loss of reputation.

Ever since the rise of urbanization and population growth, managing huge crowds has become a serious challenge. This certainly raises an interesting question, as how to solve this problem using Automation. Although there are many models that have attempted to solve this issue, only a few of them have been proven effective [5][6][7]. This is the reason why traditional Token System seems to be a better alternative and is still popular. On the other hand, the growth of automation has changed the way the traditional things would otherwise work. Thus, the

proposed model in this paper has been designed to promote automation in every aspect. The model assumes the queue dealt with, is a structured queue.

It is designed in such a way that it is cost effective as well as effective in managing the real time queue systems.

A brief walk through of the paper is given below,

- ✓ In section 2, (**Literature Review**), a brief review is discussed on the classic Queue Theory, Models of Queue and Probability Distributions that are used in the design.
- ✓ In section 3, (**Design and Implementation**), the proposal of the model as well as the design and implementation is discussed, in detail.
- ✓ In section 4, (**Results and Discussion**), test cases and results of the model are discussed. A brief discussion on emergency and error handling is done.

- ✓ In section 5 & 6, (**Conclusion and Future Work**) conclusion of the model and future work to improve rapid variations, are discussed.

II. LITERATURE REVIEW

A queue is a group of people waiting for a service one behind the other. The following gives a broad classification of queues

A. Types of Queues

1. **Structured Queue:** In this type of queue, people stand at a predictable position.
E.g.: Queues at banks and supermarkets have a predictable number of people forming a queue.
2. **Unstructured Queue:** In this type of queues, people are considered to be located at unpredictable positions and timings
3. **Virtual Queue:** This is a new form of Queue system, where people use their personal devices such as smartphones and tablets to reserve their turn as well as be updated as their turn approaches.

B. Queue Theory

Queue theory is the mathematical study of behavior of queues. It was extensively researched by Agner Krarup Erlang[8], when he created models to describe the Copen-Hagen telephone exchange.

In the proposed model, the Queue Theory is used to compute various parameters affecting the users as well as the system as a whole.

C. Kendall's Notation

The Kendall notation, after David Kendall[9], is developed to describe queuing systems. The notation is of the form A/B/c/K/m/Z where,

A stands for the arrival time distribution,
B stands for the service time distribution,
c is the number of servers available,

K the total system capacity (maximum number of customers that could be accommodated in the system), m the total source population, and Z - the type of queue discipline.

Usually, the shorter notation 'M/M/1': it is assumed that there is no limit to the length of the queue, the customer source is infinite, and the queue discipline is FCFS (First Come - First Serve).

D. The Poisson's Distribution

Poisson's Distribution is a discrete probability distribution that expresses the probability of a given number of events occurring in a fixed interval of time. If a Queue System keeps track of the number of users waiting in the queue for a specific service, and if the event of arrival of one customer is independent of arrival of others, it follows a Poisson's Distribution. The discrete values of the random variable 'x' which denotes the event of arrival of 'n' customers at time 't'. [1]

$$P_t('x') = (e^{-\lambda} * \lambda^x) \div x!$$

Where P_t is the Probability function and it describes event of 'x' number of people arriving at time t ($0 < P < 1$).

E. The M/M/1 Model

The M/M/1 queue model assumes infinite system capacity (k) and infinite number of population source (m). The system follows Poisson's Distribution. Proofs of these formulas are provided in the reference [1]. We consider total system wait time as a sum of the wait time in the queue and wait time in the service.

L: Number of People

W: Waiting time

We use a M/M/1 queue model to design the model in the paper as it is an ideal model in real-time systems. The formulas derived for the M/M/1 model are listed as follows:

$$\rho = \lambda / \mu \text{ (Traffic Intensity or Utilization parameter)}$$

L_{sys} (Number of people in the System): $\lambda / (\mu - \lambda)$

W_{sys} (Total wait time) = $W_q + W_{service}$

$W_{sys} = 1 / (\mu - \lambda)$

Little's Law : $L = \lambda W^{[10]}$

L_q (Number of people in Queue) = $L * s - (\lambda / \mu)$

III. DESIGN AND IMPLEMENTATION

The design of the model is done assuming that the queue is a structured queue. As discussed before, the structured queues include the queues that are found in banks, retails and other similar public places.

The Company/Organization has to provide the list of services they provide on the user application.

The user shall then choose the required service.

The service chosen shall be entered in the database. Since the service time differs from one service to the other, there is a need to collect the service time data for all individual services. The data is collected so as to provide better prediction of P_t using formulae listed in the M/M/1 model (Section 2). The predicted time (P_t) is computed and is provided to the user. It shall estimate the time before which the user shall have to be physically present in the service premises. The user is given virtual P Sequence Token (P_{seq}) when he/she registers in the application along with the choice of their service.

The user is regularly reminded (notified) as his/her turn comes closer. If the user confirms their presence in/around premises, they shall be given a C Sequence Token (C_{seq}). Confirmation could be done using location APIs or a QR Scanning method. And the user shall be provided the service shortly after their arrival.

The prime reason behind providing the separate Sequence Tokens to the users is to ensure that the users are physically present right around the time of their turn. In case, the user fails to confirm his/her presence, it will lead the Timeout (End of P_t). Also,

they shall be reassigned the nearest available P_{seq} Token (In place of timeouts that happen for subsequent users or the last turn at that point of time), such that it shall be minimal at that point of time. This ensures that they can still be in the line without disturbing the system. The models of the user side application and the server are discussed below.

A. User Application

The user needs to have the application to register for their turn in the queue.

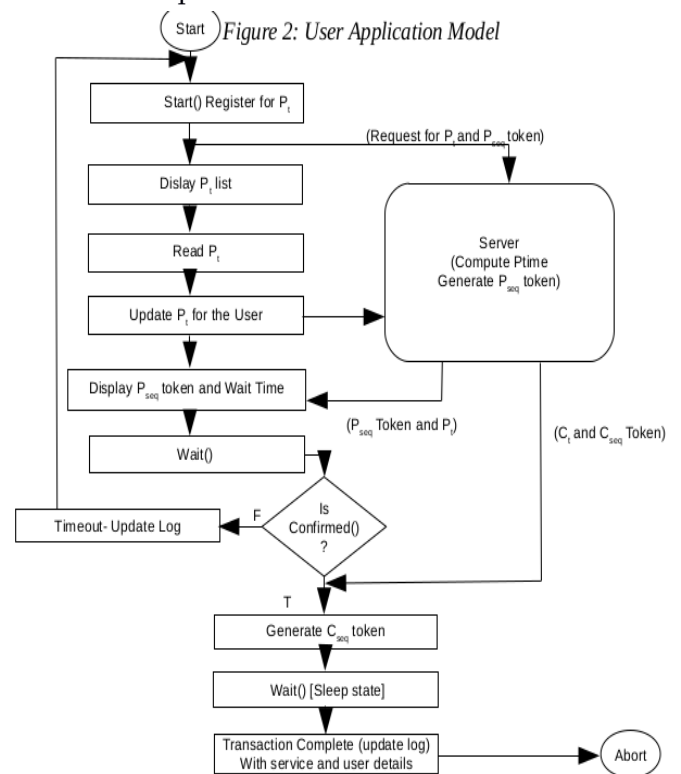


Figure 1

The application from which the user shall register has the following function

- Fetching the data from the server such as token, wait time, information of the position in the line.
- Transferring of data such as service time and other information related to emergencies.
- Update the real time queue information such as position and wait time.

1) Requesting the service:

As the user registers for a service, the request is sent to the server. This information shall contain id of the service which the user desires to receive. This in turn shall be stored in the database. The total wait time is calculated between the users' arrival and their finish of service. This information is useful in calculating the service rate for future predictions.

2) Calculate the predicted time:

The request sent by the user application shall trigger the server to generate a Token number along with its Predicted time (P_t). This data is then fetched by the user device.

3) Update the queue:

As the transactions progresses, when the customers finish their service, the server updates the time as well as the users' position in the queue.

The user application is depicted in Figure 2. This is a conceptual design of the system and it describes the work flow of the model. The notations used in the figures hold the same meaning as described earlier.

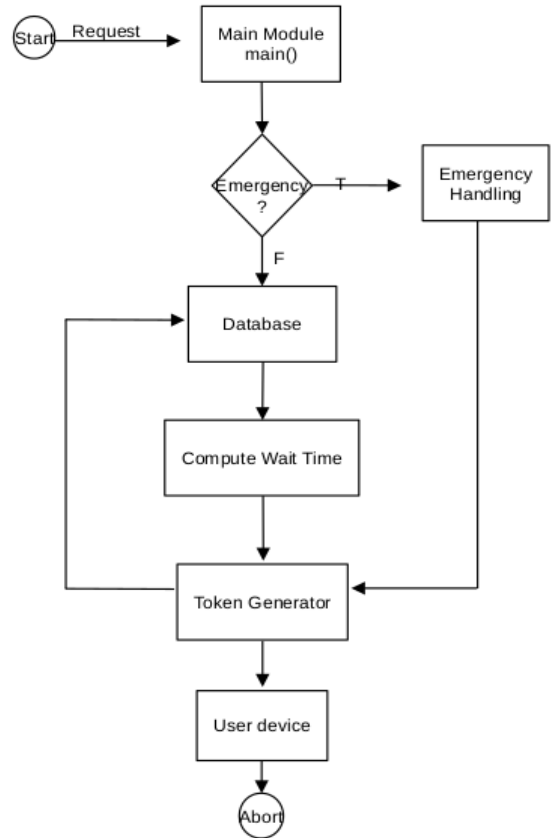
B. Server

The server on the other hand, has three major functions:

- Generate token and predict time.
- Update users as queue progresses
- Handling emergencies.

The computation of wait time depends on average service rate and arrival rate. As discussed in section 2, the P_t is calculated and transferred to the user device as depicted in Figure 3.

Figure 3: Server Model



Figuer 2

1) Database

Database holds the values of the arrival time of the user, along with the ID of the chosen service. Thus, the service rate could vary for two different services. A sample structure is depicted in the table below.

Table 1.sample database

User ID	Service ID	Arrival time	Service duration
01	S-02	8:45	4:23 min
02	S-01	8:50	2:11 min
03	S-02	9:01	3:53 min
04	S-03	9:04	1:40 min
05	S-01	9:09	2:35 min

2) Computing Wait time

It can be seen that the arrival rate of the customer varies from time to time. Thus, the arrival rate of the customer should be calculated for a specific time interval of the day. If suppose a bank records the of

arrival of customers from 10 a.m to 11 a.m, the mean arrival rate calculated will be different from that of the one which is calculated between 2 p.m and 3 p.m. The time estimation thus, should be done using the arrival rate related to a specific part of the day and not as the day as a whole. From the formula of arrival rate between time interval t_1 and t_2 ,

$$\lambda = \text{number of customers between the interval} / (t_2 - t_1)$$

3) Generate Token

As the time is estimated, the token is generated and given to the user. The token Generator will have to manage the requests in order to provide the correct token (P_{seq} or C_{seq}) as per their turn.

I. RESULTS AND TEST CASES

The test cases of the model are tabulated below. The test cases show the conceptual working of the model of a structured M/M/1 Queue model. The values of time interval could vary from service to service, person to person who is handling the service, specific time of the day or a particular day of a week.

A. Test 1: General Case

The user registers for the service at 8:26 am, and she is given a P_{seq} token (P-003). As the turn approaches, she is notified for the confirmation of her presence. The user confirms at 9:12 am and accordingly a C_{seq} token (C-003) is given. The wait thereafter is about 3 minutes.

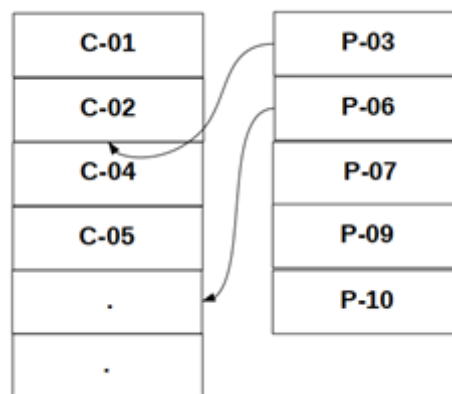


Illustration 1: General Case

Table 2.test case 1

Index	Description	Values
01	Service ID	01
02	Time of Registration	8:26
03	P_{seq} token	P-003
04	Estimated Wait Time (P_t)	9:12 min
05	Confirmed? C_{seq}	Yes (9:14)
06	C_{seq}	C-003
06	Service complete at	9:18

B. Test 2: Unconfirmed User – I

The user registers for the service at 3:47 pm, and he is given a P_{seq} token (P-002). As the turn approaches, he is notified for the confirmation of his presence. The user fails to confirm their presence and hence it will lead to Timeout. Since there is another Timeout after this user, user with P-001 token is given a position in place of that user. And further, after confirmation a C_{seq} token (C-005) is given.

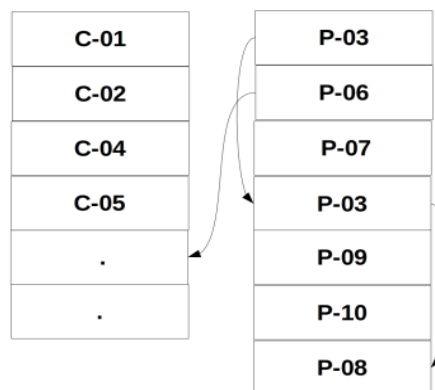


Illustration 2. Timeout Swap

Table 2. Test case 2

Index	Description	Values	Remarks
01	Service ID	02	
02	Time of Registration	3:47	
03	P _{seq} token	P-002	
04	Estimated Wait Time (P _i)	4:35 min	
05	Confirmed? C _{seq}	No	No C _{seq}
06	New P _{seq} Token (replaced in place of the nearest timeout user)	P-010	From the nearest timeout
07	New Estimated Wait time	4:55	
08	User confirmed for C _{seq} token	4:52	
09	C _{seq} token	C-010	
10	Service complete at	5:02	

C. Test 3 : Unconfirmed User – II

The user registers for the service at 2:05 pm, and he is given a P_{seq} token (P-004). As the turn approaches, he is notified for the confirmation of his presence. The user fails to confirm their presence and hence it will lead to Timeout. Since there are no other Timeout after this user, user with P-004 token is given a position in place of the nearest available turn.

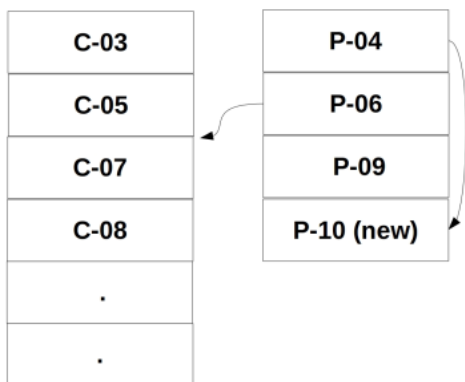


Illustration 2. Nearest Available Position

TABLE 3. TEST CASE 3

Index	Description	Values	Remarks
01	Service ID	02	
02	Time of Registration	2:05	

03	P _{seq} token	P-004	
04	Estimated Wait Time (P _i min)	3:37	
05	Confirmed? C _{seq}	No	No C _{seq}
06	New P _{seq} Token (Issue the nearest position)	P-010	New token
07	New Estimated Wait time	4:55	
08	User confirmed for C _{seq} token	4:53	
09	C _{seq} token	C-010	
10	Service complete at	5:03	

D. Test 4: Emergency Scenario

The user registers for the service at 2:33 p.m, and he is given a P_{seq} token (P-010). Since the user registered as an emergency case, the nearest Timeout after this user, user with P-007 token is swapped with P-010 user. The wait thereafter is about 4 minutes. After the service, the service time is recorded in the database.

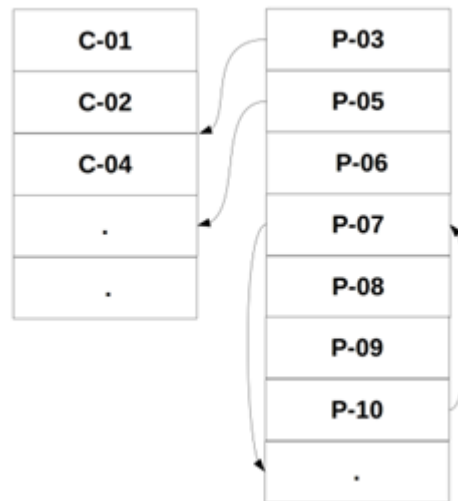


Illustration 3. Emergency Handling

TABLE 4. TEST CASE 4

Index	Description	Values	Remarks
01	Service ID	01	
02	Time of Registration	2:33	
03	P _{seq} token	P-010	Nearest

			timeout
04	Estimated Wait Time (P _t)	2:49	
05	Confirmed ?C _{seq}	Yes (2:49)	
06	C _{seq}	C-010	
06	Service complete at	2:51	

IV. CONCLUSION

The classical Queue Theory has been continuously studied for more than a century. Various models of the queues have been studied among which, the M/M/1 Queue Model is the most relevant in our model. As described before, the Model discussed in this paper is best suited for a structured queue. A structured queue with a single server follows Poisson's Distribution, and the probabilities of arrival could be computed by referring the data of arrival of customers. This takes us to the next topic of calculation of arrival and service rates. The observed values will serve as a reference to compute the average wait time for the subsequent users. It is also possible to estimate the expected number people arriving, which helps in improving the services and when there is a rapid growth.

V. FUTURE WORK

Having computed the estimated values of time and users on any particular part of the day, the prediction algorithms can be accordingly improved. The proposed model needs improvement in handling the emergencies and rapid variations in the queues. As this model directly interacts with a real world problem, there are chances that it might face a failure. Also emergencies are recommended to be handled directly by the Organization in order to make the decisions on the basis of their policies.

The system also requires an improvement in the prediction algorithms which could be enhanced through Data Analysis. The future work also involves

the addition of an error correction factor to meet the needs of real-time systems.

VI. REFERENCES

- [1]. Allen, Arnold A. (1990). Probability, Statistics, and Queueing Theory: With Computer Science Applications. Gulf Professional Publishing. p. 259. ISBN 0120510510.
- [2]. Customers' Evaluations of Queues: Three Exploratory Studies A.Th.H. Pruyn, A. Smidts - European Advances in Consumer Research Volume 1
- [3]. A Survey of Recent Developments in Queue Wait Time Forecasting Methods, Ron Davis Tamara Rogers , Yingping Huang
- [4]. Automatic Queueing Model for Banking Applications Dr. Ahmed S. A. AL-Jumaily Dr. Huda K. T. AL-Jobori
- [5]. Smart Queue Management System Using GSM Technology, Arun, R and Priyesh, P.P.
- [6]. Smart Token Bank System Prof. Mr. Ganesh Attarde, Snehal P. Shahane, Prasad Mahajan, Vaibhav Yadnik
- [7]. Erlang, Agner Krarup (1909). "The theory of probabilities and telephone conversations"
- [8]. Kendall, D.G.:Stochastic processes occurring in the theory of queues and their analysis by the method of the embedded Markov chain, Ann. Math. Stat. 1953
- [9]. Little, J. D. C. (1961). "A Proof for the Queueing Formula: $L = \lambda W$ "

Spectroscopic and Electromagnetic Interference-Shielding Effectiveness Studies on Polyaniline/DBSA/MoO₃ Composite at X-band Frequencies

NagesaSastry. D¹, Vinay. K², Hiremath Suresh Babu³, Revanasiddappa. M^{*4}

¹Department of Chemistry, Veerashaiva College, Bellary, Karnataka, India

²Department of Chemistry, Channabasaveshwara Institute of Technology, Gubbi, Karnataka, India

³Department of Chemistry, RaoBahadur Y Mahabaleswarappa Engineering College, Bellary, Karnataka, India

⁴Department of Chemistry, PESIT-Bangalore South Campus, Bangalore, Karnataka, India

ABSTRACT

Nowadays, emerging research in the areas of conducting polymer-based metal oxide composites have shown much interest among modern physical and chemical researchers due to their unique absorption properties. In the present work, the conducting polyaniline/ molybdenum trioxide nanoparticles blended in DBSA was synthesized by in-situ polymerization technique with varied weight % (10, 20, 30, 40 and 50) of molybdenum trioxide. The analysis on the EMI Shielding Effectiveness (EMI-SE) of the synthesized samples in the X-band frequencies (8.2-12.4 GHz) is presented here. The influence of molybdenum trioxide nanoparticle in Polyaniline/DBSA matrix over the EMI-SE has been studied. It is observed that the synthesized composites exhibit excellent shielding efficiency in the entire range of X-band. The absorption governed shielding effectiveness of the synthesized polyaniline/DBSA/MoO₃ composite finds cost effective applications and manifests electromagnetic compatibility in the X-band frequencies.

Keywords: Polyaniline; DBSA; molybdenum oxide; EMI shielding; composites.

I. INTRODUCTION

Composites of conducting polymer – metal oxide nanoparticles are of great research interest for scientists due to their distinct physical and chemical properties viz., high conductivity, facile synthesis, light weight, flexibility and ease of processability [15]. Due to these properties, they have recently attracted much interest in practical application as broad band microwave absorbers and electromagnetic shielding screens [1-4]. The characteristic absorption properties in particular have many areas especially in the field of aerospace and military applications, where conductive composites studied so far have been relatively poor broad band performers and such composites appears to be one of the few materials capable of dynamic

microwave absorption. Microwave absorbers have attracted greater importance because of their use in electronic devices and controlling the wave pollution [5]. Hence EMI-SE has therefore, become a matter of high priority.

II. METHODS AND MATERIAL

Doubly distilled aniline (1.0ml) monomer and 7.6 ml of dodecyl benzene sulphonic acid (DBSA) were mixed in 500 ml of milli-Q water with constant stirring. After 1hr, an aqueous solution (10ml) of 0.1mol ammonium persulfate (APS) was pour to the reaction mixture. The obtained solution was kept under magnetic stirring and over the period of 14 hr of reaction, the Molybdenum trioxide (MoO₃) is added

to the PANI/DBSA polymer matrix solution with constant stirring for 4-6 hrs at 0-5°C in order to achieve homogeneous dispersion of MoO₃ in the polymer matrix. The precipitate so obtained was filtered off by successive washing with water and acetone. Finally, the so obtained precipitate was dried at 80°C to gain constant weight. Following this procedure, PANI/DBSA/MoO₃ composites were prepared with different (10, 20, 30, 40 and 50wt%) of MoO₃ in PANI/DBSA matrix.

III. RESULTS AND DISCUSSION

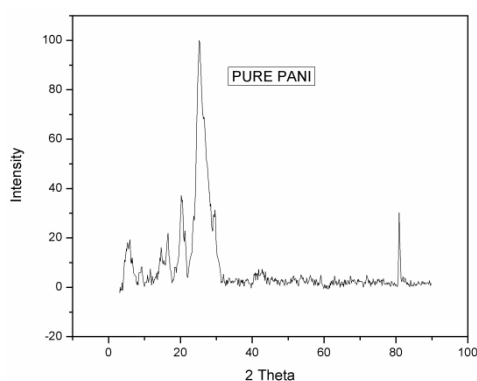


Figure 1a

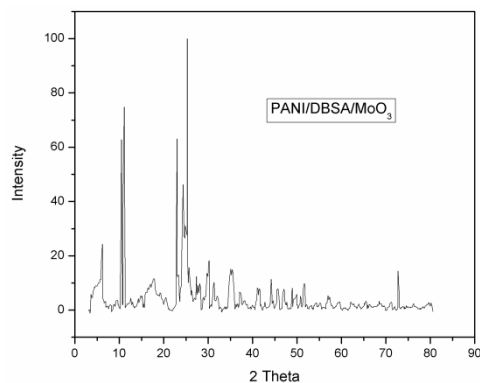


Figure 1b

Figure 1 shows XRD spectra of (a) pure PANI, (b) polyaniline/DBSA/MoO₃-50 wt %

XRD pattern clearly displays the broad peak at $2\theta=27^\circ$ indicating semi-crystalline behaviour of PANI with a crystallinity ranging from 10-30%, which is on par with the values reported by Yusoff A.N et.al. [9]. XRD spectra of polyaniline/DBSA/MoO₃-50% composite shows characteristic peaks corresponding to $2\theta = 33.51^\circ, 56.04^\circ$ and 67.05° ascribed to (010), (020), (030)

planes of MoO₃. The sharp peaks observed in these pattern, reveal the crystalline nature of the MoO₃ particles. It is seen in the XRD pattern of these composites, the sharp peaks were well retained, clearly indicating the presence of MoO₃ particles and homogeneous distribution of these particles in the PANI/DBSA matrix. Thus, XRD results reveal that MoO₃ particle does not show morphological deformation upon incorporation with PANI/DBSA matrix during the polymerization process.

It is observed from the figure 2 that, there is a constant increase in observed EMI-SE of the synthesized composites with increased weight percentage of MoO₃. Here the higher shielding efficiency observed for the composites may be attributed to the higher interfacial area and the porous network provided by the MoO₃ in polyaniline/DBSA molecular chains. The movement between the electric and magnetic dipoles present in the composites can also cause the electromagnetic wave attenuation. Altogether, the synthesized polyaniline/DBSA/MoO₃ composites exhibit absorption shielding potency in the whole X-band [10-14].

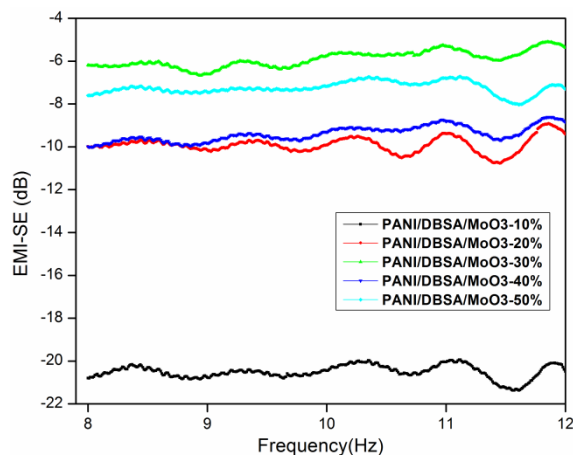


Figure 2

Figure 2. shows variation of EMI-SE with the frequency for polyaniline/DBSA/MoO₃ - 10%,20%,30%,40%&50% composites in the X-band frequencies.

IV. CONCLUSION

In summary, the conducting polyaniline/DBSA/MoO₃ composites were prepared by in-situ polymerization technique using (NH₄)₂S₂O₈ as an oxidant. The EMI shielding effectiveness of these composites has been carried out with thickness varying from 1.9-2.0 mm over a range of X-band frequencies. These EMI-SE results show good EMI-shielding properties in the X-band frequencies. Intrinsically conducting three dimensional inter connected network of conducting PANI/DBSA acted as an effective matrix for the dispersed phase of MoO₃ particles, resulted in an effective morphological change to act as wave attenuation centres. As the concentrations of MoO₃ content increases in the PANI/DBSA matrix, the EMI-SE increases. The results reveal that, the composites show good EMI shielding characteristics and can be further optimized for EMI shielding applications.

V. ACKNOWLEDGEMENT

Authors wholeheartedly acknowledge VGST, for providing financial research grant vide (No.: VGST/K-FIST (L₁)/GRD-363/2014-15 dated 02/01/15).. We are also thankful to the Principal and Management of PESIT-BSC, Bangalore for their kind cooperation to carry out this research work.

VI. REFERENCES

[1]. Salvatore Celozzi, Rodolfo Araneo, Giampiero Lovat, *Electromagnetic Shielding*, Wiley- Inter science, (2008).

[2]. J.B. Donnet, R.C. Bansal, and M.J. Wang, *Carbon Black*, 2nd ed., Marcel Dekker, New York (1993).

[3]. D.R.J. White, *A Handbook Series on Electromagnetic Interference and Compatibility*, Vol. 5, Don White Consultants, Germantown, MD (1971).

[4]. "Measuring the Electromagnetic Shielding Effectiveness of Planar Materials," ASTM Standard D 4935-89 Reapproved 1994,

American Society for Testing and Materials, Philadelphia, PA (1996).

[5]. W.C. Bushko, V.K. Stokes, and J. Wilson, *Proceedings of the Society of Plastics Engineers Annual Technical Conference*, New York, 1499, (1999).

[6]. S. C. Raghavendra, S. Khasim, M. Revanasiddappa, M. Prasad and A. B. Kulkarni, *Bull. Mater. Sci.* 26, 733 (2003).

[7]. J.C. Huang, *Adv. Polym. Technol.*, 21(3), 299 (2002).

[8]. Prasanna B P, Avadhani D N, Muralidhara H B, and Revanasiddappa M, *International Journal of Latest Technology in Engineering, Management & Applied Science.*, 3(5), 55-60, (2014).

[9]. Yusoff A.N, Abdullah M.H, Ahmad S.H, Jusof S.F, Mansor A.A, Hamid S.A.A, *J. Appl Phys.* 92, 876-882, (2002).

[10]. P Singh, T C Goel, *Ind, J, Pure Appl. Phys*, 38, 213, (2000).

[11]. A Razdan, V K Babbar, P Singh, *Ind. J. Engg. & Mat.sci.* 7, 422, (2000).

[12]. Manjula C, Sangshetty Kalyane, *International Journal of Advanced Research in Engineering and Applied Sciences*, 1(4), 55-64, (2012).

[13]. M. Revanasiddappa, D SiddalingaSwamy and S.C. Raghavendra and Y.T. Ravikiran , *IJLTEMAS*, 3(11), 1-3, (2014).

[14]. Sangappa K Ganiger, Chaluvaraju B V, Revanasiddappa M, and Murugendrappa M V, *IJLTEMAS* , 3(6), 93-97, (2014).

[15]. Vinay K, Shivakumar K and Revanasiddappa M, *International Journal of Emerging Technologies in Computational and Applied Sciences*, 21, 2017, pp. 22-26.

Numerical Modeling of Dynamically Excited Non-Resonant Piezoelectric Sensor

R. Abishek¹, V. Shrikanth²

Department of Mechanical Engineering, PES University, Bengaluru, Karnataka, India

ABSTRACT

Mass measurement of the viscoelastic or biological specimen using resonant sensor leads to missing mass effect, which affects the precision mass measurement. The non-resonant piezoelectric sensor is used in the mass measurement of these viscoelastic or biological specimen in order to eliminate the missing mass effect. In the present work, finite element analysis method of numerical modeling has been used to characterize the output of the non-resonant piezoelectric sensor. Finite element analysis of mechanical model and electromechanical coupled model is presented. In the mechanical model, the results obtained by FEA of PZT stack are in good agreement with the analytical results obtained by solving equations of motion. In the electromechanical coupled model, FEA of the non-resonant piezoelectric sensor has been carried out. The simulation results obtained for the electromechanical coupled model agrees with the published experimental results.

Keywords: Non-resonant, PZT, Actuator, Sensor

I. INTRODUCTION

Resonant sensors are used in the precise measurement of small mass because of its high measurement sensitivity at the resonance frequency. Some of the piezoelectric based resonant sensors are micro-resonators[1], micro-cantilevers[2], quartz crystal microbalance(QCM)[3], carbon nanotubes[4]. When the resonant sensors are used in the mass measurement of the biological specimens which are intrinsically viscoelastic in nature, affects the precision mass measurement due to damping effects at the resonance frequency.

Sauerbrey[5] first proposed the use of QCM to measure mass.

Voinova et al.[6] verified theoretical result on Quartz Crystal Microbalance(QCM) measurement on the supported membrane. Due to various damping effects at the resonance frequency, the accurate mass

measurement of viscoelastic material is difficult using the resonant sensor.

Shrikanth and Bobji[7] designed a non-resonant piezoelectric based mass measurement system that operates at a low frequency in order to overcome the missing mass effect. Shrikanth[8] explained the stiffness controlled operation of a sensor. For the sensor to operate in a non-resonant mode, the frequency ratio should fall under the stiffness control region. Karan Kapoor et al.[9] proposed an instrument, off-resonant tunnel fork to measure the rheological response of nanoconfined liquid. Because of its off-resonance operation, measurement can perform over a range of shear amplitude and frequency. Pan et al.[10] developed a new method for the piezoelectric charge constant measurement in shear mode (d_{15}) using non-resonant condition. Tung et al.[11] evaluate an electromechanical coupling factor for two piezoelectric materials (PZT-5A and BZT-50BCT) using finite element modeling.

From the detailed review of the literature related to mass measurement of biological specimen, it can be concluded that, as far as the liquid phase mass measurement is concerned, viscous effects of the mass to be measured and viscosity of the surrounding medium poses difficulty in the mass measurement using resonant sensors and leads to missing mass effect, which can be overcome by using a non-resonant piezoelectric sensor. Irrespective of phase/state of mass to be measured, precise mass measurement can be carried out using the non-resonant piezoelectric based mass sensor.

In the present study, we use finite element modeling method in ANSYS, in order to understand the behavior of dynamically excited Non-resonant piezoelectric sensor by characterizing its output and validate the results.

II. NON RESONANT PIEZOELECTRIC SENSOR

A. Geometry and working principle of the non-resonant piezoelectric sensor

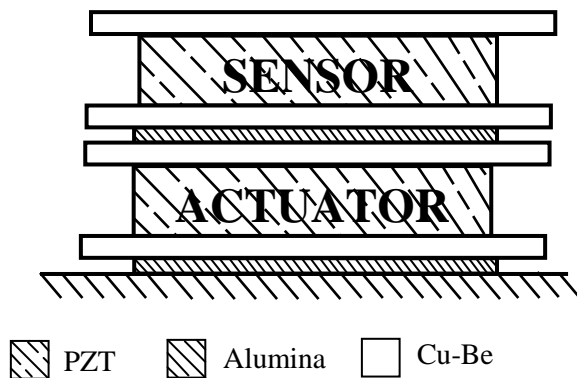


Figure 1. Sectioned view of non resonant piezoelectric sensor

The non-resonant piezoelectric sensor consists of two PZT stacks, one acts as an actuating element and another as a sensing element. Each stack of PZT consists of PZT-5A plate of area $5 \times 5 \text{ mm}^2$ and thickness 0.75 mm is bonded between two Cu-Be electrode plates of area $5 \times 6 \text{ mm}$ and thickness 0.25

mm. A skinny layer of silver based epoxy resin of thickness $50 \text{ }\mu\text{m}$ is used to join the interface of PZT and Cu-Be plates. The two stacks of PZT are separated by an alumina layer of area $5 \times 5 \text{ mm}^2$ and thickness 0.15 mm in order to create electrical isolation. Both the actuator and sensing elements are placed on the mounting block with an alumina layer in between using cyanoacrylate glue.

The actuator element undergoes elastic deformation when a voltage is applied to it, due to indirect piezoelectric effect. $V_{in} = V_0 \cos \omega t$ is the excitation voltage applied to the actuator element, where V_0 is the rms voltage. The distance moved by the sensing element is equal to the elastic deformation of the actuator element. Due to elastic deformation of the actuating element and inertia of the sensing element, the charge is generated in the sensing element.

B. Non-resonant mode of operation

Figure 2 shows the frequency response curve of a base excitation system subjected to different damping ratio.

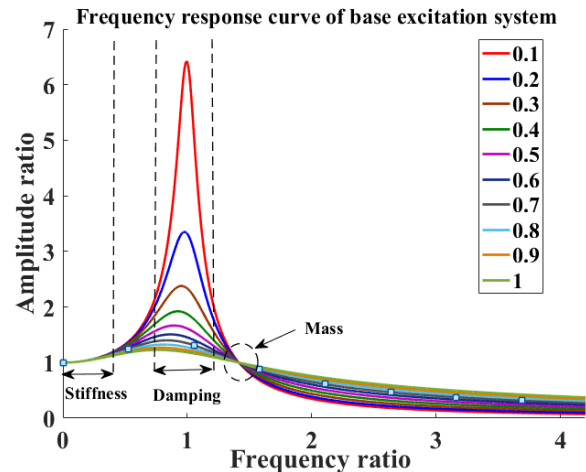


Figure 2. Frequency response system curve of base excitation system

The stiffness controlled and the mass controlled region is located before and after the resonance condition respectively, whereas the damping controlled region is located in the resonance condition. In the stiffness and mass controlled region there is no

appreciable increase in the amplitude of vibration due to change in the damping ratio. The frequency ratio in the stiffness controlled region is up to 0.3. As the mass controlled region is a point, the frequency range of operation is limited. The frequency ratio in the mass controlled region is 1.412. For the non-resonant mode of operation, the frequency ratio should fall under stiffness or mass controlled region.

III. PROBLEM FORMULATION

Finite element analysis of non-resonant piezoelectric sensors involves the analysis of mechanical model followed by electro-mechanical coupling model.

The mechanical model involves the finite element analysis of PZT stack. In mechanical model force equivalent to voltage is applied and the results obtained are compared with the analytical results.

Electro-mechanical coupling model involves the finite element analysis of complete non-resonant piezoelectric sensor considering Cu-Be plates, epoxy, alumina and the results obtained are compared with the experimentally published results.

A. Mechanical model

FEA of PZT stack has been carried out under the mechanical model. PZT stack consists of two PZT plates of area $5 \times 5 \text{ mm}^2$ and thickness 0.75 mm. PZT material type used in the analysis is PZT 5A. The bottom plate acts as an actuator and the top plate as a sensor,

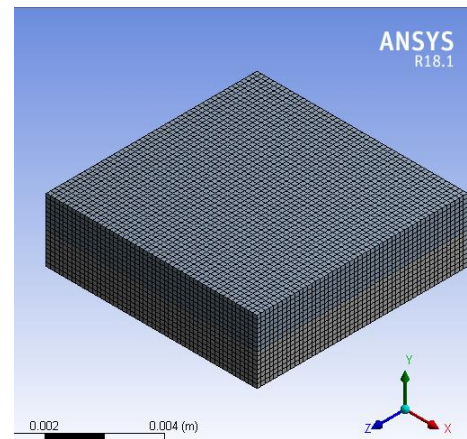


Figure 3. Meshed model of PZT Stack

The meshed model of PZT stack is shown in Figure 3 is a hexahedral mesh consists of 20000 elements with an element size 0.0001m.

Simulation is carried out for the following condition: The bottom face of an actuator is fixed and the force equivalent to voltage is applied to the top face of the actuator element.

B. Electro-Mechanical coupling model

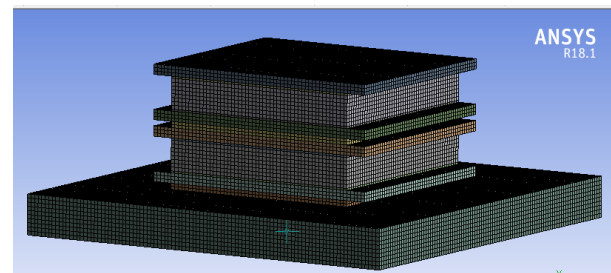


Figure 4. Meshed model of non resonant piezoelectric sensor

FEA of the non-resonant piezoelectric sensor has been carried out under electro- mechanical coupling model. The meshed model of the non-resonant piezoelectric sensor is shown in Figure 4 is a hexahedral mesh consists of 78000 elements with an element size 0.0001m.

Simulation is carried out for the following condition: the mounting block is fixed and the voltage is applied to the top face of the actuator element. For the electrical boundary condition, the bottom surface of

the actuating element should be grounded to create a potential difference.

C. Lumped model of the non-resonant sensor

Figure 5 shows the springs with a mass of the actuator element and sensing element. The force F equivalent to the input voltage is considered.

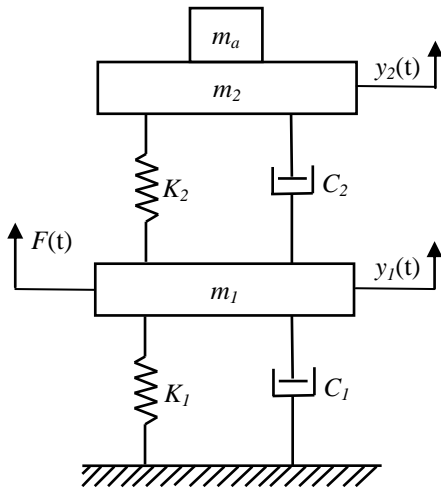


Figure 5. Lumped model of non resonant piezoelectric sensor

For the actuator element, the terms m_1 , C_1 , K_1 and $y_1(t)$ are the effective mass, effective damping coefficient, effective stiffness and displacement respectively. Similarly for the sensing element, the terms m_2 , C_2 , K_2 and $y_2(t)$ are the effective mass, effective damping coefficient, effective stiffness and displacement of the sensor respectively

The mass m_1 is due to the combined mass of actuator element, sensing element, alumina layer, Cu-Be electrode plates, epoxy resin loaded with silver and super glue.

The mass m_2 is due to the combined mass of sensing element, epoxy, and Cu-Be electrode plate at the top of the Piezo.

With the mass to be measured m_a , m_1 , and m_2 can be written as $m_1+m_a = m'_1$ and $m_2+m_a = m'_2$

The differential equations motion of non-resonant piezoelectric sensor are

$$m'_1\ddot{y}_1 + K_1y_1 + C_1\dot{y}_1 - K_2(y_2 - y_1) - C_2(\dot{y}_2 - \dot{y}_1) = F(t), \quad (1)$$

$$m'_2\ddot{y}_2 + K_2(y_2 - y_1) - C_2(\dot{y}_2 - \dot{y}_1) = 0$$

The displacement of the actuating element and sensing element can be determined by solving the above equations of motion. Force equivalent to voltage is given by $F_0 = AGd_{15}V_0 / h$, where, A , h , and G are the lateral area, thickness and rigidity modulus of the piezo respectively. and d_{15} is the piezoelectric charge constant.

IV. RESULTS AND DISCUSSION

A. Simulation results of the mechanical model

1) Displacement of PZT stack:

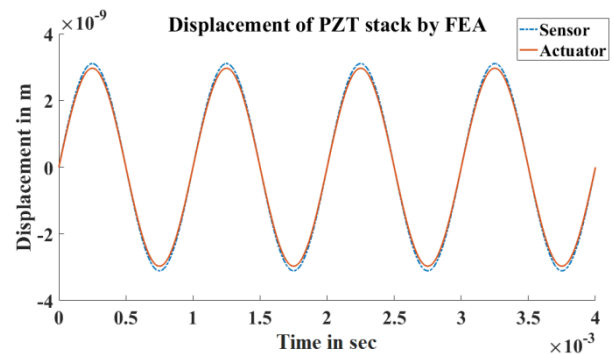


Figure 6(a). Simulation results of PZT Stack

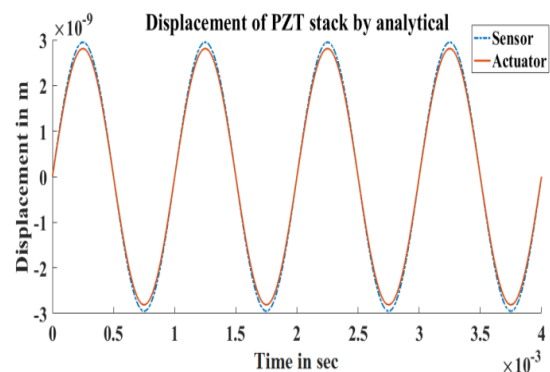


Figure 6 (b). Analytical results of PZT stack

Figure 6 (a) shows the simulation results of PZT stack obtained by FEA in ANSYS. The bottom plate is the actuator element and the top plate is the sensing element. Simulation is carried out for the following condition: sine wave force of magnitude 2.3404 N and frequency 1000 Hz is applied to the top face the actuator element in the Xdirection and the bottom face the actuator element is fixed. The magnitude of force 2.3404 N is equivalent to 5V. Displacements of an actuator and a sensor obtained by simulation are 2.97 nm and 3.11 nm respectively.

Figure 6 (b) shows the analytical results of PZT stack obtained by solving the equation of motion. Displacements of an actuator and a sensor obtained by analytically are 2.95 nm and 2.81 nm respectively. The displacement of a sensor is due to the elastic deformation of the actuating element and inertia of the sensing element. Displacements of PZT stack obtained by simulation and analytical are in good agreement.

2) Undamped frequency sweep of PZT stack

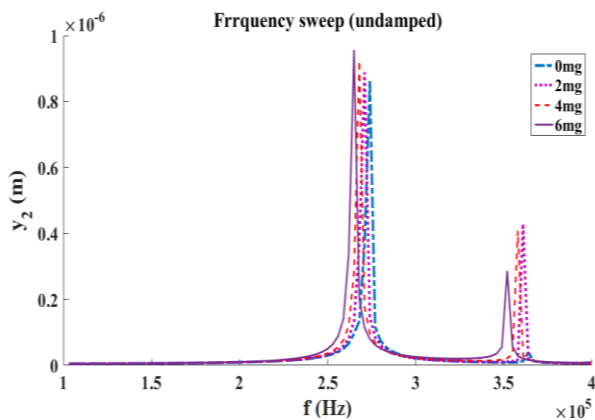


Figure 7. Undamped frequency sweep of PZT Stack for different added mass

Figure 7 shows the frequency sweep of PZT stack for different added mass that is 0mg,2mg,4mg,6mg.

Simulation is carried out for the following condition: the magnitude of the force applied is 2.3404 N on the

top face of the actuator element and the bottom face is fixed.

By neglecting the damping effect, the first natural frequency obtained by finite element analysis for 0mg, 2mg, 4mg and 6mg added mass is found to be 271 kHz, 269 kHz, 267 kHz and 264 kHz respectively. Second natural frequencies are found to be 364 kHz, 361kHz, 356 kHz and 352 kHz for added mass 0 mg, 2 mg, 4 mg and 6 mg respectively. Both first and second natural frequencies decrease with increase in the added mass.

3) Frequency sweep of PZT stack for the different damping ratio

Figure 8(a) shows the frequency sweep of PZT stack subjected to different damping ratio from 0.1 to 0.7 in steps of 0.1.

Figure 8(b) shows the normalized frequency sweep of PZT stack subjected to different damping ratio.

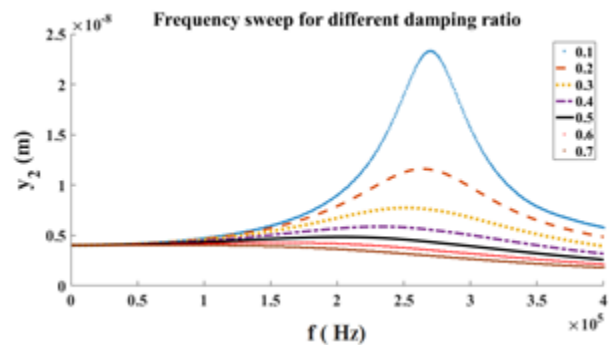


Figure 8(a). Frequency sweep of PZT stack subjected to different damping ratio.

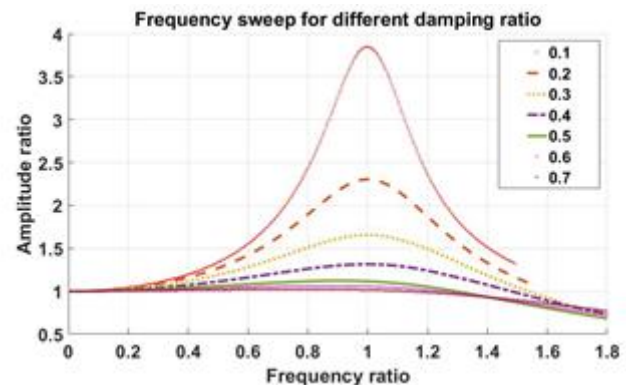


Figure 8(b). Normalised frequency sweep of PZT stack subjected to different damping ratio.

The simulation is carried out by fixing the bottom face of the actuator element and force of 2.3404 N is applied to the top face of the actuator element. It is subjected to different damping ratio from 0.1 to 0.7 in steps of 0.1. The first natural frequency for damping ratio 0.1, 0.2, 0.3, 0.4, 0.5, 0.6 and 0.7 is found to be 270 kHz, 264 kHz, 247 kHz 232 kHz, 202 kHz, 157 kHz and 75 kHz respectively. Beyond 0.7 dampingratio, the negligible amplitude of the sensor is found.

From Figure 8(b) for the frequency ratio less than 0.3, there is no appreciable increase in the amplitude of the sensor due to change in the damping ratio. It is called stiffness control region. As the frequency ratio increases beyond 0.3, the amplitude of the sensor also increases with the change in the damping ratio, which is called damping control region. For the non-resonant mode of operation, the frequency ratio should fall under the stiffness control region.

B. Simulation results of Electro-Mechanical coupled model

1) Mass calibration:

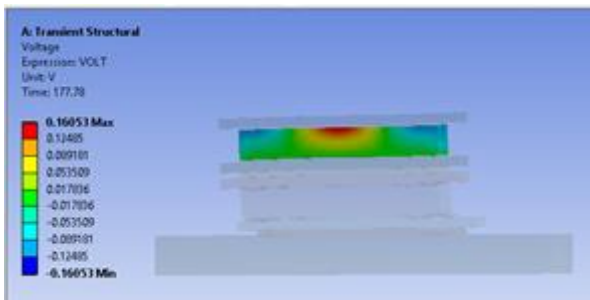


Figure 9(a). Voltage output of sensor without any added mass.

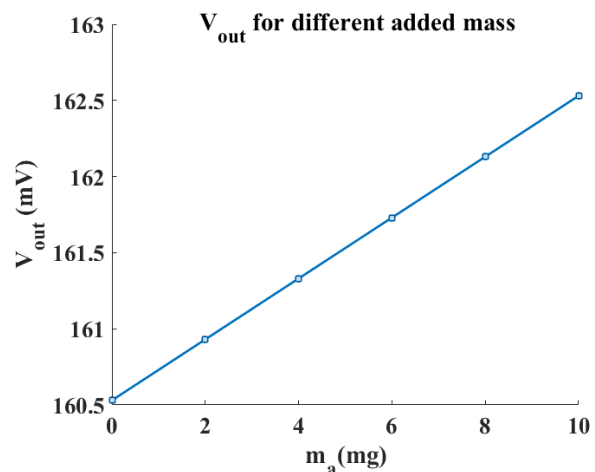


Figure 9(b). Voltage output of sensor for different added mass

Mass calibration is carried out by measuring output voltage for different mass added from 0 mg to 2 mg in steps of 2 mg.

Simulation is carried out for the following operating condition: input voltage of 5V at an excitation frequency 1000 Hz is applied to the actuator element. The output voltage is measured for different added mass from 0 mg to 2 mg in steps of 2 mg.

The voltage output of 0 mg added mass is 160.53 mV. Voltage output increases linearly with increase in the added mass. For every increase in added mass of 2 mg, the voltage output of the sensor is increased by 0.4 mV.

2) Frequency sweep of Non-resonant sensor

Figure 10 shows the frequency sweep of non-resonant piezoelectric sensor obtained by finite element analysis.

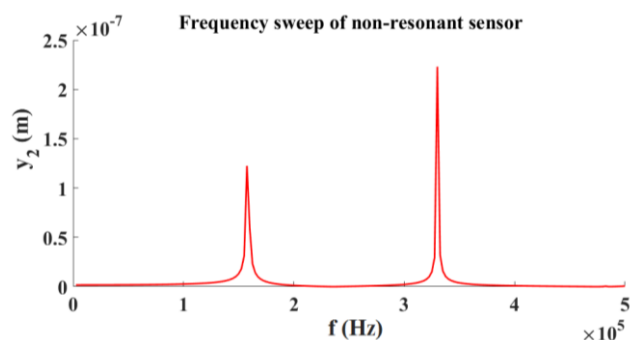


Figure 10. Frequency sweep of non resonant sensor

The frequency sweep of the non-resonant sensor is obtained by simulation for the following condition: input voltage of 5V is applied to the top face of the actuator element and bottom surface is grounded. Neglecting the damping effects, the first and the second natural frequencies obtained are 155 kHz and 340 kHz respectively. The first and the second natural frequencies in the published experimental results are 157 kHz and 350 kHz respectively. Results obtained by FEA agrees with the published experimental result.

V. CONCLUSION

FEA of mechanical and electromechanical coupled model has been carried out.

The displacements of PZT stack obtained by simulation are 2.97 nm and 3.11 nm for the actuator and the sensing element respectively, which are in good agreement with the analytical results obtained for the actuator and the sensing element that is 2.95 nm and 2.81 nm respectively. The first and second natural frequencies obtained for PZT stack by simulation is 271 kHz and 264 kHz respectively.

The voltage output of non-resonant sensor varies linearly with increase in the added mass. For every increase in added mass of 2 mg, the voltage output of sensor increased by 0.4 mV.

The first and the second natural frequencies of the non-resonant sensor considering Cu-Be electrode plates, epoxy and alumina are found be 155 kHz and 340 kHz respectively, which agrees with the published experimental results.

VI. REFERENCES

- [1]. A. P. Davila, J. Jang, A. K. Gupta, T. Walter, A. Aronson, and R Bashir, "Microresonator mass sensors for detection of Bacillus anthracis Sterne spores in air and water," *Biosensors and Bioelectronics*. 22(12), 3028–3035 (2007).
- [2]. T. Thundat, E. A. Wachter, S. L. Sharp, and R. J. Warmack, "Detection of mercury vapour using resonating microcantilevers," *Applied Physics* 66(13), 1695–1697 (1995).
- [3]. C. Fredriksson, S. Kihlman, M. Rodahl, and B. Kasemo, "The piezoelectric quartz crystal mass and dissipation sensor: A means of studying cell adhesion," *Langmuir* 14(2), 248–251 (1998).
- [4]. S. Chopra, A. Pham, J. Gaillard, A. Parker, and A. M. Rao, "Carbon nanotube- based resonant-circuit sensor for ammonia," *Applied Physics* 80(24), 4632–4634 (2002).
- [5]. G. Sauebrey, *Zeitschrift, Physica Scripta* 59,391(1999)
- [6]. M.V.Voinova, M. Jonson, B. Kasemo, "Missing mass effect in biodensor's QCM applications", *Biosensors and Bioelectronics*, 17(10),835-841(2002).
- [7]. V. Shrikanth and M. S. Bobji, "A nonresonant mass sensor to eliminate the 'missing mass' effect during mass measurement of biological materials", *Review of Scientific Instruments*, 84, 105006(2014).
- [8]. Shrikanth V, "A nonresonant piezoelectric sensor for mass, force and stiffness measurement", Thesis
- [9]. Karan Kapoor, Vinod kanawada, Vibham Shukla, and Shivprasad Patil, "A new tuning fork based instrument for oscillatory shear rheology of nanoconfined liquids", *Review of Scientific Instruments*, 84(2),0256101(2013).
- [10]. W. Y. Pan, W .Y. Gu and L. E. Cross, "Direct Measurement of the Piezoelectric Shear coefficient d15 under non-resonant condition", *Materials Letters*, 1989.
- [11]. Thanh Tung, Nguyen Tinh, Nguyen Hoang, Dang Anh Tuan, "Evaluation of Electrochemical Coupling Factor for Piezoelectric Materials Using Finite Element Modeling", *Materials and Chemistry*,59-63(2013)

Cable-Driven Constrained Traversal Mechanism for Planar Motion

B Datta Shreehari, K Lokesh Varun, P Vignesh, V Shrikanth

Department of Mechanical Engineering, PES University, Bangalore, Karnataka, India

ABSTRACT

In this paper a simple model of mobile traversal mechanism suspended by cables and actuated by motors is presented. A detailed description of the workspace on which the payload is traversed is discussed. The mechanism is actuated by cables which are driven by motors. The rate of change of length of cables and the angular velocities of motors are determined such that the payload traverses along the shortest path in the desired duration of time. The motors are programmed to operate separately as per the derived formulas. The mechanism thus designed is portable and can be applied in the field of agriculture, farming, manufacturing, surveillance etc.

Keywords: Parallel robots, traversal mechanism, portable, payload, cables, motors

I. INTRODUCTION

Cable-Driven Parallel Robots (CDPRs) are a special category of parallel robots where a moving platform is positioned by changing cable lengths. Using this type of robots, it is possible to attain completely constrained six degrees-of-freedom (DOF) despite of the fact that the cables can be subjected to only tension.

Key properties of CDPRs, which varies a great deal from conventional robots [1,2] enable the automation of completely new tasks, which were not quite possible to be automated previously. For example, cost addition in case of increasing cable length is minimal, and hence, CDPRs can be used to span very large workspaces, that are orders of magnitude larger than those covered by the biggest serial robot today. In addition, CDPR designs usually have stationary actuators. This results in a marked decrease in actuated mass, which allows the employment of greater speeds and accelerations [7] (Kawamura, Choe et al. 1995). Tasks with high payloads and large workspaces are thus ideal for automating using CDPRs.

A cable-driven parallel robot (CDPR) is composed of four basic components. A platform or payload, which is positioned within a workspace to perform a specific task, cables to control and move the payload, actuator system which change the cable length, and a frame upon which this actuator system is mounted.

The high load conveying ability, modular construction and energy-efficiency of CDPRs make them better than traditional parallel robots [8] and great prospect for an assortment of testing substantial workspace errands, for example, multidimensional cranes [3,4], very high speed robots [5], camera frameworks for stadiums [6], etc.

Planar motion of a rigid body is said to be accomplished when all the points move parallel to some fixed plane. The proposed traversal mechanism, which is constrained by cables, can be called as Cable Suspended Parallel Robot (CSPR) with 2-DOF (both translational) rather than CDPR because payload is suspended by 4 cables. Though the mechanism is predominantly planar in nature, due to mobility of the framework of the workspace and the design

considerations of the cables and also the considerations regarding the payload, it can be realised to be of three degrees of freedom (all three translational) as shown in figure 1.

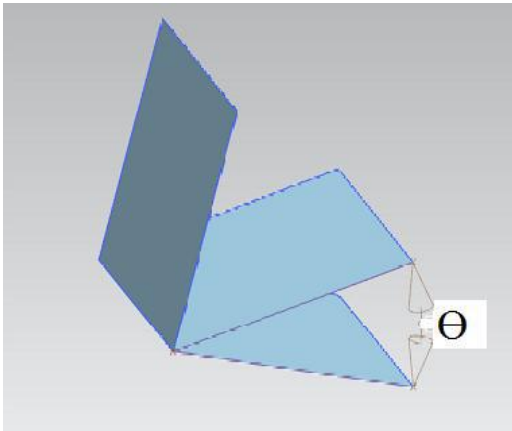


Figure 1. Base of the framework realised in three dimensions

II. THE MECHANISM

Recalling the basic components of a C SPR, it comprises of a framework, actuator system, cables and the payload. The shape of the working arena over which the payload has to traverse can be a square or a rectangle. The framework consists of four fixed columns, one each erected at four corners of the base outside the workspace. Motors, eye hooks, spools etc. constitute the actuator system. A bipolar stepper motor is stationed at each corner of the base with a spool fitted on its shaft. The columns are fitted with eye hooks in order to support the position and movement of cables. A flexible cable – more than 1.5 times the length of the diagonals of the workspace – is wound around each motor (spool) and their free ends are connected to the platform of the payload. These cables form the connecting links of the mechanism. The end-effector is thus constrained to achieve only translational motion in the workspace making it a planar mechanism as shown in Figure 2.

The position of the payload is determined by the length of each cable. In order to achieve the required motion of the payload, the length of the cables should

vary in tandem such that it guides the payload to cover the shortest path – straight line – between the two desired points in the desired duration of time.

Figure 3 depicts the workspace with the four motors and their corresponding cables. Let a and b be the length and breadth of workspace and $L1, L2, L3$ and $L4$ be the lengths of the cables between the vertical support and the payload as shown in figure 3.

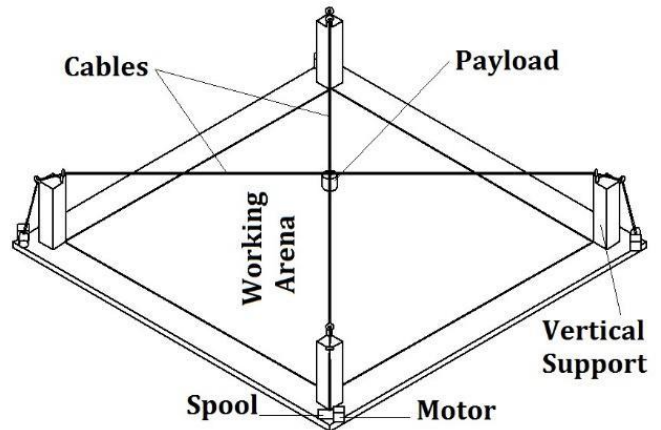


Figure 2. Schematic sketch of the construction of the mechanism

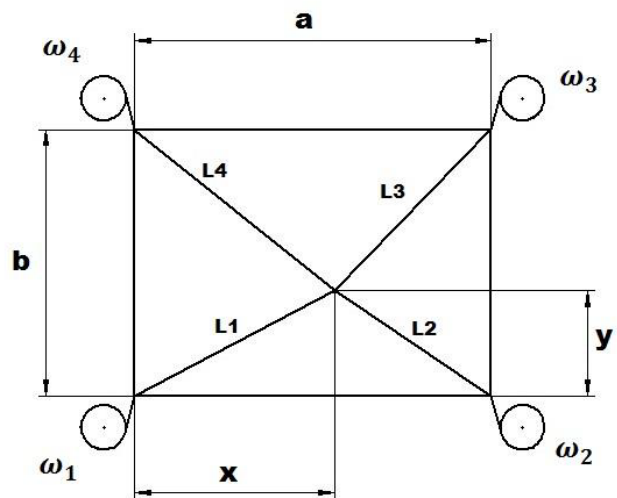


Figure 3. Schematic sketch depicting the notations used

The rate of change of length of the cable 1 is given by

$$v_1 = \frac{x \dot{x} + y \dot{y}}{\sqrt{x^2 + y^2}}$$

Likewise, the rate of change of length of the cables 2, 3 and 4 are given by

$$v_2 = \frac{-(a-x)\dot{x} + y\dot{y}}{\sqrt{(a-x)^2 + y^2}}$$

$$v_3 = \frac{x\dot{x} - (b-y)\dot{y}}{\sqrt{x^2 + (b-y)^2}}$$

$$v_4 = \frac{-(a-x)\dot{x} - (b-y)\dot{y}}{\sqrt{(a-x)^2 + (b-y)^2}}$$

These changes in lengths of cables are effected by 5 V bipolar stepper motors. The voltage supply to each of the motors is varied separately using a microcontroller kit (Arduino Uno) and A3967 stepper motor drivers as shown in figure 4 in order to vary their speed of revolution which in turn varies the rate of change of length of the cables. Considering the workspace to be x-y plane, the angular velocity of motor 1 is given by

$$\omega_1 = \frac{v_1}{r} \hat{k}$$

Similarly, the angular velocity of motors 2, 3 and 4 A are given by

$$\omega_2 = \frac{v_2}{r} \hat{k}$$

$$\omega_3 = \frac{v_3}{r} \hat{k}$$

$$\omega_4 = \frac{v_4}{r} \hat{k}$$

where 'r' denotes the radius of the spool.

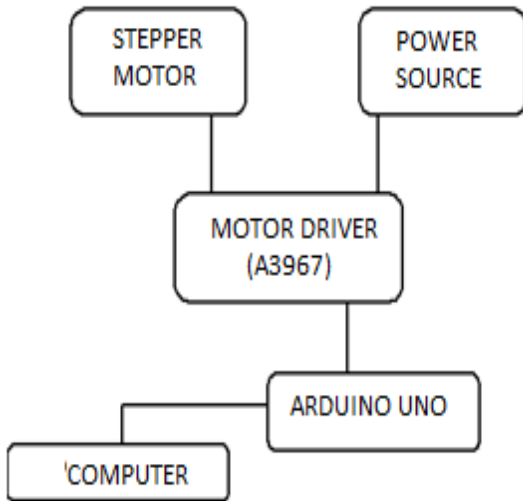


Figure 4. Block diagram of the circuit to vary the speed of revolutions of the stepper motor

III. RESULTS AND DISCUSSION

Assuming the dimensions of the workspace to be 100 cm x 100 cm, simulation of the mechanism was carried out and the results were obtained as discussed below.

Consider the initial position of the payload to be (50, 10), as shown in figure 5. By virtue of the changes in the length of the cables, the payload has to reach its destination at (90, 90) along the shortest path in the stipulated duration of time.

The trends followed by the motors and the cables are discussed below:

1. Motor 1 undergoes constant anticlockwise rotation which unwinds the cable 1.
2. Motor 2 undergoes small clockwise rotation initially, which winds the cable 2, and then changes to anticlockwise rotation with gradually increasing speed such that the cable unwinds accordingly.
3. Motor 3 undergoes constant clockwise rotation which winds the cable 3.
4. Motor 4 undergoes clockwise rotation initially with gradually decreasing speed, which winds the cable 4, and later changes to gradually increasing anticlockwise rotation, thus unwinding the cable.

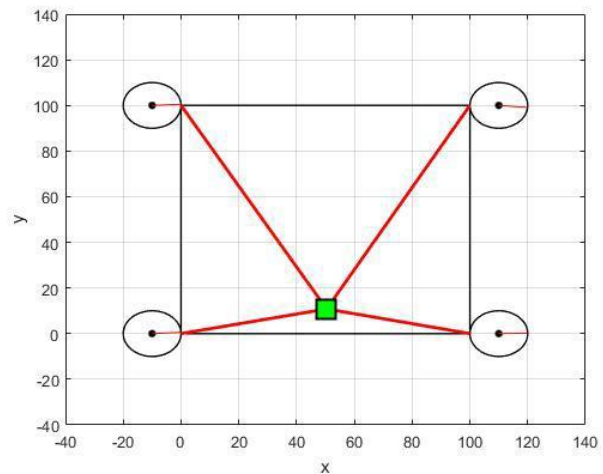


Figure 5. Initial position of the payload

IV. CONCLUSION

A thorough study of CSPRs and CDPs is done and a simple constrained traversal mechanism for planar motion is formulated. The mechanism is made mobile and portable, which aids in extending the mechanism from being purely a 2-dimensional fixed mechanism to a portable, table-top, 3-dimensional mechanism. Depending upon the payload employed, this mechanism can be applied in various areas as in understanding the surface roughness along a particular line, sowing of seeds at particular intervals, spraying of fertilizers and pesticides on plants, handling of toxic chemicals in a laboratory, 3-D printing, monitoring the conditions in a closed environment, and so on and so forth.

V. REFERENCES

- [1]. Landsberger, S. E., and Sheridan, T. B., 1993, "A Minimal, Minimal Linkage: The Tension-Compression Parallel Link Manipulator," *Rob. Mechatron. Manuf. Syst.*, 2, pp. 81–88.
- [2]. Valentin Lorentz Schmidt, 2017, "Modeling Techniques and Reliable Real-Time Implementation of Kinematics for Cable-Driven Parallel Robots using Polymer Fiber Cables," University of Stuttgart.
- [3]. Higuchi, T., Ming, A., and Jiang-yu, J., 1988, "Application of Multi- Dimensional Wire Cranes in Construction," *Proc. of 5th International Symposium on Robotics in Construction*, Tokyo, June 6–8, pp. 661–668.
- [4]. Albus, J., Bostelman, R., and Dagalakakis, N., 1992, "The NIST Robocrane," *J. Rob. Syst.*, 10~5!, pp. 709–724.
- [5]. Kawamura, S., Choe, W., Tanaka, S., and Pandian, S. R., 1995, "Development of an Ultrahigh Speed Robot FALCON Using Wire Drive System," *Proc. Of IEEE International Conference on Robotics and Automation*, IEEE, New York, pp. 215–220.

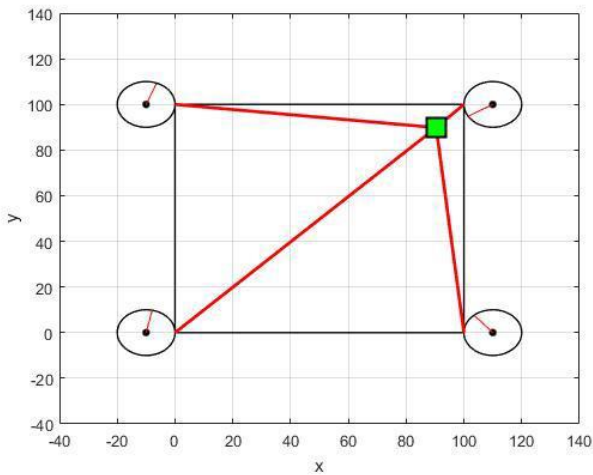


Figure 6. Final position of the payload

The variation of length of each cable with respect to abscissa of the position of the payload is shown in figure 6.

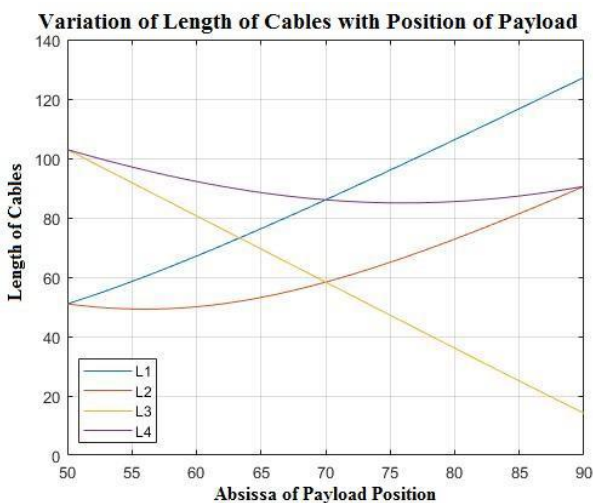


Figure 7. Plot to show the variations of length of cables with respect to positions of payload

As a result of these variations in lengths of cables, the payload is traversed from its initial point (50, 10) to its final point (90, 90). It is to be observed that the time of travel or the speed of travel is specified initially, along with the initial and final positions, as the requirement may be but the path followed remains a straight line. It is worth to be mentioned that the path to be traversed can also be programmed as per the requirement, which has its own applications such as 3-D printing *etc.*

- [6]. Cone, L. L., 1985, "Skycam: An Aerial Robotic Camera System," *BYTE*, Oct. pp. 122–132.
- [7]. Kawamura, Sadao, Choe, Won, Tanaka, S., and Pandian, S. R., 1995. "Development of an ultrahigh speed robot FALCON using wire drive system", In: *IEEE International Conference on Robotics and Automation*, 1995, pp. 1764–1850.
- [8]. Guillaume Barrette, Cle'ment M. Gosselin, 2005, "Determination of the Dynamic Workspace of Cable- Driven Planar Parallel Mechanisms," DOI: 10.1115/1.1830045

EyesPRO - Protect Your Eyes

Pranav Manjunath, Nimisha V Arun
(Equal Contributions)

PESIT Bangalore South Campus, Department of Information Science and Engineering, Hosur Road, Electronic City, Bangalore, Karnataka, India

ABSTRACT

Myopia or nearsightedness is a major health problem especially in young children, owing to repeated use of mobile phones at a suboptimal distance relative to one's eyes. EyesPRO is a mobile application that calculates the distance between the user and the phone, compares this value with the optimum value and warn the user to move the phone appropriately to attain a safe distance if needed.

Keywords: EyesPRO, myopia, nearsightedness, android application, vision, mobile phone, smart phone, health risk

I. INTRODUCTION

Eye is an important sensory organ that perceives light as input, converts to a neuronal signal, which is conducted through optical nerve to the visual cortex of the brain where the signal is processed and interpreted as an image. Eye is a complex structure, with its architecture analogous to a camera and the distance between the object - lens - retinas needs to be ideal for perception of a clear image.

There are three common structural changes to the eye that lead to impaired vision due to refractive errors. Myopia or near-sightedness, is a condition where the eyeball is elongated and the light that enters the eye does not converge on the retina properly leading to blurred vision of the far away objects. Myopia first occurs in children since the eye continues to grow during childhood and typically progresses until about age 20. The "near work" hypothesis states that spending a lot of time doing close works can increase the risk of myopia. In hyperopia or farsightedness, the eyeball is shortened again leading to impaired vision. In another condition called astigmatism, imperfections of the cornea leads to blurred vision. These changes can happen at birth or with age and can be corrected with appropriate lenses.

A major concern in the last 30 years is that myopia is becoming more prevalent especially in younger children due to extensive and improper use of electronic devices such as mobile phones, tablets, computers and televisions. Prolonged usage of these devices leads to dry eyes, sore eyes, headaches and blurred vision causing serious damage to the eyes, collectively referred to as "Computer Vision Syndrome" or "Digital Eye Strain". Several precautionary measures are recommended to prevent extensive damage to the eyes: the 20-20-20 rule suggests that for every 20 minutes of staring at the screen, one must look at an object that is 20 meters away for a duration of 20 seconds. An optimum distance of at least 30 cm between the mobile screen and the eyes is suggested in order to keep are eyes safe and free from strain. In addition, it is important to maintain a proper position while using smartphones. While these can certainly help maintain eye health in the longer term, compliance is a major issue. Hence, it is important to come up with a more reasonable practical solution to help solve the problem of myopia induced by misuse of electronic devices such as smartphones.

Following a thorough review, we have come up with an android application called "EyesPRO" that

constantly monitors and helps maintain an optimal screen to face distance. It uses the front camera of the smartphone to calculate the distance, incorporates the 20-20-20 rule and warns the user appropriately in real time.

Overall project objectives are to develop a mobile application that is user-friendly, not phone resource intensive, and help users to maintain optimum distance to avoid potential development of Myopia due to use of mobile phones.

For implementation, we have divided the project into 2 phases as described in the methods section. This report will focus on Phase 1 of the project, which includes analysing the problem and an initial version of the mobile phone application.

II. METHODS AND MATERIAL

2.1 Method description

We have divided our project into two phases. The outlook of these phases is given below:

Phase I:

1. Problem statement
2. Assessment of the problem
 - a. Expert advice
 - b. Population analysis
3. Preliminary version of EyesPRO mobile phone application

Phase II:

1. Addition of power saving mode
2. Implementation of 20-20-20 rule
3. Identification and addressing issues from Phase I

2.1.1 Phase I

1. Assessment of the problem

a. Expert Advice

We spoke to a leading ophthalmologist, Dr. Adrian Sandeep Braganza from NarayanaNethralaya,

Bangalore to gain information about myopia as a health problem.

b. Population Analysis

We conducted a population survey to evaluate the smartphone usage and knowledge of myopia induced by electronic gadgets. This survey was created using Google Forms and was sent to a limited number of people between the age groups of 15-50.

2. Methodology

Phase 1 methodology describes the algorithm used in detecting the screen to face distance. The optimum screen to face distance that the user must maintain in 30 cms.

Screen to Face Distance

Optometry and Vision Science, official journal of the American Academy of Optometry [5] suggests that the average working distance when viewing a web-page or a text message on a mobile falls in the range of 30-36 cms. One must maintain a minimum distance of 30 cms while viewing the mobile screen. Therefore we have set the threshold level for our app to be 32 cms (+2 cms to nullify any possible error).

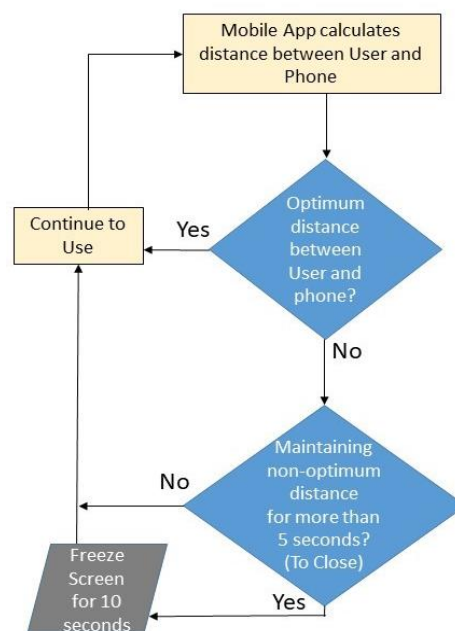


Figure 1. Phase 1 - Preliminary version of EyesPRO Flowchart

The application first calculates the distance between the screen and the face using the Screen-to-face-distance Algorithm [1] which is explained in the next section. Depending on the calculated distance the following two cases arise.

Case I

If(calculated distance >= optimum distance):

The user can continue to use the mobile phone.

Case II

If(calculated distance < optimum distance):

The user is given a warning and is requested to move away from the screen. If the warning continues for 5 seconds, the app will automatically freeze the screen for the next 10 seconds.

Screen-to-face-distance Algorithm

The objective of our app is evaluating the screen-to-face-distance based on an algorithm initially developed by König et al. [1], which depends on interpupillary distance to measure the screen to eye distance. The interpupillary distance is inversely proportional to the screen-to-face-distance. We have made significant modifications integrating Google's face detection software with interpupillary distance measurement along with threshold values to check and warn the user based the proximity of the phone.

The Screen-to-face-distance equation is:

$$D_{comp} = Prf/P_{comp} * Drf \quad (1)$$

Here,

P_{comp}: The interpupillary distance to be obtained using the Google's API

Prf: The reference interpupillary distance obtained experimentally

D_{comp}: The the screen-to-face-distance that we need to obtain from the equation

Drf: The reference screen-to-face-distance obtained experimentally

Google's API Facedetector.Face [3] is a class that has a method called 'eyesDistance()' which returns the distance between the eyes. P_{comp} is obtained from this method. However the app incurs a delay of 2.5 seconds to calculate the eye to eye distance.

2.1.2 Phase II Plan

1. Power Saving Mode:

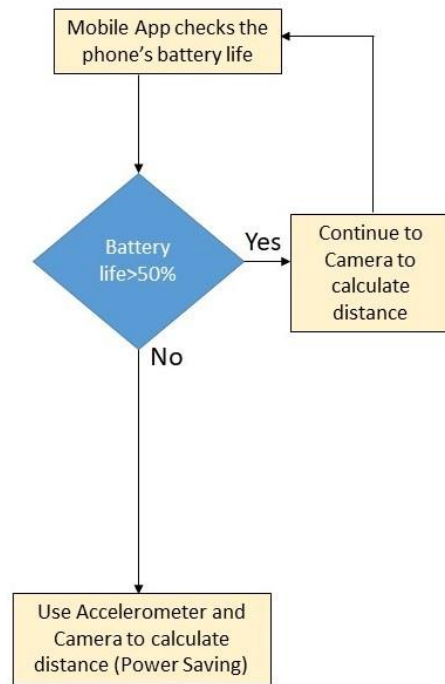


Figure 2. Power Saving Mode Flowchart

The plan is to use Google BatteryManager class [4] in order to determine the health of the battery (Battery Percentage).

The variable BATTERY_PROPERTY_CAPACITY returns an integer value by which we can determine the battery percentage. As shown in the flowchart above, depending on the percentage of the battery the following two cases arise.

Case I

If (Mobile's battery percentage >= 50%):

The front camera continuously measures the distance between the eyes and the screen using the Screen-to-face-distance Algorithm [1]. In this state, the camera takes the picture of the user automatically for every 5

seconds. For every picture, the eye to eye distance (Pcomp) is determined using the Google's FaceDetector.Face class. Now, Pcomp is substituted in the formula (1) and the screen-to-face-distance (Dcomp) is computed.

Case II

If (Mobile's battery percentage < 50%):

Here in this case, we plan to employ the methodology mentioned in the paper presented by Zhuqi Li et al.[2]. It is an optimization method that is used to minimise the battery consumption by using the camera to take pictures (using Screen-to-face-distance Algorithm [1]) only when there is movement detected by the built-in accelerometer (a sensor that is used to determine the devices position and orientation). If the accelerometer does not show any movement, it indicates that the user is standing still and the camera is inactive, else, the camera is activated and continues to behave in similar manner as mentioned in the case I and remains in the active state for the next 5 minutes.

2. The 20-20-20 Rule:

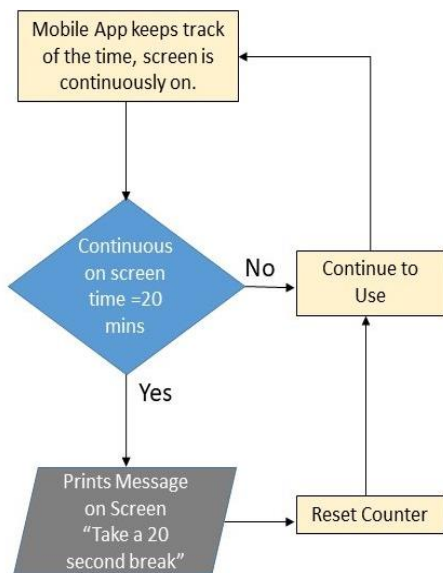


Figure 3. 20-20-20 rule flowchart

EyesPRO plans to implement the 20-20-20 rule. This rule states that for every 20 minutes that a user stares at the mobile screen, he/she must look at an object 20

feet away for 20 seconds. EyesPRO keeps a track of the time, the screen is continuously on. If the screen has been continuously on for 20 minutes, EyesPRO prints a message on the screen “Take a break for 20 seconds”, reminding the user of the 20-20-20 rule.

We plan to use the Google CountdownTimer class to schedule a countdown timer for regular intervals of 20 minutes. The timer is in the active state only when the mobile screen is on. This timer starts when the application (EyesPRO) is turned on and repeats its activity every 20 minutes until it stops when application is turned off. The timer is reset every time the camera switches from active to inactive state, if the camera remains in the inactive state for 15 minutes the application pops up a message requesting the user to take a 20 seconds break. This process is repeated for every 20 minutes.

III. RESULTS AND DISCUSSION

3.1 Problem statement:

Improper constant use of smartphone in close proximity leads to myopia.

3.2 Population Survey Analysis:



Figure 4. Daily usage of phone or tablet.

It is clear from [Figure 4] that close to 40% of the people spend at least 3-6 hours on smartphone per day while a similar number of people spend 1-3 hours. It is

also concerning to see close to 20% of the people spend more than 6 hours on smartphone per day.

Are you aware of the optimum distance that should be maintained between your eyes and your phone? Do you maintain that distance?

162 responses

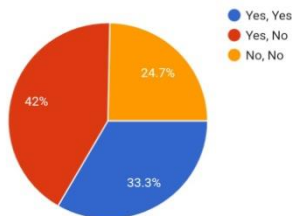


Figure 5. Awareness among people about the Screen-to-face optimum distance

Figure 5 indicates that 66.7% of the people do not follow the optimum distance, of which, close to 25% of this population are not even aware of it.

Have you heard of the 20-20-20 rule?

164 responses

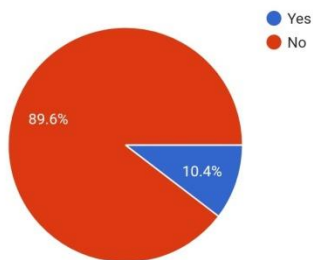


Figure 6. Awareness about the 20-20-20 rule

It is alarming that nearly 90% of the people who took the survey do not know about the 20-20-20 rule.

Have you seen small children below the age of 9 using smartphones and tablets for a long duration of time?

162 responses

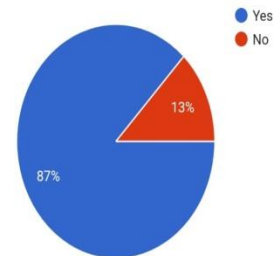


Figure 7. Usage of smartphone by young children

As expected, a high majority (87%) of responders claim to have seen children use smartphones and tablets for long duration of time.

The survey clearly states that there is a problem with prolonged improper use of smartphones amongst population and there is a lack of awareness of the precautionary recommendations. Further, this is substantiated by discussions with an ophthalmologist. This clearly requires additional interventions that are practical and easy to use to reduce the incidences of eye problems caused by use of smartphones.

3.3 Preliminary Version of EyesPRO

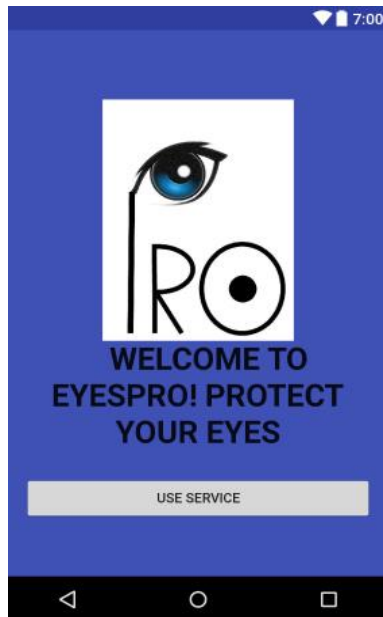


Figure 8. EyesPRO Front Screen

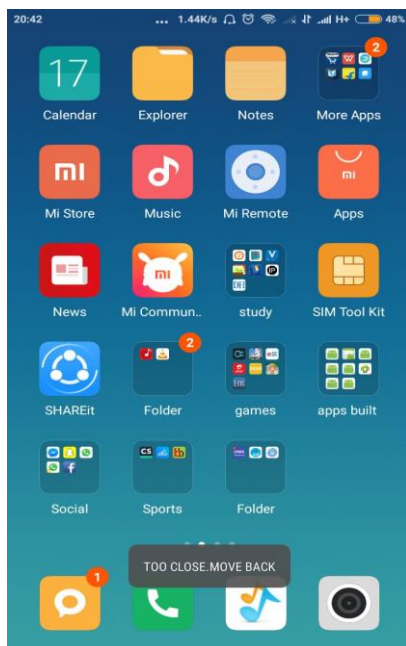


Figure 9. EyesPRO Warning Message

1. Accuracy of distance: We have tested this app in different mobile phones to measure the accuracy of the distance and it was found that distance measured was within +/- 2 cm of the distance. Further, if the distance was less than 30 cm, a warning message would appear as “TOO CLOSE MOVE BACK” [Fig. 9].

2. Response latency: We tested EyesPRO amongst various mobile phones and calculated the average time each phone took to measure the screen-face distance.

Table 1. Response Latency

Mobile Brand	Processor	Processor Make	Avg. Response Latency in secs
Asus	1GHz octa-core	MediaTek MT6750	10.2
Lenovo	1.2GHz octa-core	Qualcomm Snapdragon 415	10.5
Micro max	1.3GHz quad-core	MediaTek MT6582 M	11.4
Samsung	1.3GHz quad-core	Exynos	9.6
Vivo	1.5GHz octa-core	MediaTek MT6750	1.3
Xiaomi	2Ghz octa-core	Qualcomm Snapdragon 625	5.1
OnePlus	2.45Ghz octa-core	Qualcomm Snapdragon 835	8.3
Lenovo	2.15GHz octa-core	Qualcomm Snapdragon 820	3.5

3.4 Future improvements

1. Measure the number of hours a user uses his/her's phone per day. Nowadays, the use of mobile phones and tablets have increased significantly among various age groups. For example, Smart Classroom implementations require the students to use tablets for their work. Users do not have an idea of how much they use their phones on a daily basis. Therefore we plan to add this as an added feature in which EyesPRO can graphically monitor and display the phone consumption patterns to the user.

2. Along with smartphones, many users hooked up with their laptops in their office and also find many users watching TV at their home. Adding a similar feature in these devices is necessary. Hence this plan can also be implemented on laptops and smart televisions to ensure that the user can operate any electronic device harming their eyes.

IV. ACKNOWLEDGEMENT

We would like to acknowledge the support of Professor SaiPrasanna, who was our faculty mentor for this project and Dr.ManjunathRamarao for his guidance.

V. CONCLUSION

Technology has enabled us to increase our comfort and achieve efficiency in every aspects of our life. With the increase in the use of these devices, it's no surprise that many individuals suffer from vision related problem and computer-vision syndrome. EyesPRO helps us tackle such very common problem faced by the world today.

"EyesPRO" utilizes the camera and accelerometer to estimate the distance between the user and the mobile screen, and accordingly requests the user to monitors his position with respect to device. Along with this, EyesPRO incorporates the 20-20-20 rule. And thus help us lead a healthy lifestyle.

VI. REFERENCES

- [1]. I. Konig, P. Beau, and K. David. A new context: Screen to face distance. In 2014 8th International Symposium on Medical Information and Communication Technology (ISMICT), pages 1–5. IEEE, 2014.
- [2]. Zhuqi Li, Weijie Chen, Zhenyi Li and Kaigui Bian, "Look into My Eyes: Fine-grained Detection of Face-screen Distance on Smartphones". In 2016, Mobile Ad-Hoc and Sensor Networks (MSN), 2016 12th International Conference , pages 1-8, IEEE, 2017
- [3]. Google .Facedetector.face .<http://developer.android.com/intl/zh-cn/reference/android/media/FaceDetector.Face.html>
- [4]. Google BatteryManager <https://developer.android.com/reference/android/os/BatteryManager.html>
- [5]. Optometry and Vision Science Journal, American Academy of Optometry <https://www.aaopt.org/home/section-ovs>

VII. AUTHOR PROFILE

PranavManjunath currently pursuing 2nd year in Department of Computer Science And Engineering, PESIT- Bangalore South Campus, Bangalore, India.

Nimisha V Arun currently pursuing 2nd year in Department of Computer Science And Engineering, PESIT- Bangalore South Campus, Bangalore, India.

Effect of Schiff Base Ligands as Corrosion Inhibitors on Mild Steel

Avinash Anupam¹, Atmanand Udameeshi¹, Revanasiddappa M^{*2}

¹Department of Mechanical Engineering, Bengaluru, Karnataka, India

²Department of Chemistry, PESIT Bangalore South Campus, Bengaluru, Karnataka, India

ABSTRACT

Corrosion is recognized as a major problem in today's manufacturing industries where every industry pays for the cost of corrosion and pays for its control. If we consider mild steel which is extensively used in industries gets corroded when exposed to different industrial corrosive environments. Therefore, this experiment deals with the effort to control the rate of corrosion and increase the stability of the material. Mild steel which is being used is dissolved in 0.1M H₂SO₄ and corrosion inhibitors can be used to restrain the corrosive attack of acids on the structure. Using organic corrosion inhibitors having hetero atoms in the organic molecule such as nitrogen, oxygen and sulphur are acting as donor atoms. Newly synthesized organic corrosion inhibitors viz., IM1 to IM4 in 0.1M H₂SO₄. This helped us to understand acid and inhibitors concentration, immersion time and temperature on dissolution rate and polarization potential have been studied. The mild steel follows adsorption of inhibitors molecules which is been proved through the study of Arrhenius adsorption isotherm.

Keywords: inhibitors; polarization; Arrhenius adsorption isotherm;

I. INTRODUCTION

This experiment deals with the dissolution study of mild steel in 0.1M H₂SO₄. It is significant practice since the acid is highly corrosive and extensively used in various industrial operations¹. The usage of corrosion inhibitors is essential so that it restrains the corrosive attack of acids on metallic materials². Organic compounds containing nitrogen, sulphur and oxygen has been found to function as very effective corrosion inhibitors. The effectiveness of these compounds as corrosion inhibitors can be attributed to the number of mobile electron pairs present, the π -electron character of free electron and the electron density around the nitrogen atoms³. This has prompted us to study the new inhibitors IM₁ to IM₄ in 0.1M H₂SO₄ medium. The effect of acid concentration, immersion time and temperature on dissolution rate and polarization studies has been explored. The

inhibitors action on the mild steel follows absorption of inhibitors molecule which has been proved through the study of Arrhenius adsorption isotherm. It could be obtained from the current potential plots and corrosion rates from Tafel extrapolation method. The corrosion rates obtained from cathodic and anodic polarization techniques are compared to get useful information about the corrosion test in presence of inhibitors tools for mild steel. The thermodynamics parameters were also deduced from the resulting adsorption isotherms and surface coverage values of inhibitors. In view of the above facts we thought of discussing the effects of corrosion inhibitors on mild steel for anodic and chemical dissolution.

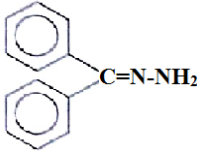
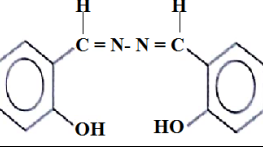
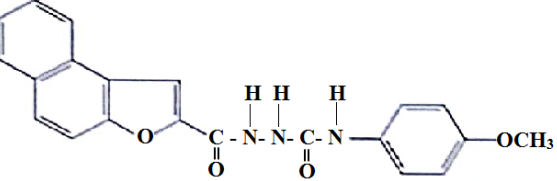
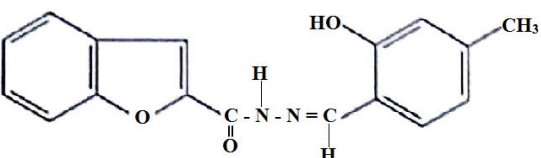
II. EXPERIMENTAL

Material and methods

All chemical and reagents were used in this projects were of AR-grade. Further solvents, reagents and

chemicals were purified. The following corrosion inhibitors were used in this paper.

Table 1

Inhibitor code	Name of the corrosion inhibitor	Structure
IM ₁	1-(Diphenyl methylene) hydrazine	
IM ₂	2-Hydroxybenzaldehyde[(1E)-(2-hydroxyphenyl)methylene] hydrazone	
IM ₃	N-(4-methoxyphenyl)-2-(naphtha[2,1-b] furan -2-yl-carbonyl)hydrazine carbothioamide	
IM ₄	N'[(1E)-(2-hydroxy- 4-methylphenyl)methylene]-1-benzofuran - 2-carbohydrazide	

Preparation of the Electrode Surface:

Mild steel having a surface area of 0.985cm² were fixed in a Tygon tubing exposing only the required surface. The metal plates were cleaned mechanically and also emery paper for the removal of organic deposits like grease oil which can be removed by washing with ethanol and orthophosphoric acid. The metal plates were dipped in 0.1M H₂SO₄ or HCL solution, stirred without and with different concentration of inhibitors for the desired interval of time (1 to 6hrs).

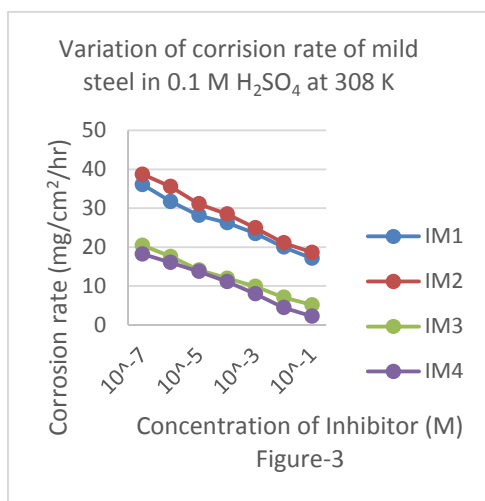
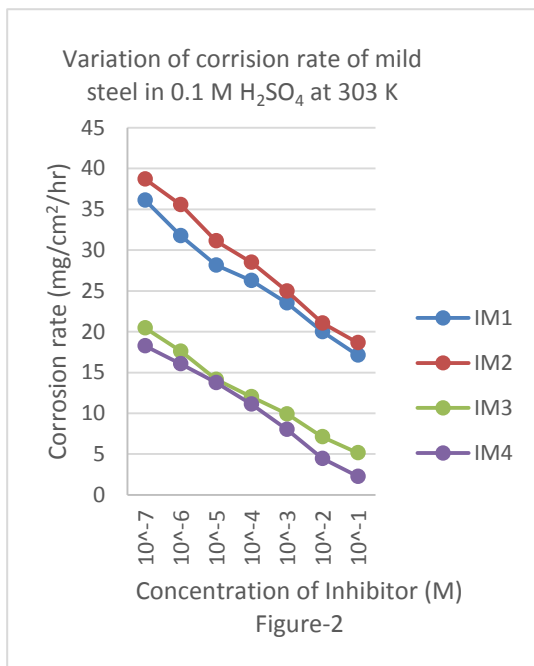
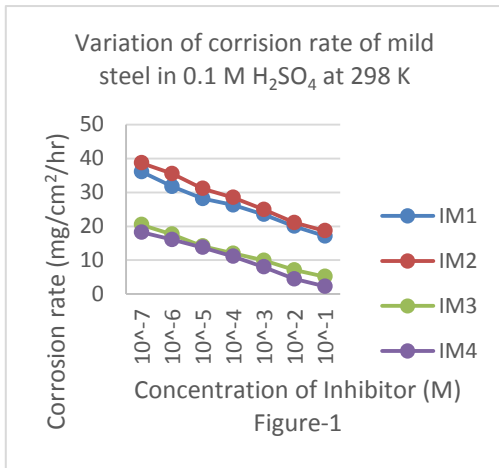
Preparation of corrosive medium:

Analytical graded Sulphuric or Hydrochloric acids used for each anodic or chemical dissolution studies was distilled using 1:1 acid-tri-pe water proportion. Distilled was subjected to anodic pre-electrolysis in a cell with platinum electrodes for 12 hours at current density greater than that used in dissolution studies.

III. RESULTS AND DISCUSSION

Dissolution Rates:

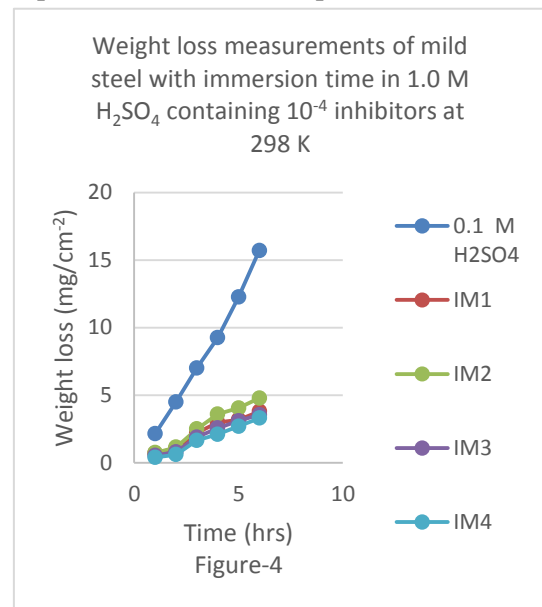
The mild steel surface was exposed to 0.1M H₂SO₄ under stirred and unstirred conditions in the temperature range of 298-308 K for about 1 to 6 hrs with and without inhibitors at various concentrations (10⁻⁷ M to 10⁻¹ M). The dissolution rates (mg/cm²/hr) of mild steel plates were calculated in corrosive medium spectrophotometrically. The inhibitory effect of inhibitors on the significant dissolution rate of the mild steel was observed. Decrease in the corrosion rate of the mild steel was observed as change in the concentration of inhibitors. The decrease in rate of corrosion was indicated in the graphs. The graph were plotted against "concentration of inhibitors (M) Vs Corrosion rate (mg/cm²/hr)" as shown in Figures-1, 2, 3.



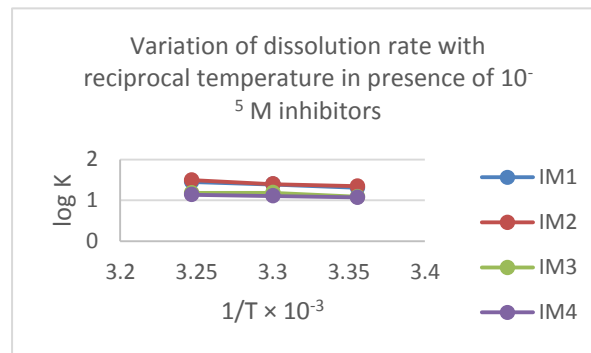
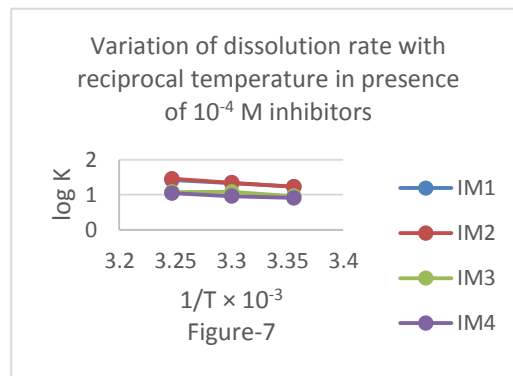
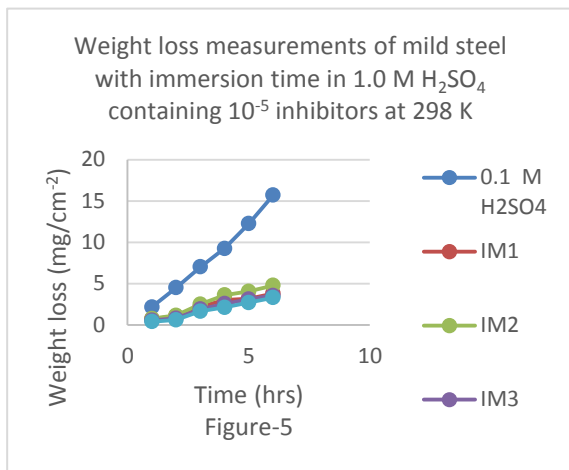
Based on the experimental data clearly reveals under stirred aerated conditions in 0.1M H₂SO₄ to study the effects of stirring rates on the dissolution of mild steel. The dissolution rates increased with increase in the rate of stirring till to reach optimum stirring rate. Above optimum stirring rate, the dissolution rate of mild steel was independent.

Effects of Immersion time:

Mild steel surface was immersed at different intervals of time in 0.1M H₂SO₄ with different concentrations (10⁻⁷- 10⁻¹ M) of inhibitors at 298K. Graphs has been plotted "Time Vs Weight loss" Figs- 4, 5 shows the effects of immersion time on the weight loss of mild steel in 0.1M H₂SO₄ with (10⁻⁴- 10⁻⁵ M) inhibitors at room temperature. Inference from the graph is that the mild steel dissolved with steady rate and weight loss was a linear as a function of immersion time. It was observed in the both Figures represents the absence of the insoluble film of corrosion product deposited on the surface. The inhibitor efficiency was calculated and it was found to be independent of immersion period.



Effects of Stirring:



Effects of Temperature:

To study the effects of temperature on the corrosion rate of mild steel in 0.1M H₂SO₄ contains 10⁻⁴ M - 10⁻⁵ M of inhibitors in the temperature range 298 – 308 K. As increasing in the rate of corrosion by increasing the temperature with or without corrosion inhibitors. However, the inhibitor efficiency was decreased with increase in temperature due to the decomposition of organic inhibitor so the rate of corrosion inhibition is depending on temperature.

The graph has been plotted (log k) Vs 1/T (Figure 6 and 7). These plots clearly reveals the activation energies of the dissolution process in presence of 10⁻⁴ M - 10⁻⁵ M concentration of inhibitors.

The activation energy of different corrosive inhibitors values were tabulated in Table-1. The activation energy of different corrosion inhibitors values are different for different organic molecule. The thermodynamic parameters are obtained at 303K but the entropy value indicates for different corrosion inhibitors reduces the dissolution of the mild steel.

Table 1. Thermodynamics parameters at 303K in presence of 10⁻³ M inhibitors

Thermodynamics parameters	IM ₁	IM ₂	IM ₃	IM ₄
E _a (KJ mol ⁻¹)	070.417	082.89	047.100	027.943
-ΔG ^o _a (KJ mol ⁻¹)	045.309	046.295	046.800	022.655
ΔH ^o _a (KJ mol ⁻¹)	045.355	046.342	046.847	022.678
ΔS ^o _a (KJ mol ⁻¹)	152.190	155.510	157.200	076.100

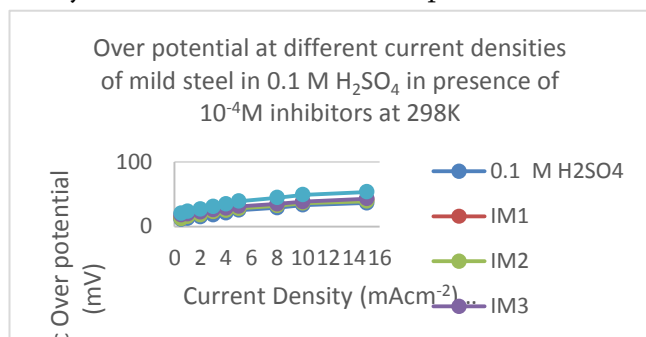
Corrosion Potential:

In the presence of different concentration corrosion inhibitors the mild steel is immersed and corrosion potential was studied. In absence of corrosion inhibitor the corrosion potential is increased with

increase in immersion time to a certain extent and remains constant. The same trend is observed in variation of corrosion potential in presence of inhibitors. As depicted in Figure 2 and 3.

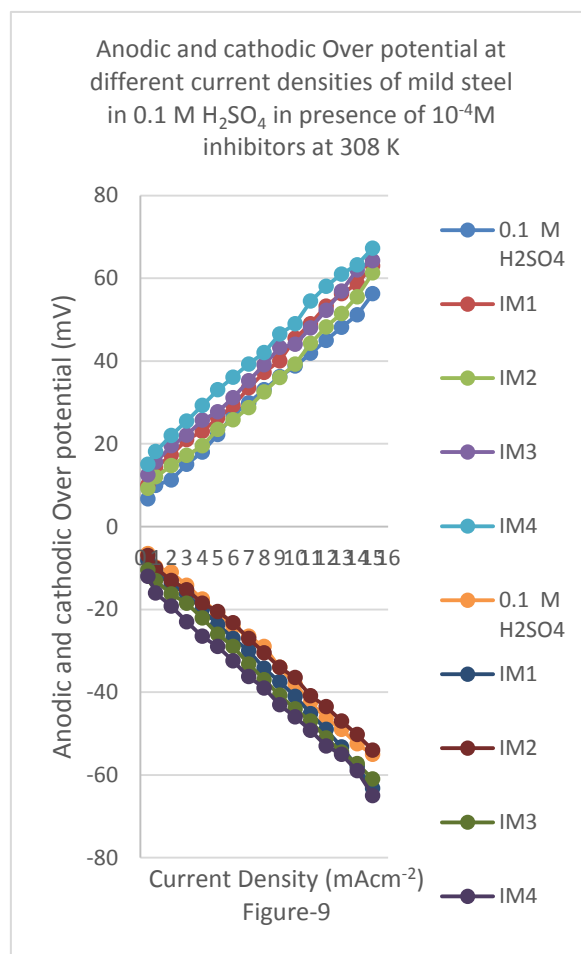
Polarization measurements:

Mild steel surface was studied under anodic polarization galvanostatically in stirred 0.1M H₂SO₄ in the presence of different concentration of inhibitors, current densities is maintained between 0.5 and 15mA/cm² at 303K. During anodic polarization at each current density, the over potential drifted slightly with time and finally attained a steady value on the surface of the mild steel at all current densities, the anodic over potential increased with time and reached a steady state value in 0.1M H₂SO₄ as summarized. The same trend was observed in the variation of over potential in presence of different concentration (10⁻⁷ - 10⁻¹M) of inhibitors. The value of initial and final over potential were always higher in the presence of inhibitors compared to that of pure acid. Figure 8 represents the variation in over potential with current density in 0.1M H₂SO₄ at room temperature.



The steady state over potential values were used to construct Tafel plots with and without corrosive inhibitors. Anodic Tafel lines shifted to higher potential region on the surface of metal. The anodic Tafel slope of 40 ± 5mV obtained in 0.1M H₂SO₄ increased with increasing concentration of inhibitory action of inhibitors. The value of Tafel slopes obtained in presence of inhibitor on the surface of the metal shown in Figure 9. The same trend was observed in the case of cathodic Tafel slope as shown in Figure 9

and this depicts both the anodic and cathodic Tafel slope.



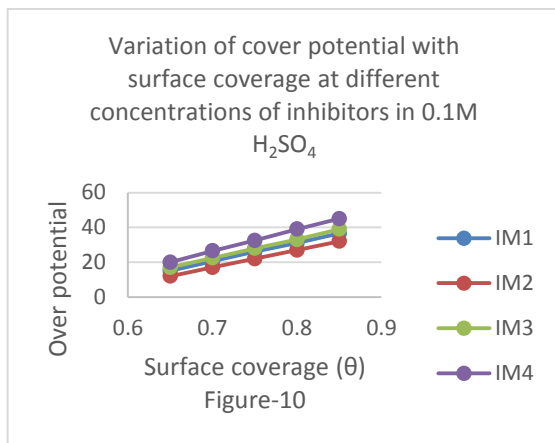
The %P obtained from polarization technique values are aggregable with weight loss method. The surface coverage values obtained from weight loss measurements and polarization technique values and variation in over potential at different concentration in 0.1M H₂SO₄ is shown in Figure 10.

Table 2

Inhibitors	Corrosion current (<i>i</i> _{corr}) mA/cm ²	Anodic Tafel slope (β _a) mV/decade	Inhibitor efficiency %P
0.1 M H ₂ SO ₄	0.35	35.2	-
IM ₁	0.29	41.1	82.00
IM ₂	0.10	39.25	80.24

IM ₃	0.62	98.0	87.00
IM ₄	0.85	40.0	91.02

$$\text{Surface coverage } (\theta) = \frac{\text{Weight loss without inhibitor} - \text{Weight loss with inhibitor}}{\text{Weight loss without inhibitor}}$$



The percentage protection from the polarization data were evaluated by using the Fisher's equation as follows,

$$\%P = \frac{i - i^*}{i} \times 100$$

Where i and i^* are corrosion current with and without corrosive inhibitors respectively. The %P was calculated using Fisher equation and same values were tabulated in Table- 2.

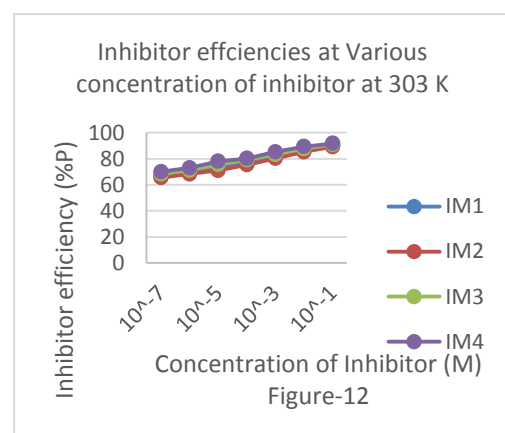
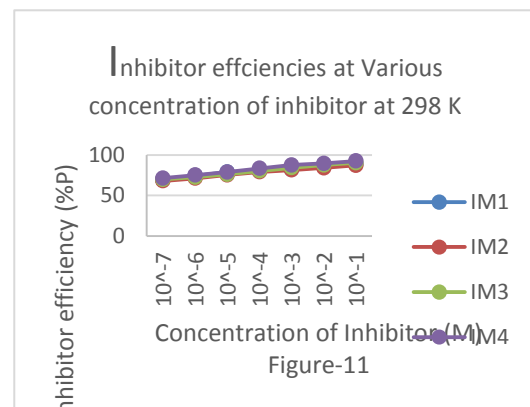
Table-2 Values of Corrosion current (i_{corr}), Tafel slope (β_a) and %P of mild steel stirred condition.

The weight loss of mild steel in 0.1M H₂SO₄ and in the presence of the different inhibitors (IM₁- IM₄) was determined by maintaining the time duration for about 1 to 6 hrs of immersion. The value of inhibitors efficiency (I.E), corrosion rate and surface coverage (θ) were calculated from the weight losses of the specimen with and without corrosive inhibitor using the following equations.

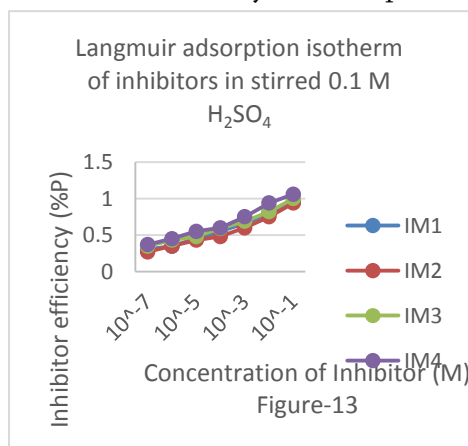
$$\text{I.E} = \frac{\text{Weight loss without inhibitors} - \text{Weight loss with inhibitor}}{\text{Weight loss without inhibitor}} \times 100$$

$$\text{Corrosion rate} = \frac{534 \times \text{Weight loss in mg}}{\text{Density} \times \text{Area in sq.inch} \times \text{Time in hours}}$$

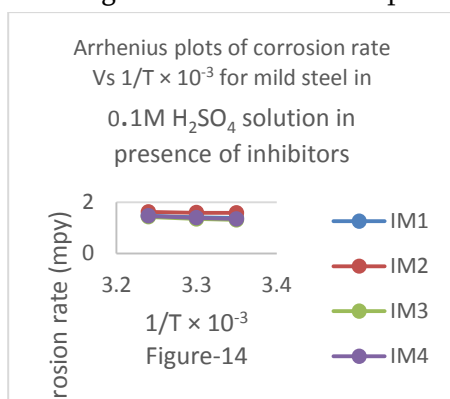
Figure 11 and Figure 12 show the IE for different concentrations of the inhibitors (10⁻⁷M- 10⁻¹ M) in 0.1M H₂SO₄. It is evident from this figure that all the compounds inhibit the corrosion of mild steel even at very low concentrations. The very high IE of these compounds is understandable from the electron donating properties of different nitrogen atoms present in the molecules. From the molecular structure of the inhibitors it is clear that an extensively delocalized orbit covers all the molecular atoms and the orbit is filled up with a number of π -electrons, they being contributed by different anchoring atoms of the molecule. It is apparent from the molecular structure that these molecules are able to absorb on the metal surface through nitrogen, imine groups and aromatic rings^{4,5}.



The degree of surface coverage (θ) for the different concentrations of the inhibitors evaluated from weight loss measurement. Inhibitor efficiency is increased as increase in inhibitor concentration. The same indicated in Figure 13. The Langmuir isotherm was tested by plotting c/θ Vs C for all compounds (Figure 13). A straight line obtained in all the cases providing the fact these compounds adsorbed on the mild steel surface obeys the Langmuir adsorption isotherm. This is substantiated by earlier report⁶.



At different temperature in the range of 298K - 308K with and without corrosive inhibitors (IM₁ to IM₄) at different concentration (10⁻⁷M to 10⁻¹M). The corresponding results are shown in Figure 14 and 15, clearly indicates the rate of corrosion increases with decrease in inhibitor efficiency with increase in temperature. The decrease in IE values by increasing the temperature this may be due to desorption of the inhibitors from the metal surface and thus exposing the metal surface for fresh attack by acid⁷. This observation is agreeable with earlier report.



Values of E_a and ΔG°_a are given in Table- 1. The less negative values of ΔG°_a with increase in temperature indicate physical absorption of the inhibitors on the metal surface⁸. The increase in E_a values for the inhibited solution in comparison with uninhibited solution may be due to the presence of reactive centres on the inhibitors that can block the active sites for corrosion⁹.

The cathodic and anodic polarization curves of mild steel in 0.1M H₂SO₄ with and without corrosive inhibitors of 10⁻⁴ concentration (IM₁ to IM₄) as shown in Figure 14. Similarly, polarization studies were made for other temperature (298K and 303K). Electrochemical parameters such as corrosion current (I_{corr}) and %P calculated from Tafel plots are given in Table-2. It is evident from the Tafel slope that it is affected to some extent by the addition of corrosive inhibitors, which shows that the inhibitors are efficient to control the rate of corrosion. Bentisset. al.,¹⁰ have reported such Tafel slopes.

IV. CONCLUSION

We have studied the effects of corrosion inhibitors on mild steel for anodic and chemical dissolution. In general the efficiency of corrosive inhibitors of different types of organic molecules IM₁ to IM₄. It is observed from the weight loss from Tafel slopes and thermodynamic parameters that these inhibitors are effective and efficient inhibitors in the presence of corrosion of mild steel in mineral acidic medium.

V. REFERENCES

- [1]. J.T. Patel, B.N. Oza, Trans. SAEST 38 (2003) 37.
- [2]. S.K.A. Ali, M.T. Saeed, S.V. Rahman, Corros, Sci. 45(2003).
- [3]. R. Hariharaputran, A. Subramania, A.A. Antony, P.M. Sankar, A. Gopaln, T.Vasudevan, S.V.K.Iyer, Br. Corr. J.33 (1998).

- [4]. S. Muralidharan, M.A.Quaraishi, S.V.K Iyer, *Corr. Sci.* 37 (1995)
- [5]. A. Selvaraj, S. Chitra et.al., *Bull.Electrochemistry* 21(6), 2005, 247-251.
- [6]. S. Rengamani, S. Muralidharan, M.Anbukulanthainathan, S.V.K.Iyer, *J.Appl.Electrochemistry*.24 (1994).
- [7]. S.T. Keera, *Br.Corr.J.*36 (2001).
- [8]. T.Murakawa, N.Hackerman, *Corros.Sci.*4(1964).
- [9]. M.S.Abdel-Aal, M.S. Morad, *Br.Corr.J.*36(2001).
- [10]. F.Bentiss, M.lagrennee, M.Trainsnel, J.C Hornez, *Corr.Sci.* 41(1999).

Effects Of Different Types of Water Solutions on Corrosion of Mild Steel

Revanasiddappa.M*, Avinash Anupam , Atmanand Y. Udameeshi

Department of Mechanical Engineering, Department of Chemistry , PESIT South campus Bengaluru, Karnataka, India

ABSTRACT

This paper aims to understand the effect of different water samples on rate of corrosion of mild steel at room temperature. this paper emphasis on three water samples those are salt water (NaCl+ water), one time distilled water, ground water. The experimental result helps to understand the cause of corrosion and its consequences.

Keywords: corrosion, mild steel, turbidity.

I. INTRODUCTION

Gradual deterioration or loss of metal at its surface by chemical, electrochemical reaction between the metal and as corrosion.

Metals are thermodynamically unstable. natural the surrounding environment is called metals are present in the form of metallic compounds(oxidized form).during extraction lot of energy is put to reduce metal ions into metal atoms. hence metals are always at higher energy state and are thermodynamically unstable hence metals try to lower their energy by spontaneously reacting with the chemicals present in surrounding environment like O₂ and H₂O.thus metals get back to their compound state and hence metal is lost. this process of loss of metal is termed as metallic corrosion.

Corrosion is an electrochemical process that appears in several forms like atmospheric corrosion and chemical corrosion .when acidic substances (water) come in contact with metal such as iron, steel rusting process gets started. Rust is result of corroding steel and iron (Fe).which is exposed to oxygen and moisture (humidity, vapor).when steel is exposed to water, the iron particles are oxidized due to water's

acidic electrolyte. The iron particles then become oxidized, which result in formation of Fe⁺⁺.when Fe⁺⁺ is formed, two electrons are released and flow through the steel to another area the steel which is cathodic area.

Oxygen allows these electrons to rise up and form hydroxyl ions (OH⁻).The hydroxyl ions on reaction with Fe⁺⁺ to form hydrous iron oxide (FeOH),better known as rust. Where the affected iron particles were, now formed into corrosion pit and where they are now is called corrosion product (rust).

Corrosion can happen at any rate, depending on environment that the metal is in.due to low oxygen content,even marine sediments favor growth of anaerobic organisms that influences the corrosion processes in mild steel in marine media .since atmospheric corrosion gets spreadat faster rate ,it is advised to follow effective precautionary procedures when it comes to prevention of corrosion.

II. OBJECTIVE OF THE STUDY

To study the rate of corrosion of mild steel in salt water, distilled water, ground water and in open atmosphere and discuss the results.

III. METHODOLOGY

Four mild steel pieces of 50*70 mm were taken and rust was removed using emery paper. Three solutions were prepared in 250 ml beaker consisting salt water (NaCl + water), one time distilled water (water that has

been boiled into steam and condensed back into liquid on a separate container and this process is conducted only one time), ground water respectively and other piece was kept open to atmosphere. They were observed at regularly intervals of 24 hours and amount of corrosion was checked.

IV. RESULTS AND DISCUSSION



Figure 1. picture of water samples after 24 hrs.



Figure 2.metal surfaces on exposure to salt water ,distilled water and ground water



Figure 3.Metal in distilled water after 48 hrs



Figure 4.metal in ground water after 48 hrs.



Figure 5.metal in salt water after 48 hrs.

As the beaker is partially filled with water solution, part of tank just below water level is exposed to lower concentration of oxygen therefore becomes anodic and undergoes corrosion .part of above water line which is exposed to higher concentration of oxygen becomes cathodic and remains cathodic.

[concentration of oxygen in atmosphere is 20.95%
Concentration of oxygen in water is 9.03mg/l]

We observed that all the three were corroded but the quantity was different. Salt water had the highest amount of corrosion while distilled water had lowest amount of corrosion. Ground water had medium level of corrosion

Higher the salt content higher the corrosion rate. This is explained as increased solution electrical conductivity of the solution facilitate the cathodic reaction (oxygen reduction) and anodic reaction (iron dissolution). salt water has higher viscosity than ground water because of its higher salinity . corrosion also depends on temperature and also environment .oxygen content decreases with increase in pressure .it is to be noticed that the distilled water causes considerable rate of corrosion for the whole

time. The occurrence of corrosion in distilled water may be attributed to the presence of little amount of salts.

It is also noted that rate of corrosion increases with decrease in pH. The rate of corrosion increases with increase in conductance of medium.as the conductance of medium increases, ions can move easily through the medium.

Turbidity:

Turbidity can be defined as blurriness or cloudiness in the water due to impurities or dirt. We observe in the corrosion aspect, turbidity due to corrosion product. We observe that turbidity in salt is highest and turbidity in distilled water is lowest. Corrosion product insalt water does not stick to the surface of mild steel .it suspends in the solution. Whereas, in distilled water corrosion product sticks to the surface. Corrosion product covers the whole surface .it does not allow corrosion for inner surface.

V. CONCLUSION

We observed that the metal gets corroded faster in salt water than in distilled water and ground water. Metal gets more corrode in salt water than in other two solutions. More the salt concentration or solution conductivity higher corrosion.it was also proved by turbidity concept.

VI. REFERENCES

- [1]. BASUCHANDRA'S ENGINEERING CHEMISTRY.2012 edition.
- [2]. Fundamentals of metallic corrosion in fresh water. J R.Rossom.
- [3]. Effect on corrosion rate on steel pipe in turbulently flowing solution .Dr. Basim O.Hassan.
- [4]. comparision of the mineral water,tap water and bottled water.J.Genn Intern med.
- [5]. Ph.Rafait. .R .Sabot.Corrosion at sea water interface and mechanism.
- [6]. Harold J.Cleary.On the mechanism of Corrosion of steel immersed in Saline water.
- [7]. www.Britannica.com/seawater.

Qualitative Analysis of Ground Water Samples of 4 Sites in Hosakerehalli Locality of Bangalore South, Karnataka, India

Sankarshana Rao R, Sanath Krishna, Pushkar Pramod Wani, S Sourav Revanasiddappa M

PESIT Bangalore South Campus, Department of Electronics and Communication Engineering, Bangalore, Karnataka, India

ABSTRACT

Water is an important source for many purposes especially for drinking and we get water especially from ground water which is considered to be the purest form and most reliable form but due to various human activities such as industrialization, irrigation and polluting the water by the means of releasing harmful wastes. Hence these are considered to be the major factors of pollution of ground water. To use water for various day to day purposes, it must meet the standards prescribed by World Health Organization (WHO) and Central Ground Water Board. Therefore the ground water is tested for various factors such as Total Hardness (TH), Alkalinity, pH, Conductivity, Chemical Oxygen Demand (COD). This paper presentation is to check the samples of ground water for the above mentioned parameters and report the comparative study the same with the standards prescribed as per WHO and other organizations and boards.

I. INTRODUCTION

Every living creature on the planet Earth needs water for its survival. Water is a very Essential component of human survival. Human body is made up of 80%-90% of water. Cell, blood and bones contain 90%, 75% and 22% of water respectively. We can hardly leave for a very few days without water. The general survey reveals that the total surface area of earth is 51 crore km² out of which 36.1 crore km² is covered by sea which needs some sophisticated processes to make it fit for drinking and other daily chores. We get fresh water from rivers, underground, lakes, tanks which are fit for drinking and other daily chores. Among this urban areas are more dependent on the underground sources of water for consumption which is considered as the purest form of water containing no dissolved impurities. But due to the industrialization and modernization of the agricultural practices, the chances of polluting the ground water has increased. Harmful chemical fertilizers used in agricultural

fields and also untreated industrial chemical waste left into water bodies enters the ground water sources by seepage through surface soil. So in order to detect and calculate pH, hardness, conductivity and other parameters we can use cost effective remote sensors which connects the mobile phone through Bluetooth or Wi-Fi by generating an application for this. By doing this we can get instantaneous reading of various parameters and if at all the readings are exceeding the normal range as prescribed by WHO then the concerned authorities will get notified about this, through this the concerned authorities can take necessary action.



HOSAKEREHALLI LAKE AFTER CLEANING

Ward no. 161- HOSAKREHALLI MAP



II. MATERIAL AND METHODS

2.1 Study area:

Ward number 121 Hosakerehalli, BSK3rd stage, Bangalore, Karnataka, India.

Geographical Coordinates: 12.9290° N, 77.5370° E

This area is densely populated and has a good commercial activity in one part of it. These areas have fairly good wide roads with a few exceptions. The area contains a lake which was cleaned and brought back to its form in 2017. Till that it was polluted with the domestic sewage. This area being a connective one between Raja Rajeshwari Nagar (Mysore Road) and outer ring road, has high amount of traffic flow which brings in great amount of air pollution in the peak hours. Though it is a very old one, it has been witnessing all the types of development in recent times. The area has a good sanitary system except some few parts. The area has a very large amount BOREWELLS dug up for supply of Drinking Water. Some are dug by the government and others of the residents. It has splendid road connectivity.

Due to its elevation, Bangalore enjoys a pleasant and equable climate throughout the year. The highest temperature recorded was 38.9°C (102.0°F) on 22 May 1935 and the lowest was 7.8°C in 1884. Bangalore receives about 970 mm of rain annually, the wettest months being August September, October and in that order. The summer heat is moderated by fairly frequent thunderstorms and

occasional squalls causing power outages and local flooding. The heaviest rainfall recorded in a 24-hour period was 159.7 mm recorded on 1 October 1997. October 2005 was recorded as one of the wettest months in Bangalore with heavy rains causing severe flooding in some areas, and closure of a number of organizations for over a couple of days.

2.2 Sample collection:

A total of 4 water samples were collected in the month of March of the year 2018 in pre-summer season in Hosakerehalli Ward no. 161, Bangalore, Karnataka, India.

2.3. Parameters under monitoring:

The groundwater samples were analysed by using chemical and physical parameters such as pH, TH (Total Hardness), Electrical Conductivity, Alkalinity and COD (Chemical Oxygen Demand) using standard protocols and the quality of the data was ensured through careful standardization.

III. RESULTS AND DISCUSSIONS

3.1 Electrical Conductance of water samples:

The conductivity of the ground water is being measured by the conductivity electrode dipped in water and connected to conductivity meter which shows the conductivity values. As per the WHO and the Indian Ground water Board, the permissible limit of Electrical Conductivity in the potable water is stated as 5mS/m to 50mS/m. From the Qualitative analysis of the ground water samples we can conclude that all the water samples tested have the electrical conductivity as per the standards and hence it is fit for drinking.

3.2 Total Hardness:

Hardness is majorly caused due to the presence of carbonates and bicarbonates of calcium and magnesium salts including sulphates, chlorates and nitrates. The hardness of water is found out

experimentally by the method of titration. By using the titre values we can calculate the accurate values of the total hardness of water. As per the WHO and Indian Ground Water Board, the normal permissible limit for drinking water is 200ppm, but in extreme cases where there is severe water shortage, the permissible limit can be raised up to 600ppm. As per the Qualitative analysis of water samples, we get to know that hardness values of all the samples lie in the range of 200ppm-600ppm. This range is not the normal permissible range, but the water can be used for drinking in severe drought conditions mainly in summer season as there will be less/no drinking water supply from the Water Board. As per the result we can conclude that, the above mentioned water samples is not advisable to use them for drinking when there is abundant other resources of water. They can only be used in extreme cases i.e. when there is no other source of drinking water.

3.3 Chemical Oxygen Demand (COD):

Chemical Oxygen Demand (COD) can be referred to as an indicative measure of the amount of oxygen that can be consumed by reactions in a measured amount of water or solution. Greater the value of COD, it means that there is greater amount of contaminants (Chemicals) in water. As per the WHO and Indian Ground Water Board, there is no mention of any limitations but the COD for drinking water must be zero or negligible. As per the Qualitative analysis of water, the water samples are not contaminated with chemicals which shows the ideal conditions for drinking water and hence it can be concluded that the tested water samples are very much fit for drinking with respect to Chemical Oxygen Demand (COD) of water.

3.4 pH:

pH is a numeric scale used to specify the acidity or basicity of an aqueous solution. Typically it is the measure of hydrogen ion concentration in the liquid (water). It ranges from 1

to 14. pH of a pure water is 7 which is considered as NEUTRAL pH. If the pH of a solution is <7 it is considered acidic and if it is >7 , it is considered basic. According to the WHO and Indian Ground Water Board, the permissible range of pH for drinking water is 6.5 --- 8.5. The samples that we have tested, the sample 1, sample 3 and sample 4 has pH in the permissible limit and hence fit for drinking. But the sample 2 shows slight variation from the permissible limit and as mentioned by WHO that there must be no compromise in pH of drinking water, it can be strictly stated that the water sample 2 is not fit for drinking purpose.

POISONED WATER OF HOSAKEREHALLI DRAINAGE



3.5 Alkalinity:

Alkalinity is a measure of the capacity of water to neutralize acids. The Alkalinity is mainly caused due to the presence of carbonates, bicarbonates and hydroxides. Alkalinity has the same limitations as that of Total Hardness i.e. 200ppm – 600ppm. From the Qualitative analysis of the water samples, we found out that all the samples had alkalinity less than 200 ppm which is perfectly placed in the permissible limits of drinking water and hence can be concluded that all the water samples are safe for drinking with respect to the Alkalinity factor.

For all samples:

Odour – Odourless

Taste – Tasteless

Colour – Colourless

IV. CONCLUSIONS

This study has let us know the water quality in the area of Hosakerehalli, ward no. 161. This is significant in making people know about the water quality in the area and also helps in building required technical devices that help in purifying the contaminated water and make it fit for drinking.

The Qualitative study of the hardness of water indicates that:

- All the samples shows the hardness level more than normal permissible limit but it is below the extreme permissible limit.
- Therefore all the water samples can be used for drinking in extreme drought conditions.

The Qualitative study of Chemical Oxygen Demand (COD) indicates that all the water samples are fit for drinking as they all showed 0 COD.

The Qualitative study of pH of the samples indicates that sample 1,3 and 4 are very much fit for drinking as they are in permissible limits and sample 2 shows a slight variation from the permissible limit which indicates that it is not fit for drinking.

The Qualitative study of Alkalinity of the water samples indicates that there is no presence of hydroxyl ions and shows presence of carbonate and bicarbonates. The presence of carbonates and bicarbonate are within the prescribed limits of WHO and hence can be concluded that the water samples are fit for drinking.

The Qualitative study of Electrical conductivity of Water samples indicates that all samples have electrical conductivity within the range of prescribes limits from WHO and hence can be concluded that the water is fit for drinking.

Hence from the overall study of all the characteristics, it can be concluded that the ground water of Hosakerehalli, Ward no. 161 is fit for drinking in Extreme cases as it shows slight variation in pH in some regions. The area regularly has a good drinking water supply, hence the citizens must be advised to use the water supplied from the BWSSB (Bangalore Water Supply and Sewage Bard) rather than using ground water.

Table 1.Shows the measurement of bore well water quality parameters by using chemical and physical methods

Sample no.	X(Latitude) (Degrees)	Y(Longitude) (Degrees)	1 st Source (Feet)	2 nd Source (Feet)	3 rd Source (Feet)	Casing Depth (Feet)	Total Depth (Feet)	Yield (Inches)	Total Hardness	Chemical Oxygen Demand (COD)	Total Alkalinity	pH	Conductivity
<u>01</u>	12.55336	77.32259	10	45	--	80	100	4.5	379.6ppm	nil	116.0ppm	7.92	32.6 mS
<u>02</u>	12.929927	77.535577	85	145	--	80	400	6	423.23ppm	nil	132.0ppm	8.6	36.4 mS
<u>03</u>	12.931426	77.534832	50	160	400	150	450	6	528.86ppm	nil	196.0ppm	7.91	35.6 mS
<u>04</u>	12.928657	77.533521	20	50	--	50	80	4	507.49ppm	nil	174.0ppm	8.23	28.2 mS

Crime Patterns and Prediction: A Data Mining and Machine Learning Approach

Saptarshi Dutta Gupta, Vaibhav Garg

Computer Science and Engineering, PES Institute of Technology, Bangalore, Karnataka, India

ABSTRACT

Studying and analysing patterns in crime is of paramount importance in today's world. With the increase of rapes, burglary, kidnapping and theft we need to provide a comprehensive framework for the government and law-makers for planning and informed decision making to control the increase of a particular kind of crime in various locations. Again, location and time of a crime have huge effects on the severity of the crime. According to a report published by the National Crime Records Bureau, which noted the crime rates between 1953 and 2006, the number of house burglaries in the country had dropped by 79.84% over a period of 53 years. However, the number of kidnapping cases in the country increased by 47.80% during that time. In addition to that, the total number of cognisable crimes under the Indian Penal Code (IPC) had shown a 1.5% increase in its numbers from 2005 to 2006. Looking at these statistics, we can understand the duplicity of crime data and how it changes over the years. Because of its dynamic nature, we need to find patterns in a crime which will help the police in the process. Multiple datasets were selected from government websites, which were used to find a pattern in the different classes of crime occurring in different states of the country. The dataset contains instances of reported crimes ranging from the year 1993-2014. With this information, we plan on predicting the crime rates in the future years using various machine learning algorithms and decide which algorithm is providing the most accurate values. Prediction of crimes can help the individual state police departments to concentrate their efforts more in the regions which recorded a higher concentration of crime or which shows a steady increase in its cases of reported crimes. 21 years of data is being used for training the model and extrapolating future values. This research aims at providing the people with an almost accurate prediction of the total number of crime instances in a State/UT within a span of 10 years from the last recorded year of data.

Keywords: crime prediction, data mining, time series, machine learning, regression, decision tree, support vector, random forest

I. INTRODUCTION

As per the National Crime Records Bureau's 'Crime in India' Report 2012 edition, it stated India as one of the most violent countries to live in. After the 2016 edition of the report, it was evident that literate people had more involvement in the criminal activities. Metro cities like Delhi, Mumbai and Bengaluru had the highest crime rates in the country respectively.

To keep a check on these ever increasing crime rates in the major cities of the country the law enforcement needs to be made stricter. The punishment for anybody who commits a heinous crime should be as strict as ethically possible so that anybody thinks twice before breaking the law. For effective law enforcement it is necessary to know the current trends of different crimes, for example which crime is the most prevalent in an area. To provide the law-makers with this information, we have done extensive research on crime data across the country and have

implemented machine learning models to make these predictions. The model is trained with a dataset of all the number of reported cases of multiple crimes for each state/Union Territory from 1993 to 2014.

Multiple learning algorithms have been applied so as to arrive at an output with the highest accuracy possible. The dataset is trained differently for every algorithm. We plot different time-series graphs for our dataset using various regression algorithms like Support Vector Machine, Decision tree regression, Random Forest Regression. Once a model has been trained it is put to use by trying to predict the expected number of instances of a particular crime in a state/Union Territory in a given year with minimal acceptable error.

II. TIMES SERIES ANALYSIS FOR PATTERNS

The factor which is of paramount importance in ensuring success in a business is Time. In today's world, it is difficult to keep up with the pace of time. Time Series Modelling is a powerful method by which we can see ahead of time.

A continuous list of data points listed or graphed in time order is used for time series analysis. Time series plots are usually plotted with the help of line charts. Time series is largely used in any science and engineering domain where temporal measurements are involved.

Time series analysis can be defined as the method for examining and scrutinizing the time series data so that meaningful statistics and useful information can be extracted from it. This information may not be visualized normally. Time series analysis is also the first step to time series forecasting where future values are predicted depending on the previously observed values. This kind of analysis finds its application in diverse kinds of data which includes continuous data,

real-valued data, discrete numeric data and discrete symbolic data.

Statistical inference is a part of time series prediction and a particular approach to such an inference is known as predictive inference. Time series analysis of the data will give a visualization of the data which will help us to assess the pattern of the dataset i.e. whether the particular factor we are measuring is increasing or decreasing with respect to a certain period of time.

A common notation specifying a time series X that is indexed by the natural numbers is written

$$X = \{X_1, X_2, \dots\}$$

We have datasets for each crime for ex. Murder, rape, kidnapping for individual states/Union Territories. The datasets comprises of the numerical value of that crime in each state according to increasing order of time.

III. MACHINE LEARNING FOR PREDICTING FUTURE RATES

A kind of supervised learning problem for predicting future rates is time series forecasting. We develop a time series model to best capture or describe an observed time series in order to understand the underlying causes. Here we seek the 'why' behind a time series dataset. The method by which predictions about the future is made is called extrapolation and refer to it as time series forecasting.

Supervised learning is a form of learning in which we have to enter the input variable(X) and an output variable(y) and an appropriate algorithm is used in order to map the function from the input to the output.

$$Y=f(x)$$

Supervised learning problem can be divided into two types:

(i) **Classification** where we classify the output variable into a particular type for example summer or winter

(ii) **Regression** problems are the ones in which the output variable has a specific real value.

Our problem is a supervised regression problem.

Sliding Window: For a time series problem, in order to apply supervised learning, we need to restructure our data so that it corresponds to a sliding window. Here we use the value at the previous step in order to predict the value at the next step. Therefore the dataset needs to be reorganized in order to predict the correct values.

In sliding window, we reorganized our dataset as shown in the table Fig1 and Fig2. Fig 1 shows the original dataset and Fig2 is the data after modifying it according to the sliding window method

YEARS	MURDERS
2001	2602
2002	2525
2003	2667

Figure 1. Murder statistics for three years in Andhra Pradesh

?	2602
2602	2525
2525	2667
2667	?

Figure 2. The reorganized data according to sliding window method

The first and last rows are removed and we use the rest of the dataset to train the model. In our supervised learning problem, the input(x) will be the

previous time step and the next time step is the output(y). Next we will be able to apply any regression algorithms in order to predict the future values.

We have primarily used three regression algorithms and compared the result to find out which algorithm is giving us the maximum accuracy.

1. **Support Vector Regression:** It is an extension of the classification theorem Support Vector Machine (SVM). It is used as a regression algorithm with only a few minor differences between the two algorithms. It becomes comparatively difficult to predict a value with the information at hand that can have infinite possibilities. When used as a regression algorithm, a margin of tolerance is set in approximation to the SVM which is a user input at the start of the algorithm itself. SVR has other benefits over SVM, like it minimizes the error in prediction, individualises the hyperplane which maximizes the margin while tolerating a part of the error.

The model produced by SVR depends only on a subset of the training data, because the cost function for building the model ignores any training data that lie close to the prediction model.

2. **Decision Tree Regression:** A decision tree generates a classification or a regression model in the form of a tree. It divides the dataset into many small subsets, simultaneously incrementally developing a decision tree. The final tree has two different types of nodes, decision nodes and leaf nodes. The decision nodes have two or more child nodes, each representing values for the attribute tested. Leaf nodes represents the target numeric value to be predicted.

Regression Decision Trees are used when the target values takes continuous values, like in our case.

3. **Random Forest Regression:** It is an ensemble learning method for classification and regression. It operates by constructing multitude of decision trees during training and outputting the class that is the mean prediction of the individual trees. Random Forests are a way of averaging multiple deep decision trees, trained on different parts of the same training dataset, with the goal of reducing the variance. This comes at the expense of a small increase in the bias and loss of interpretability, but greatly boosts the performance in the final model.

IV. IMPLEMENTATION

The aim of this paper is to find patterns in criminal activities and find the future increase or decrease of a particular criminal activity in the state. This is done so that necessary actions can be taken to curb such activities in that state. In order to achieve the goals, we have used the architecture/workflow diagram as shown in Figure 3.

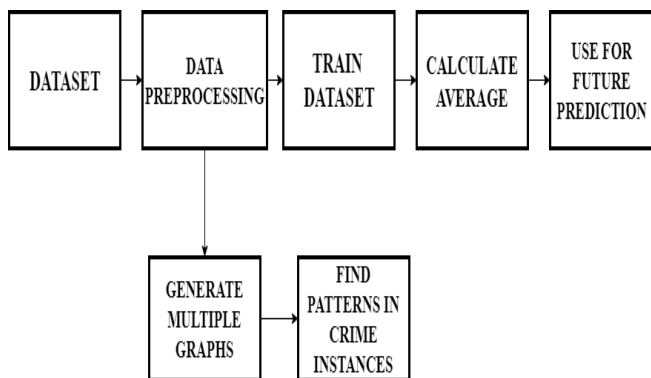


Figure 3. Workflow Diagram

Multiple dataset files were obtained from government websites which contained the reported number of incidents of each type of crime from 1993 to 2014. After gathering the data, the first step was to preprocess the data. This included two main steps: *first*, handling the missing values. The data was cleaned by removing any inconsistencies and some

missing values were filled in by calculating the mean of the particular attribute and deciding a value around it. *Second*, data reduction techniques were applied to remove any attribute (crime) based on whether it has at least one recorded instance in each state or not. Subsequently, the entire dataset was divided into multiple datasets according to the state and crime using a Python script.

This data was analysed using various time series charts, bar graphs in order to see a pattern in the data. RapidMiner was used for the visualization of the data. The time series graphs was generated using RapidMiner modules and visualization according to various states and crimes. We also generated time series graphs for multiple states and a particular crime in order to get a picture of the scenario of the crime in various states.

After finding patterns in the data, the next step is to predicting future values. This is achieved by training the dataset using various machine learning algorithms. Therefore, we have to convert the dataset into the sliding window format in order to apply supervised learning algorithm as discussed in Section III. This was also achieved using a Python script.

The data was then trained using various machine learning algorithms. The supervised learning algorithms that were applied in the paper were Support Vector Regression, Decision Tree Regression and Random Forest Regression. We divided our data set into the training and testing data. We applied each algorithm separately and trained the training data set. We used Python programming language for each of the algorithm. The scikit_learn library was used for implementing the machine learning algorithms.

We generated plots for every model for the training set in order to visualize the fitness of the model. Following this, we generated the predicted values for the testing data and matched how accurate the actual

results are from the predicted results. The model which gave the least error was used for the prediction of the crime rates for the future years.

V. RESULTS AND ANALYSIS

After preprocessing the data multiple time series graphs were generated for various states. The states with the maximum number of murders were obtained as Uttar Pradesh, Maharashtra and Bihar as shown in the Fig4.

Individual time series graphs were also generated for each state and for each crime and the rate of increase/decrease of crime rates in each state could also be analysed. In this way, the government can plan more suitable techniques to handle criminal activities in the area and focus on one or more state or one or more crime than the other.

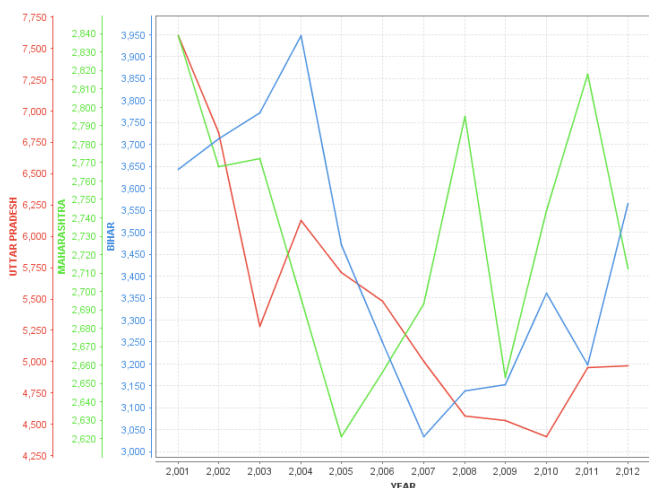


Figure 4. Time series graph for the states Maharashtra, Uttar Pradesh and Bihar

Next the sliding window dataset was trained using the Support Vector Regression, Decision Tree Regression and Random Forest Regression and the training data was plotted as shown in the figures below. The graphs were generated taking into consideration the crime 'Murder' for the years 1993-2014 for the state Andhra Pradesh.

Fig5 shows the regression line Decision Tree Regression, Fig6 for Support Vector Regression and Fig7 for Random Forest regression.

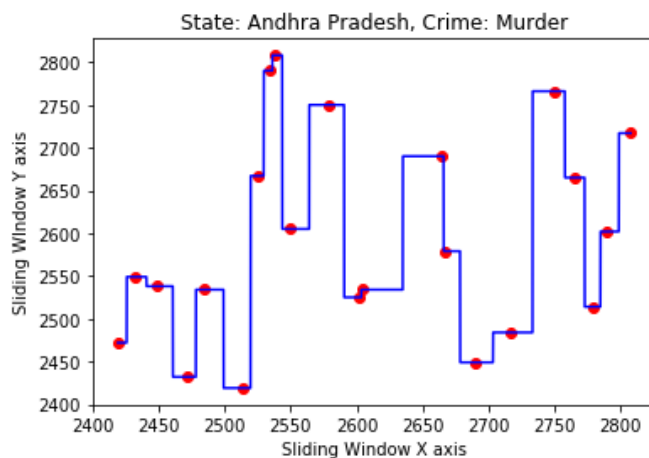


Figure 5 Regression Line using Decision Tree Algorithm

From the graphs it can be understood that Decision Tree Regression is giving the most accurate results. We have calculated the R-squared value which is a statistical measure of how close the predicted data is from the generated regression line. For each of the regression algorithms, we have calculated this value and the results are displayed as shown in the table given by Fig8. This value is calculated taking into consideration the murder rates in Andhra Pradesh. Even after running on several different datasets, Decision Tree Regression always gave us the highest R-squared value.

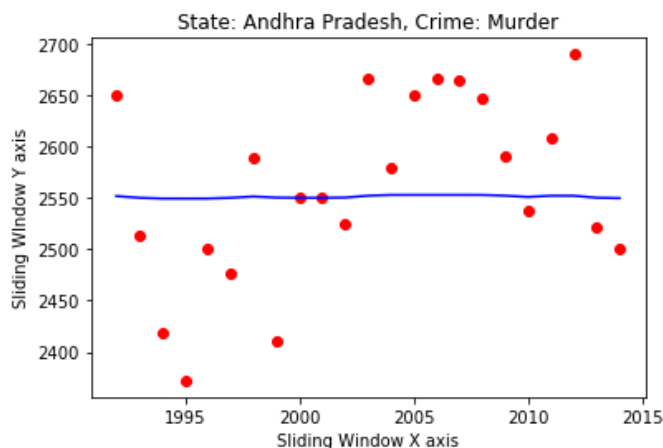


Figure 6. Regression line using Support Vector Regression

Therefore the R-squared value also gives us the proof that predicting using Decision Tree will give us the best result.

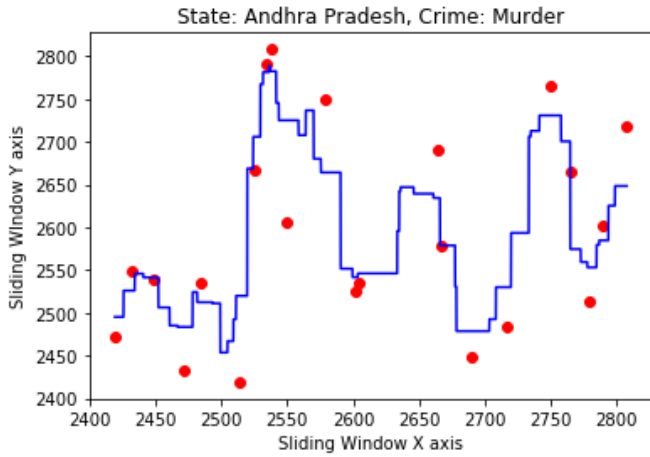


Figure 7. Regression Line using Random Forest Regression

Regression Algorithm	R-Squared value (in %)
Support Vector Regression	29.6
Decision Tree Regression	80.8
Random Forest Regression	64.3

Figure 8. R-Squared value for the algorithms

Thus we have calculated the future values of the crimes using the Decision Tree Regression Algorithms. Since we are measuring crime rates and it depends on human psychology, very high R-squared value could not be achieved. The following table in Fig9 shows us the predicted value for some of the crimes in Andhra Pradesh in the year 2018 after applying the Decision Tree algorithm.

CRIME	EXPECTED VALUE 2018
Murder	2432
Rape	1070
Dacoity	145
Kidnapping	2119

Murder	2432
Rape	1070
Dacoity	145
Kidnapping	2119

Figure 9.Expected crime rates in Andhra Pradesh, 2018

VI. CONCLUSION

The proposed model aims at predicting the total number of incidents of a particular crime in a state. We approached the problem with three different approaches, Support Vector Regression, Decision Tree Regression and Random Forest Regression. The original dataset had to be trained and processed differently for each algorithm. This was accomplished by implementing python scripts.

The data was then fed into the method and a test model was generated. This model was then tested with the help of test values and the model was then made to predict the number of a particular crime that will occur in that state in the given year. The error in the test predictions were very high which led to further training of the models. From the test run of the algorithms it was evident that the Decision Tree Regression algorithm gave the predictions with the best R-squared value.

Once an acceptable model was ready for each algorithm, it was made to predict the number of crime instances in 2018. Government bodies can use this data and predictions to come up with different policies and laws for each state depending on the type of crime which is expected to be prevalent in the next year. More police force can be deployed in the areas which have a history of crimes being committed around them. The people living in these states can also

use this data to learn how to defend themselves from these threats.

According to our predictions the number of murders in the state of Andhra Pradesh should decrease by 3.68% compared to 2017. The numbers of rape instances are expected to be 1070. Dacoity should decrease down to only 145. A little more effort from everyone and we can bring down this number to 0 in the years to come.

In our analysis high R-squared values could not be achieved. This is not due to wrong training of the model but rather because this is a human psychological analysis. There are numerous factors which affect a person's psychological state, which could lead to committing a crime. The values predicted are based on the past trends in the numbers of crimes committed and does not put a hard value on the numbers predicted.

VII. REFERENCES

- [1]. Tom M. Mitchell, "Machine Learning"
- [2]. Vojislav Kecman, "Learning and Soft computing: support vector machines, neural networks and fuzzy logic models"
- [3]. <https://machinelearningmastery.com/time-series-forecasting-supervised-learning/>
- [4]. <https://data.gov.in/>

IoT Based Intelligent Lock

Nidhi Shivhare¹, Aashi Garg¹, Ananda M.²

¹Department of Computer Science and Engineering , PESIT South Campus Bangalore, Karnataka, India

²Asst. Professor, Department of Electronics and Communication PESIT South Campus Bangalore, Karnataka, India

ABSTRACT

Security is an entity that cannot be compromised. There has been an increase in rate of theft and crime, attacks by intruders and vandals, despite of all the different forms of security gadgets and lock. The concept of remotely connecting and monitoring real world objects through the Internet comes from Internet of Things(IoT). We can aptly incorporate it to make our homes smarter, safer and automated. We live in the world dominated by technology and we still use the mechanical locks and combinational locks for the security of our loved ones, valuable belongings. To end this we have designed an effective security system for buildings, safes, doors and gates, so as to prevent unauthorized person from having access to ones properties. The proposed system provides strengthened security functions that sense the surrounding for the presence of an invalid user and based on that alarm the user to live stream the surroundings. Thus the accessibility is totally in hands of the owner.

I. INTRODUCTION

The advancement in science and technology throughout the world has lead to an increase in the rate of crime and so has the necessity for us to ensure the security of our valuable belongings. The crime rate still has increased with the use of mechanical locks as these locks can be easily broken. While with the use of combination locks (also known as keyless gates) the rate of crime has decreased but it still can be broken by guessing or hacking. The leverage obtained by preferring the proposed system over the other similar kinds of existing systems is that the alerts and the status sent by the Wi-Fi connected micro-controller managed system can be received by the user on his phone through E-mail and SMS from any distance.

The main aims of this design are: (1) To design a cheap and effective security system for buildings, safes, doors and gates etc., (2) To experiment the application of electronic devices as locks, and (3) To prevent unauthorized person from having access to ones

properties through the use of IFTTT which is a free web-based service to create applets. In this paper, we propose the design of an IoT based digital door lock to enhance the various security and monitoring functions using IoT technologies.

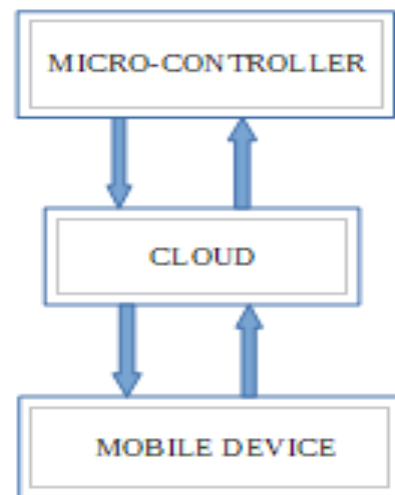


Figure 1. General Connectivity

II. EXISTING METHOD

In the RFID technology if someone tries to open the door it will be sensed and sends the indication message to the user via GSM. In the pattern matching method, the door will be opened only when the unique graphical security is drawn on the screen but the pattern can be easily identified by unknown person and that person can easily open the door without any exception from the user. The main drawback is that it will not be identifying who is opening the door. In this paper the technique implemented is that the door can be opened only by the user authenticated by the owner on the basis of live streaming done after sensing the presence of a person nearby. Thus the access to be given or denied is entirely in the hands of the owner.

III. PROPOSED METHOD

The main goal of this project is to overcome the major drawbacks of different door security systems such as GSM and RFID, Pattern Analyser and Fingerprint methods. In this proposal, if a person tries to access the door the sensor unit will activate the complete circuit and it will be sending the E-mail and SMS to the authenticated user via IFTTT [3]. In addition, the person who is trying to access the door will then be live streamed by ESP8266 ArduCAM 5MP OV5642 camera Wi-Fi video-streaming to the owner. If the person is known to the owner, he/she would be permitted to open the door. Else if the person is of unknown to the user, he/she can make the door to be in a closed state and could take the appropriate action. Thus the door will be of highly secured from unknown person.

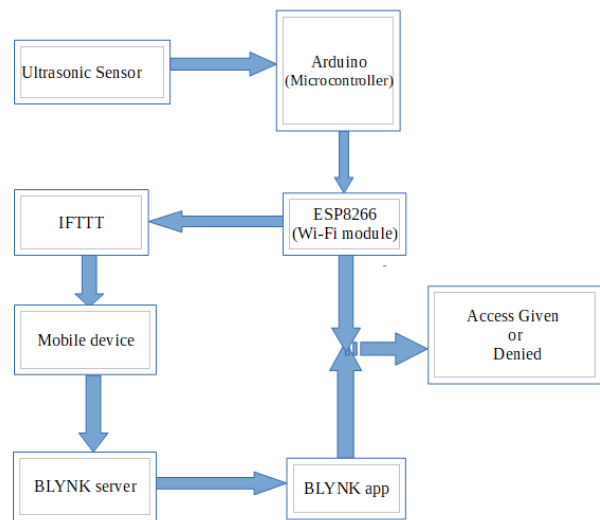


Figure 2. Block Diagram

IV. HARDWARE DESCRIPTION

Ultrasonic Sensor: Device used to measure the distance to an object by sending out a sound wave a specific frequency and recording the time taken by the sound wave to bounce back.



Figure 3. Ultrasonic Sensor

Arduino: Microcontroller used to construct programmed devices and intelligent object to perform detection and control operations in the real world. [2]



Figure 4.Arduino

ESP8266 12e (NodeMCU): Wi-Fi modulo used to connect system to the cloud to perform various transfers over the internet. The workable advancement framework that require a serial TTL-to-USB connector and an outside 3.3 volt control supply. [1]

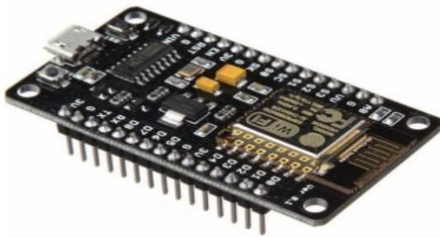


Figure 5.NodeMCU

Web-camera: A video camera that feed or streams its image in real time. The ArduCAM mini has miniature size with benefit that can be used in any platforms if they have SPI and 12C interface for it to use hardware interface and open source code library. Also it can be mated with standard Arduino boards.



Figure 6. Web camera

Breadboard and Jump wire: A breadboard is utilized to build and test circuits expeditiously afore finalizing any circuit design. Apertures on the breadboard route components like ICs and resistors to be connected. Top and bottom power distribution rails are present in a typical breadboard. To establish connectivity with bread board we use Jump wires.

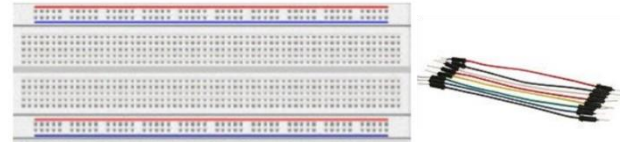


Figure 7. Breadboard and Jump wires

V. IMPLEMENTATION

An ultrasonic sensor is required to recognize a nearby user which in turn is connected to the microcontroller, required to control the door lock, and a Wi-Fi module is used for communicating with the mobile device using IFTTT server and BLYNK server. The sensor activates the circuit sending a message and an E-mail through the IFTTT server to the mobile device of the user, with the web portal address which will be used for live streaming.

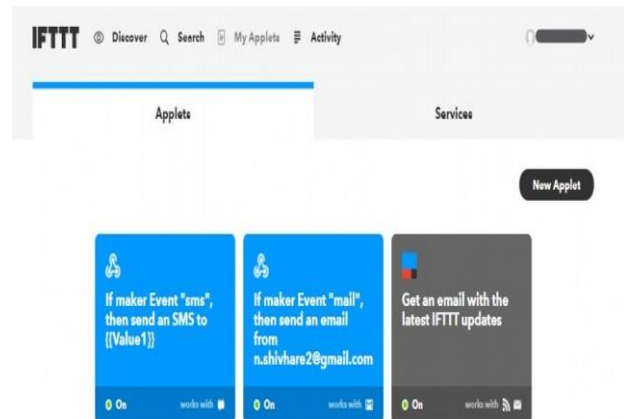


Figure 8. IFTTT Interface

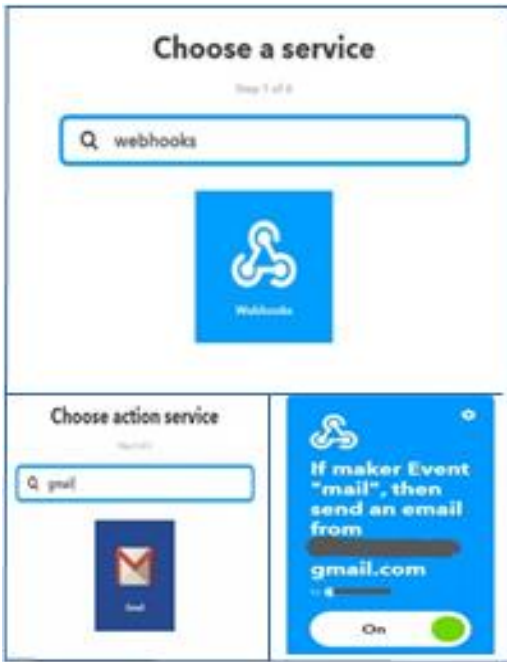


Figure 9. Procedure to send a mail



Figure 11. Live streaming using the web portal

The accessibility based on the authentication is provided using the BLYNK app which connects to the NodeMCU through the BLYNK server.



Figure 10. Procedure to send a message

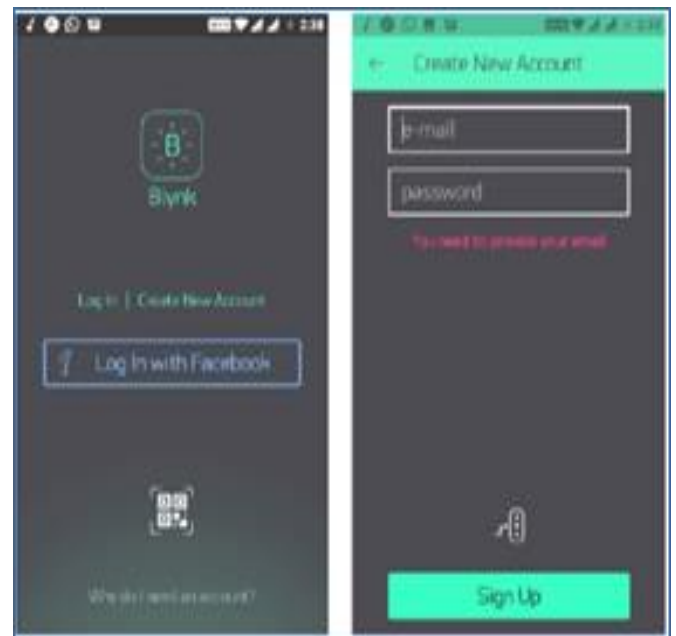


Figure 12. Create a new account

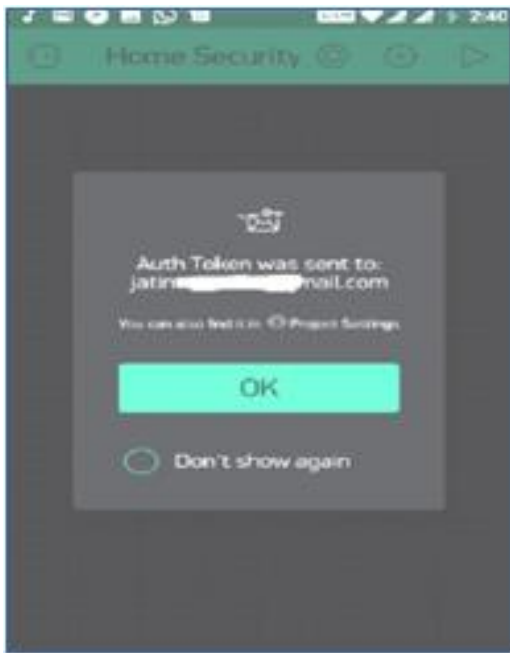


Figure 13. Authentication token



Figure 15. Screenshot of Notification

VI. FLOWCHART



Figure 14. Adding Widgets

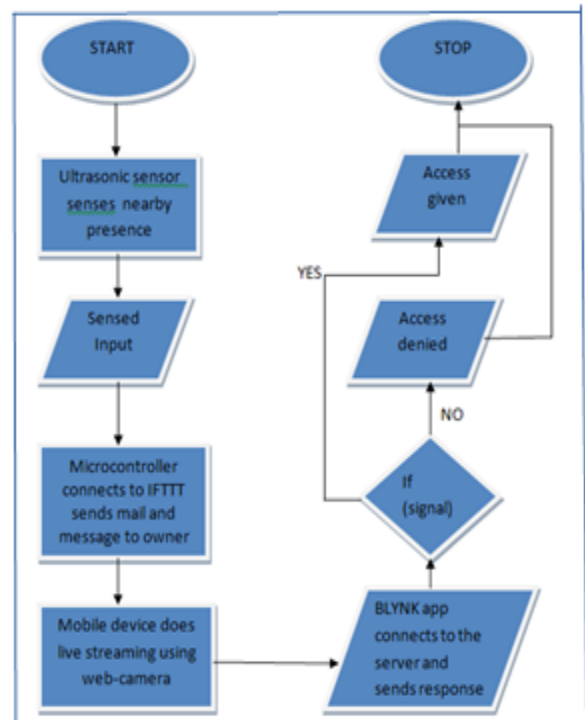


Figure 16. Flowchart

Based on the indication received the accessibility is provided or denied.

VII. CONCLUSION

The proposed system is platform independent therefore can be accessed from a wide range of phones with different operating systems. Also connectivity problems are removed as the notifications will also be delivered through SMS. Data connections need not be

enabled on user's phone all the time. The major utility of this system compared to others is the minimal use of hardware which in turn reduces its cost and chances of failure.

VIII. ACKNOWLEDGEMENT

We would like to express our heartfelt gratitude to the institute, PESIT-BSC for providing us with a conducive environment and the required facilities that helped us in completing the project. We would like to express a deep sense of gratitude to Mr.Ananda M, Asst. Professor who has been very supportive. He has been extremely important in the completion of this project.

IX. REFERENCES

- [1]. NodeMCU – an open-source firmware [Online]. Available: nodemcu.com/index_en.html
- [2]. Arduino–Open-source electronics platform. Based on easy-to-use hardware and software. Available: <http://www.arduino.cc>
- [3]. IFTTT–a free web based service to create applets. Available: <https://ifttt.com/discover>

Structural and Modal Analysis of Composite Leaf Spring

Rohan P Sakale, Sharanbassappa Patil

Department of Mechanical Engineering, PES University, Bengaluru, Karnataka, India

ABSTRACT

The suspension system is one of the imperative parts of an automobile and is responsible for the ride comfort and handling of the vehicle. In suspension system, two types of springs are used helical spring and leaf spring. In addition to energy absorbing device, the ends of a leaf spring behave as a guided along a definite path as it deflects act as a structural member, this behaviour of leaf spring proves to be an advantage over helical spring. In the present work, fabricated mono-leaf spring comprises of steel and unidirectional glass fiber reinforced composite. To analyze the behavior of the fabricated steel and composite leaf spring, experimental modal testing and FEA has been carried out with free-free boundary condition. For FEA, ANSYS workbench environment has been used. By FEA it is found that natural frequencies of steel leaf spring are greater than natural frequencies of composite leaf spring and it has been also noticed that the experimental modal testing results showed a similar trend.

Keywords: Mono leaf spring, Metal leaf spring, Experimental modal analysis, Harmonic analysis

I. INTRODUCTION

Leaf spring is a simple form of a spring, commonly used for the suspension in wheeled vehicles. It is also one of the oldest forms of springing, dating back to medieval times. An advantage of a leaf spring over a helical spring is that the end of the leaf spring may be guided along a definite path. Sometimes referred to as a semi elliptical spring or cart spring it takes the form of as lender arc-shaped length of spring steel of rectangular cross-section. The center of the arc provides location for the axle, while tie holes are provided at either end for attaching to the vehicle body. For very heavy vehicles, a leaf spring can be made from several leaves stacked on top of each other in several layers, often with progressively shorter leaves. Leaf springs can serve locating and to some extent damping as well as springing functions.

This project mainly focused on modal analysis of laminated mono composite leaf spring with

unidirectional fiber with an orientation of $(0^\circ/90^\circ/45^\circ/-45^\circ/-45^\circ/45^\circ/90^\circ/0^\circ)$. The probability Glass fiber/ Epoxy composite material for leaf springs of a suspension system to interchange in conventional spring to increase the deflection, stresses, gain the comfort is studied.

Shokrieh *et al.* [1] determine stresses and deflection in the leaf spring utilized in back suspension of vehicles by FEA. As the width decreases, the thickness increases linearly from spring eye towards the axel seat.

Abdul Rahim Abu Talib *et al.* [2] studied the fabric material and geometry of the composite curved spring was optimized utilizing FEM by considering versatility properties of $a/b = 2$ of composite elliptic springs had an ideal spring parameter and it can be utilized for all trucks.

Karditsaset *al.* [3] designed two parabolic leaf spring for front axles of heavy duty vehicles was done using finite element methods. The permissible stress were determined using Wohler curve. The results shown that the stress limitations or exceeded and nearly uniform stress distribution were achieved along the length of the two leaves.

Kong et *al.*[4] worked on failure assessment of a leaf spring eye design under various load cases. They presented a transient dynamic multibody simulation of a truck leaf spring and suspension module. They analyzed the various leaf spring eye design extreme load condition such as cornering, breaking and striking

Stephan Krall *et al.* [5] this work carried out experimental modular investigation (impact test and shaker test) for examining energetic quality of CFRP cantilever leaf springs. Classical lamination theory of composite was utilized in arriving at the measurements. The results obtained by Euler Bernoulli beam hypothesis were compared the experimental results.

N Suprithet *al.*[6] FEM analysis of three multi leaf springs made up of three distinctive materials viz. 65Si7, composite leaf spring, and hybrid leaf spring. Structural analysis was carried out for these leaf springs and they found that under the same static conditions the stresses in leaf springs were with great contrast.

R M Patilet *al.*[7] found that the conventional metallic leaf springs include significant static weight to the vehicles and diminishes their fuel productivity. Hand lay-up vacuum bagging process using fabrication of composite leaf spring. Experimental tests were performed to load carrying capacity and stiffness of composite leaf spring compare to metallic.

II. METHODS AND MATERIAL

In leaf springs made of strong materials, the energy is stored as elastic strain energy. Further, since a portion of the spring's mass is associated with vertical motion of the wheel, it is desirable to reduce its mass as well as other contributing unsprung mass to increase vehicle control. Therefore the spring setup and fabric material of construction should be chosen to maximize the strain energy storage capacity per unit mass without outstanding stress horizontal surface with reliable long life method.

Steel leaf spring

The material used for leaf springs is generally pure carbon steel having 0.90% to 1.0% carbon. The leaves are warm treated after the making process. Greater range of deflection and better fatigue properties.

Table 1. Measurements of steel leaf spring

Parameter	Value mm
Straight length	985
Camber	112
Leaf width	50
Leaf thickness	8

Mechanical properties of steel leaf spring

Table 2

Sr. No	Properties	value
1	Hardness	BHn 388-461
2	Tensile strength	1300-1700MPa
3	Yield Strength	1170-1550MPa
4	Density of material	7800kg/m ³

A. Finite Element Analysis

Finite Element Analysis of steel leaf spring. It can be used to calculate deflection, natural frequency, and many other phenomena.

The modeling of metal leaf spring is done with CATIA V5. For the finite element analysis, ANSYS is selected due to its simplicity and quick results. For modelling the steel spring, the dimensions of a conventional leaf spring are chosen.

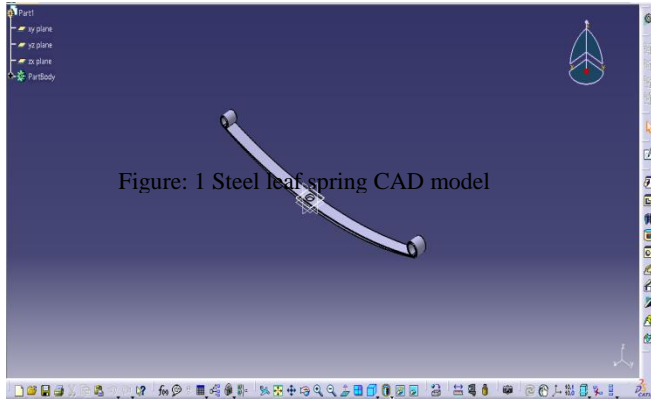


Figure 1. Steel leaf spring CAD model

Vehicle specifications:-

Here weight and initial dimension of four wheeler “Maruti Suzuki Omni” vehicle are taken.

- Max. load carrying capacity = $5 \times 70 = 350\text{kg}$
- Weight of vehicle = 785kg
- Acceleration due to gravity (g) = 9.81m/s^2
- Total weight = $785 + 350 = 1135\text{kg}$
- Total weight = 11135.34N
- Load on each eye of spring is 2784N
- Load on each wheel is = 1392N

Since the vehicle is 4-wheeler, a single leaf spring comparing to one of the wheel takes up one fourth of the overall weight.

Composite Leaf Spring

The capacity to absorb and store more expense of energy ensures the comfortable operation of a suspension system. In any case, the problem of heavy weight of spring is still determined. This can be cured by presenting composite material, in place of the conventional leaf spring. From several studies, it is found that the E-glass/Epoxy is better material for replacing the conventional steel as per strength.

MATERIAL PROPERTIES OF E-GLASS EPOXY

Table 3

Sr. No	Properties	Value
1	Young's modulus Y-direction (E_y)	8060 MPa
2	Young's modulus X-direction (E_x)	52060 MPa
3	Young's modulus Z-direction (E_z)	8060 MPa
4	Shear modulus XY-direction (G_{xy})	4500 MPa
5	Shear modulus ZX-direction (G_{yz})	4500 MPa
6	Shear modulus YZ-direction (G_{zx})	3846.2 MPa
7	Poisson ratio XY-direction (ν_{Uxy})	0.26
8	Poisson ratio ZX-direction (ν_{Uyz})	0.4
9	Poisson ratio YZ-direction (ν_{Uzx})	0.26
10	Density of material	1800kg/mm^3

Table 4. Measurements of composite leaf spring

Parameter	Value (mm)
Straight length	985
Leaf thickness at the end	08
Leaf thickness at the centre	20
Leaf width at the centre	32
Camber	112
Leaf width at the end	50

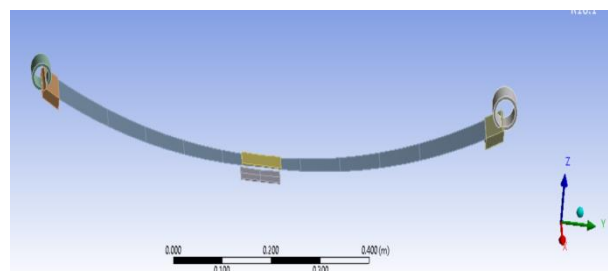


Figure 2. composite leaf spring shell model

The shell model of composite leaf spring is shown in figure 2 is developed in ANSYS Composite PRE-POST. To create layers for different thickness and different width of composite leaf spring and connected metal parts to shell bounded contact.

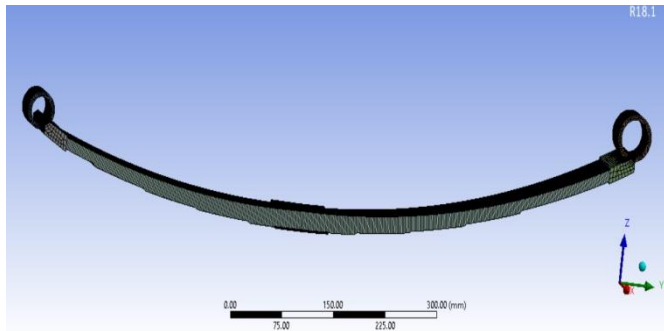


Figure 3. Meshed model of composite leaf spring

The meshed model of composite leaf spring is shown in Figure 3 is a hexahedral mesh consists of 108176 elements with an element size 5mm.

Simulation is carried out for free-free boundary condition to determined natural frequency and deflection of composite leaf spring.

B. Experimental modal testing

The leaf spring is suspended by two elastic strips within a designed setup, to make it hang a free-free condition. When the leaf spring is excited at resonant frequencies, it causes to vibrate and gives special shapes called mode shapes. By understanding the modal parameters or “mode shapes”, all possible type of vibration can be predicted. The excitation is applied by the impact roving hammer and the input force is measured by the force measuring transducer. The accelerometer is mounted on specified point to measure the frequency response at several points on the leaf spring and data acquisition system computes the frequency response function (FRF) and output is measured.

To perform an impact test the following equipment's are required:

1. An impact hammer
2. An accelerometer
3. A 8 channel FFT data analyser
4. Post-processing software

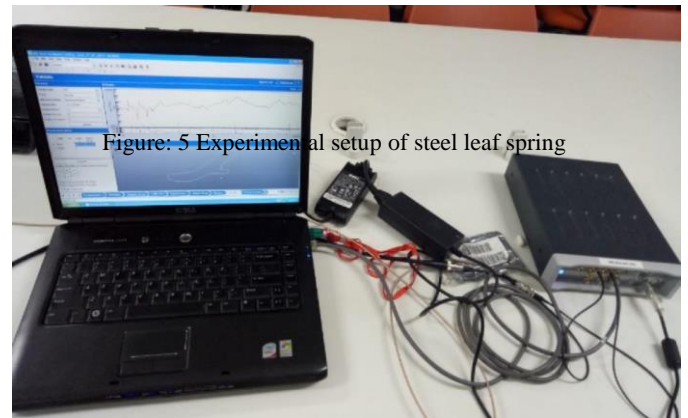


Figure 4. Actual impact testing Experimental setup

Generally, experimental modal analysis is used to solve a dynamic problem. Most of vibration and acoustic problems are function of both initial conditions and inherent characteristics of a system which described by the modal analysis. Thus, it helps to understand the various mode of vibration response of any structure.



Figure 5. Experimental setup of steel leaf spring

III. RESULTS AND DISCUSSION

A. Numerical Results of Steel Leaf Spring

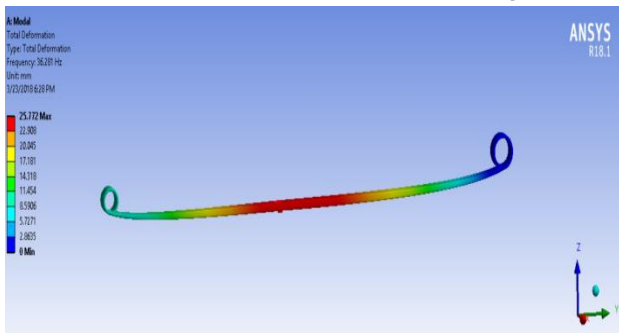


Figure 7. Steel leaf spring 1st Mode shape

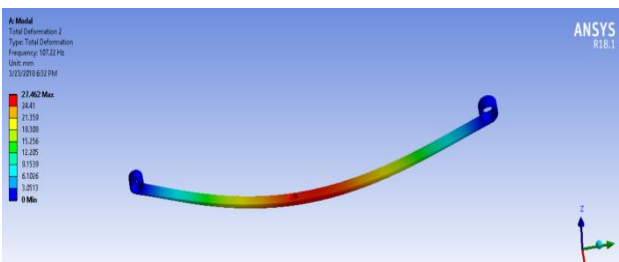


Figure 8. Steel leaf spring 2nd Mode shape

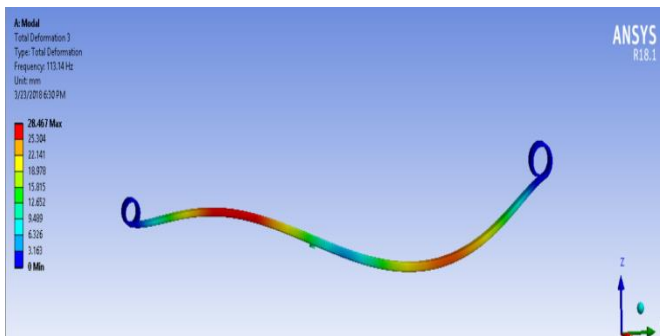


Figure 9. Steel leaf spring 3rd Mode shape

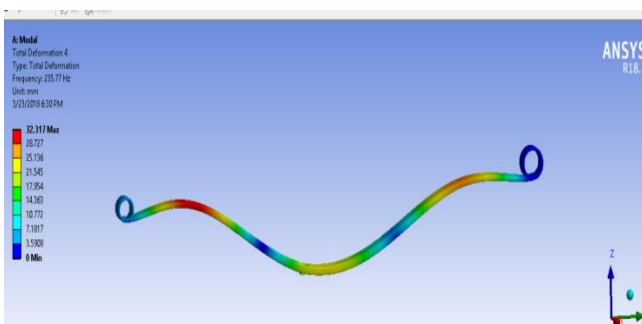


Figure 10. Steel leaf spring 4th Mode shape

B. Numerical Results of composite Leaf Spring

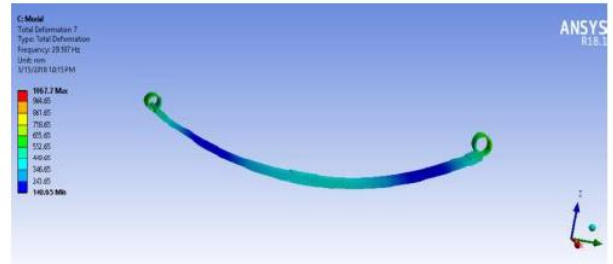


Figure 11. Composite leaf spring 1st Mode shape

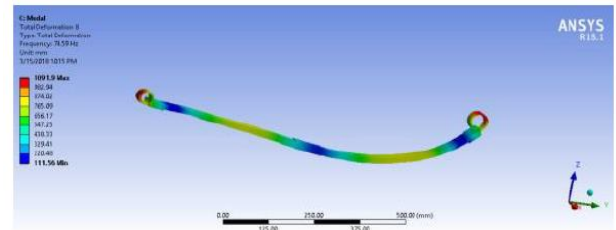


Figure 12. Composite leaf spring 2nd Mode shape

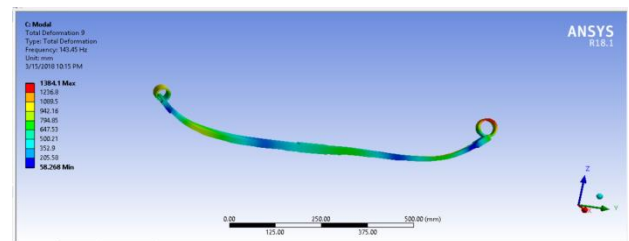


Figure 13. Composite leaf spring 3rd Mode shape

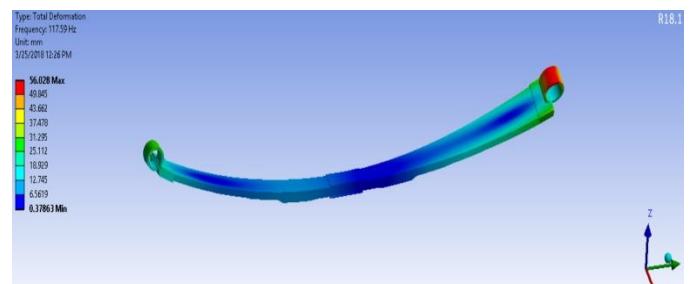


Figure 14. composite leaf spring 4th Mode shape

Table 4. Natural frequency of Steel Leaf Spring

Modes	Experimental Results (Hz)	FEA Results (Hz)
1	32.08	36.28
2	75.30	107.22
3	150.13	113.14
4	225.73	235.77

Table 5. Natural frequency of Composite Leaf Spring

Modes	Experimental Results (Hz)	Numerical Results (Hz)
1	26.09	29.18
2	79.10	74.43
3	89.74	98.35
4	116.91	119.20

From Above results, it is observed that there is good agreement between experimental and simulated natural frequencies of both steel and composite leaf spring.

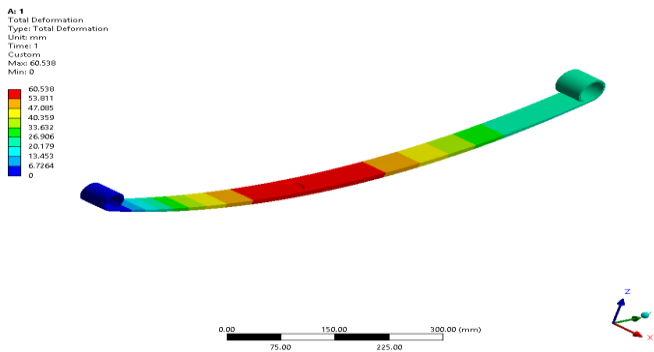


Figure15. Deformation of steel leaf spring 60.53mm

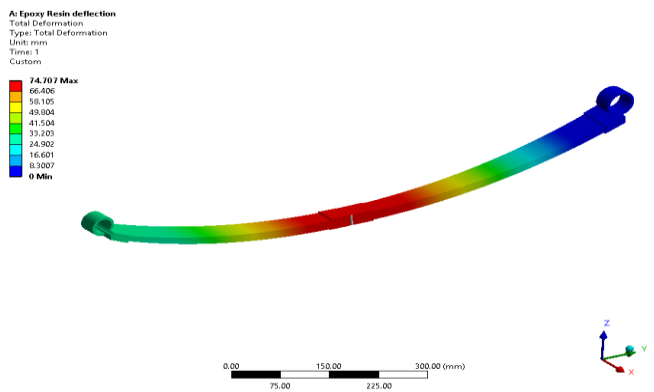


Figure16. Deformation of composite leaf spring 74.70mm

Deflection of composite and steel leaf spring obtained from simulation is 74.70 mm and 60.53 mm is same load carrying capacity respectively.

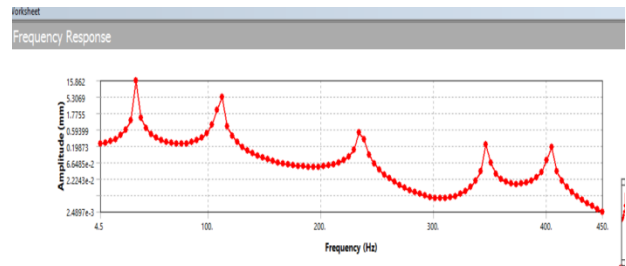


Figure 17. FRF of Steel leaf spring

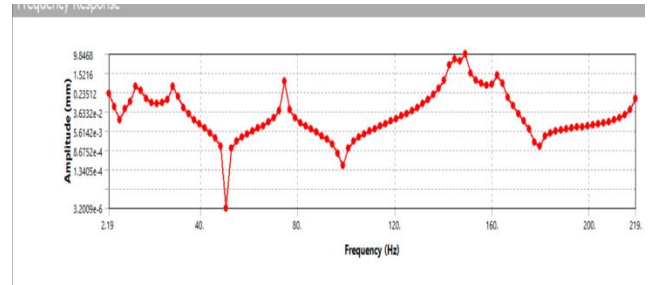


Figure 18. FRF of Composite leaf spring

Figure 17 and figure 18 shows the response analysis of composite leaf spring and steel leaf spring. This technique exploits the Frequency Response Function (FRF) of the structure, which represents the relation between the excitation and the vibrational response of the structure. Resonance frequencies appear as peaks in the measured frequency response functions.

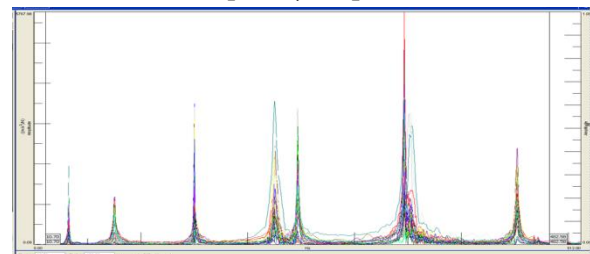


Figure 19. Experimental FRF of Steel leaf spring

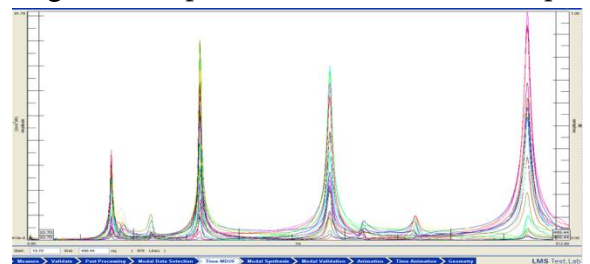


Figure 20. Experimental FRF of Composite leaf spring

Figure 19 and figure 20 shows the experimental response analysis of composite leaf spring and steel leaf spring good agreement with numerical results.

IV. CONCLUSIONS

This work is to compare load and deformation in Glass/Epoxy composite leaf spring compared to steel leaf spring for automobile suspension system.

It can be observed from the comparison that the deflection and load induced in the Glass/Epoxy composite leaf spring is higher than the conventional steel leaf spring for the same load carrying capacity.

This design helps in the replacement of conventional steel leaf springs with Glass/Epoxy mono composite leaf spring with better ride quality.

Comparative modal analysis of mono composite Leaf spring has been carried out.

The mode shapes and frequencies are carried out of both steel leaf spring and composite leaf spring. The numerical results from Finite Element Analysis showed in general a good agreement with the experimental results.

Totally it is found that the composite leaf spring is the better than that of steel leaf spring. Therefore, it is concluded that composite mono leaf spring is an effective replacement for the existing steel leaf spring in vehicles.

V. REFERENCES

- [1]. Mahmood M. Shokrieh, Davood Rezaei, "Analysis and optimization of a composite Leaf spring", *Composite Structures* 60 (2003) 317–325
- [2]. Abdul Rahim Abu Talib, Aidy Ali, G. Goudah, Nur Azida Che Lah, A.F.Golestanesh "Developing a Composite based elliptic spring for automatic applications", *Materials and Design* 31(2010) 475-484
- [3]. S. Karditsas, G. Savaidis, A. Mihailidis, A. Savaidis, R. Fragoudakis. "Leaf springs- Design, Calculation, and testing requirements research gate publication June 2014
- [4]. Kaveri A Katake, Sham. H. Mankar, Sandip A. Kale, Prakash S. Dabeer, S.J. Deshmukh " Numerical and Experimental Stress Analysis of a Composite Leaf Spring", *International Journal of Engineering and Technology* Oct-Nov 2016
- [5]. Y.S.Kong, S. Abdullah, M.Z. Omar, S.M. Haris "Failure assessment of a leaf spring eye design under various load cases", *Engineering Failure Analysis* 63(2016) 146-159
- [6]. Stephan Krall and Richard Zemann "Investigation of the Dynamic Behaviour of CFRP Leaf Spring", *Procedia Engineering* 100 (2015) 646-655
- [7]. N Suprith, K. Annamalai, C.D. Naiju, Arjun Mahadevan "Design and analysis of Automotive Multi-Leaf Springs Using Composite Materials", *Applied Mechanics and Materials* Vol.372 (2013)
- [8]. R M Patil, S. M. Hatrote, A. K. Pharale, V S Patil, G V Chiniwar, A S Reddy "Fabrication and Testing of composite Leaf Spring for Light Passenger Vehicle", *International Journal of Engineering and Technology* April 2014
- [9]. P.S.Fancher, R.D. Ervin, C.C. Mac Adam, and C.B.Winkler: "Measurement and Representation of the Mechanical properties of leaf springs", *SAE paper*, 1980,800905 pp.26-35.
- [10]. Suichi Takano & Masahiro Suzuki "study of a vehicle dynamic model for improving roll stability", *society of automotive Engineers SAE Inc* 1969, 69176pp.11-15.
- [11]. Autar K. Kaw "Mechanics of Composites" Second Edition Published in 2006 by CRC Press Taylor & Francis Group 6000 Broken Sound Parkway NW, Suite 300 Boca Raton, FL 33487-2742
- [12]. Manual on Design and Application of leaf springs, *Spring Design Manual*, AE-11, Society of Automotive Engineer Hs 788, 1990
- [13]. Release 15.0, November 2013 ANSYS Composite PrePost User's Guide. ANSYS, Inc.

Synthesis and Mechanical Properties of Araldite/Wooden Powder/Lead oxide/PPY/PANI Composites

P M Surendar, Nagaraja K B , Navyakiran R M , N Rahul , J Yashas , Pachappan C , M Revanasiddappa
Department of Mechanical Engineering, PESIT Bangalore South Campus , Bangalore , Karnataka, India

ABSTRACT

In the Present day world, there is a huge amount of work and research being done for various advancements in Composites. This, in turn has led to the innovations in materials and discovery of wide variety of new composites. A **composite material** is basically a material which is made from two or more constituent materials with significantly different physical or chemical properties, which when combined, produce a material with characteristics different from the individual components. This feature helped us to develop various composite materials with desired properties of interest. The mechanical properties of the composites developed is due to the combined effects of matrix composition, reinforcement, hardener and solvents used. This paper highlights the experimental study on the synthesis and mechanical properties such as Ultimate Tensile strength, UL and cross breaking strength of Araldite/wooden powder/Lead oxide/PPY/PANI reinforced epoxy composites. Various Studies were performed by varying the concentrations of Lead oxide, wooden powder, PANI, PPY (by weight percent) keeping the concentration of Entire composite constant (100%) in the epoxy matrix. The hardener used was HY951 which is hydrophilic in nature. The particles of wooden powder and lead oxide adds to the enhancement of mechanical properties. It was observed that the mechanical properties enhanced for higher concentration of Lead oxide, wooden powder, PANI, PPY while decreased for lower concentrations, keeping pure epoxy composite as the reference.

Keywords: Lead oxide; Wooden powder ;PANI; PPY; epoxy; Cross breaking; Tensile ; UL;

I. INTRODUCTION

Due to the rise in the new technologies, there is a need for materials which are Light weight in nature and must be possessing Good strength in order to replace the current Existing materials. Our literature survey reveals that the composites which are made from Lead oxide, wooden powder etc. Have good mechanical properties than the fiber reinforced composites. One of the reasons for Good mechanical properties is due to the size of particles which makes them possess high Grain efficiency. In our research work, we used Araldite/wooden powder/Lead oxide/PPY/PANI to make composites. The hardener (HY951) used has low viscosity and helps curing of

epoxy resin at room temperature. It undergoes an exothermic reaction with the resin and releases heat. These hardeners being hydrophilic in nature tend to get contaminated on exposure to atmospheric moisture hence, they are stored in a dry place at room temperature in air-tight containers.

The following research work was carried out by using epoxy LY556 as the matrix material. Epoxies are widely used as metal coatings, electronic components, electrical insulations and also as structural adhesives. The advantage of using Epoxy resins is that, it has less Shrinking capacity during curing and great Flexibility and as well as Higher Strength.

The hardener (HY951) used has low viscosity and helps curing of epoxy resin at room temperature very easily and higher filler addition possibility. It undergoes exothermic reaction with the resin releasing heat.

Hardeners being hydrophilic in nature tend to get contaminated on exposure to atmospheric moisture hence, they are stored in a dry place at room temperature in air-tight containers. Polypyrrole (PPy) are conducting polymers which are formed by the polymerization of pyrrole.

In this Research, we have studied the Tensile strength and Cross breaking strength of Araldite/wooden powder/Lead oxide/PPY/PANI composites.

II. EXPERIMENTAL PROCEDURE AND METHODOLOGY

A mold of dimension 200mmX150mmX3mm made of Glass was used. Wax material were applied to the edges of the mold ,so that the composite material once solidified,can be easily removed from the mold ,rather than being sticky onto the surface of the moldcavity.The various composites were prepared by varying the compositions of araldite , lead oxide, PPy, PANI in terms of weight percentage 4%, 2% (Keeping 100% wt as the total wt). Initially a pure epoxy composite was prepared which was used as reference. The reinforcements, matrix and the hardener were mixed thoroughly in a beaker and stirred continuously in magnetic stirrer. Acetone was slightly added for dissolving the reinforcements. The prepared mixture was poured into the wax coated mold cavity and was allowed to cure under room temperature for three days. Thus, fabrication of composites was completed.

The following composites were made and named accordingly, for easy study purpose:

- R1 – Pure Epoxy
- R2 – Epoxy + 4g Pbo2
- R3 – Epoxy + 2g Pbo2 + 2g PANI
- R4 – Epoxy + 2g Pbo2 + 2g PPy
- R5 – Epoxy + 2g Pbo2 + 2g PANI + 2g Wood powder

- R6 – Epoxy + Pure Wood
- R7 – Epoxy + 4g Pbo2 + 4g Wood powder
- R8 – Epoxy + 2g Wood + 2g PANI
- R9 – Epoxy + 2g Wood + 2g PPy

The composites were taken out of the mold cavity and specimens of suitable dimensions were obtained . Composite specimens were prepared according to Indian standards IS: 1998-1962 , Clause 5 for testing the Tensile strength and IS: 1998-1962, Clause 6 for cross breaking strength. The edges of the specimen was filed for finishing and the mechanical properties were tested on a Universal Testing Machine (UTM) .



Figure 1. – Pure Epoxy composite



Figure 2. - Epoxy + 2g of Pbo2 + 2g of PANI

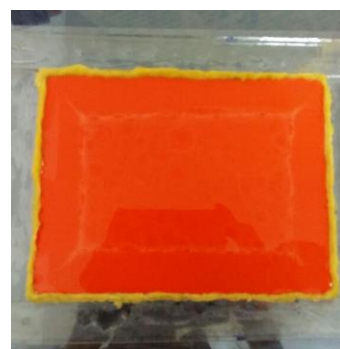


Figure 3. – Epoxy + 4g of Lead Oxide



Figure 4.- Epoxy + Pure Wood

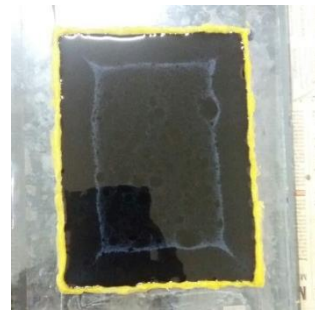


Figure 5. - Epoxy + 2g of PbO₂ + 2g of PPY

III. RESULTS AND DISCUSSIONS

The following images shows the various results obtained by synthesizing these composites :

1) **R1 – Pure Epoxy**

TENSILE TEST

Parameters	Observations
Width x thickness,mm	6.30x3.63
Area,mm ²	22.869
UL,N	915.00
Tensile strength,Mpa	40

CROSS BREAKING TEST

Parameters	Observations
Width x thickness,mm	14.85x3.70
Span length,mm	59
Cross Breaking load,N	203.25
Cross Breaking strength,Mpa	88.5

2) **R8 – Epoxy + 2g Wood + 2g PANI**

TENSILE TEST

Parameters	Observations
Width x thickness,mm	5.92x3.60
Area,mm ²	21.312
UL,N	440.00
Tensile strength,Mpa	21

CROSS BREAKING TEST

Parameters	Observations
Width x thickness,mm	15.00x3.61
Span length,mm	58
Cross Breaking load,N	112.25
Cross Breaking strength,Mpa	50.0

3)R6 – Epoxy + Pure Wood

TENSILE TEST

Parameters	Observations
Width x thickness,mm	6.18x3.63
Area,mm ²	22.433
UL,N	830.00
Tensile strength,Mpa	37

CROSS BREAKING TEST

Parameters	Observations
Width x thickness,mm	14.90x3.69
Span length,mm	59
Cross Breaking load,N	114.25
Cross Breaking strength,Mpa	49.8

4) R4 – Epoxy + 2g Pbo2 + 2g PPY

TENSILE TEST

Parameters	Observations
Width x thickness,mm	6.28x3.43
Area,mm ²	21.540
UL,N	545.00
Tensile strength,Mpa	25

CROSS BREAKING TEST

Parameters	Observations
Width x thickness,mm	15.03x3.35
Span length,mm	54
Cross Breaking load,N	98.25
Cross Breaking strength,Mpa	47.2

5) R 3 – Epoxy + 2g Pbo2 + 2g PANI

TENSILE TEST

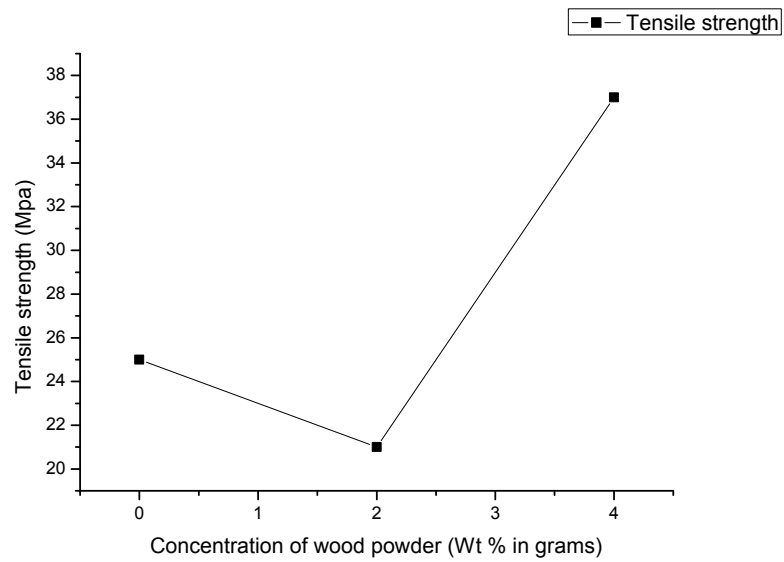
Parameters	Observations
Width x thickness,mm	6.26x3.68
Area,mm ²	23.037
UL,N	822.50
Tensile strength,Mpa	36

CROSS BREAKING TEST

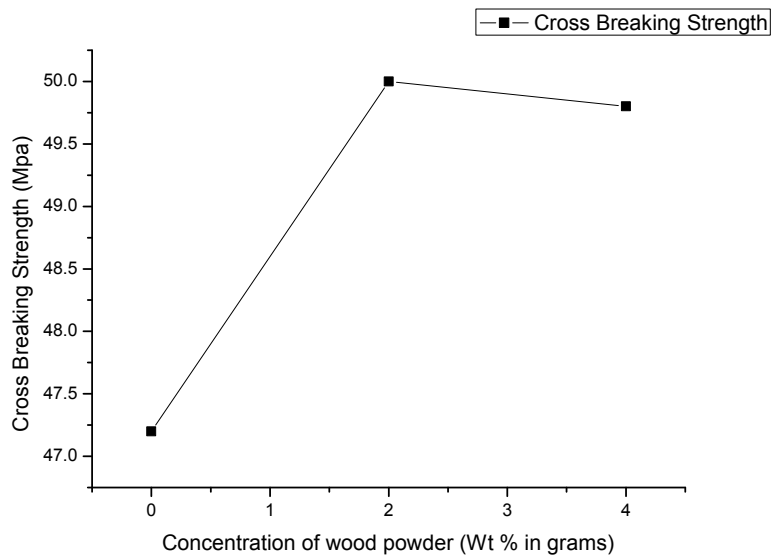
Parameters	Observations
Width x thickness,mm	14.80x3.75
Span length,mm	60
Cross Breaking load,N	202.00
Cross Breaking strength,Mpa	87.4

Following are the Graphs obtained by testing the various composites:

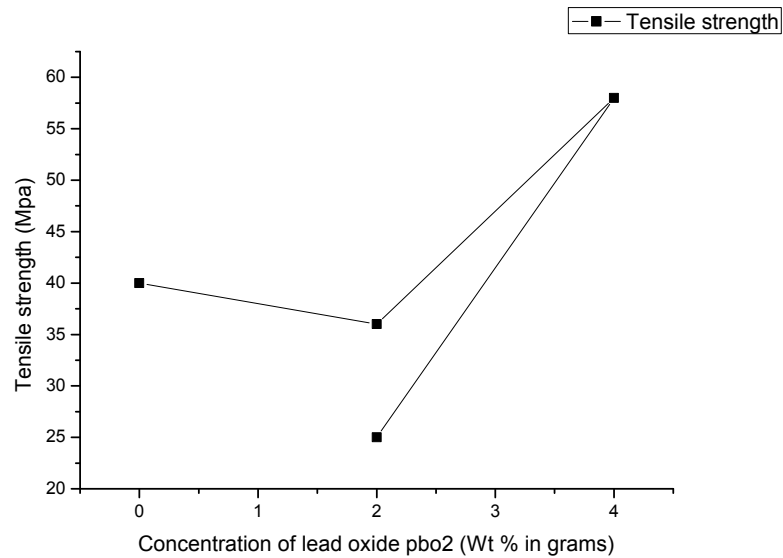
1) Graph 1



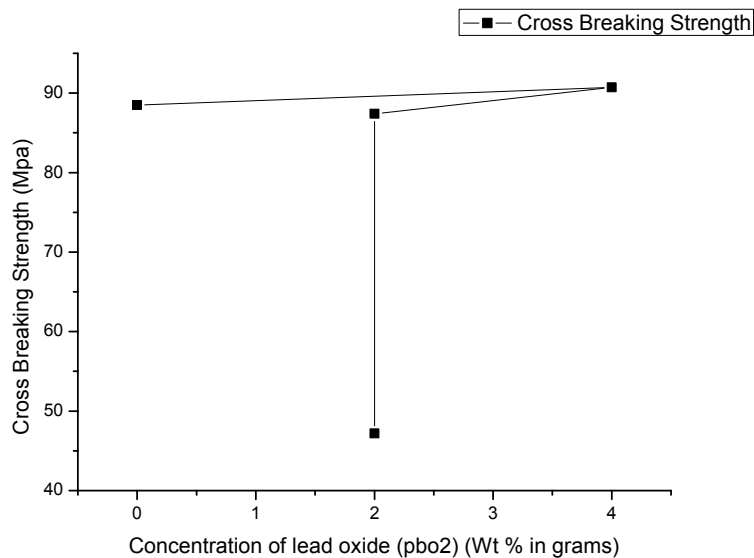
2) Graph 2



3) Graph 3



2) Graph 4



III. MECHANICAL PROPERTIES

The ultimate tensile strength of the pure epoxy sample was Lesser compared to other sample containing Epoxy with Lead oxide . The 4 % Lead oxide reinforced composite shows 14.5%increase in tensile strength with respect to pure epoxy composite. While the 2% Pbo2 along with 2 % PANI and 2% Wood along with 2% PANI reinforced composites show 9.93% and 52.5% decrease in tensile strength respectively with respect to pure epoxy composite.

Thus, it can be concluded that the tensile strength of Lead oxide reinforced epoxy composite increases in its Tensile strength and increases with the further increase in amount of Lead oxide.

The cross breaking strength of the pure epoxy sample was lesser than the Lead oxide matrix composite.

The 4 % Lead oxide reinforced composite shows 1.015% increase in Cross breaking strength with respect to pure epoxy composite. While the 2% Pbo2

along with 2 % PANI and 2% Wood along with 2% PANI reinforced composites show 1.029% and 55.5% decrease in Cross breaking strength respectively with respect to pure epoxy composite.

Table 1. Variation of tensile strength for various composites

Test sample	Tensile strength (MPa)
R1	40
R2	58
R3	36
R4	25
R6	37
R8	21
R3	36

Table 2. Variation of cross breaking strength

Test sample	Cross breaking strength (MPa)
R1	88.5
R2	90.7
R3	87.4
R4	47.2
R6	49.8
R8	50

IV. CONCLUSION

From the above Research work it can be concluded that , higher concentration of Lead oxide enhances mechanical properties such as Tensile strength and Cross breaking strength to the composite. It is the small size of these particles responsible for special characteristics. When we look at future of composites, the advanced composite value in the market share is expected to rise rapidly . Even the aerospace industries working with composite materials is anticipated to grow at elevated rates in comparison to past years. As time progresses, these lighter weight, incredibly strong materials will gain a lot of Importance and dominate the other materials used in almost any given industry .With the increase in demand for these special materials, prices will be forced down, and the technology to make these advanced materials will become more readily available and become very easy. These epoxy polymer

composites can be used in real time day to day technological applications.

V. ACKNOWLEDGEMENT

The authors are acknowledge to Geological and metallurgical laboratories - A division of IRCLASS Systems and solutions Private Limited CIN :U74120MH2014PTC254091 for helping us perform and obtain all the experimental results .

We are also Thankful to Dr.Revanasiddappa M and Principal and as well as the Management of PESIT Bangalore South Campus, Bangalore, for providing facilities in the department.

VI. REFERENCES

- [1]. J. Jayaseelan, P. Palanisamy and K. R. Vijayakumar 'Design, fabrication and

characterization of nano tubes reinforced epoxy - carbon fiber composites' Volume: 3, Issue: 2, February 2013, ISSN - 2249-555X

- [2]. Devaraj E. and Haseebuddin M.R., "Study of mechanical and wear behavior of carbon fiber reinforced epoxy resin composites with alumina filler additions". International Journal of Engineering Research & Technology (IJERT) eISSN: 2278-0181, Vol. 2, No.10, Oct-2013 P.P2602-2607.
- [3]. <http://www.scirp.org/journal/PaperInforCitation.aspx?PaperID=20720>
- [4]. <https://www.ijmter.com/papers/volume-2/issue-8/development-and-characterisation-of-epoxy-resin-based-granite-powder-a.pdf>
- [5]. Pritish Shubham, S K Tiwari 'Effect of fly ash concentration and its surface modification on fiber reinforced epoxy composite' s mechanical properties' International Journal of Scientific & Engineering Research, Volume 4, Issue 8, August-2013 ,1173 ISSN 2229-5518
- [6]. Ibtihal A. Mahmood, Wafa A. Soud, Orhan S. Abdullah, "Effect of different types of Fillers on Wear characteristics of Carbon-Epoxy composites" Al-Khwarizmi Engineering Journal, 2013, Vol. 9, No.2, P.P-85-93.
- [7]. [Characterization%20and%20Studies%20of%20Mechanical%20Properties%20ofFly%20ash_Nano%20clay%20Epoxy%20Resin%20Polymer%20Composites.pdf](#)
- [8]. Amit Kumar Tanwer 'Effect on mechanical properties for jute, coir and bamboo natural fiber reinforced epoxy based composites' ISSN (Print): 2328-3491, ISSN (Online): 2328-3580, ISSN (CD-ROM): 2328-3629
- [9]. Characterization and Studies of Mechanical Properties of Fly ash/Nano clay Epoxy Resin Polymer Composites Komal kumar B. N1 , Prajwal G1 , Prateek J. P1 , Karthik J1 and Revanasiddappa M2* 1Department of Mechanical Engineering, PES Institute of technology ISBN: 978-81-8487-599-7

Real Time Analysis of Pollutants in Vehicles [R.T.A.P.V]

Yash Bhardwaj, Shakti Ratan

Information Science and Engineering, PES Institute of Technology, Bangalore South Campus, Bangalore,
Karnataka, India

ABSTRACT

Air pollution has had devastating impacts on public health and environment, hence it has become a major concern especially in urban areas. A real-time system is essential because conventional systems are not scalable resulting in limited data of pollution levels available to us for detailed research. The need is for a gadget which can sense the level of pollutants at any time instant and help us know about the condition of the vehicles. This project of ours aims to automate the process of checking quantity of pollutants in cars and send data to a cloud system using local Wi-Fi for regular analysis of pollution levels. The real time analysis is the need of the hour and we strive to achieve that aim through this project. The device has been created to be of aid to the environment and the society.

Keywords: Research Paper, Technical Writing, Science, Engineering and Technology, real time analysis, pollution.

I. INTRODUCTION

Research has begun on air pollution all over the world due its hazardous impacts on human health. The concern on air pollution has increased significantly due to the serious hazards caused by it to the public health. The toxic gases emitted by the vehicles are also a chief source of pollution. The condition of the engine majorly decides the gas emissions pollution rate of the vehicle.

The improper combustion of the gases inside the combustion chamber is one of the chief cause of the pollution as these emissions include hazardous gases like carbon monoxide, volatile organic compounds, compounds of sulphur etc. The traditional way of measuring pollution are highly reliable and accurate in measuring wide range of pollutants by gas chromatography - mass spectrometers. The drawback of these conventional monitoring instruments, however, is that they are large in size, heavy and quite expensive.

Our project aims to overcome these drawbacks. The project uses cheap, easily available and portable sensors connected to a module that can access the local Wi-Fi and send the data on to a cloud-based web host. This data can then be analysed as desired. According to a survey in the national capital, 99% of the vehicles got their Pollution Under Control(PUC) certificates but in the same year this data was analysed, car pollution had caused major health issues in the national capital, hence making these PUC certificates unreliable.

In order to overcome this problem, we have made a device that performs Real Time Analysis of Pollutants in Vehicles [R.T.A.P.V], which is cost effective and portable, measuring pollution at regular intervals, as opposed to the stationary machines that vehicles are taken to for measuring the pollution levels every three months, because that's how long the PUC certificate is valid for.

II. EXPERIMENT

The paper elucidates the measurement of Carbon Monoxide concentration from the exhaust of vehicles and send the measured data to a website over the local Wi-Fi at regular intervals.

The working model, currently, only measures the concentration of carbon monoxide, and sends data to a simple web host and not the cloud-based web host. It is a basic model that simulates the working of the complete device on a smaller scale.

Construction:

The device consists of:

Arduino UNO R3

MQ-7 CO sensor

esp8266 Wi-Fi module

Jumper wires

Breadboard

N-channel MOSFET

Description of Important components:

ARDUINO UNO microcontroller:

The Arduino UNO R3 acts as the base and brain of our device. This helps us to program the different modules that we have used for our purpose in this project effectively and easily, allowing us access to a wide range of applications. The Arduino IDE, that is required for writing the code and uploading it to the microcontroller, is effortless to use.

It is a microcontroller board based on the Atmega328P. It has 14 digital input/output pins, 6 analog input pins, a 16 MHz quartz crystal, a USB connection jack, a power jack, an ICSP header and a reset button. It contains everything needed to support the microcontroller.

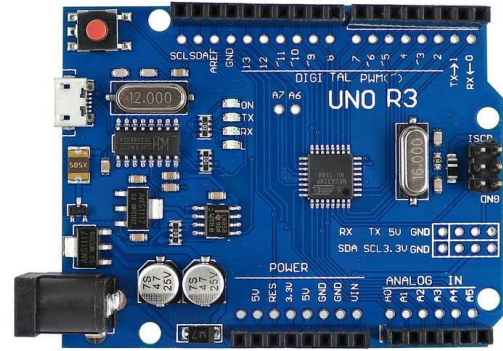


Figure 1

MQ-7 Carbon Monoxide Sensor:

This is a simple and easy to use Carbon Monoxide (CO) sensor, suitable for sensing CO concentrations in the air. The MQ-7 can detect CO-gas concentrations anywhere from 20 to 2000ppm.

This is a semiconductor gas sensor tuned to detect carbon monoxide. It measures the change in surface conductivity of tin dioxide in the presence of carbon monoxide. This sensor has a high sensitivity and fast response time. The sensor's output is an analog resistance.



1 = GND
2 = DOUT
3 = AOUT
4 = VCC

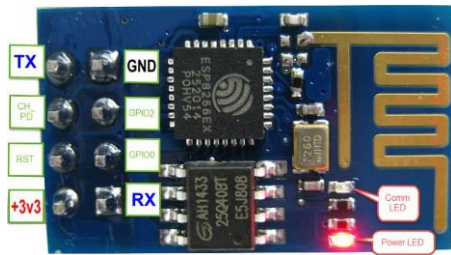
(bottom view)

Figure 2

ESP8266 Wi-Fi Module:

ESP8266 provides a complete solution to Wi-Fi networking, which allows it to either host the application or to offload all Wi-Fi functions from another application processor. The module has an integrated cache which improve the performance of

the system, and minimizes the memory requirements.



Figuer 3

The Vcc(input voltage pin) of the MQ – 7 sensor is connected to the 5v pin of the power port of an Arduino board. Analog pin of CO sensor is connected to the analog port of Arduino board. Digital pin 13 of the Arduino board is connected to the Gate pin of the N-channel MOSFET. The Drain pin of the MOSFET is connected to the GND pin of the CO sensor. Source pin of the MOSFET is connected to the GND of the Arduino UNO board. The Vcc of the esp8266 Wi-Fi module is connected to the 3.3v pin of the power section on the Arduino board. GND pin is connected to the GND pin of both the devices. CH_PD pin of esp8266 is connected to the Vcc of esp8266 module. The UTXD pin of esp8266 is connected to the TX (pin 1) on the digital section of the Arduino UNO and the URXD of the Wi-Fi module is connected to the RX (pin 0) of the microcontroller.

III. WORKING

The Arduino UNO is connected to the computer through a USB cable, which also energizes the Arduino board. The MQ-7 sensor works most accurately on a 60-90 second cycle. The coil is heated for 60 seconds and then allowed to cool for 90 seconds. This 60-90 cycle is controlled by the MOSFET which basically acts as a switch. It switches the voltage between 5v and 1.4v. At the end of the 90 second cycle the sensor is supplied with 5v and the data is read through the sensor.

This data can be displayed using the serial monitor that comes in-built with the Arduino IDE. The values sent by the sensor are voltage values and not in ppm format. We can change these values to the ppm format using appropriate code that we'll write in the Arduino ide. Alternately, we can calculate the Ro value of the sensor and determine the ppm level; 1:28 is the ratio of CO in fresh air to that of 400 ppm of CO, i.e.

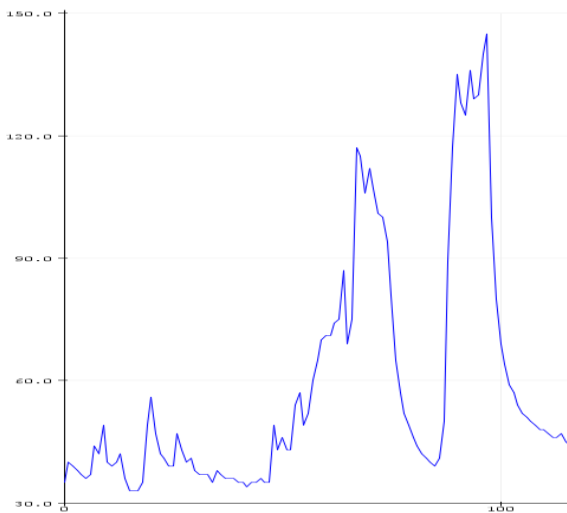
The values sent by the sensor in clean air is 1/28 times the value sent by the sensor at 400 ppm.

The code is:

```

-----
const int PinA0=A0
const int Pin13=13
//int limit;
float value;
float R0;
void setup() {
  Serial.begin(9600);
  pinMode(PinA0, INPUT);
  pinMode(Pin13, OUTPUT);
}
void loop() {
  digitalWrite(Pin13,HIGH);
  delay(60000);
  digitalWrite(Pin13,LOW);
  delay(90000);
  digitalWrite(Pin13,HIGH);
  delay(100);
  value = analogRead(PinA0);
  //Serial.print("CO value :");
  Serial.println(value);
  R0 = 10*(1023-value)/value;
  Serial.print("R0=");
  Serial.println(R0);
}

```



Figuer 4

Pollution data from a Hyundai Xcent (the peak value is when the sensor was closest to the exhaust)

Cloud computing many abilities like flexibility, disaster recovery, automatic software updates and many others, it is being preferred more than normal web hosting.

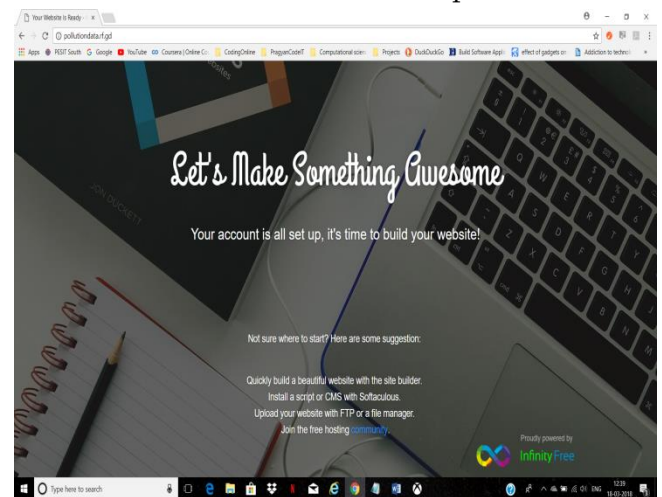
According to mckinsey.com,” Yet while automotive digital technology has traditionally focused on optimizing the vehicle’s internal functions, attention is now turning to developing the car’s ability to connect with the outside world and enhance the in-car experience. This is the connected car—a vehicle able to optimize its own operation and maintenance as well as the convenience and comfort of passengers using onboard sensors and Internet connectivity.”

This project tries to incorporate both ‘cloud computing’ and ‘connected cars’ to make the device relevant in the current era and easy to manufacture and low priced so that it can be preferred by the general public. Sending real time data of pollution of cars to a server (currently, a normal web server), would enable further research and better understand the problem at hand, i.e., the ever-increasing pollution and find better ways to solve it.

The ESP8266 Wi-Fi Module has integrated TCP/IP protocol stack that can give any microcontroller (Arduino UNO R3, in this case) access to a local Wi-Fi network. The device will use the features of esp8266 to connect to the in-car Wi-Fi and send data to our website.

We have created our own website using one of the many free domain and hosting websites. This project uses <https://infinityfree.com> for that job, which is convenient for our work. We send data to the server by directly uploading it through MonstaFTP, a MFTP provider.

The website where the data will be posted:



<https://pollutiondata.rf.gd>

Figure 5

HTTP works as a request-response protocol between a client and server. A web browser may be the client, and an application on a computer that hosts a web site may be the server. The response basically contains the status information of the request and might also contain the requested content. In this case, the esp8266 is the client and server is the one that is hosting the above website.

The sever-side script can be written in a number of languages, one of them being PHP, which is very good for handling medium - sized websites. The PHP script is uploaded to the using the file

manager(filezilla). When the esp8266 module requests the server for the php file, the server will process the request by performing all the functions specified in the script and then send the response(if required) back. We can then view that data on the website.

Esp8266 Wi-Fi module also helps us determine the location of the person through the help of the geo-location API. In order to get the geo-location API, a person needs to get a key from the Google API to use the geo-location API. The key provides us the access to know the location of the given module we have attached to the gadget, i.e., the esp8266 module. What it actually does is send the location of the device connected to the internet and providing Wi-Fi to the module. The API gives us the latitude as well as longitude thus providing accurate location of the module. Hence, the gadget is able to perform spatio-temporal analysis of pollutants in vehicles.

The code that we upload into Arduino for our device to work is:

```
#include "SoftwareSerial.h"
String ssid ="thessid";
String password="thepassword";
SoftwareSerial esp(6, 7);// RX, TX
const int AOUTpin=A0;
//const int DOUTpin=13;
const int ledPin=13;
String data;
String server = "www.pollutiondata.rf.gd"; //
www.example.com
String          uri          =
"www.pollutiondata.rf.gd/datasend.php";//
our example is /esppost.php
void setup() {
pinMode(AOUTpin, INPUT);//sets the pin as
an input to the arduino
pinMode(ledPin, OUTPUT);//sets the pin as
an output of the arduino
esp.begin(9600);
```

```
Serial.begin(9600);
reset();
connectWifi();
}
//reset the esp8266 module
void reset() {
esp.println("AT+RST");
delay(1000);
if(esp.find("OK") ) Serial.println("Module
Reset");
}
//connect to your wifi network
void connectWifi() {
String cmd = "AT+CWJAP=\" +ssid+\"\",\" +
password + \"\"";
esp.println(cmd);
delay(4000);
if(esp.find("OK")) {
Serial.println("Connected!");
}
else {
connectWifi();
Serial.println("Cannot connect to wifi"); }
}
String read_data () {
String value;
digitalWrite(ledPin,HIGH);
//delay(60000);
delay(2000);
digitalWrite(ledPin,LOW);
//delay(90000);
delay(3000);
digitalWrite(ledPin,HIGH);
delay(100);
value = analogRead(AOUTpin);
//Serial.print("CO value :");
Serial.println(value);
return value;
}
void loop () {
String vall = "tom";
//vall=read_data ();
```

```

data = "CO_level="+val1;
httppost();
delay(1000);
}
void httppost () {
esp.println("AT+CIPSTART=\\"TCP\\","\\" +
server + "\",80");//start a TCP connection.
if( esp.find("OK")) {
Serial.println("TCP connection ready");
} delay(1000);
String postRequest =
"POST " + uri + " HTTP/1.0\r\n" +
"Host: " + server + "\r\n" +
"Accept: *" + "/" + "*" + "\r\n" +
"Content-Length: " + data.length() + "\r\n" +
"Content-Type: application/x-www-form-
urlencoded\r\n" +
"\r\n" + data;

String          sendCmd          =
"AT+CIPSEND=";//determine the number of
characters to be sent.
esp.print(sendCmd);
esp.println(postRequest.length() );
delay(500);
if(esp.find(">")) { Serial.println("Sending..");
esp.print(postRequest);
if(          esp.find("SEND          OK"))          {
Serial.println("Packet sent");
while (esp.available()) {
String tmpResp = esp.readString();
Serial.println(tmpResp);
}
// close the connection
esp.println("AT+CIPCLOSE");
}
}
If everything goes successfully, we will be
able to see the data on to our websit

```

age because of the ever-increasing pollution. The efforts taken to reduce pollution has not had large enough impact due to world governments being unable to enforce necessary policies in their respective countries. There is also a technological gap between developed and underdeveloped countries that adds into the problem. The device helps to automate the process of checking pollution level in cars and sending data to a cloud system using local Wi-Fi for regular analysis of pollution level. This project helps to fill that technological gap, providing a cheap, reliable and real-time method of measuring carbon monoxide(currently) in the car exhaust.

The This project has helped us to gain knowledge about a lot of new subjects that we never explored before. It has changed our way of thinking and helped us see the surroundings in a different light. This project would have not been possible without the help and guidance of the professors of our college and our family, who were very generous and helpful throughout the making of our project.

We would like to show our gratitude to Prof. Revannasiddappa M for his guidance and mentoring throughout the endeavour. We would like to thank Prof. Prashanth Reddy for his guidance and funding for the project. We would also like to thank Prof. Muhammad Faisal for providing us with novel ideas and support.

IV. REFERENCES

- [1]. <https://www.ncbi.nlm.nih.gov/pmc/articles/PMC4721779/#!po=0.261780>
- [2]. <https://www.areresearch.net>
- [3]. <https://www.instructables.com>

Design and Analysis of CMOS Based Temperature Sensor and Its Readout Circuit

Pankaja. H. C, Dr. Shashidhar Tantry

Electronics and Communication, PESIT South Campus, Bangalore, Karnataka, India

ABSTRACT

In this paper, the proposed sensor utilizes the temperature dependency of MOSFET and BJT for designing of this sensor. The voltage or current across MOSFETs and BJT always varies with the temperature, but the challenge in this project is to design these types of sensors to linearize this variation. This task is accomplished by proper selection of circuit architecture by adjusting W/L Ratio of the transistors and choosing the proper resistor value so that the non-linearity can be reduced. After achieving the linearity, readout circuit is designed for to digitize the obtained temperature information. The proposed temperature sensor is simulated in Cadence Analog Design Environment with GPDK180nm library.

I. INTRODUCTION

Temperature is one of the most important fundamental physical quantity and is almost common in our daily life and which is independent of the amount of material i.e. temperature is having intensive property. As we know hundreds or thousands of devices are formed on thin silicon wafers[2]. Before the wafer is scribed and cut into individual chips, they are usually laser trimmed. Temperature is a physical quantity that is a measure of hotness and coldness on a numerical scale. In a body in its own internal thermal equilibrium, the temperature is spatially uniform. Temperature is important in all fields of natural science. One popular use of temperature sensors in VLSI implementation is in the emergence of RFID and wireless sensor network (WSN) applications.

With microprocessors scaling to higher performance and faster speed, heat dissipation has become a growing concern. Excessive heat degrades performance and increases power consumption of the entire system. Safe operation of the integrated circuits requires the prevention of excessive chip temperatures.

To prevent overheating, multiple integrated temperature sensors are employed in the microprocessor to monitor its thermal distribution.

II. PROPOSED SCHEME

In this paper, proposed sensor investigates two cases. In the first case, temperature sensor is designed by utilizing temperature dependency characteristics of BJT and MOSFET in Saturation region and in the second case, temperature sensor is designed by utilizing temperature dependency characteristics of only MOSFET in Sub threshold region.

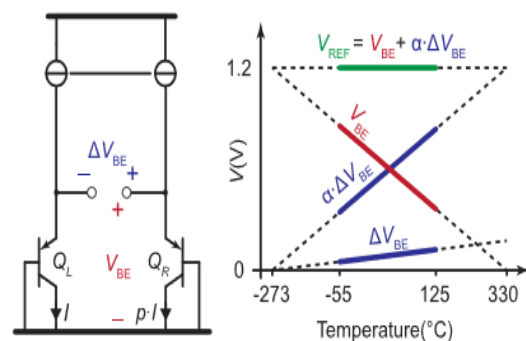


Figure 1. Basic operation of PTAT and CTAT curve.

The main aim of this project is to design a circuit to obtain Proportional to absolute temperature value (PTAT). To obtain this PTAT voltage, necessary design conditions has been considered. Basic operation of a PNP based circuit showing PTAT and CTAT behaviour is as shown in figure 1.

$$V_T = KT/q \dots \dots \dots (1)$$

Where,

V_T denotes thermal voltage.

T denotes temperature.

Q denotes electric charge.

K denotes proportionality constant.

From equation (1), it is clear that the V_T is directly proportional to temperature.

Voltage across BJT is given by equation (2)

$$V_{BE} = V_T \ln (I/I_s) \dots \dots \dots (2)$$

$$I = I_s e^{V_{BE}/V_T} \dots \dots \dots (3)$$

Where,

V_{BE} denotes base to emitter voltage.

I denotes the current flowing through each transistor.

I_s denotes reverse saturation current.

Equation (2) shows CTAT behaviour because of I_s term.

When 'n' number of transistors are considered, equation becomes as shown in (4)

$$V_{BE1} = V_T \ln (I/n I_s) \dots \dots \dots (4)$$

$$\Delta V_{BE} = V_{BE} - V_{BE1} \dots \dots \dots (5)$$

$$\Delta V_{BE} = V_T \ln (n) \dots \dots \dots (6)$$

Where,

'n' denotes number of transistors.

ΔV_{BE} denotes difference between base to emitter voltage .

In equation (6), ΔV_{BE} represents PTAT voltage since it is equal to V_T because $\ln(n)$ is constant.

In equation (2), term (I/I_s) represents complementary to absolute temperature since I_s depends upon

temperature. In this work, the main concentration is on obtaining Thermal voltage because it is PTAT, so it is necessary to cancel the CTAT term.

To cancel the CTAT term, the necessary circuits have been designed by employing a technique which connects pnp transistors in parallel and so that voltages across them are same. The difference between the base to emitter voltages have been taken into consideration, which gives the required PTAT value.

A. Temperature dependency characteristics of BJT and MOSFET in Saturation region

In this proposed scheme, Temperature dependency characteristics of BJT and MOSFET in Saturation region is investigated . In the schematic shown in figure 2, the first circuit gives the voltage that is proportional to absolute temperature and this voltage is given as the input to the pmos of the differential amplifier in order to get the required amplification range. In the final stage of the circuit, comparator is designed by giving the differential amplifier output as the input to the first input of the comparator and pulse is given to the 2nd input so that necessary digitized temperature information is obtained. The drain current of an NMOS transistor in the saturation region is given by

$$I_D = 1/2 \mu_n C_{OX} W/L (V_{GS} - V_{TH}) \dots \dots (7)$$

Where,

W/L is the aspect ratio of the transistor.

μ is the carrier mobility .

C_{OX} is the gate-oxide capacitance .

V_{TH} is the threshold voltage of a MOSFET.

In the above equation threshold voltage and mobility are the main temperature dependent parameters. As the temperature increases, both the threshold voltage and the mobility decrease. But the decrease of V_{TH} and mobility have opposing effects on the drain current; a lower threshold voltage tends to increase

the drain current, but a lower mobility tends to decrease it.

B. Temperature dependency characteristics of only MOSFET in Sub threshold region

Sub threshold region operates with the gate to source voltage less than the transistors threshold voltage V_T . This is done to ensure that all the transistors are indeed operating in the sub threshold region[1]

The sub-threshold drain current I_D of a MOSFET is an exponential function of the gate-source voltage V_{GS} , and given by

Where,

$$I_D = KI_0 e^{(V_{GS} - V_{TH}) / \eta V_T} \dots \quad (8)$$

$$I_0 = \mu C (\eta - 1) \times V_T^2$$

K is the aspect ratio ($=W/L$) of the transistor

μ is the carrier mobility

C_{OX} is the gate-oxide capacitance .

V_T is the thermal voltage .

V_{TH} is the threshold voltage of a MOSFET .

η is the sub-threshold slope factor.

III. BLOCK DIAGRAM OF THE PROPOSED TEMPERATURE SENSOR

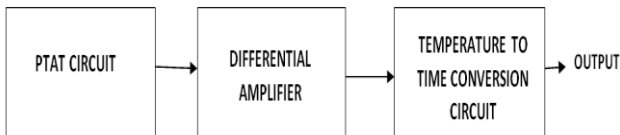


Figure 2. Block Diagram of the Proposed Temperature Sensor

This block diagram depicts the concept of whole operation where in the PTAT circuit block, the obtained voltage is given as an input to differential amplifier to obtain the amplified version and good linear range of the PTAT voltage versus temperature. In temperature to time conversion circuit, the obtained temperature information is converted into time.

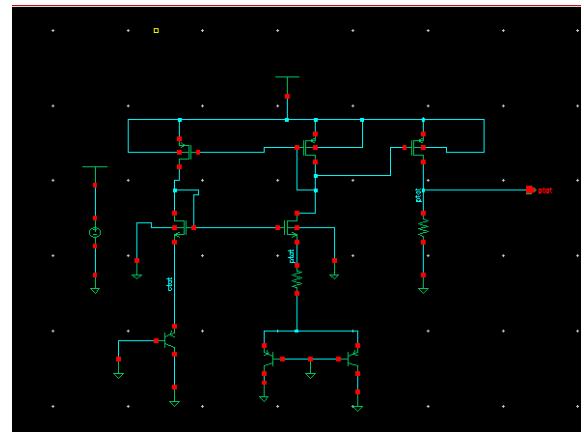


Fig3.Schematic of the PTAT circuit in saturation region.

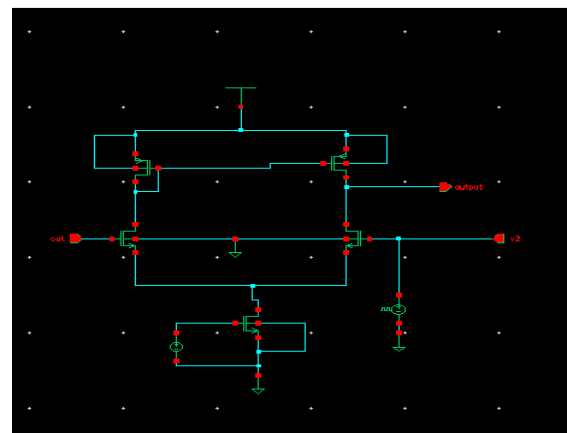


Fig4.Schematic of the Temperature to Time conversion circuit in saturation region.

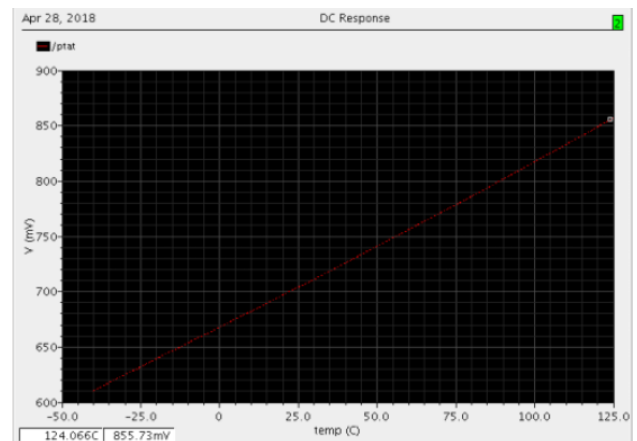


Figure 5. DC response of the proposed ptat circuit showing the linear relationship of voltage and temperature.

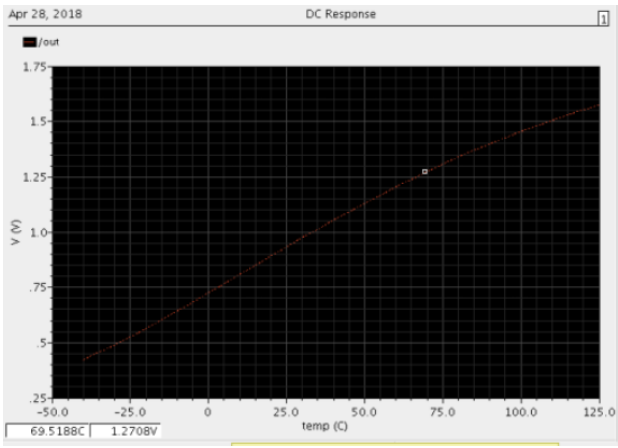


Figure 6. DC response of the proposed differential amplifier circuit showing the linear relationship of voltage and temperature.

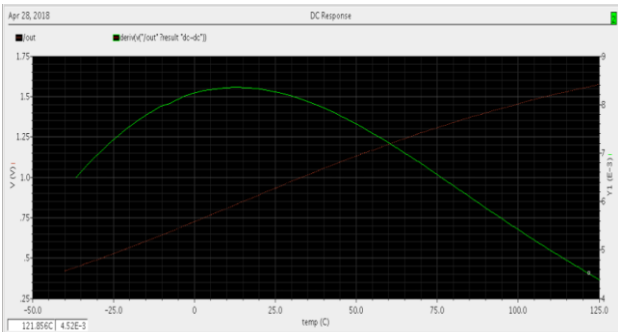


Figure 7. DC response showing the slope of the proposed ptat circuit.

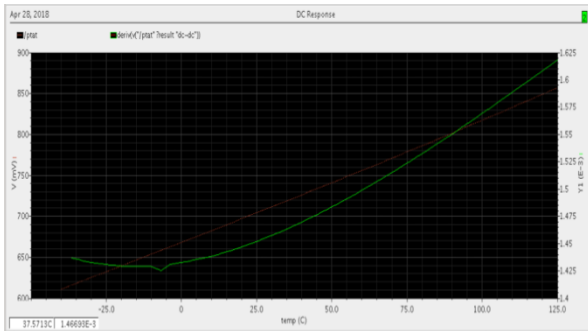


Figure 8. DC response showing the slope of the differential amplifier circuit.

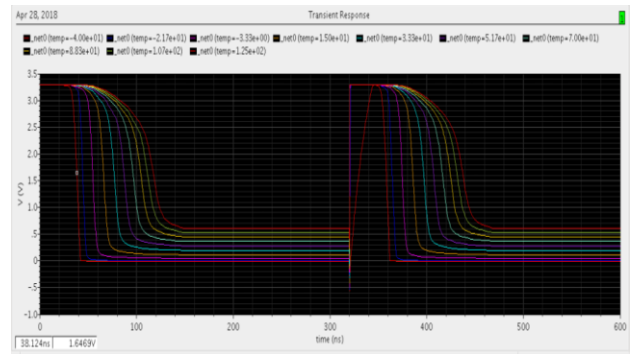


Figure 9. Transient response of varying pulse width for different temperature values.

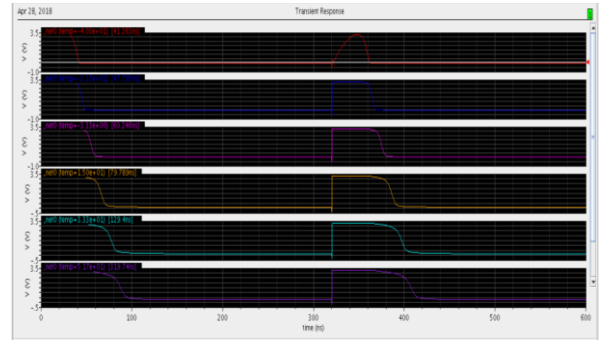


Figure 10. Expanded version of Transient response of varying pulse width for different temperature values.

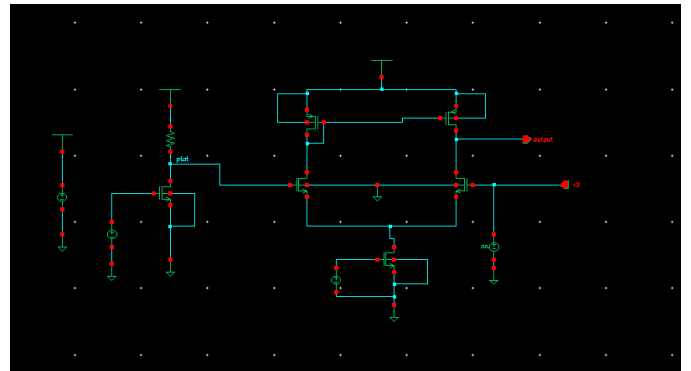


Figure 11. Schematic of the proposed temperature sensor in subthreshold region.

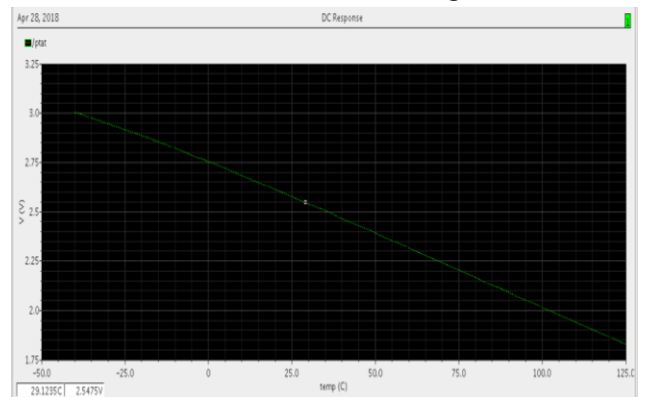


Figure 12. DC Response of the proposed temperature sensor in sub-threshold region showing the linear relationship of voltage and temperature.

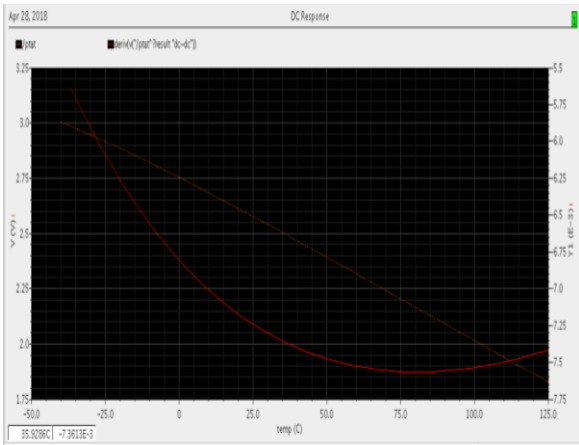


Figure 13. DC response showing the slope of the proposed temperature sensor.

Figure 14. Transient response of varying pulse width for different temperature values

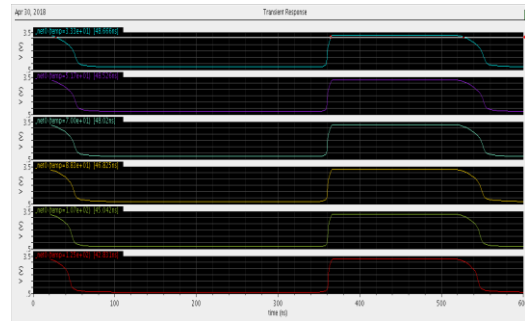
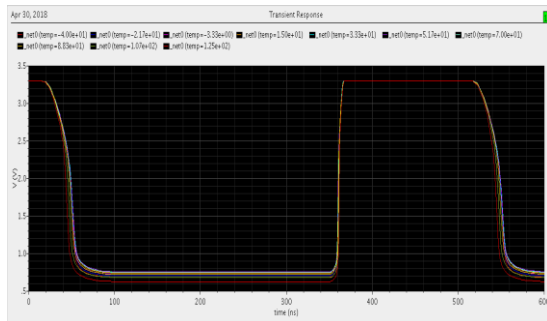


Figure 15. Expanded version of Transient response of varying pulse width for different temperature values.



IV. COMPARISON TABLE OF TEMPERATURE DEPENDENCY CHARACTERISTICS IN SATURATION AND SUBTHRESHOLD REGION

PARAMETER	Proposed PTAT circuit in saturation region	Differential amplifier circuit	Proposed PTAT circuit in sub-threshold region
Voltage Range	(857.24mV-611.93mV)=245.31mV	(1.5745-423.61mV)=1.15V	(3.005V-1.832V)=1.173V
Temperature Range	-40°C to +125°C	- 40°C to +125°C	- 40°C to +125°C

V. COMPARISON TABLE OF SLOPE VERSUS TEMPERATURE RANGE IN SATURATION AND SUBTHRESHOLD REGION

PARAMETER	TEMPERATURE RANGE	SLOPE in E-3
Proposed PTAT circuit in saturation region	-36°C to +60 °C	1.432 to 1.499
	65 °C to 115 °C	1.5 to 1.599
	116 °C to 125 °C	1.618
Differential amplifier circuit	-36 °C to -29 °C	6.55 to 6.99

	-28°C to -10°C	7.07 to 7.96
	-9°C to 61°C	8 to 8.24
	62°C to 64°C	7.1 to 7.02
	65°C to 87°C	7 to 6.01
	88°C to 109°C	5.9 to 5.01
	110°C to 125°C	4.96 to 4.4
Proposed PTAT circuit in sub-threshold region	-36°C to +27°C	-5.65 to -5.99
	-28°C to 9°C	-6 to -6.99
	10°C to 125°C	-7.012 to -7.414

VI. CONCLUSION

This paper proposes a design of temperature sensor by utilizing the temperature dependency characteristics of BJT and MOSFET. The voltage or current across MOSFETs and BJT always varies with the temperature, but the challenge in this project is to design these types of sensors to linearize this variation. In this proposed work, the required linearity is achieved within the sensing range. In the next level, Amplification circuit is designed to increase the voltage range which results in achieving more linearity. After achieving the linearity, readout circuit is designed to digitize the obtained temperature information. The proposed temperature sensor is simulated in Cadence Analog Design Environment with GPDK180nm library.

VII. REFERENCES

- [1]. Suraj Kumar Saw, Vijay Nath, "A 10.8 nW LOW POWER CMOS TEMPERATURE SENSOR FOR WIRELESS APPLICATION" 978-1-4799-7678-2/15/ IEEE 2015.
- [2]. Bahman Yousefzadeh, Saleh Heidary Shalmany, and Kofi A. A. Makinwa, "A BJT-Based Temperature-to-Digital Converter With ± 60 mK (3σ) Inaccuracy From -55 °C to $+125$ °C in $0.16\mu\text{m}$ CMOS" 0018-9200 IEEE 2017.
- [3]. Subhra Chakraborty, Abhishek Pandey, Suraj Kumar Saw and Vijay Nath, "A 1.37nW CMOS Temperature Sensor with Sensing Range of -25 °C to 65 °C" 978-1-4799-8553-1/15/ IEEE 2015.
- [4]. Sheng-Cheng Lee and Herming Chiueh, "A $69\mu\text{W}$ CMOS Smart Temperature Sensor with an Inaccuracy of $\pm 0.8^\circ\text{C}$ (3σ) from -50°C to 150°C " 978-1-4577-1767-3/12/ IEEE 2012.
- [5]. Poki Chen, Chun-Chi Chen, Chin-Chung Tsai and Wen-Fu Lu "A Time-to-Digital-Converter-Based CMOS Smart Temperature Sensor" IEEE JOURNAL OF SOLID-STATE CIRCUITS, VOL. 40, NO. 8, AUGUST 2005.
- [6]. Michiel A. P. Pertijs, Gerard C. M. Meijer and Johan H. Huijsing, "Precision Temperature Measurement Using CMOS Substrate PNP Transistors "IEEE SENSORS JOURNAL, VOL. 4, NO. 3, JUNE 2004.
- [7]. A. Bakker, "CMOS smart temperature sensors—An overview," Proc. IEEE Sensors, vol. 2, pp. 1423–1427, Jun. 2002.
- [8]. Gerard C. M. Meijer, Guijie Wang and Fabiano Fruett, "Temperature Sensors and Voltage References Implemented in CMOS Technology "IEEE SENSORS JOURNAL, VOL. 1, NO. 3, OCTOBER 2001.
- [9]. A. Bakker and J. H. Huijsing, "Micropower CMOS temperature sensor with digital output," IEEE J. Solid-State Circuits, vol. 31, no. 7, pp. 933–937, Jul. 1996.
- [10]. Ali Sahafi, J.Sobhi et.al "Nano Watt CMOS temperature sensor" Springer (2013) 75: p-343-348.

4th National Conference on “Recent Innovations in Science and Engineering”

Organised by

PES Institute of Technology - Bangalore South Campus,
Electronic City, Hosur Road, Bangalore - 560 100,
Karnataka, India

Publisher

Technoscience Academy

Website : www.technoscienceacademy.com

Email: info@technoscienceacademy.com

